Synthetic Transformations Based on Homolysis of Iodine and Bismuth Complexes

Dissertation

Zur Erlangung des Doktorgrades der Naturwissenschaften

(Dr. rer. nat.)

an der Fakultät für Chemie und Pharmazie

der Universität Regensburg

vorgelegt von

Rok Narobe

aus Bizovik, Slowenien

2023

The experimental work has been carried out between October 2018 and September 2022 under the supervision of Prof. Dr. Burkhard König at the University of Regensburg, Institute of Organic Chemistry.

Date of submission:	13.2.2023
Date of colloquium:	27.3.2023

Board of examiners:

Prof. Dr. Arno Pfitzner	(chair)
Prof. Dr. Burkhard König	(1st referee)
Prof. Dr. Oliver Reiser	(2nd referee)
Prof. Dr. Frank-Michael Matysik	(examiner)

„Science is magic that works.“

Kurt Vonnegut

TABLE OF CONTENTS

Chapter 1

1 Transformations Based on Direct Excitation of Hypervalent Iodine(III) Reagents

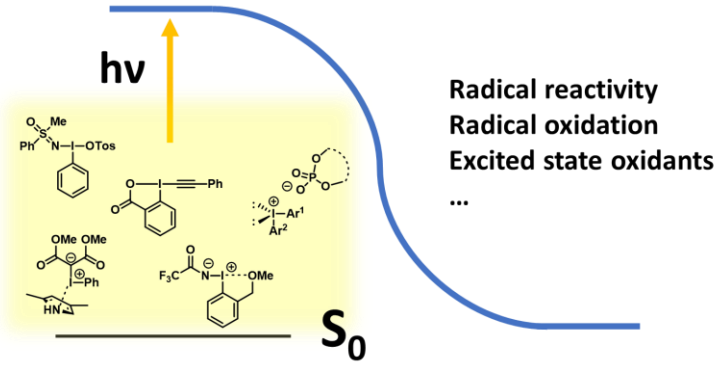

Hypervalent iodine compounds have evolved from structural curiosities into useful reagents owing to their unique polar and radical reactivity. In the last decade, many reactions based on their direct excitation have been reported as strong visible light sources became more available. In this review, we present different synthetic examples of the diverse reactivity of five different structural classes of hypervalent iodine compounds and their complexes.

This chapter has been published. For reference see:
Narobe, R.; König, B., Transformations based on direct excitation of hypervalent iodine(III) reagents.
(***Manuscript submitted***)

Author contribution: RN collected the presented literature and wrote the manuscript with the input of all authors. BK supervised the project.

1.1 Introduction

Hypervalent iodine reagents (HIRs) became an important and diverse class of compounds fulfilling multiple roles in organic synthesis.[1] Different applications of these metal-free reagents stem from their good oxidizing abilities, unique electrophilic properties, convenient structural modifications, and generally environmentally benign character.[2] They are used in different oxidative processes as chemoselective oxidants or as group transfer reagents.[3] Moreover, applications of HIRs are not only limited to their use as stoichiometric additives, but they can also serve as catalysts when combined with appropriate oxidants.[4] Different chiral iodoarenes have been utilized as organocatalysts in several impressive stereoselective transformations.[5] Furthermore, relatively weak iodine–ligand bonds in HIRs allow their use in radical chemistry as well.[6]

Homolysis of HIRs resulting from their photoactivation under UV mercury lamp has been studied since the late 80s.[7] However, most of the synthetically useful examples have been reported only in the last few years under visible light irradiation (LEDs). HIRs are mostly colourless, and excitation by visible light may seem paradoxical at first glance. The efficient light-driven reactions, irradiated at wavelengths far from absorption maxima were explained by Nakajima and Namoto in 2020.[8] They showed that HIRs in fact do absorb negligibly at higher wavelengths; the low absorption comes from a normally spin-forbidden electronic transition from the ground state directly into triplet excited state. Nevertheless, this transition and its follow up reactivity become more probable because of iodine's internal heavy atom effect.

In this review, we present synthetically useful transformations resulting from the direct excitation of different classes of HIRs (Scheme 1.1). In general, the main advantage of the direct excitation approach is additional control over reactivity compared to purely outer sphere radical species formation. Another benefit is operational simplicity, as these reactions typically do not require any additional photo- or metal catalyst.

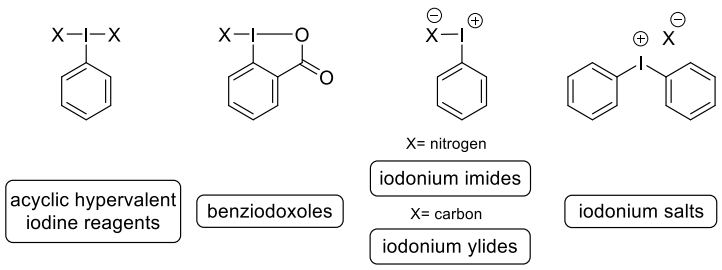

Scheme 1.1: Different structural classes of hypervalent iodine(III) reagents (HIRs) which are covered in this review.

We will not cover numerous examples of light-induced reactions in which photocatalysts are used in combination with iodine(III) reagents as these have been a subject of other recent reviews.[9]. Similarly, we will not describe examples of reactions requiring the addition of a catalytic amount of molecular iodine (I_2), which rely on the direct excitation of iodine intermediates in lower (I) oxidation state. Such examples have been reviewed by Muñiz in a book chapter.[10] Some individual examples from our review have been covered in reviews about homolysis[11] and direct photoexcitation strategy.[12]

1.2 Reactions of different types of reagents

1.2.1 Reactions of acyclic hypervalent iodine(III) reagents

Radical addition to nitrogen containing heterocycles

Radical additions of nucleophilic radicals to electron-poor nitrogen heterocycles were the first reactions performed by direct excitation of hypervalent iodine reagents (Scheme 1.2). Irradiation of simple acyclic hypervalent iodine reagents with carboxylate ligands leads to homolytic I–O bond cleavage followed by decarboxylation of the carboxyl radical, resulting in a corresponding nucleophilic alkyl radical. These radicals can add to the electron-poor protonated nitrogen heterocycles.[13] In this process, aromaticity breaks, and a second oxidation event is required to restore the aromaticity of the nitrogen heterocycle. This can happen by oxidation with intermediate A or by another molecule of HIR (radical chain process). Overall such coupling is an oxidative process involving a transfer of two electrons (decarboxylation and rearomatization).[14]

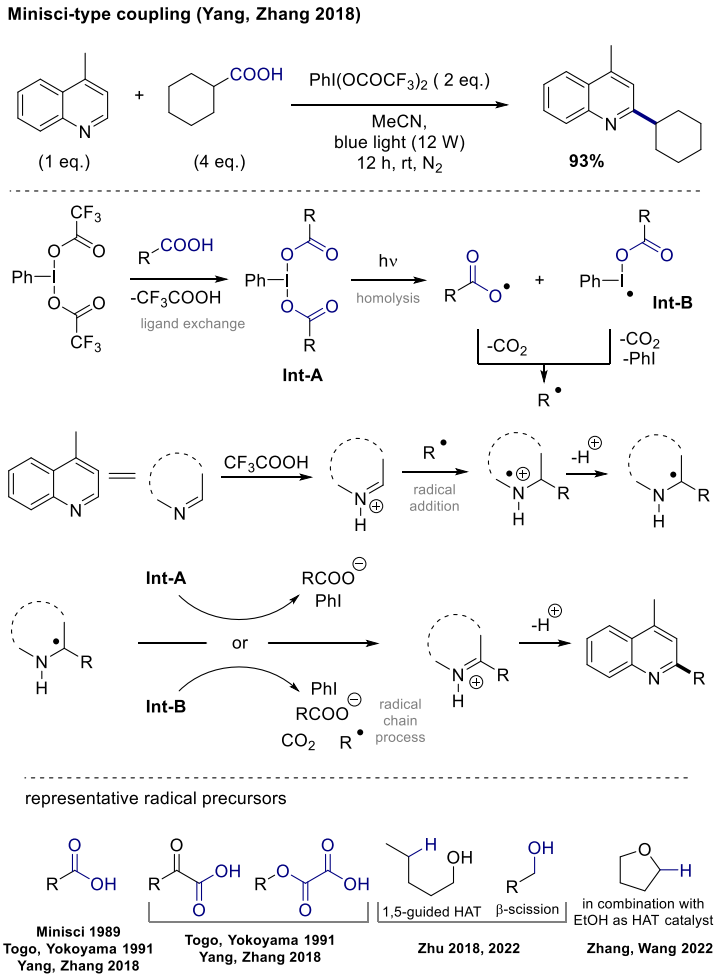

Scheme 1.2: Examples of Minisci-type coupling with different radical precursors.

In 1989 Minisci used phenyliodine diacetate and different carboxylic acids as radical precursors under low-pressure mercury lamp irradiation (254 nm) to perform radical additions to electron-poor protonated pyridine and quinoline derivatives.[7a] These conditions were an improvement of previously reported harsh thermal conditions requiring silver salts in combination with persulfate oxidant and strong acids.[13] Later, Togo and Yokoyama used similar reaction

conditions and expanded the scope of viable radical precursors from carboxylic acids also to α-keto carboxylic acids generating acyl radicals, and oxalate monoesters.[15] The latter are prepared in a simple reaction from the corresponding alcohol substrate, and as such allow utilization of very abundant alcohol substrates as radical precursors. In 2018, Yang and Zhang improved the reaction conditions by using 400 nm LEDs with previously established radical precursors.[16] Apart from carboxyl radicals, also other oxygen-centered radicals can be generated in I-O bond homolysis. Zhu designed a system in which alkoxy radicals abstract a hydrogen atom from the aliphatic chain in a 1,5-guided fashion.[17] The formed alkyl radicals undergo Minisci coupling reaction similarly as described in previous examples. Later, the authors reported an adaptation of the system in which iodobenzene has been used in a catalytic fashion enabled by the addition of a stoichiometric amount of *m*-CPBA as oxidizing agent.[18] Recently, Zhang and Wang reported a system in which ethanol was used as a HAT catalyst allowing functionalization of C(sp^3)-H bonds in different substrates.[19]

Marouka expanded the scope of nitrogen heterocycles to more electron-rich heterocycles in a similar class of radical addition reactions to aromatic systems (Scheme 1.3A).[20] They used a hypervalent iodine reagent (HIR 1) prepared from inexpensive difluoroacetic acid and *para*-substituted iodobenzene. Under irradiation with 400 nm LEDs I-O bond homolysis, followed by decarboxylation lead to formation of difluoromethyl radicals. These radicals are more electrophilic and, as such, more likely to add to electron-rich systems.[21] This allowed functionalization of pyridine derivatives with electron-donating groups and other nitrogen heterocycles such as caffeine. Importantly, the protonation of nitrogen heterocycle is not required due to the different philicity of the fluoroalkyl radicals.

Recently, Prakash reported a similar system (Scheme 1.3B) in which chlorodifluoromethyl radicals are reacted with different nitrogen heterocycles.[22] In this case the hypervalent iodine reagent was prepared *in situ* from the corresponding carboxylic acid and HIR-2. Interestingly, the yield of some substrates is significantly higher upon the addition of a catalytic amount of 1,3,5-trimethoxybenzene. The authors rationalize this observation by a mechanistic proposal, in which an excitation of the EDA complex between HIR and 1,3,5-trimethoxybenzene operates as a parallel productive pathway.

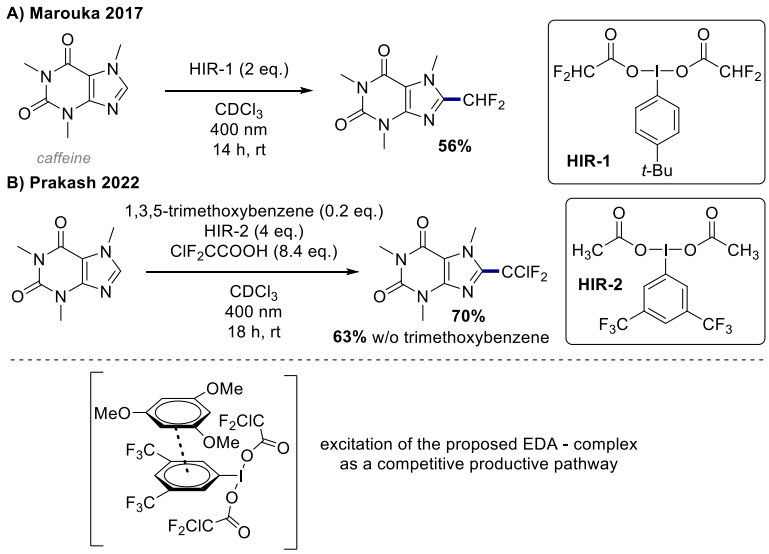

Scheme 1.3: Transformations based on radical addition of electrophilic fluoroalkyl radicals to nitrogen heterocycles.

Radical addition to alkenes and alkynes

In 1993 Togo and Yokoyama reported examples of nucleophilic radical addition to electron-poor alkenes (Scheme 1.4A).[23] Similarly, as in their previous studies of Minisci coupling, they used a mercury lamp to generate alkyl radicals from the corresponding carboxylic acids. In this reaction, the addition of a hydrogen atom donor (1,4-cyclohexadiene) is required to obtain the desired saturated product after the radical addition to the double bond.[24] In 2022 Li performed a similar radical addition with fluoroalkyl radicals and THF as a hydrogen donor under blue LEDs irradiation (Scheme 1.4B).[25] The reaction gives easy access to valuable fluorinated products from the substrates with unactivated terminal double bonds. Liu, Zhou, and Lu developed a different hydrodifluoroalkylation reagent which enabled them to functionalize different unactivated alkenes and also alkynes (Scheme 1.4C).[26] Recently, the same group also developed an elegant multicomponent reaction system (Scheme 1.4D) in which fluoroalkyl radicals first add to the double bond of a styrene derivative, and the newly formed benzylic radical then adds to an electron-poor nitrogen heterocycle.[27] The developed multicomponent system requires two additional equivalents of a HIR-based oxidant (PIFA).

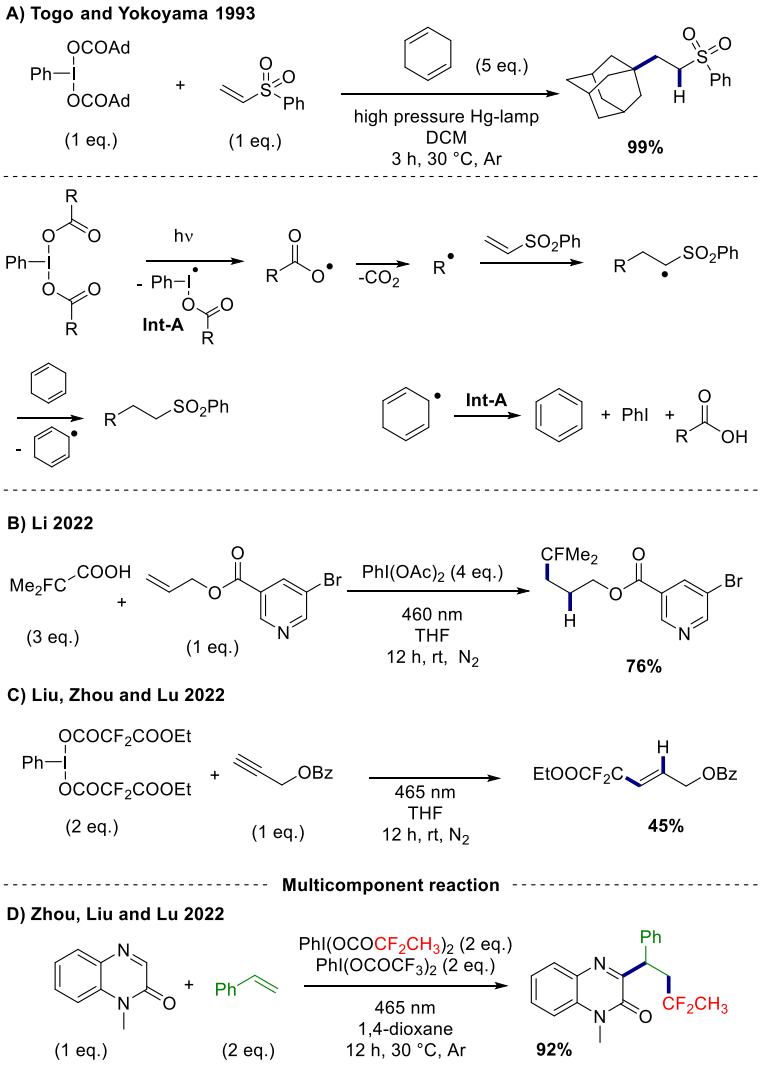

Scheme 1.4: Decarboxylation followed by addition of corresponding radicals to multiple bonds (A-C) and an example of multicomponent reaction (D). Ad = adamantly.

Iodine bond homolysis is not limited to the generation of oxygen radicals, it works well also with other atoms. In 2020 the Bolm group reported a reaction system in which HIRs with sulfoximidoyl ligands were irradiated under blue LEDs to release the corresponding electrophilic sulfoximidoyl radicals (Scheme 1.5).[28] These nitrogen-centered radicals reacted first with terminal alkynes, and the corresponding radical intermediates then formed *N*-α-ketoacylated sulfoximines upon reaction with oxygen.

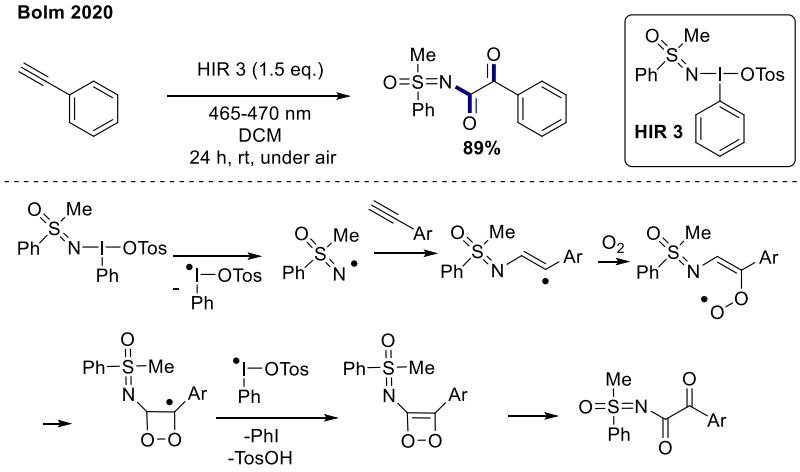

Scheme 1.5: Sulfoximination of alkynes.

Decarboxylative bromination

Recently, Miyamoto and Uchiyama reported a method for decarboxylative bromination of different aliphatic carboxylic acids (Scheme 1.6).[29] It allowed them to use readily available carboxylic acids for the preparation of different alkyl bromides using inexpensive and safe KBr as a bromide source. The application of the method was demonstrated on a variety of sterically bulky and strained alkyl substrates. Authors hypothesized that the iodine-bromine bond of *in situ* formed HIR intermediate is prone to undergo homolysis, leading to radical decomposition of the formed reagent. The decomposition results in alkyl and bromine radicals, with a possibility of a radical chain process to the desired brominated product.

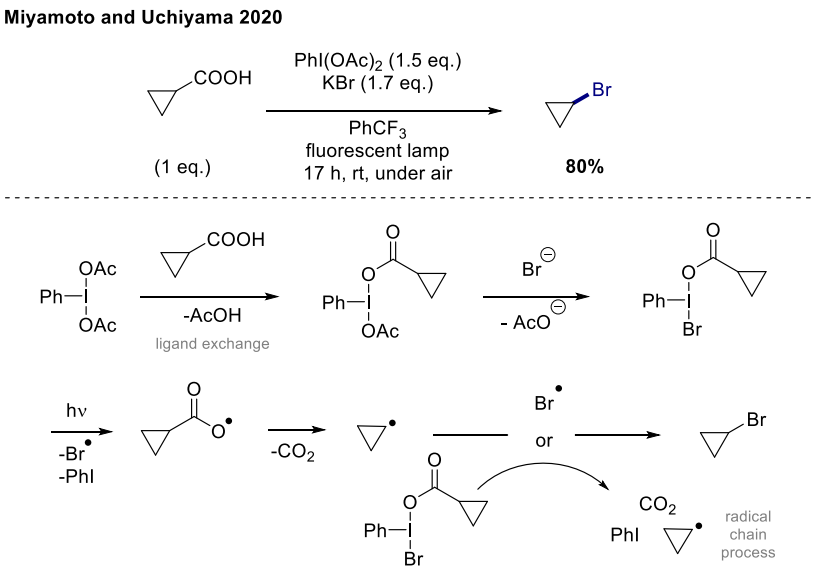

Scheme 1.6: Decarboxylative bromination of carboxylic acids.

Oxidation of radicals to carbocations – Ritter amination

Complexes of hypervalent iodine(III) and BF_3 are known for their enhanced oxidation properties.[30] The complexation of HIRs with aliphatic carboxylic acids as ligands also redshifts the absorption by almost 100 nm giving these complexes a slightly yellowish appearance. We developed a system in which such complexes are formed *in situ* from iodobenzene, Selectfluor as oxidant, carboxylic acid as a ligand, and Lewis acid BF_3.[31] The excitation of these complexes leads to the decarboxylative formation of a radical, which is rapidly oxidized to a carbocation. These were reacted with wet acetonitrile to give Ritter amination products (Scheme 1.7A). The strategy is unique as it can be applied to substrates which are considered challenging, e.g., aliphatic and benzylic positions with electron-withdrawing substituents. A similar reactivity was also observed by the Waser group in their report of intramolecular cyclisation of dipeptide derivatives.[32] However, for their substrates light input was not required.

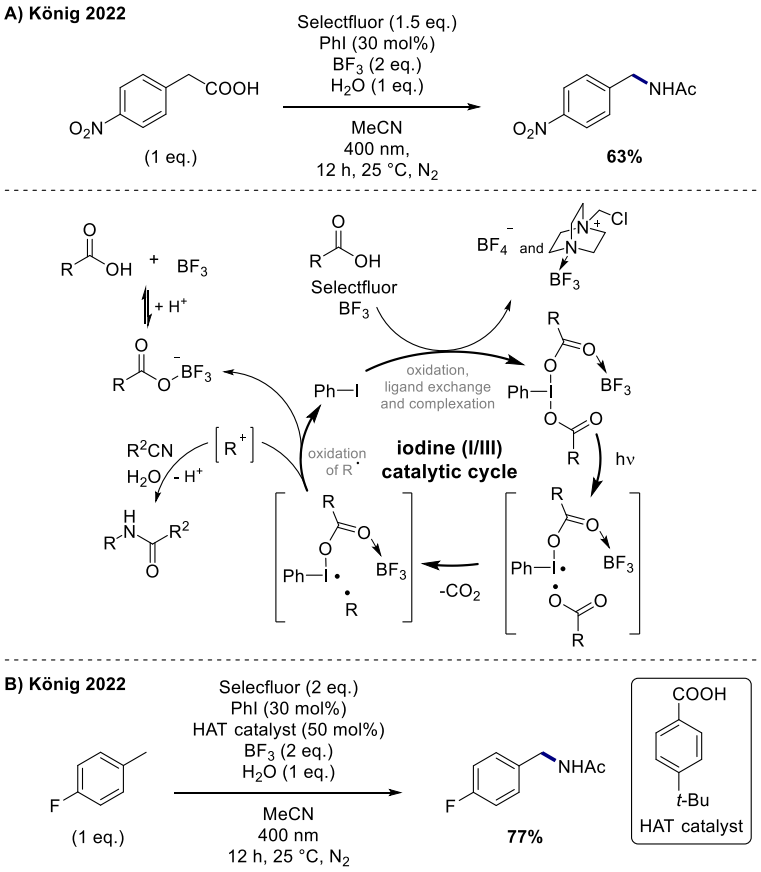

Scheme 1.7: Oxidation of radicals to carbocations by HIR-BF_3 complexes from carboxylic acids (A) or from C-H precursors (B).

We expanded our method also to the functionalization of benzylic C(sp^3)-H bonds in toluene derivatives (Scheme 1.7B). This reaction was enabled by carboxylate ligands that do not undergo decarboxylation, but instead serve as hydrogen abstracting agents.[33]

1.2.2 Reactions of cyclic hypervalent iodine(III) reagents

Decarboxylative couplings with alkenes and alkynes

In 2015 Li and Wang reported an example of decarboxylative alkynylation of α-keto acids with bromoacetylene derivatives enabled by cyclic HIR under sunlight irradiation (Scheme 1.8).[34] The reaction works well with aliphatic and aromatic derivatives of both α-keto acids and bromoacetylene derivatives. Importantly, only a catalytic amount of 1-hydroxy-3-oxobenziodoxole (BI-OH) is required. Under the reaction conditions the -OH group of BI-OH first undergoes ligand exchange with the carboxyl group of the substrate α-keto carboxylic acid. Visible light excitation of the formed intermediate triggers decarboxylation generating benzoyl radicals and an iodanyl radical fragment (BI•). In this radical process the iodanyl radical BI• is reoxidized back by either acetylene bromide or bromine radical (catalytic cycles I and II, respectively). In the first case (cycle I), a PhEBX reagent is formed, which acts as a radical trap for previously formed benzoyl radicals. After the radical addition the desired product is formed together with an iodanyl radical BI•. The latter is reoxidized by bromide radicals to form BI-Br (cycle II) that undergoes hydrolysis to a BI-OH intermediate, which perpetuates the catalytic cycles.

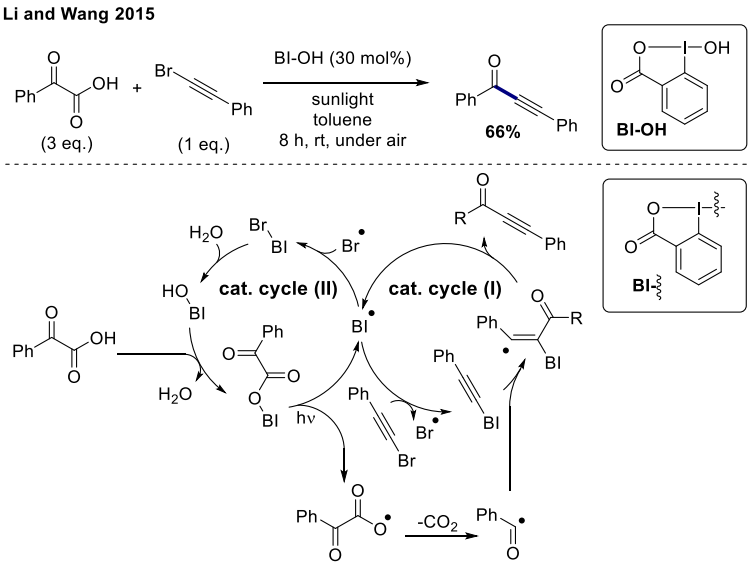

Scheme 1.8: Practical decarboxylative alkynylation with BI-OH as a catalyst.

Soon after, the group of Wang reported two more examples of reactions relying on the excitation of benziodoxole derivatives (Scheme 1.9).[35] In both cases, light promotes the decarboxylative radical formation and radical addition to an alkene or alkyne followed by an intermolecular radical cyclisation with a tethered phenyl moiety. The iodanyl radical BI• abstracts hydrogen from the dearomatized ring allowing its rearomatization along with the formation of BI-H. The role of BI-H is very interesting, because it allows hydrogen gas (H_2) evolution upon reaction with a substrate, α-keto carboxylic acid. In such a way a carboxy group substituted benziodoxole derivative is formed again, and the catalytic cycle can continue upon another light excitation.

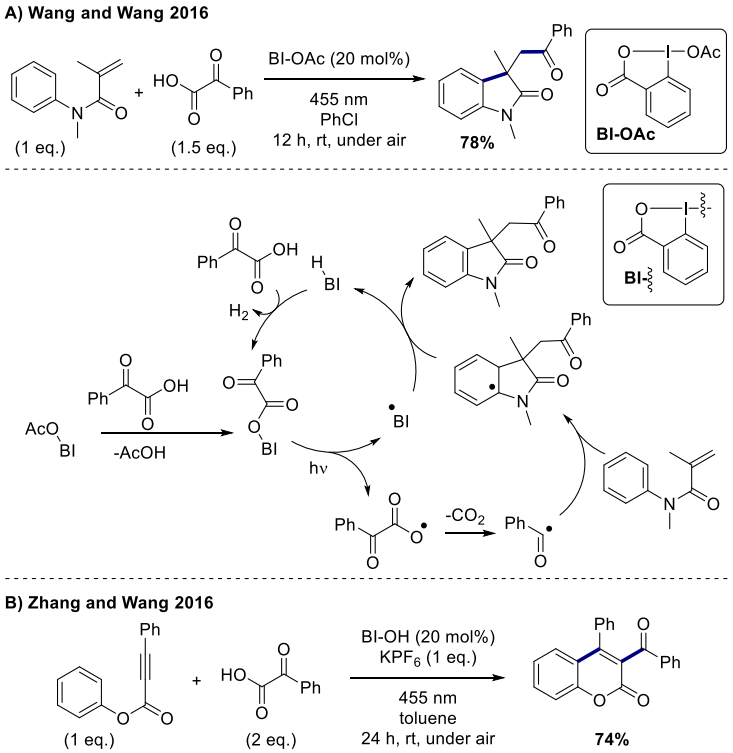

Scheme 1.9: Dehydrogenative intermolecular cyclization reactions of alkenes (A) and alkynes (B) with hydrogen gas evolution.

EBX derivatives as excited state oxidants

Ethynylbenziodoxolones (EBXs) are commonly used as radical traps in photocatalytic alkynylations. Recently, the Waser group reported an unexpected discovery about these reagents acting as excited state oxidants upon irradiation with higher intensity 440 nm light source.[36] The finding is mechanistically interesting and has practical value as it simplifies the reaction system which otherwise requires the addition of a photocatalyst (Scheme 1.10A). In their report of decarboxylative alkynylation of oxalate ester it was shown that the reaction proceeds similarly well in conditions with- and without an external photocatalyst. Moreover, by performing many different types of reactions, they demonstrated that excited EBXs are quite a general reaction platform. Examples of decarboxylative and deboronative alkynylations, oxyalkynylation of enamides, deaminative alkynylation via an aryl imine and C-H alkynylation of THF all proceed in good yields. In these reactions, the main observed side product was dyne which also forms upon excitation of EBX without any reactants.

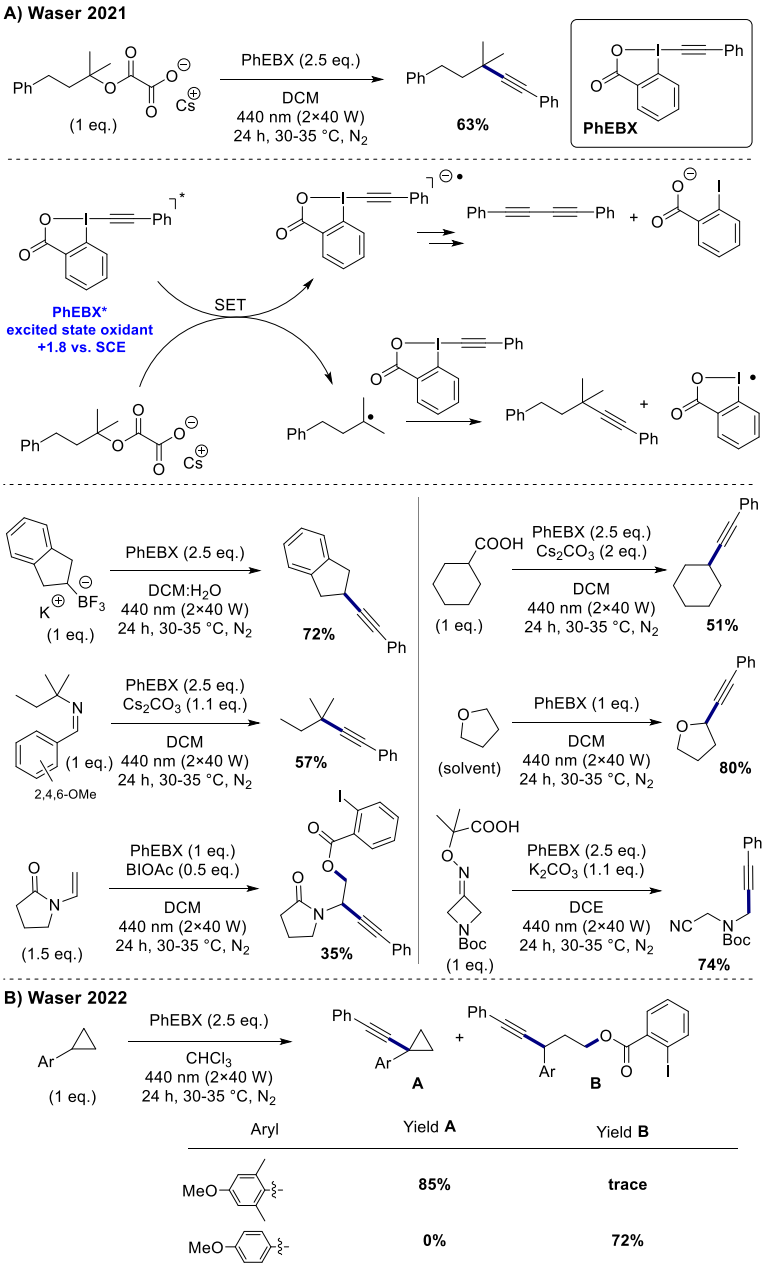

Scheme 1.10: Ethylene benziodoxoles (EBXs) as excited state oxidant in different transformations (A and B).

Recently, Waser et al. extended the repertoire of reactions based on direct excitation of EBX to C–H alkynylation of arylcyclopropanes (Scheme 1.10B).[37] The aryl group was found to have an important effect on the reaction outcome. The ortho substituents of the aryl group steer the reaction towards C–H alkynylation, and in the absence of ortho substituents oxyalkynylation of the C–C bond product prevails. The latter was also performed on aminocyclopropanes and styrene derivatives.

1.2.3 Reactions of iodonium imides

Iodonium imides are commonly used in organic synthesis in combination with metal catalysts as precursors of nitrenes in aziridations of alkenes and amination reactions of various organic substrates.[38]

In 2017 Takemoto reported a series of iodonium imides with a methoxymethyl group in the ortho position of the phenyl ring.[39] The substitution improved the solubility of these reagents in organic solvents. Moreover, the authors hypothesized that ortho substitution would stabilize the molecule upon excitation and prevent the generation of free nitrene intermediate, which may cause undesired side reactions. Indeed, under 370 nm irradiation, additive-free amination of silyl enol ethers was achieved in very good yields (Scheme 1.11A). The mechanism is not well understood, however, the absence of the side products, which would stem from a reaction with the reaction solvent (acetonitrile), hints that free nitrenes are not involved. Soon after, Takemoto reported a new series of iodonium imides and tested them in the aziridation of styrenes.[40] Ortho-nitrosubstituted (HIR 5) derivative showed the best performance in this reaction, giving 73% yield (Scheme 1.11B). Reaction with substituted alkenes gave an additional insight into the reaction mechanism. From the ratios of syn/anti substituted aziridine products, it was concluded that the reaction proceeds via stepwise rather than concerted mechanism.

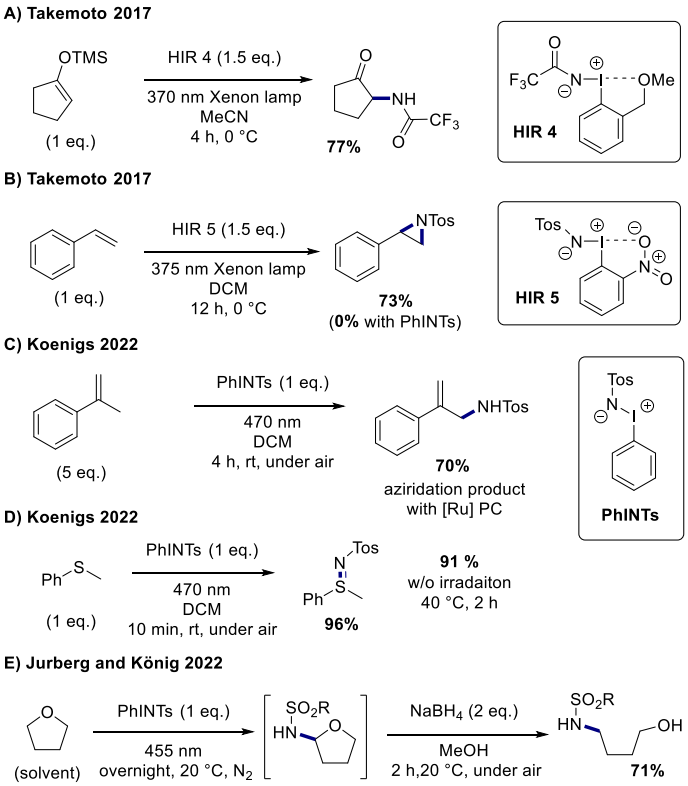

Scheme 1.11: Reactions of iodonium imides with different substrates.

Recently, Koenigs group reported a study in which they irradiated simple PhINTs under blue LEDs in the presence of different alkenes (Scheme 1.11C).[41] Depending on the substrate, they observed two different reactions, either C-H amination or aziridation. The authors show an interesting example of α-methyl styrene giving different products when PhINTs was directly excited (C-H amination) and when it was sensitized with a ruthenium dye (aziridation). The difference in reactivity was explained by formation of triplet nitrene upon direct excitation and formation of nitrene radical anion in the presence of the photosensitizer.

Soon after Koenigs reported a reaction of nitrenes with sulfides resulting in sulfinimies (Scheme 1.11D).[42] The reaction gives high yields in very short reaction time (10 min) under blue LEDs irradiation and, interestingly, works similarly well also at slightly elevated temperatures and longer reactions times. The authors conclude that there are two mechanisms operating. Under direct excitation, singlet nitrenes are liberated and react rapidly with the sulfide substrate. The other possibility is a thermal process, a formal metathesis reaction that has a higher activation barrier and proceeds only slowly at room temperature.

Lately, Jurberg and König reported a two-step protocol allowing the C(sp^3)-H amination of cyclic ethers with iodonium imides, followed by the reduction of the resulting intermediate (Scheme 1.11E).[43] The amino alcohol products have been obtained in good yields under photochemical or thermal conditions. In many examples it was found that light has a beneficial effect on the reaction yield. Spectroscopic measurements have shown that both, singlet and triplet nitrene intermediates are present and possibly interconverting under photochemical reaction conditions. Equilibrium between the two species was found to be solvent dependent.

1.2.4 Reactions of iodonium ylides

Iodonium ylides are used in organic synthesis as precursors of carbenes for the cyclopropanation of alkenes and in the preparation of heterocyclic compounds. Older examples of their photochemical reactivity under harsh UV irradiation have already been summarized in a review from 2016 by Yusubov and Zhdankin.[44] Therefore, we will focus our discussion on the newer examples performed under milder visible light irradiation.

In 2019 Quideau, Hopkins and Murphy reported a method based on direct excitation of β-dicarbonyl-derived iodonium ylides in the presence of different alkenes (Scheme 1.12A).[45] Under blue LEDs irradiation, cyclopropane derivatives are formed in very high yields. The authors performed a detailed computation study to explain a good chemoselectivity of the reaction. The study revealed that reactivity comes exclusively from HOMO-LUMO excitation without free carbenes generation. The excited species can be either a iodonium ylide or the EDA complex between iodonium ylide and styrene.

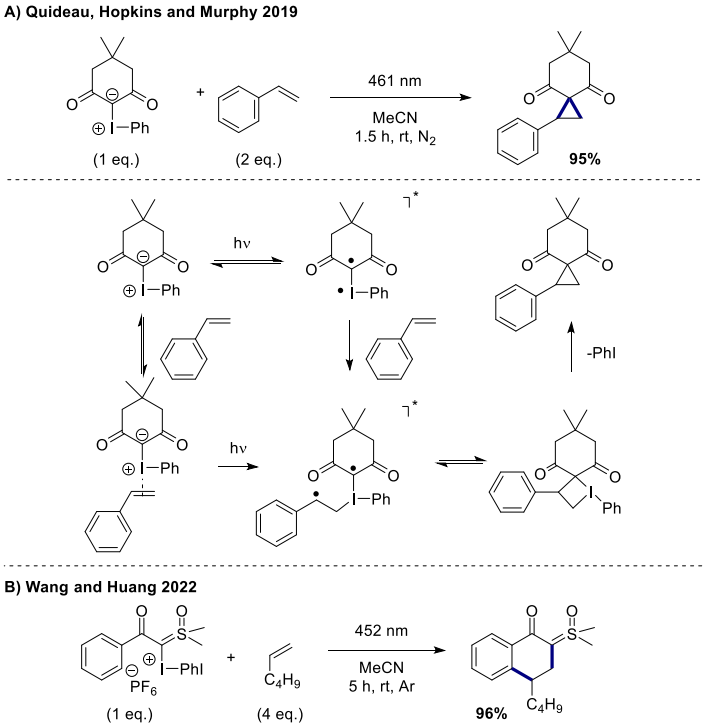

Scheme 1.12: Reactions of iodonium ylides.

Recently, Wang and Huang designed and prepared a series of mixed I, S-ylides and used them in photocycloaddition reactions with different unsaturated systems (Scheme 1.12B).[46] Alkenes, alkynes, nitriles, and allenes have been used to prepare a broad range of sulfoxonium-containing cyclic structures under 452 nm irradiation in moderate to excellent yields. The authors speculate that different mechanism operate depending on the type of the unsaturated system, but exact mechanistic details remain unclear.

Sen reported a system in which different pyrrole and indole derivatives are functionalized with iodonium ylides under blue LEDs irradiation (Scheme 1.13A).[47] In their mechanism they propose an excitation of the EDA complexes between substrates and iodonium ylides, similarly as mentioned in the earlier report by Murphy and coworkers.[45]

Lately, Li and Xuan reported a method for the synthesis of biologically relevant indolines through the cyclization of tertiary aryl amines with iodonium ylides (Scheme 1.13B) under blue LEDs. In their mechanistic studies, they conducted UV-Vis measurements which clearly indicate the redshift in absorption when reactants are mixed. This strongly supports the formation and excitation of the EDA complexes under reaction conditions.

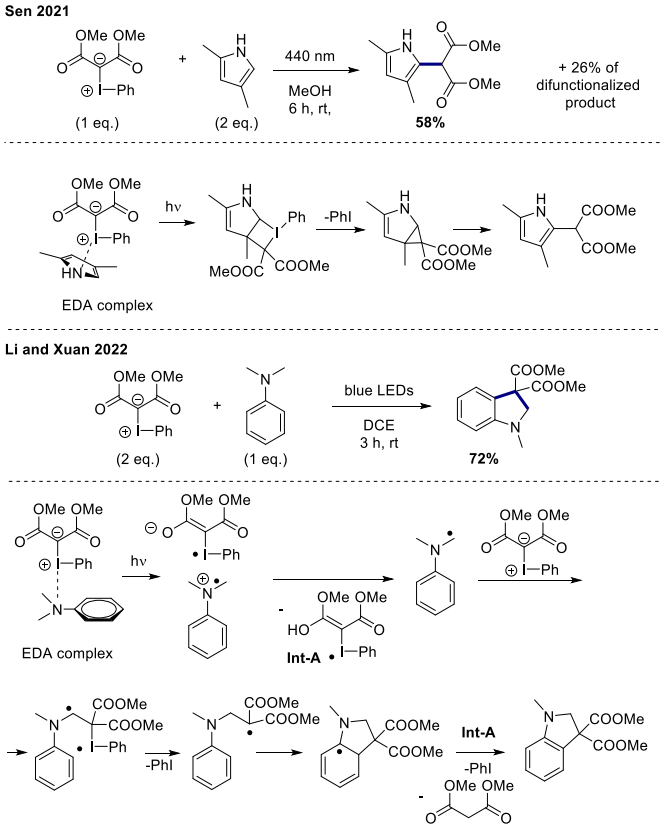

Scheme 1.13: Excitation of EDA complexes of iodonium ylides.

1.2.5 Reactions of iodonium salts

Direct excitation of phenyl iodonium salts leads to a variety of different products Involving phenyl radicals, cation radicals and cations. The photochemical properties of the iodonium salts have been mainly exploited in cationic polymerizations as they can produce very strong protic acids upon photolysis (photoacids).[48]

In 2013 Tobisu and Chatani showed that iodonium salts and electron-rich *N*-methylpyrrole form EDA complexes when mixed.[49] The irradiation of these complexes under white LEDs triggers an electron transfer, which leads to their coupling product (Scheme 1.14).

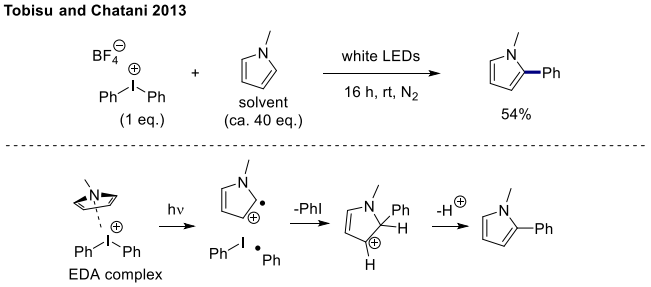

Scheme 1.14: EDA complexes with iodonium salts.

Iodonium salts are charged and, as such, can undergo specific ion-pairing interactions with counterions, e.g., phosphoric acids. Toste reported an interesting system (Scheme 1.15) using an insoluble iodonium salt precursor, which, combined with a chiral phosphoric acid, acts as a phase transfer catalyst and forms a soluble ion pair.[50] Impressively, by the optimization of aryl substituents of the iodonium salt and substituents of chiral phosphoric acid

derivatives, they managed to tune the regio- and diastereoselectivity of the hydrogen abstraction and also the selectivity of addition of the alcohol (cis or trans). Using different enantiomers of phosphoric acids (R or S), they obtain either cis or trans isomers of the functionalized THF derivative. The authors propose two different paths leading to the product.

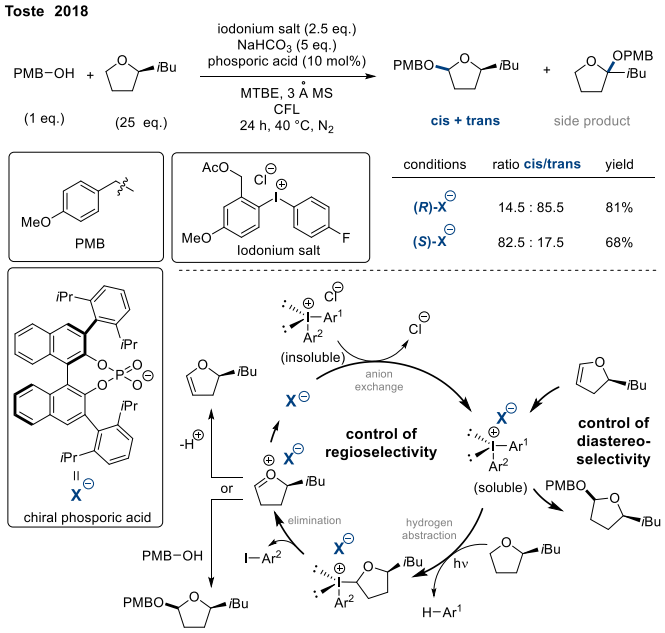

Scheme 1.15: Regio- and diastereoselective functionalization of THF derivatives.

1.3 Conclusion

In summary, we presented synthetic examples of the reactivity of five different classes of hypervalent iodine reagents upon their excitation. The observed reactivity patterns are mechanistically very diverse, and we think that more of them will be discovered in the near future. The new reactivity classes may emerge from entirely new iodine complexes or from exploiting weak interactions between iodine complexes and substrates. In any case, we hope the review will inspire and accelerate future developments in the broader hypervalent iodine and photochemical community.

1.4 References

1. (a) Yoshimura, A.; Zhdankin, V. V., Advances in Synthetic Applications of Hypervalent Iodine Compounds. *Chem. Rev.* **2016,** *116* (5), 3328-3435; (b) Zhdankin, V. V.; Stang, P. J., Chemistry of Polyvalent Iodine. *Chem. Rev.* **2008,** *108* (12), 5299-5358.
2. (a) Frey, B.; Maity, A.; Tan, H.; Roychowdhury, P.; Powers, D. C., Sustainable Methods in Hypervalent Iodine Chemistry. In *Iodine Catalysis in Organic Synthesis*, 2022; pp 335-386; (b) Yusubov, M. S.; Zhdankin, V. V., Iodine catalysis: A green alternative to transition metals in organic chemistry and technology. *Resource-Efficient Technologies* **2015,** *1* (1), 49-67; (c) Ishihara, K., Concepts in Iodine Catalysis. In *Iodine Catalysis in Organic Synthesis*, 2022; pp 11-26.
3. (a) Ghosh, M. K.; Rajkiewicz, A. A.; Kalek, M., Organocatalytic Group Transfer Reactions with Hypervalent Iodine- Reagents. *Synthesis* **2019,** *51* (02), 359-370; (b) Brand, J. P.; González, D. F.; Nicolai, S.; Waser, J., Benziodoxole-based hypervalent iodine reagents for atom-transfer reactions. *Chem. Commun.* **2011,** *47* (1), 102-115.
4. (a) Francke, R., Recent progress in the electrochemistry of hypervalent iodine compounds. *Current Opinion in Electrochemistry* **2021,** *28*, 100719; (b) Francke, R., Electrogenerated hypervalent iodine compounds as mediators in organic synthesis. *Current Opinion in Electrochemistry* **2019,** *15*, 83-88.
5. (a) Dong, D.-Q.; Hao, S.-H.; Wang, Z.-L.; Chen, C., Hypervalent iodine: a powerful electrophile for asymmetric α-functionalization of carbonyl compounds. *Org. Biomol. Chem.* **2014,** *12* (25), 4278-4289; (b) Boelke, A.; Nachtsheim, B. J., Design of Chiral Organoiodine(I/ III) Catalysts for Asymmetric Oxidative Transformations. In *Iodine Catalysis in Organic Synthesis*, 2022; pp 185-209; (c) Singh, F. V.; Shetgaonkar, S. E.; Krishnan, M.; Wirth, T., Progress in organocatalysis with hypervalent iodine catalysts. *Chem. Soc. Rev.* **2022,** *51* (18), 8102-8139.
6. Wang, X.; Studer, A., Iodine(III) Reagents in Radical Chemistry. *Acc. Chem. Res.* **2017,** *50* (7), 1712-1724.
7. (a) Minisci, F.; Vismara, E.; Fontana, F.; Claudia Nogueira Barbosa, M., A new general method of homolytic alkylation of protonated heteroaromatic bases by carboxylic acids and iodosobenzene diacetate. *Tetrahedron Lett.* **1989,** *30* (34), 4569-4572; (b) Dektar, J. L.; Hacker, N. P., Photochemistry of diaryliodonium salts. *J. Org. Chem.* **1990,** *55* (2), 639-647.
8. Nakajima, M.; Nagasawa, S.; Matsumoto, K.; Kuribara, T.; Muranaka, A.; Uchiyama, M.; Nemoto, T., A Direct $S_0 \rightarrow T_n$ Transition in the Photoreaction of Heavy-Atom-Containing Molecules. *Angew. Chem. Int. Ed.* **2020,** *59* (17), 6847-6852.
9. (a) Jia, K.; Chen, Y., Photochemistry of Hypervalent Iodine Compounds. In *PATAI'S Chemistry of Functional Groups*, 2018; pp 1-42; (b) Wang, L.; Liu, J., Synthetic Applications of Hypervalent Iodine(III) Reagents Enabled by Visible Light Photoredox Catalysis. *Eur. J. Org. Chem.* **2016,** *2016* (10), 1813-1824; (c) Singh, F. V.; Wirth, T., Hypervalent iodine chemistry and light: photochemical reactions involving hypervalent iodine chemistry. *ARKIVOC* **2021,** *2021* (7), 12-47.
10. Bosnidou, A. E.; Romero, R. M., Catalytic Transformations Based on Iodine(I) Involving Radical Pathways. In *Iodine Catalysis in Organic Synthesis*, 2022; pp 121-149.
11. Protti, S.; Ravelli, D.; Fagnoni, M., Designing radical chemistry by visible light-promoted homolysis. *Trends Chem.* **2022,** *4* (4), 305-317.
12. Sumida, Y.; Ohmiya, H., Direct excitation strategy for radical generation in organic synthesis. *Chem. Soc. Rev.* **2021,** *50* (11), 6320-6332.
13. Proctor, R. S. J.; Phipps, R. J., Recent Advances in Minisci-Type Reactions. *Angew. Chem. Int. Ed.* **2019,** *58* (39), 13666-13699.
14. Reed, N. L.; Yoon, T. P., Oxidase reactions in photoredox catalysis. *Chem. Soc. Rev.* **2021,** *50* (5), 2954-2967.
15. (a) Togo, H.; Aoki, M.; Kuramochi, T.; Yokoyama, M., Radical decarboxylative alkylation onto heteroaromatic bases with trivalent iodine compounds. *J. Chem. Soc., Perkin trans. 1* **1993,** (20), 2417-2427; (b)

Togo, H.; Aoki, M.; Yokoyama, M., Alkylation of Aromatic Heterocycles with Oxalic Acid Monoalkyl Esters in the Presence of Trivalent Iodine Compounds. *Chem. Lett.* **1991,** *20* (10), 1691-1694.

16. Zhang, X.-Y.; Weng, W.-Z.; Liang, H.; Yang, H.; Zhang, B., Visible-Light-Initiated, Photocatalyst-Free Decarboxylative Coupling of Carboxylic Acids with N-Heterocycles. *Org. Lett.* **2018,** *20* (15), 4686-4690.

17. Wu, X.; Zhang, H.; Tang, N.; Wu, Z.; Wang, D.; Ji, M.; Xu, Y.; Wang, M.; Zhu, C., Metal-free alcohol-directed regioselective heteroarylation of remote unactivated C(sp3)–H bonds. *Nat. Commun.* **2018,** *9* (1), 3343.

18. Cao, Z.; Wang, X.; Wu, X.; Zhu, C., Iodobenzene-catalyzed photochemical heteroarylation of alcohols by rupture of inert C–H and C–C bonds. *Tetrahedron Chem* **2022,** *4*, 100031.

19. Li, X.; Liu, C.; Guo, S.; Wang, W.; Zhang, Y., PIFA-Mediated Cross-Dehydrogenative Coupling of N-Heteroarenes with Cyclic Ethers: Ethanol as an Efficient Promoter. *Eur. J. Org. Chem.* **2021,** *2021* (3), 411-421.

20. Sakamoto, R.; Kashiwagi, H.; Maruoka, K., The Direct C–H Difluoromethylation of Heteroarenes Based on the Photolysis of Hypervalent Iodine(III) Reagents That Contain Difluoroacetoxy Ligands. *Org. Lett.* **2017,** *19* (19), 5126-5129.

21. Parsaee, F.; Senarathna, M. C.; Kannangara, P. B.; Alexander, S. N.; Arche, P. D. E.; Welin, E. R., Radical philicity and its role in selective organic transformations. *Nat. Rev. Chem.* **2021,** *5* (7), 486-499.

22. Lin, D.; Krishnamurti, V.; Prakash, G. K. S., Visible Light-Mediated Metal-Free Chlorodifluoromethylation of Arenes and Heteroarenes by a Hypervalent Iodine EDA Complex. *Eur. J. Org. Chem.* **2022,** *2022* (35), e202200607.

23. (a) Togo, H.; Aoki, M.; Yokoyama, M., Reductive addition to electron-deficient olefins with trivalent iodine compounds. *Tetrahedron* **1993,** *49* (36), 8241-8256; (b) Togo, H.; Taguchi, R.; Yamaguchi, K.; Yokoyama, M., Reactivity of [bis(1-adamantylcarbonyloxy)iodo]arenes in substitution and addition reactions. *J. Chem. Soc., Perkin trans. 1* **1995,** (17), 2135-2139.

24. Kitcatt, D. M.; Nicolle, S.; Lee, A.-L., Direct decarboxylative Giese reactions. *Chem. Soc. Rev.* **2022,** *51* (4), 1415-1453.

25. Guo, C.; Han, X.; Feng, Y.; Liu, Z.; Li, Y.; Liu, H.; Zhang, L.; Dong, Y.; Li, X., Straightforward Synthesis of Alkyl Fluorides via Visible-Light-Induced Hydromono- and Difluoroalkylations of Alkenes with α-Fluoro Carboxylic Acids. *J. Org. Chem.* **2022,** *87* (14), 9232-9241.

26. Liu, R.; Zhou, N.; Zhao, T.; Zhang, Y.; Wang, K.; Zhao, X.; Lu, K., Visible-Light-Induced Difluoroalkylation of Alkenes and Alkynes with Fluoro-Containing Hypervalent Iodane (III) Reagents Under Photo-Catalyst-Free Conditions. *J. Org. Chem.* **2022.**

27. Zhou, N.; Liu, R.; Zhang, C.; Wang, K.; Feng, J.; Zhao, X.; Lu, K., Photoinduced Three-Component Difluoroalkylation of Quinoxalinones with Alkenes via Difluoroiodane(III) Reagents. *Org. Lett.* **2022,** *24* (19), 3576-3581.

28. Wang, C.; Ma, D.; Tu, Y.; Bolm, C., Use of Hypervalent Iodine Reagents in Visible Light-Promoted α-Ketoacylations of Sulfoximines with Aryl Alkynes. *Org. Lett.* **2020,** *22* (22), 8937-8940.

29. Watanabe, A.; Koyamada, K.; Miyamoto, K.; Kanazawa, J.; Uchiyama, M., Decarboxylative Bromination of Sterically Hindered Carboxylic Acids with Hypervalent Iodine(III) Reagents. *Org. Process Res. Dev.* **2020,** *24* (7), 1328-1334.

30. (a) Dasgupta, A.; Thiehoff, C.; Newman, P. D.; Wirth, T.; Melen, R. L., Reactions promoted by hypervalent iodine reagents and boron Lewis acids. *Org. Biomol. Chem.* **2021,** *19* (22), 4852-4865; (b) Izquierdo, S.; Essafi, S.; del Rosal, I.; Vidossich, P.; Pleixats, R.; Vallribera, A.; Ujaque, G.; Lledós, A.; Shafir, A., Acid Activation in Phenyliodine Dicarboxylates: Direct Observation, Structures, and Implications. *J. Am. Chem. Soc.* **2016,** *138* (39), 12747-12750.

31. Narobe, R.; Murugesan, K.; Schmid, S.; König, B., Decarboxylative Ritter-Type Amination by Cooperative Iodine (I/III)—Boron Lewis Acid Catalysis. *ACS Catal.* **2022,** *12* (1), 809-817.

32. Robert, E. G. L.; Le Du, E.; Waser, J., Synthesis of polycyclic aminal heterocycles via decarboxylative cyclisation of dipeptide derivatives. *Chem. Commun.* **2022,** *58* (21), 3473-3476.

33. Narobe, R.; Murugesan, K.; Haag, C.; Schirmer, T. E.; König, B., C(sp^3)–H Ritter amination by excitation of in situ generated iodine(III)–BF_3 complexes. *Chem. Commun.* **2022,** *58* (63), 8778-8781.
34. Tan, H.; Li, H.; Ji, W.; Wang, L., Sunlight-Driven Decarboxylative Alkynylation of α-Keto Acids with Bromoacetylenes by Hypervalent Iodine Reagent Catalysis: A Facile Approach to Ynones. *Angew. Chem. Int. Ed.* **2015,** *54* (29), 8374-8377.
35. (a) Yang, S.; Tan, H.; Ji, W.; Zhang, X.; Li, P.; Wang, L., Visible Light-Induced Decarboxylative Acylarylation of Phenyl Propiolates with α-Oxocarboxylic Acids to Coumarins Catalyzed by Hypervalent Iodine Reagents under Transition Metal-Free Conditions. *Adv. Synth. Catal.* **2017,** *359* (3), 443-453; (b) Ji, W.; Tan, H.; Wang, M.; Li, P.; Wang, L., Photocatalyst-free hypervalent iodine reagent catalyzed decarboxylative acylarylation of acrylamides with α-oxocarboxylic acids driven by visible-light irradiation. *Chem. Commun.* **2016,** *52* (7), 1462-1465.
36. Amos, S. G. E.; Cavalli, D.; Le Vaillant, F.; Waser, J., Direct Photoexcitation of Ethynylbenziodoxolones: An Alternative to Photocatalysis for Alkynylation Reactions. *Angew. Chem. Int. Ed.* **2021,** *60* (44), 23827-23834.
37. Nguyen, T. V. T.; Wodrich, M. D.; Waser, J., Substrate-controlled C–H or C–C alkynylation of cyclopropanes: generation of aryl radical cations by direct light activation of hypervalent iodine reagents. *Chem. Sci.* **2022,** *13* (43), 12831-12839.
38. Yoshimura, A.; Yusubov, M. S.; Zhdankin, V. V., Iodonium imides in organic synthesis. *ARKIVOC* **2019,** *2019* (1), 228-255.
39. Kobayashi, Y.; Masakado, S.; Takemoto, Y., Photoactivated N-Acyliminoiodinanes Applied to Amination: an ortho-Methoxymethyl Group Stabilizes Reactive Precursors. *Angew. Chem. Int. Ed.* **2018,** *57* (3), 693-697.
40. Masakado, S.; Kobayashi, Y.; Takemoto, Y., Photo-Induced Aziridination of Alkenes with N-Sulfonyliminoiodinanes. *Chem. Pharm. Bull* **2018,** *66* (6), 688-690.
41. Guo, Y.; Pei, C.; Koenigs, R. M., A combined experimental and theoretical study on the reactivity of nitrenes and nitrene radical anions. *Nat. Commun.* **2022,** *13* (1), 86.
42. Guo, Y.; Pei, C.; Empel, C.; Jana, S.; Koenigs, R. M., Photochemical Nitrene Transfer Reactions of Iminoiodinanes with Sulfides. *ChemPhotoChem* **2022,** *6* (5), e202100293.
43. Jurberg, I. D.; Nome, R. A.; Crespi, S.; Atvars, T. D. Z.; König, B., Visible Light-Enhanced C–H Amination of Cyclic Ethers with Iminoiodinanes. *Adv. Synth. Catal.* **2022,** *364* (23), 4061-4068.
44. Yusubov, M. S.; Yoshimura, A.; Zhdankin, V. V., Iodonium ylides in organic synthesis. *ARKIVOC* **2016,** *2016* (1), 342-374.
45. Chidley, T.; Jameel, I.; Rizwan, S.; Peixoto, P. A.; Pouységu, L.; Quideau, S.; Hopkins, W. S.; Murphy, G. K., Blue LED Irradiation of Iodonium Ylides Gives Diradical Intermediates for Efficient Metal-free Cyclopropanation with Alkenes. *Angew. Chem. Int. Ed.* **2019,** *58* (47), 16959-16965.
46. Li, L.; Deng, K.; Xing, Y.; Ma, C.; Ni, S.-F.; Wang, Z.; Huang, Y., Synthesis of I(III)/S(VI) reagents and their reactivity in photochemical cycloaddition reactions with unsaturated bonds. *Nat. Commun.* **2022,** *13* (1), 6588.
47. Sar, S.; Das, R.; Barman, D.; Latua, P.; Guha, S.; Gremaud, L.; Sen, S., A sustainable C–H functionalization of indoles, pyrroles and furans under a blue LED with iodonium ylides. *Org. Biomol. Chem.* **2021,** *19* (35), 7627-7632.
48. Crivello, J. V., Diaryliodonium Salt Photoacid Generators. In *Iodine Chemistry and Applications,* 2014; pp 457-478.
49. Tobisu, M.; Furukawa, T.; Chatani, N., Visible Light-mediated Direct Arylation of Arenes and Heteroarenes Using Diaryliodonium Salts in the Presence and Absence of a Photocatalyst. *Chem. Lett.* **2013,** *42* (10), 1203-1205.
50. Ye, B.; Zhao, J.; Zhao, K.; McKenna, J. M.; Toste, F. D., Chiral Diaryliodonium Phosphate Enables Light Driven Diastereoselective α-C(sp^3)–H Acetalization. *J. Am. Chem. Soc.* **2018,** *140* (26), 8350-8356.

CHAPTER 2

2 Decarboxylative Ritter-Type Amination by Cooperative Iodine (I/III) - Boron Lewis Acid Catalysis

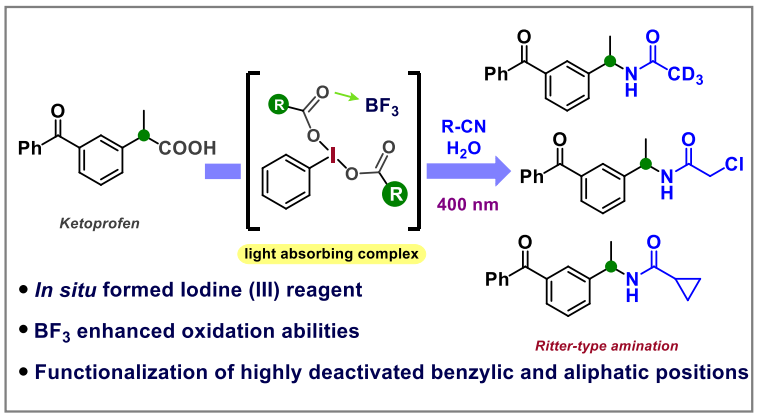

Abstract: Recent years have witnessed important progress in synthetic strategies exploiting the reactivity of carbocations via photo- or electrochemical methods. Yet, most of the developed methods are limited in their scope to certain stabilized positions in molecules. Herein we report a metal-free system based on iodine (I/III) catalytic manifold, which gives access to carbenium ion intermediates also on electronically disfavoured benzylic positions. The unusually high reactivity of the system stems from a complexation of iodine (III) intermediates with BF_3. The synthetic utility of our decarboxylative Ritter-type amination protocol has been demonstrated by the functionalization of benzylic as well as aliphatic carboxylic acids, including late-stage modification of different pharmaceutical molecules. Notably, the amination of Ketoprofen was performed on a gram-scale. Detailed mechanistic investigations by kinetic analysis and control experiments suggest two mechanistic pathways.

This chapter has been published. For reference see:
Narobe, R.; Murugesan, K.; Schmid, S.; König, B., Decarboxylative Ritter-Type Amination by Cooperative Iodine (I/III)—Boron Lewis Acid Catalysis. *ACS Catal.* **2022,** *12* (1), 809-817. Reproduced with permission from the American Chemical Society.

Author contribution: RN discovered the reaction, performed the optimization, synthesized the scope and carried out the mechanistic investigations. SS helped in the initial screenings and optimization of the reaction. KM helped with the preparation of substrates, isolation of products, and design of the mechanistic experiments. RN wrote the manuscript with the input of all authors. BK supervised the project and is the corresponding author.

2.1 Introduction

Catalytic aminations are widely applied in research laboratories and industry for the synthesis of fine and bulk chemicals[1] as well as pharmaceuticals, agrochemicals, and biomolecules.[2] The Ritter reaction, first reported in 1948,[3] allows for the preparation of amides, which are present in many functional molecules.[4] Crucial for the success of the Ritter amination is an efficient formation of carbenium ion intermediates, which can react with a variety of less reactive nucleophiles, like MeCN.[5] The quest to expand the scope of viable precursors for the formation of carbenium intermediates by applying new strategies is an ongoing challenge in chemistry.

In this regard, carboxylic acids are attractive starting materials, as they are abundant and inexpensive. Single-electron transfer (SET) oxidation of carboxylates leads to irreversible decarboxylation and the formation of the corresponding radical. Their role as radical precursors in different radical coupling processes is well established.[6] Comparably more challenging and less explored are methodologies of radical-polar crossover to generate an ionic intermediate from the corresponding radical by its oxidation or reduction.[7] The most straightforward approach to access carbocations by two sequential oxidations of carboxylate anions was synthetically exploited on electrode surfaces in some impressive transformations.[8] A redox neutral photocatalysis produces carbanions efficiently from carboxylates by a reductive radical-polar crossover.[7b, 9] Similarly, carbocations can be accessed by employing the corresponding redox-active phthalimide esters[10] or cyclic hypervalent iodine (III) reagents[11] as starting materials (Scheme 2.1a). While these sequential SET-based methods carry a remarkable impact and are highly valuable, they are also limited to certain types of stabilized positions in molecules, as the efficient oxidation of transient radicals is difficult due to the short lifetimes and relatively high oxidation potentials.[12]

A conceptually different approach to access carbocations is based on the trapping of radicals by iodine to form stable alkyl iodides.[13] Subsequent chemical oxidation of alkyl iodides to transient alkyl iodine (III) compounds converts the iodine moiety into a "hyper leaving group",[14] which gives access to carbenium intermediates (Scheme 2.1b). Among pioneering contributions to the field of iodine (I/III) catalytic reactions are also reports of photocatalytic decarboxylative oxygenation[15] and amination[16] from Kiyokawa and Minakata. Synthetic opportunities arising in this field are very appealing as they offer many benefits in terms of low reagent cost and a generally environmentally benign profile.[17]

As aforementioned, hypervalent iodine (III) precursors have shown very promising potential for the generation of carbocations in two mechanistically very different contexts. Still, the developed methods typically work best on the electronically stabilized positions. We sought to overcome the scope limitations by modifying properties of the used hypervalent iodine (III) reagents with simple additives such as BF_3. The complexation of iodine (III) reagents with BF_3 drastically changes their properties (*e.g.* oxidation potential),[18] and it was shown in the past to be the enabling factor in different types of iodine-mediated transformations.[19] Behavior of these complexes has so far not been investigated under photochemical conditions,[20] which has triggered our research interest.

Herein we report a photocatalyst-free catalytic system for decarboxylative amination. The system relays on the excitation of the colored *in situ* formed iodine (III) × BF_3 complexes, and can be used to functionalize molecular positions, which were not accessible by previously reported iodine (I/III) catalytic approaches.[21] The presented protocol is an alternative to achieve decarboxylative amination in a single step, instead of three classical synthetic steps - formation of the activated carboxylic acid analogue, coupling it with a nitrogen atom source, such as ammonia or azide, and triggering the respective Hoffman[22] or Curtius[23] rearrangement

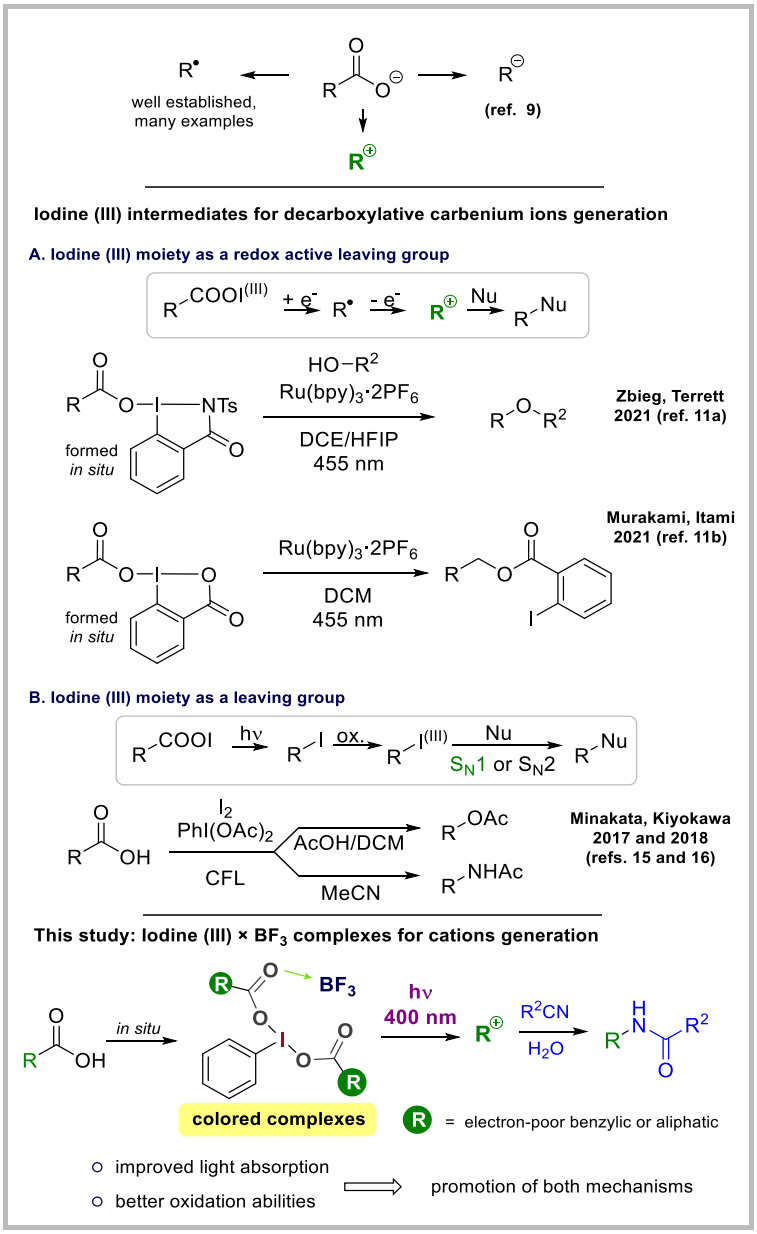

Scheme 2.1: Iodine (III) mediated decarboxylative transformations and our method, which overcomes some limitations in the generation of carbenium ions.

2.2 Reaction development

We started our investigations by *in situ* generation of hypervalent iodine (III) reagents from catalytic amounts of iodobenzene, Selectfluor as a terminal oxidant, and the reactant 4-nitrophenylacetic acid (**1a**) as ligand.[24] Upon irradiation in MeCN, the formed cations were expected to react in a Ritter-type amination to give product **1b**. The selected starting material **1a** is a challenging substrate because the generation of a carbocation at the benzylic position is strongly disfavored due to the electron-withdrawing effect of the nitro group. Irradiation at 400 nm without any additives gave a low 8% yield (Table 2.1, entry 1). Screening of different acids and bases (entries 2-3) revealed that bases (entry 2) completely inhibit the reaction, and the majority of the tested acids do not have any significant effect on the reaction outcome (entry 3). A significant improvement in the product yield was observed only with different BF_3 complexes, which can coordinate to the hypervalent iodine reagents (Table S2.1).[18-19] BF_3 in MeCN gave the highest product yield of 72% (entry 4) among the tested complexes. Contrary to other reports in iodine catalysis, our approach does not require neither a photocatalyst nor external molecular iodine (I_2) in combination with iodobenzene.

Table 2.1. Screening of the reaction conditions for decarboxylative amination.

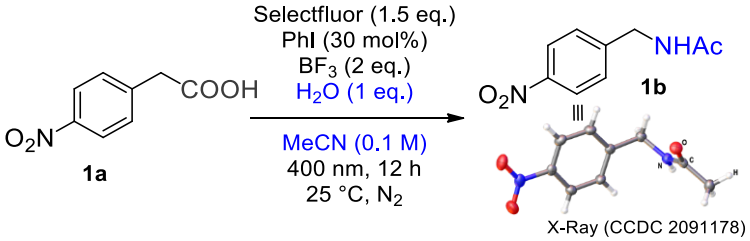

Entry	Deviation from optimized conditions	Yield of 1b (%)
1	No BF_3	8
2	Cs_2CO_3 (2 eq.) instead of BF_3	0
3	H_2SO_4, TFA, or HFIP (2 eq.) or $Sc(OTf)_3$ (0.5 eq.) instead of BF_3	8-11
4	**$BF_3 \times MeCN$ (2 eq.) as acid**	**72 (63)[d]**
5	without PhI or without light	0
6	I_2 (0.3 eq.) instead of PhI	46
7	NIS (0.3 eq.) instead of PhI	54
8	$PhI(OAc)_2$ (1.5 eq.)[b]	18
9	$PhI(OCOCF_3)_2$ (1.5 eq.)[b]	36
10	I_2 (0.5 eq.) + $PhI(OAc)_2$ (2 eq.) *(Ref. 20)*[c]	3
11	455 nm LED	67
12	525 nm LED	7
13	80 °C instead of irradiation	47

[a]Reaction conditions: 0.1 mmol substrate, 30 mol% PhI, 1.5 eq. Selectfluor, 2 eq. Lewis acid ($BF_3 \times MeCN$ unless otherwise noted), 1 eq. H_2O, 1 ml MeCN (0.1 M) under N_2 atmosphere, 25 °C, 12 h, yields were determined by ^1H NMR using acetanilide as internal standard. [b]Indicated iodine (III) reagent instead of combination of Selectfluor and PhI. [c]Previously reported conditions under CFL irradiation. [d]Isolated yield.

In the absence of iodobenzene the reaction does not give any product (entry 5). We continued optimization by screening the reactivity of different iodoarenes (Scheme S2.2) and found that many iodoarenes perform equally well, giving 72% product yield almost irrespective of their electronic properties or substitution pattern. Some iodoarenes with very easily oxidizable aromatic moieties (*e.g.*, naphthyl or methoxybenzene) gave lower product yields (<15%), probably because of their fast oxidative decomposition under the reaction conditions. We continued with iodobenzene as it is the simplest iodoarene and easiest to separate from the product after the reaction completion.

Molecular iodine (I_2) or N-iodosuccinimide (NIS) alone are also competent iodine sources leading to the product formation, albeit in slightly lower yields (entries 6 and 7, respectively). We did not pursue further optimization with them, because they are also good electrophilic "I^+" sources,[25] and might therefore potentially trigger electrophilic iodination of the aromatic ring as a side reaction.

Gratifyingly, our approach by *in situ* generation of hypervalent iodine (III) reagents (entry 4) is advantageous in terms of yields over using stoichiometric amounts of commercially available hypervalent iodine (III) reagents PIDA and PIFA (entries 8 and 9, respectively). Moreover, the previously reported conditions for the decarboxylative amination[16] turned out to be ineffective when applied to our starting material (entry 10 in Table 2.1, and Tables S2.14-2.15). The developed reaction does not work in the absence of light (entry 5), whereas irradiation with 455 nm blue light LEDs gave a slightly lower yield of 67%, and irradiation with 525 nm green light lead to a significantly lower 7% yield. Alternatively, the reaction can be run also under thermal conditions which might be a more suitable option for scale-up purposes (entry 13).

2.3 Synthetic application

With the optimized conditions in hand, we started exploring the general applicability of this transformation. The reaction conditions gave reliably good yields with mono- and poly-substituted arene moieties of phenylacetic (**1a**-**21a**) and phenylpropionic acids (**22a**-**28a**). Halogens and different hydrolysable groups (-CN, -OTos. -OAc) remained untouched under the reaction conditions. In most cases the position of substituents on the aromatic ring did not have a significant effect on the product yields. Notably, this protocol was further extended to a few approved drug structures - Ketoprofen (**26b**), Ibuprofen (**27b**) and Flurbiprofen (**28b**).

To demonstrate the scope beyond simple acetamide derivatives, other nitriles were used as coupling partners in this transformation. The obtained versatile products can be further functionalized, *e.g.*, by cyclopropyl ring-opening (**29b**), or act as alkylating agents (**30b**). The method is also suitable for the preparation of a fully deuterated acetamide derivative **31b**, which was not before with the I_2/PIDA system due to acetate ligands interference.[16]

The optimization of the reaction conditions for aliphatic substrates (**32a-37a**) revealed that addition of iodine is beneficial to achieve higher yields (Table S2.4). Impressively, the developed conditions allowed the functionalization of primary carboxylic acids **32a** and **33a**, which proceed via a non-stabilized primary carbenium intermediate. However, the overall reaction yield is lower, and as observed in the case of **33a**, carbenium intermediates preclude the functionalization of more complexes substrates as they undergo rearrangements to form more stable cations. Secondary cyclic and acyclic motifs (**34b-37b**) were obtained in moderate yields.[26] Notably, the acetylated drug Memantine **39b** and the unnatural amino acid building block **41b** were synthesized via a functionalization of tertiary positions.

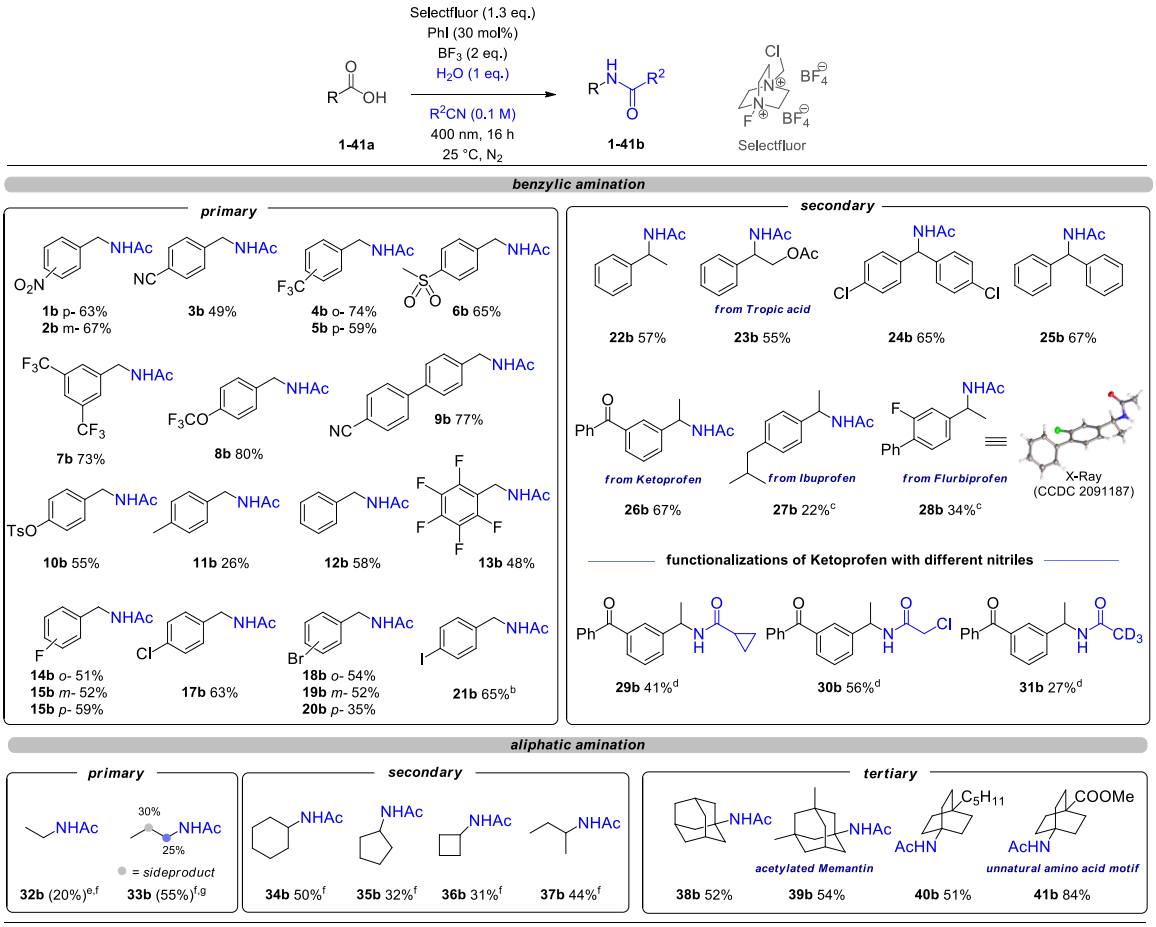

Scheme 2.2. Substrate scope for the synthesis of amides. [a]Reaction conditions: 0.4 mmol substrate, 30 mol% PhI, 2 eq. BF_3, 1.3 eq. Selectfluor, 1 eq. H_2O, 4 ml R^2CN (0.1 M) under N_2 atmosphere, 25 °C, 16 h, isolated yields. [b]No PhI was used.[c]2 eq. TFA were used instead of BF_3.[d]2 eq. $BF_3 \times Me_2O$ complex were used instead of $BF_3 \times$ MeCN complex. [e]In parenthesis is ^1H NMR yield using acetanilide as internal standard. [f]10 mol% of I_2 and 2 eq. Selectfluor were used. [g]Combined ^1H NMR yield using acetanilide as internal standard.

To show the practical value of our single-step methodology, a gram-scale reaction was performed (Scheme 2.3). In this case, the isolated yield of **26b** was slightly higher (74%) than in the small-scale reaction (67%), presumably due to a better control of the water content. An important practical aspect of the developed protocol is also a simple isolation, which does not rely on the separation by silica column chromatography, but it can be achieved by extraction followed by a simple filtration through a plug of basic alumina.[27]

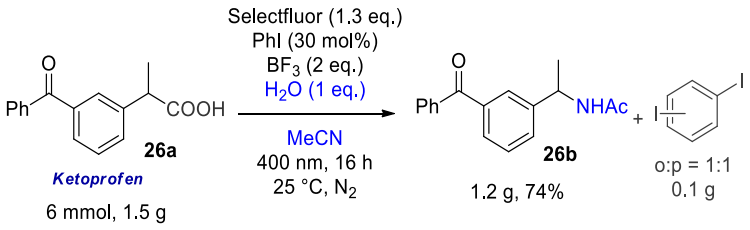

Scheme 2.3: Gram-scale decarboxylative amination of Ketoprofen.

2.4 Mechanistic investigations

To get a better insight into the reaction mechanism, Hammett kinetic plots analysis with differently substituted phenylacetic acids and iodoarenes have been performed. The reaction proceeds via carbenium intermediates at benzylic positions, and therefore we were expecting a strong influence of the electronic properties of the substrate on the reaction rate. Surprisingly, the reaction rate is relatively insensitive to different electron-withdrawing substituents (Figure 2.1a), even in case of the most electron-withdrawing group in the series (-NO_2). However, slower reaction rates have been observed with electron-rich substrates, probably due to competitive side reactions such as formation of diaryl iodanes.[18, 28] The main parameter affecting the overall reaction rate was found to be the substitution of the iodoarene (Figure 2.1b). The obtained negative ρ value (-1.95)[29] strongly indicates a buildup of positive charge on the iodine atom of the iodoarene (oxidation) as the rate limiting step.

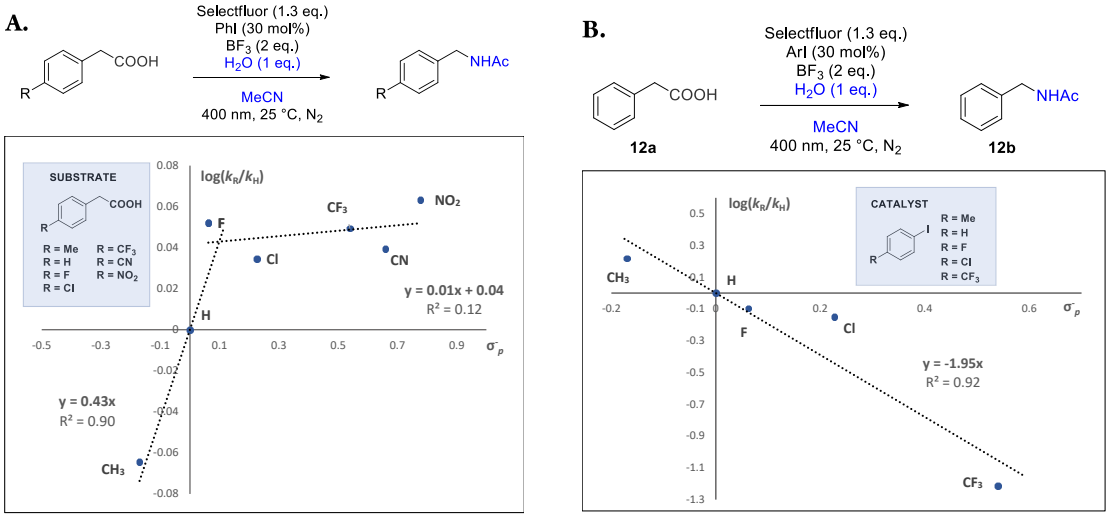

Figure 2.1: Hammett plots for differently substituted phenylacetic acids (A) and iodoarenes (B).

Starting the reaction from intermediate **1i** (Figure 2.2a), which is presumably formed after the oxidation of iodobenzene, gave 56% product yield. The yield is in very good agreement with the result obtained with the PhI/Selectfluor system with 1 eq. of Selectfluor (58%, entry 4 in Table S2.3). The result indicates that the reaction most likely proceeds via **1i** or alike intermediates and it is also an indication that Selectfluor plays no additional role in the system apart from being a terminal oxidant. The performance of **1i** formed *in situ* by ligand exchange from commercially iodine (III) reagents PIDA or PIFA is worse (18% and 36%, entries 8 and 9 in table 2.1), possibly due to competitive unproductive decarboxylation of (trifluoro)acetate ligands. The reaction from the intermediate **1i** in the absence of BF_3 resulted only in traces of the product.

The complexation of the hypervalent iodine (III) reagents with BF_3 results in a significantly better light absorption in the visible region (Figure 2.2b). A very similar light absorption pattern was observed with a variety of complexes containing different aliphatic and phenylacetic carboxylic acids (Figure 2.2c). Moreover, addition of BF_3 makes these reagents completely soluble in acetonitrile, which is also an important aspect for the efficient progress of the reaction.

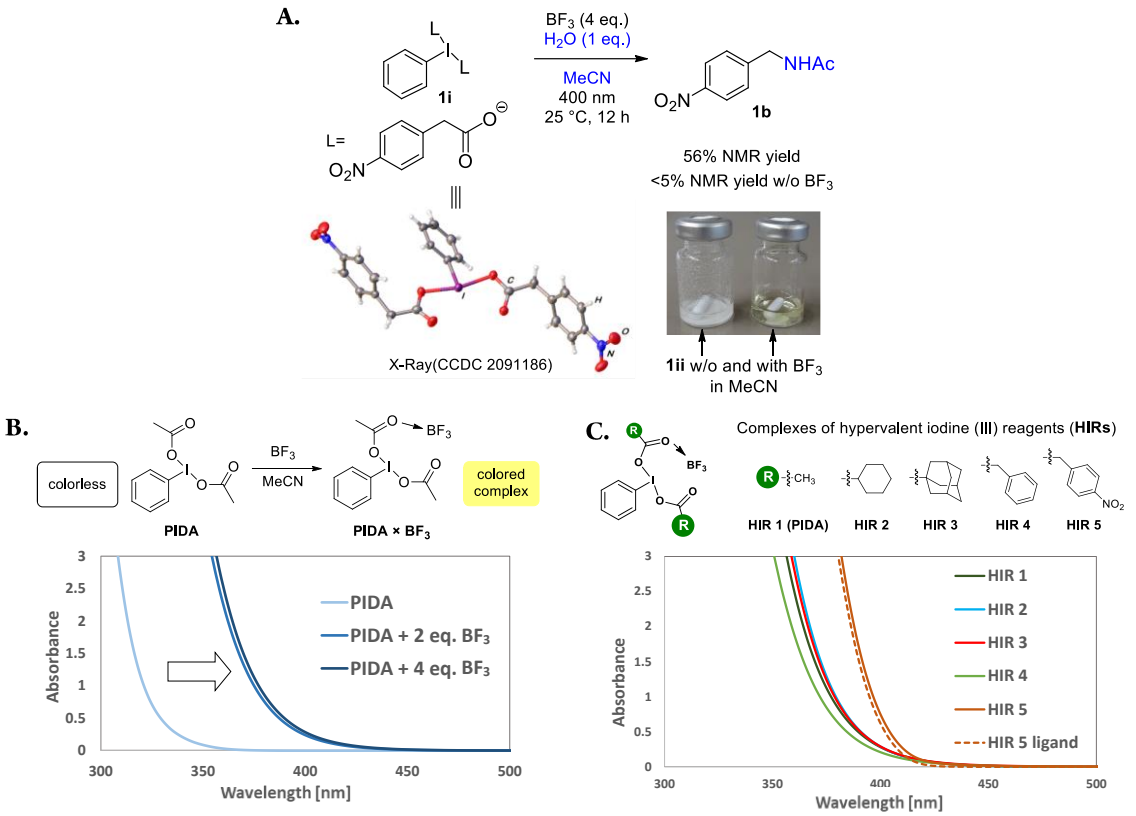

Figure 2.2: Reaction from the proposed intermediate 1i (A). Changes in visible light absorption properties of PIDA upon addition of BF_3 (B), and absorption properties of other hypervalent iodine (III) × BF_3 complexes (C). UV-vis spectra were measured at 25 mM in MeCN.

As shown, the excitation of the coloured hypervalent iodine (III) × BF_3 complexes leads to the product formation. However, with an appropriate "I^+" source such as I_2 or NIS (entries 6 and 7 in Table 2.1), the reaction proceeds also in the absence of iodobenzene. This is a good indication that the excitation of the *in situ* formed acyl hypoiodite (RCOOI) is also a productive mechanistic pathway in the system. As shown earlier, the photochemical iododecarboxylation step leads to the formation of the corresponding alkyliodide (RI),[30] which is a precursor of carbenium ions under oxidative conditions.

To confirm alkyl iodide's (RI) role as a potential intermediate in our reaction conditions and investigate the role of all reaction components, we used the proposed benzyl iodide intermediate **1ii** and subjected it to different reaction conditions (Table 2.2). In the presence of all the reaction components of our catalytic system, the intermediate **1ii** is efficiently converted into product **1b** in synthetically useful 95% yield (entry 1). The Lewis acid BF_3 alone (entry 2) is not sufficient to trigger the formation of carbenium species like in Friedel-Crafts alkylation reactions[31] and the oxidative conditions to access the transient alkyliodine (III) intermediates are required. Selectfluor as an oxidizing agent is giving a low 28% yield (entry 3). Addition of PhI to form a hypervalent iodine (III) complex (entry 4), or addition of PhI in combination with a carboxylate ligand (entry 5) have a positive, but minor effect on the product yield. Major improvement in the product yield (78%, entry 6) was observed upon addition of BF_3 with Selectfluor. In these conditions, also the formation of benzaldehyde as a side product was completely suppressed. Addition of PhI in combination with BF_3 and Selectfluor increased the yield to 90% (entry 7), which is already comparable with the result in the presence of the additional ligand **1a** (95%, entry 1). For comparison, we have also performed reactions with a stoichiometric amount of PIDA instead of the PhI/Selectfluor system. The results (entries 8 and 9) are consistent with the previous observations about the necessity of coordination with BF_3 resulting in better oxidation properties[18-19] and once again confirm that Selectfluor acts only as a terminal oxidant.

Table 2.2: Evaluating the role of the reagents with the proposed intermediate **1ii**.

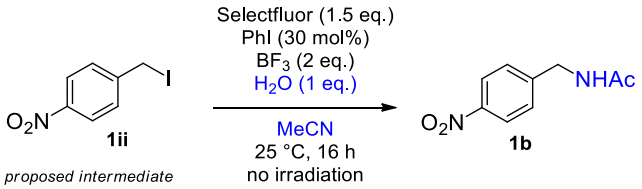

Entry	Selectfluor	PhI	BF_3	1a (1 eq.)	Yield of 1b (%)
1	Yes	yes	yes	yes	95
2	-	-	yes	-	0
3	Yes	-	-	-	28
4	Yes	yes	-	-	34
5	Yes	yes	-	yes	41
6	Yes	-	yes	-	78
7	Yes	yes	yes	-	90
8	$PhI(OAc)_2$ (1.5 eq.)	-	-	-	4
9	$PhI(OAc)_2$ (1.5 eq.)	yes	-	-	95

Reaction conditions: 30 mol% PhI, 2 eq. BF_3, 1.5 eq. Selectfluor, 1 eq. H_2O, 1 ml MeCN (0.1 M) under N_2 atmosphere, 25 °C, 16 h. Yields were determined by ^1H NMR using acetanilide as internal standard.

As we used additional iodine for functionalization of aliphatic carboxylic acids, we also performed similar experiment on a chiral aliphatic iodide (Scheme 2.4).[32] The chiral starting material allows us to get additional insight into the mechanism by distinguishing between the S_N1 (racemization of the product) and S_N2 (inversion of the chirality) reaction mechanism. The results obtained by chiral GC, indicate that the reaction proceeds mostly (60%)[33] via a carbocation mechanism, but still with a significant S_N2 component.

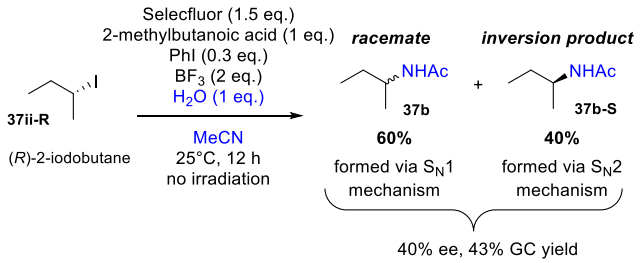

Scheme 2.4: Oxidation of enantiopure 2-iodobutane.

After these experiments, it was unclear whether the reactivity of the system can be explained by the released inorganic iodine as a result of photodegradation of iodine (III) reagents like **1i** and BF_3 complexes thereof.[34] The reaction of aliphatic carboxylic acids and phenylacetic acids worked well without additional iodine, however, in both cases we observed a positive effect on the reaction yield when iodine was added (entry 16 in Table S2.1 and Table S2.4). A noteworthy observation, supporting the release of inorganic iodine under the reaction conditions, was the isolation of small amounts of *ortho*- and *para*-diiodobenzene in the gram scale experiment (Scheme 2.3).[35] A mechanistic alternative to the alkyl iodide mediated mechanism is a direct single electron oxidation of the radical to a cation (Scheme 2.5a), similarly as proposed in the systems which contain a photocatalyst.

In order to identify the dominating mechanism, we have compared the reaction rates of compound **1a** in the presence of different PhI and "I^+" sources. If the release of iodine was a requirement for the successful progress of the reaction, we should be able to observe some specific traits in the kinetic profile of the reaction such as induction period and rate

acceleration upon addition of iodine. Surprisingly, the measurements revealed that the reaction catalyzed by "I⁺" precursors I_2 and NIS is quite slow compared to the iodobenzene catalyzed reaction (Figure 2.3a). Combination of iodobenzene with "I⁺" sources also displayed a bit slower reaction rate. From these experiments we can conclude that iodine release is not required for the reaction to proceed. Small amounts of released iodine do not significantly contribute to the overall reaction rate, because the direct radical oxidation pathway is a much faster process. Similarly, the effect of added iodine was tested also in the reaction of the hypervalent iodine (III) intermediate **1i-F** (Figure 2.3b). The intermediate has a blocked *para* position, to prevent consumption of iodine in electrophilic aromatic iodination under the reaction conditions. The kinetic profiles of the reactions with- and without iodine are almost identical, which additionally confirms that iodine is not required in the reaction and supports the direct oxidation of the radical as the main reaction pathway.

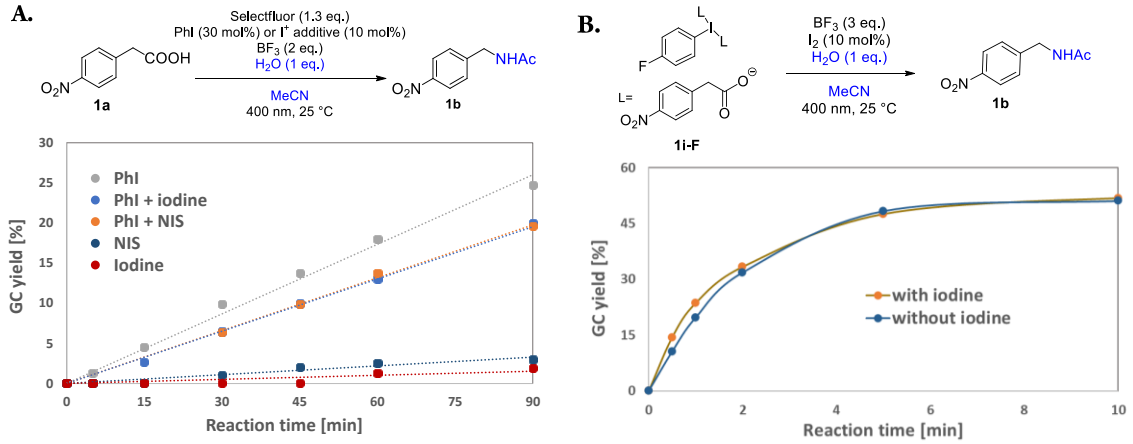

Figure 2.3: Kinetic profiles of the reactions of **1a** with different iodine sources. (A) and kinetic profile of the reactions of intermediate **1i-F** with and without iodine (B).

Next, quantum yield measurements have been performed to find out whether the oxidation of the radical is happening within the complex or intermolecularly by another equivalent of complex **1i** (radical chain). Relatively low quantum yields of the model reaction (1.3%; Table S2.12) and the reaction of the intermediate **1ii** (5.2%; Table S2.13) indicate that radical chains are most likely not involved in the mechanism.

Based on the performed experiments, we are proposing the following mechanistic picture (Scheme 2.5). In the predominat mechanism, Selectfluor oxidizes iodobenzene to a hypervalent (III) iodine reagent, which in the presence of carboxylate ligands and BF_3 forms an iodine (III) × BF_3 complex B.[18-19] An additional role of BF_3 in this step is scavenging of the nucleophilic byproducts of the Selectfluor oxidation. Consequently, BF_3 has to be used as a stoichiometric additive in the reaction. Excitation of the colored iodine (III) × BF_3 complex B leads to homolytic cleavage of the I–O bond and subsequent decarboxylation of the carboxyl radical ($RCOO^{\cdot}$). The obtained radical ($R^{\cdot}$) is then oxidized to a carbocation (R^+) which reacts with the solvent MeCN to give the Ritter-type amination product (C). The released iodobenzene perpetuates the iodine (I/III) catalytic cycle, and the other molecule of ligand and BF_3 can re-enter the catalytic cycle after the protonolysis of their complex (D).

An alternative mechanism (Scheme 2.5b) is operating in parallel with the main mechanism under the reaction conditions with additional iodine (I_2). It proceeds via an alkyl iodonium (III) species and relies on the improved oxidation abilities of the *in situ* formed iodine (III) × BF_3 complexes. In the first step, iodine reacts with the carboxylic acid A to form acyl hypoiodite species (B) which upon irradiation undergoes decarboxylation to give the corresponding alkyl iodide (C). [30] Oxidation of the alkyl iodide (C) by either Selectfluor or the aryl iodine (III) reagent complexed with BF_3 leads to a transient alkyl hypervalent iodine (III) species (D). The species undergoes

rapid nucleophilic substitution with the solvent MeCN to give the Ritter amination product (E).[16] Acyl hypoiodite species (B) released from the iodine (III) leaving group moiety, perpetuates the alkyl iodine (I/III) catalytic cycle.

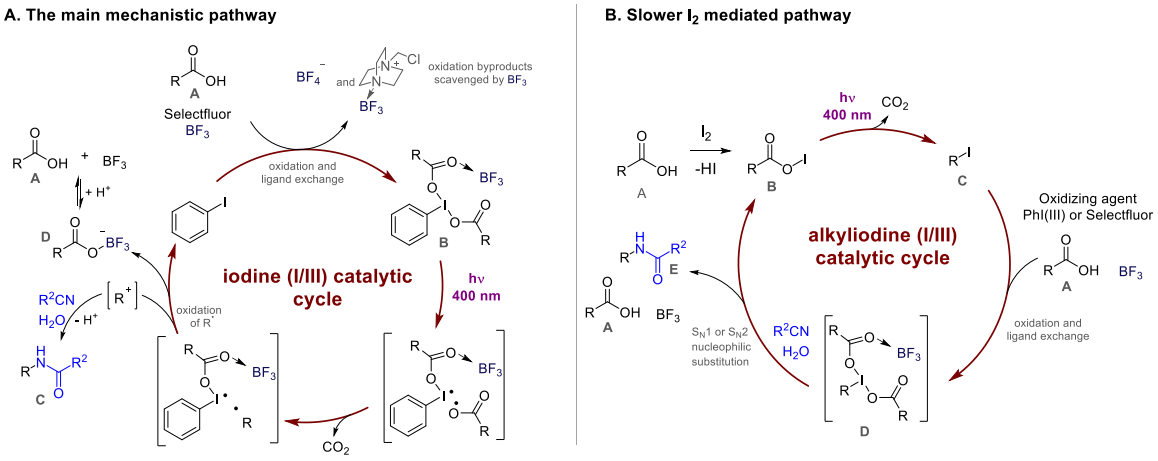

Scheme 2.5: Proposed reaction mechanisms.

2.5 Conclusion

In summary, we have developed a practically simple protocol for a Ritter-type amination which expands the scope of positions which can be functionalized by an iodine (I/III) catalytic manifold. BF_3 was found to be the enabling additive, which complexes the *in situ* formed iodine (III) intermediates and significantly improves their solubility, light absorption, and oxidation properties. Applying this methodology gives access to reactive carbenium ions from the corresponding carboxylic acids. The synthetic value of the presented decarboxylative amination protocol was demonstrated on 41 examples which also include functionalization and synthesis of pharmaceutically relevant molecules. Mechanistic investigations revealed two operating mechanisms for this transformation. The main mechanism is the oxidation of the carboxylic acid to a carbenium ion within the hypervalent iodine (III) × BF_3 complex upon excitation. Further investigations on the utilization of the presented approach are in progress.

2.6 Experimental information

2.6.1 General info

Starting materials and reagents were purchased from commercial suppliers (Sigma Aldrich, Alfa Aesar, Acros or Fluka) and were used without further purification. Solvents were used as p.a. grade. Reactions were monitored by analytic thin layer chromatography (TLC) using Fluka silica gel or NH2-Modified Silica Plates with a fluorescent indicator. Visualization of the developed TLC chromatogram was performed using 254 nm UV light source. Organic solutions were concentrated using Buchi rotary evaporator. Flash column chromatography was performed by hand using Pasteur pipettes filled either with Silica gel (60-200 μm) or basic alumina (50-200 μm).

NMR spectroscopy
All NMR spectra were recorded at room temperature using a Bruker Avance 300 (300 MHz for ^{1}H, 75 MHz for ^{13}C, 282 MHz for ^{19}F) or a Bruker Avance 400 (400 MHz for ^{1}H, 101 MHz for ^{13}C, 376 MHz for ^{19}F) NMR spectrometer. All chemical shifts are reported in δ-scale as parts per million [ppm] (multiplicity, coupling constant J, number of protons), relative to the solvent residual peaks as the internal standard. Coupling constants J are given in Hertz [Hz]. Abbreviations used for signal multiplicity: ^{1}H-NMR: br = broad, s = singlet, d = doublet, t = triplet, q = quartet, dd = doublet of doublets, dt = doublet of triplets, and m = multiplet.

Gas chromatography
GC measurements were performed on a GC 7890 from Agilent Technologies system coupled to a FID. The system was equipped with a capillary column (HP-5ms UI, length 30 m, diam. 0.25 mm, film 0.25 μm) and worked with H_2 as carrier gas. GC program: The initial temperature of the GC was set to 40 °C and kept for 1.5 minutes. Subsequently, the oven temperature was increased at a rate of 25 °C/min. until reaching 280 °C, which was maintained for 3 min. Then, temperature was further increased (42 °C/min) until reaching 300 °C and final temperature was hold for 5 minutes. Injector temperature was set to 280 °C and temperature of the detecting unit to 310 °C. A split ratio of 30:1 (split flow 42 mL/min) was applied, and the column flow was set to 1.4 mL/min. Data acquisition and evaluation was done with Agilent ChemStation Rev.C.01.04.
For instrumental details of chiral GC chromatography see chapter 2.6.4.4

Mass spectrometry
High resolution mass spectrometry (HRMS) was performed at the Central Analytical Laboratory of the University of Regensburg. Mass spectra were measured on a Finnigan MAT 95, ThermoQuest Finnigan TSQ 7000, Finnigan MAT SSQ 710 A or Agilent Q-TOF 6540 UHD instrumenta and a Waters Acquity UPLC system equipped with Waters PDA, sample manager, sample organiser, column oven and Waters Xevo QTOF mass spectrometer.

Photochemical setups
Photochemical reactions were performed in sealed reaction vials, placed approximately 2 cm above a 400 nm LED array (each LED has 3 W electrical power) and stirred under irradiation (Figure S2.1). The reaction temperature was controlled by a thermostated (25 °C) metal cooling block. The reactor setup is a custom-made device (University of Regensburg workshop) and is not a commercially available product.

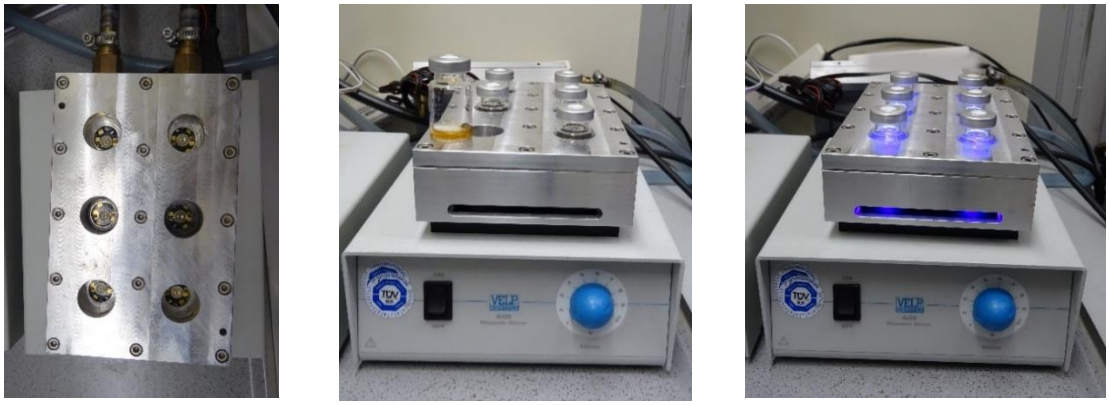

Figure S2.1: Photochemical setup for screening reactions from different perspectives

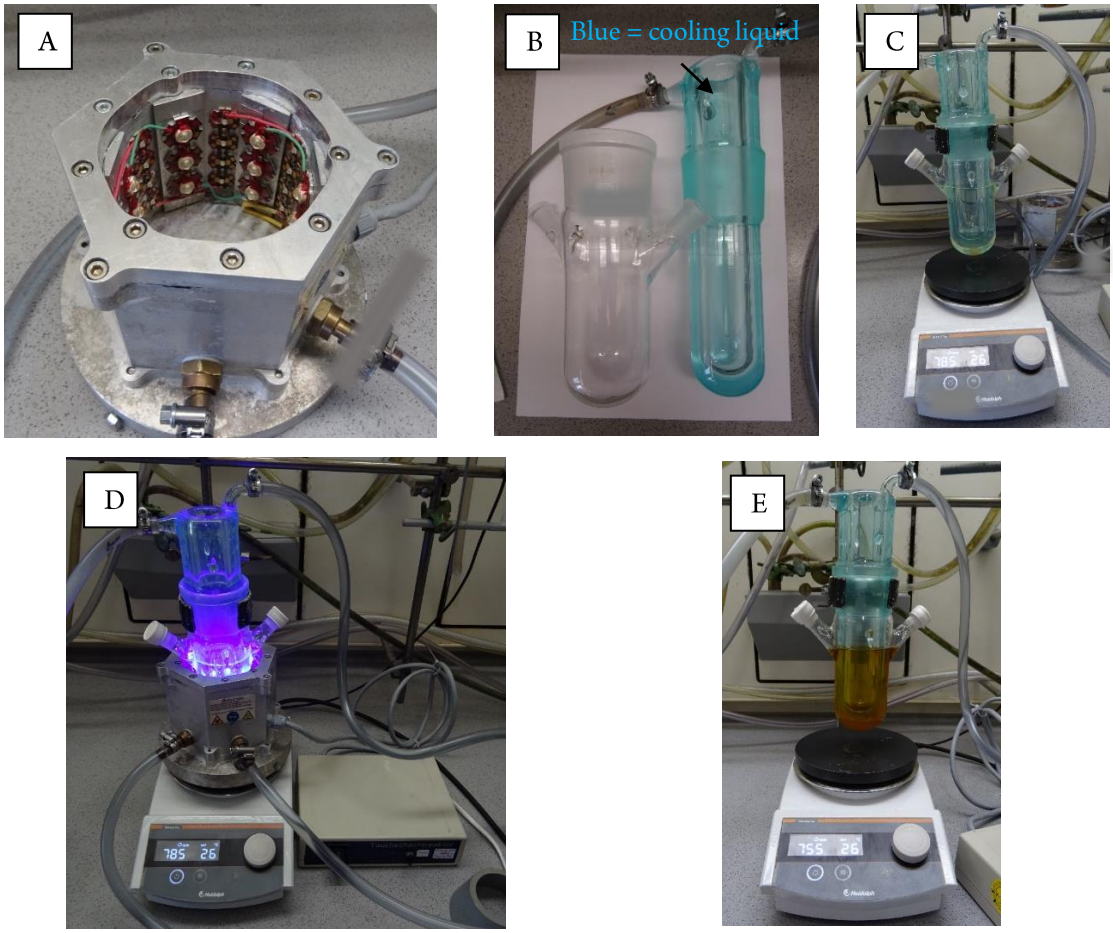

Figure S2.2: Pictures of large-scale setup. A) LEDs glued on a cooling block. B) Disassembled reaction vessel. The inner part is temperature controlled (blue liquid). C) Reaction vessel containing reaction mixture. D) reaction in progress. E) Reaction after completion.

The sample was irradiated with 18 LEDS (400 nm, 3 W electrical power each). The temperature was actively controlled by a thermostat (not shown in the photos).

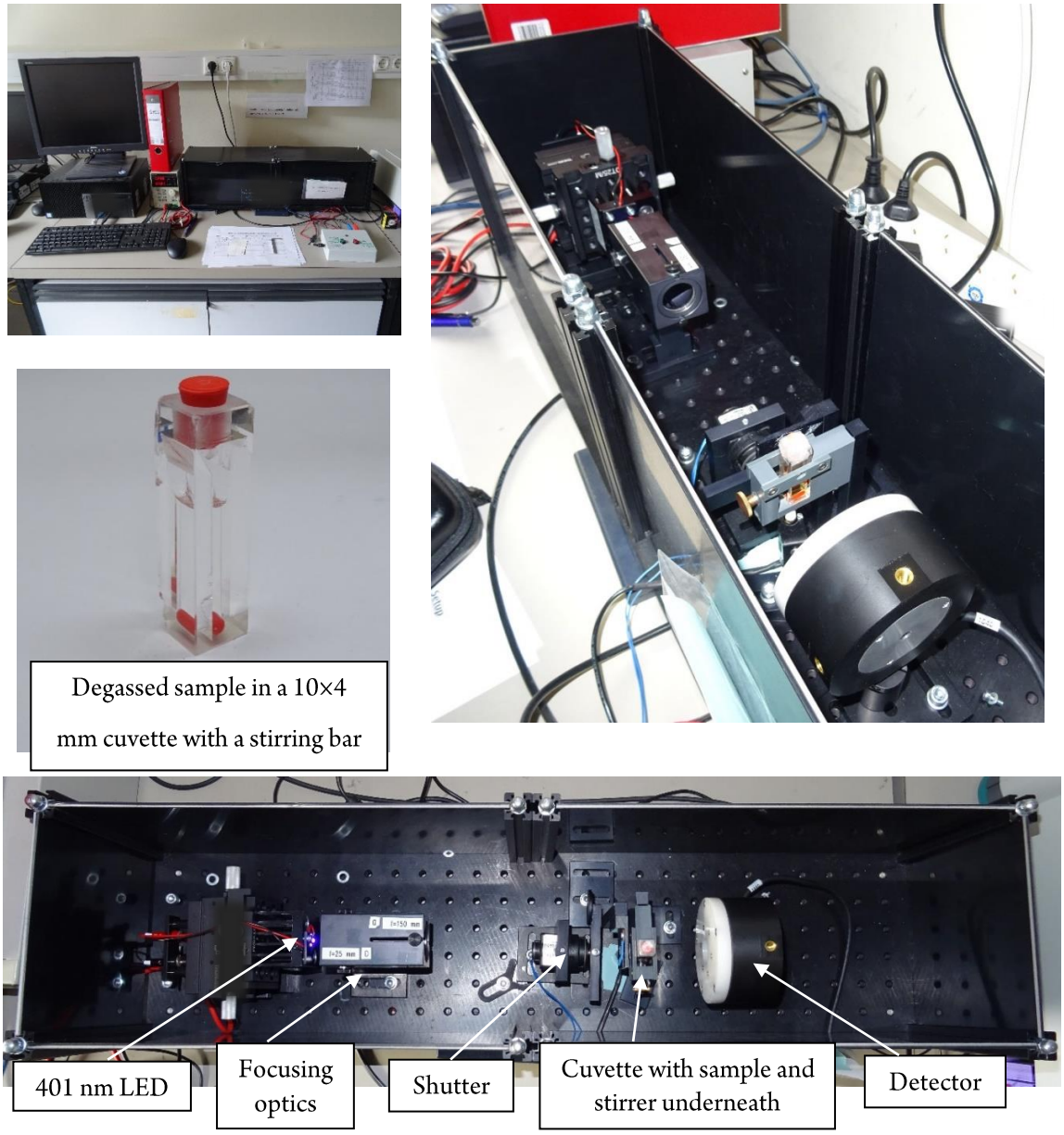

Figure S2.3: Quantum yield determination setup from different perspectives.

2.6.2 General experimental procedures

General procedure 1

Carboxylic acid (0.2 mmol, 1 eq.) and Selectfluor (92 mg, 0.26 mmol, 1.3 eq.) were weighed into a crimp reaction vial. Then, 2 ml of a stock solution containing iodobenzene (6.7 µl, 0.06 mmol, 0.3 eq.) and H_2O (3.6 µl, 0.2 mmol, 1 eq.) in dry MeCN were added. A stirring bar was added and the vial was capped. The reaction mixture was degassed by 4 nitrogen-vacuum cycles. Afterwards BF_3 (200 µl of 16% BF_3 in MeCN, 0.4 mmol, 2 eq.) was added, and the vial was placed in a thermostated cooling block (25 °C) and irradiated through the plane bottom side of the vial by a 400 nm LED (3 W electrical power) for 16 hours (see Figure S3.1). After the completion, the two reaction batches were combined, and the solvent was removed *in vacuo*. The solid residue was dissolved in 2 ml H_2O and 4 ml EtOAc and transferred into a separatory funnel containing 2 ml of brine. The aqueous layer was washed two times with 5 ml of EA. Combined organic phases were concentrated *in vacuo* and redissolved in a minimal amount of DCM and filtered through a small basic alumina column (packed in a Pasteur pipette). The column was washed with approximately 5 ml of DCM. After removal of the solvent, analytically pure product was obtained.

Note: A bit higher yields can be achieved by washing the basic alumina column with EtOAc. However, we have observed that with some substrates it may lead also to elution of remaining carboxylic acid (starting material).

General procedure 2:

Solid carboxylic acid (0.2 mmol, 1 eq.) and Selectfluor (142 mg, 0.4 mmol, 2 eq.) were weighed into a crimp reaction vial. Then, 2 ml of a stock solution containing iodine (5.1 mg, 0.02 mmol, 0.1 eq.), iodobenzene (6.7 µl, 0.06 mmol, 0.3 eq.) and H_2O (3.6 µl, 0.2 mmol, 1 eq.) in dry MeCN were added. A stirring bar was added and the vial was capped. The reaction mixture was degassed by 4 nitrogen-vacuum cycles. In case of liquid carboxylic acids, they were added after degassing. Afterwards BF_3 (200 µl of 16% BF_3 in MeCN, 0.4 mmol, 2 eq.) was added, and the vial was placed in a thermostated cooling block (25 °C) and irradiated through the plane bottom side of the vial by a 400 nm LED (3 W electrical power) for 16 hours (see Figure S3.1). After the completion, two reaction batches were combined, and the solvent was removed *in vacuo*. The solid residue was dissolved in 2 ml H_2O and 4 ml EtOAc and transferred into a separatory funnel containing 2 ml of brine. Aqueous layer was washed two times with 5 ml of EA. Combined organic phases were concentrated *in vacuo* and redissolved in a minimal amount of DCM and filtered through small basic alumina column (packed in a Pasteur pipette). The column was washed with approximately 5 ml of DCM. The solution was concentrated and filtered through another small silica containing column. First, the column was washed with DCM to remove remaining di- and tri-iodobenzenes. Then, the product was washed from the column with EtOAc. After removal of the solvent, analytically pure product was obtained.

Note: A bit higher yields can be achieved by washing the basic alumina column with EtOAc. However, we have observed that with some substrates it may lead also to elution of remaining carboxylic acid (starting material).

General procedure for screening and optimization studies:

Selectfluor (typically 53 mg, 0.15 mmol, 1.5 eq.) was weighed into a crimp reaction vial together with any other solid materials (different Lewis acids/bases, PIDA, PIFA, NIS…). Then, 1 ml of a stock solution containing 4-nitrophenylacetic acid 18.1 mg, 0.1 mmol, 1 eq.), iodobenzene (3.3 µl, 0.03 mmol, 0.3 eq.) and H_2O (1.8 µl, 0.1 mmol, 1 eq.) in dry MeCN were added. A stirring bar was added and the vial was capped. The reaction mixture was degassed by 4 nitrogen-vacuum cycles. Afterwards, BF_3 (100 µl of 16% BF_3 in MeCN, 0.2 mmol, 2 eq.) or any other liquids (Lewis acids) were added, and the vial was placed in a thermostated cooling block (25 °C) and irradiated through the plane bottom side of the vial by a 400 nm LED (3 W electrical power) for 16 hours (see Figure S2. 1). After the completion, the analysis was done following the typical procedure for NMR yield determination (*vide infra*).

Note: The reaction is relatively sensitive to the amount of water in the reaction mixture. Stock solutions containing 4-nitrophenylacetic acid, H_2O and PhI were always used to set all the reactions in order to have all the entries within the series (optimization table) comparable.

Procedure for NMR yield determination

The screening and optimization reactions were all done on a 0.1 mmol scale following GP1 or GP2. After the reaction completion, the crimp vial was opened and the solvent (acetonitrile) was removed from the reaction vial by using rotary evaporator. To the dry residue 0.5 ml of distilled water were added and 1 ml of a stock solution of internal standard (0.66 M acetanilide in EA). The two-phasic solution was transferred to a 2 ml round-bottom Eppendorf tube containing 0.5 ml of brine. The Eppendorf tube was briefly shaken to facilitate the extraction. The aqueous layer (bottom) was transferred back into the reaction vial by using a Pasteur pipette. Then, 1 ml of ethyl acetate was added to wash the reaction vial and extract remaining organics from the aqueous phase. The extraction was done in the Pasteur pipette by first quickly drawing in/pushing out the solution and then letting the layers separate in the pipette. The aqueous layer was put back in the reaction vial, and the combined organic layers in the Eppendorf tube were dried over sodium sulfate. Then, the solution was decanted in a glass vial from which the solvents were then removed using a rotary evaporator. The residue in the vial, was dissolved in deuterated chloroform and submitted to NMR. Sometimes an ultrasound bath was used to facilitate dissolution of the residue in chloroform.

Procedure for GC yield determination.

The internal standard (octane or benzonitrile) was present in the reaction mixture from the beginning. 100 µl aliquot of the reaction mixture were taken out of the reaction vial and transferred into a 1.5 ml conical-bottom Eppendorf tube. Then, 100 µl of ethyl acetate were added to the reaction mixture to precipitate most of the Selectfluor. The suspension in the Eppendorf tube was centrifuged for 1 min and the clear solution was submitted for GC analysis.

Procedure for gram-scale reaction

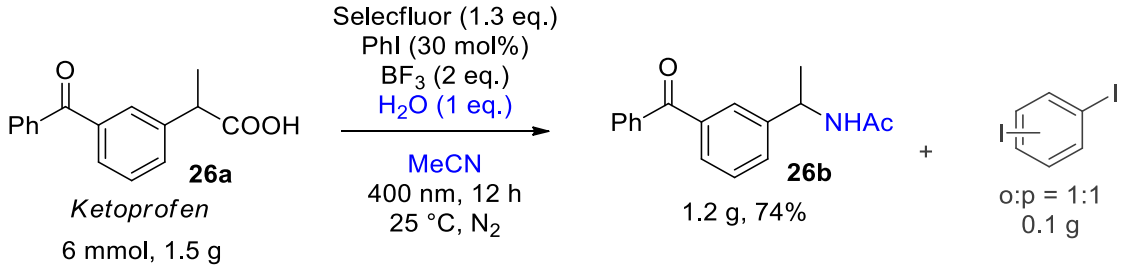

Scheme S2.1: Gram-scale reaction.

Ketoprofen (1524 mg, 6.0 mmol, 1 eq.) and Selectfluor (2761 mg, 7.8 mmol, 1.3 eq.) were charged in a reaction vessel (see Figure S2.2). Then, dry MeCN (50 ml), PhI (200 µl, 367 mg, 1.8 mmol, 30 mol%), and water (108 µl, 108 mg, 6 mmol, 1 eq.) were added, and the suspension was stirred for a few minutes to become a clear solution. Then, the reaction vessel was closed (see pictures of the setup) and degassed by 4 nitrogen-vacuum cycles. Afterwards, BF_3 (6.0 ml of solution of 16% BF_3 in MeCN, 12 mmol, 2 eq.) was added and the solution was irradiated for 16 hours at 25 °C. After the completion, the reaction mixture was transferred into a round bottom flask and the solvent was removed by a rotary evaporator. The remaining residue was dissolved in 5 ml of H_2O and 20 ml of EtOAc and transferred into a separatory funnel containing 10 ml of brine. The aqueous layer was washed two times with 20 ml of fresh EtOAc. The combined organic layers were dried over Na_2SO_4. After filtration of the drying agent, dry load for flash column chromatography was prepared by adding 2 spoons of basic alumina to the organic phase and evaporating the solvent. The dry load was transferred on the column containing ca. 20 g of basic alumina and was washed with 200 ml of ethyl acetate. 2 spoons of silica gel were added to the organic phase to prepare a dry load. The dry load was transferred on column containing ca. 20 g of silica gel. The column was washed first with ca. 100 ml of DCM and then with ca. 200 ml of EA. The DCM fraction contained 105 mg (0.32 mmol) of a mixture of diiodobenzenes (o:p=1:1), and the EtOAc fraction contained 1.192 g (4.46 mmol, 74%) of the desired product as a colorless oil.

Remark: The formation of diidobenzenes is also an indication that iodine may be liberated under the reaction conditions. The liberated iodine reacts with iodobenzene to give diiodobenzenes.

2.6.3 Screening and optimization

Screening of Lewis acids

First, we screened different acids and bases (Table S2.1). Bases (entry 2, others are not shown) completely inhibits the reaction, and the majority of the tested acids did not have any significant effect on the reaction outcome. Different complexes of BF_3 showed the highest yields (entries 7-9). BF_3 in MeCN performed best (entry 7) among the tested acids, and therefore we used it in the following screening and optimization steps.

Table S2.1: Screening of different Lewis acids.

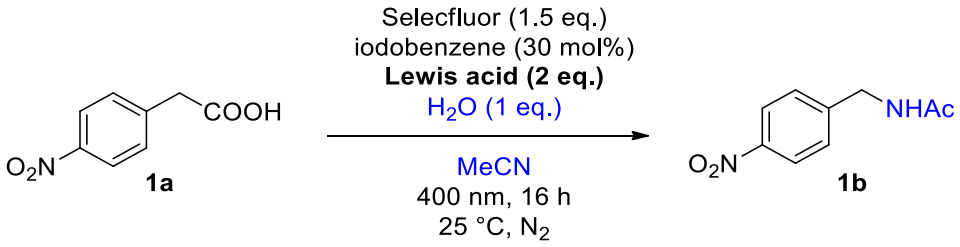

Entry	Acid/base	I_2	Yields [%]
1	-	-	8
2	Cs_2CO_3 (2 eq.)	-	0
3	TFA (2 eq.)	-	11
4	H_2SO_4 (2 eq.)	-	8
5	$HClO_4$ (70%, 2 eq.)	-	4
6	HFIP (2 eq.)	-	8
7	**BF_3 (16% in MeCN, 2 eq.)**	**-**	**73**
8	$BF_3 \times Et_2O$	-	15
9	$BF_3 \times Me_2O$ (2 eq.)	-	47
10	$BF_3 \times 2\ H_2O$	-	4
11	$B(OH)_3$ (2 eq.)	-	5
12	HBF_4 (32% in water, 2 eq.)	-	2
13	$LiBF_4$ (2 eq.)	-	9
14	$Zn(OTf)_2$ (0.5 eq.)	-	5
15	$Sc(OTf)_3$ (0.5 eq.)	-	10
16	BF_3 (16% in MeCN, 2 eq.)	0.1 eq	78

[1]H NMR yields determined by using acetanilide as internal standard.

The reaction yield can be improved a little by adding a catalytic amount of iodine (entry 16). However, we did not continue optimization in this direction because of the potential electrophilic iodination of the arene ring of more electron-rich arenes.

Screening of iodine sources

Screening of different iodine sources (Table S2.2) revealed that iodobenzene in combination with Selectfluor (Entry 1) is the optimal combination. The reaction also works when starting with a catalytic amount of preformed hypervalent iodine reagents (entries 2 and 3), but the yield seems to be dependent on the ligands of the used hypervalent iodine reagent.

Table S2.2: Screening of other iodine sources

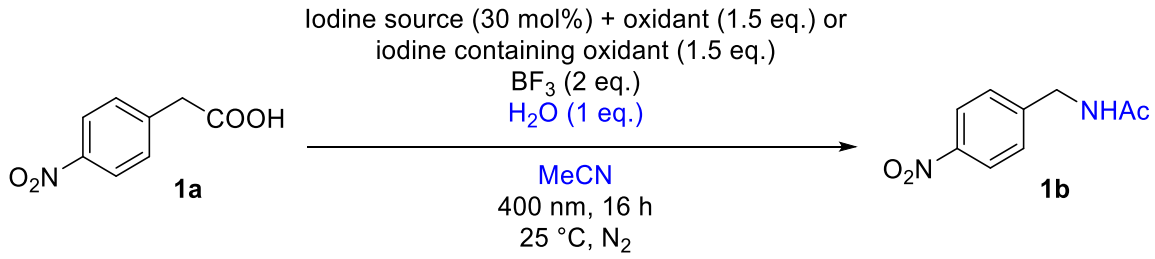

Entry	Iodine source (0.3 eq)	Terminal oxidant (1.5 eq.)	Yields [%]
1	**PhI**	**Selectfluor**	**73**
2	PIDA	Selectfluor	62
3	PIFA	Selectfluor	74
4	KI	Selectfluor	21
5	I_2	Selectfluor	54
6	NIS	Selectfluor	46
7		NIS (1.5 eq.)	53
8		HIO_3 (1.5 eq.)	3
9		H_5IO_6 (1.5 eq.)	1

[1]H NMR yields determined by using acetanilide as internal standard.

Screening of iodoarenes

Then, different iodoarenes were surveyed (Scheme S2.2). Contrary to our expectations, easily oxidizable iodoarenes (1, 2, 11, and 12) did not perform well under the reaction conditions. The reaction mixtures turned dark (brown/black) immediately after the addition of BF_3. The iodoarenes which did not undergo immediate color change performed similarly, giving 60-74% yields. The exception is iodoarene **10**, which gave a lower yield, probably because of the difficulties in oxidation to the corresponding I(lll) reagent.

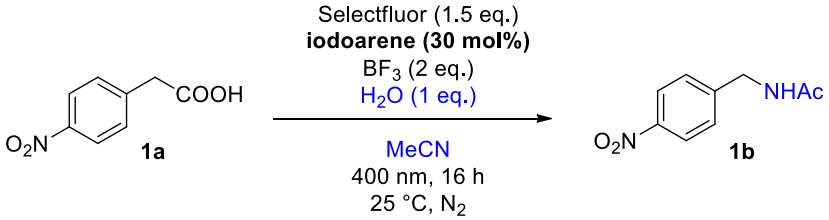

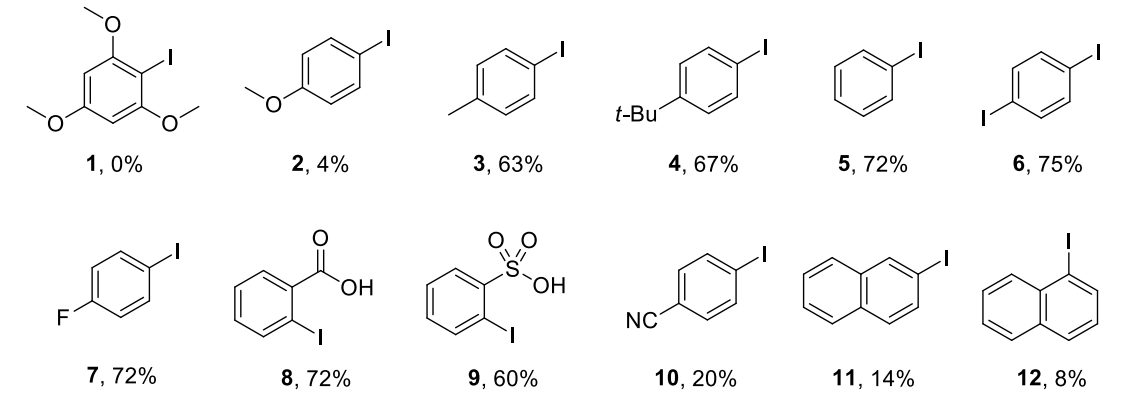

[1]H NMR yields determined by using acetanilide as internal standard.

Scheme S2.2: Screening of different iodoarenes.

The highest yield was achieved by using arene **6**. However, we decided to continue optimization with iodoarene **5** because, the differences in yields are almost negligible, and the removal of remaining iodoarene is much simpler with iodoarene **5** (evaporation).

Optimization of reaction conditions

Table S2.3: Optimization of reaction conditions

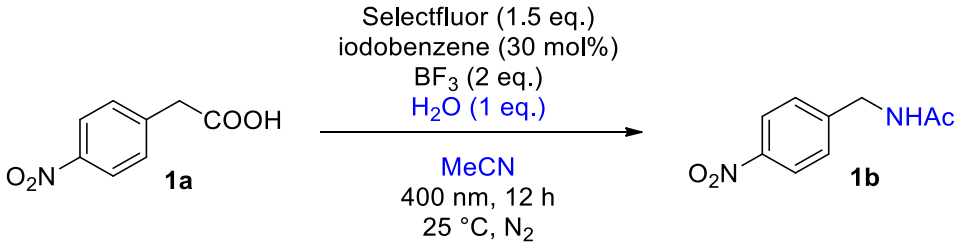

	Entry	λ [nm]	Selectfluor [eq.]	PhI [mol%]	BF_3 [eq.]	H_2O [eq.]	Reaction time [h]	Atmosphere	Yield [%]
Model conditions →	1	400	1.5	30	2	1	16	N_2	73
	2	455	1.5	30	2	1	16	N_2	67
	3	525	1.5	30	2	1	16	N_2	7
	4	400	1.0	30	2	1	16	N_2	58
Optimal conditions →	5	400	1.3	30	2	1	16	N_2	73
	6	400	1.5	20	2	1	16	N_2	68
	7	400	1.5	10	2	1	16	N_2	53
	8	400	1.5	30	1	1	16	N_2	48
	9	400	1.5	30	3	1	16	N_2	60
	10	400	1.5	30	2	5	16	N_2	5
	11	400	1.5	30	2	1	8	N_2	51
	12	400	1.5	30	2	1	16	O_2	43
	13	400	1.5	30	2	1	16	Air	42

^{1}H NMR yields determined by using acetanilide as internal standard.

Short optimization of amination of aliphatic substrates

Catalytic amounts of iodine were found to significantly improve the yields of more challenging aliphatic substrates. We have observed iodination of iodoarene giving a mixture of *ortho*- and *para*-diiodobenzene and even small amounts of triiodobenzene in entries where additional iodine was used.

Table S2.4: Optimization of reaction conditions for aliphatic substrates.

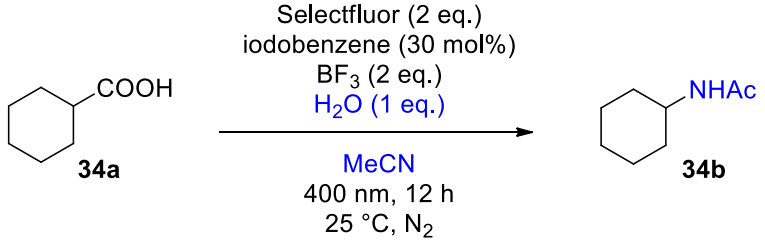

	Entry	Selectfluor [eq.]	Additive	Yield [%]
	1	1.5	-	24
	2	1.5	10 mol% I_2	47
Optimal conditions →	3	2	-	30
	4	2	10 mol% I_2	50

^{1}H NMR yields determined by using acetanilide as internal standard.

2.6.4 Mechanistic studies

2.6.4.1 Control experiments and comparison with other hypervalent iodine (III) sources

Control experiments confirmed that the reaction is actually photocatalytic and requires PhI (entries 1 and 2). Yields are lower when starting with preformed hypervalent iodine reagents (entries 3-6) compared to our PhI/Selectfluor conditions (entry 8). One potential reason could be that ligands get decarboxylated and consume the iodine to form CH_3I or CF_3I. Therefore, we have performed reactions with addition of ligands (entries 9 and 10). Acetic acid indeed inhibited the reaction progress quite significantly to obtain only 20% yield, and TFA did not give any major effect on the reaction outcome.

Table S2.5: Control experiments and comparison with other hypervalent iodine (III) sources

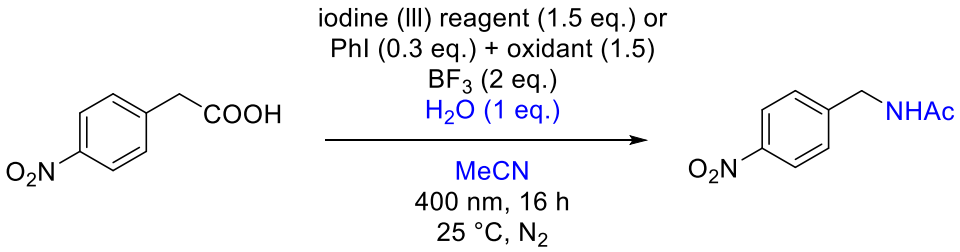

Entry	Iodine (III) reagent	BF_3	Additive	Yield [%]
1	Selectfluor (1.5 eq.) + PhI (0.3 eq.)	yes	No irradiation	0
2	Selectfluor (1.5 eq.), without PhI	Yes	-	0
3	$PhI(OAc)_2$ (1.5 eq.)	Yes	-	18
4	$PhI(OAc)_2$ (1.5 eq.)	-	-	0
5	$PhI(OC(O)CF_3)_2$ (1.5 eq.)	Yes	-	36
6	$PhI(OC(O)CF_3)_2$ (1.5 eq.)	-	-	11
7	Selectfluor (1.5 eq.) + PhI (0.3 eq.)	-	-	9
8	**Selectfluor (1.5 eq.) + PhI (0.3 eq.)**	**Yes**	**-**	**74**
9	Selectfluor (1.5 eq.) + PhI (0.3 eq.)	Yes	AcOH (3 eq.)	20
10	Selectfluor (1.5 eq.) + PhI (0.3 eq.)	Yes	TFA (3 eq.)	72

[1]H NMR yields determined by using acetanilide as internal standard.

The experiments were set following GP1 and the NMR yields were determined following the standard procedure described in general procedures.

2.6.4.2 UV-vis spectra of the hypervalent iodine (III) × BF_3 complexes

The measurements were performed in 10 × 10 mm quartz cuvette at indicated concentrations in dry MeCN under air atmosphere.

Upon the addition of BF_3 to PIDA, a slightly yellowish complex in 1:1 stoichiometry is formed (Figure S2.4). Additional equivalents of BF_3 do not have any significant effect on the absorption properties of the formed complex.

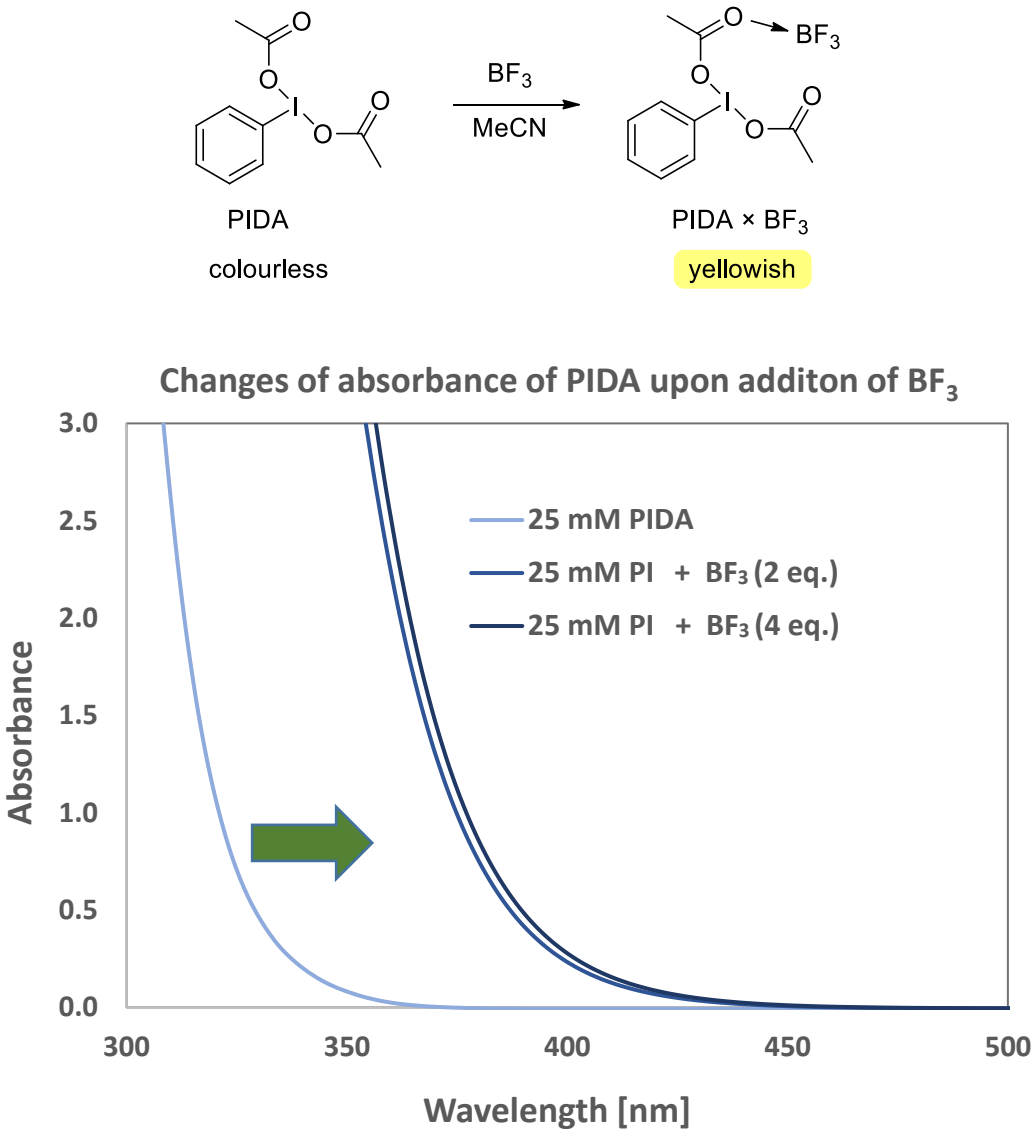

Figure S2.4: Absorption properties of PIDA × BF_3 complex.

A very similar behaviour has been observed also with the other hypervalent iodine (III) reagents upon addition of BF_3 (Figure S2.5). Interestingly, the absorption spectra of different reagents do not differ significantly, unless there is an additional chromophore present in the system (like in the case of HIR 5).

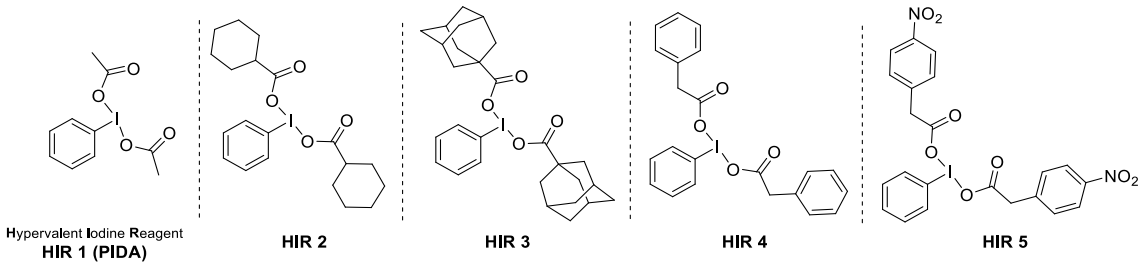

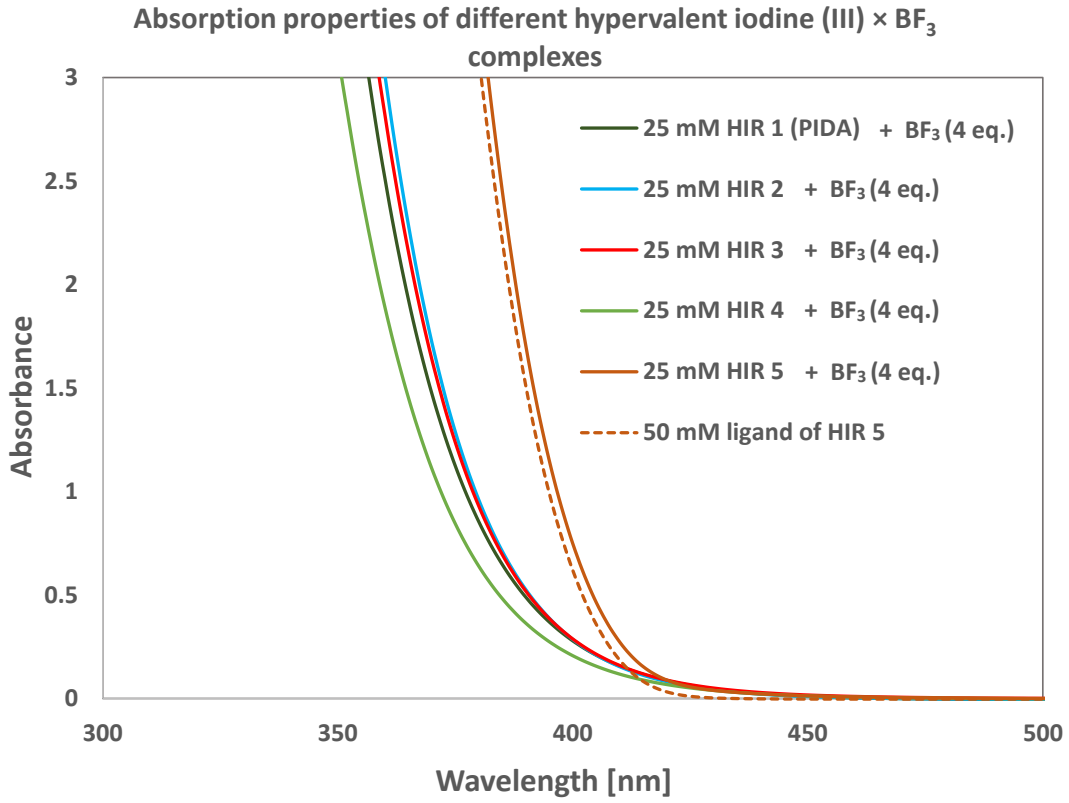

Figure S2.5: Absorption properties of different hypervalent iodine (III) × BF_3 complexes.

2.6.4.3 Testing different reaction conditions on the proposed alkyl iodide intermediates.

Effects of different reagents were tested on the proposed benzyl iodide intermediate (**1ii**).

Table S2.6: Testing different conditions for the oxidation of benzyl iodide intermediate **1ii**.

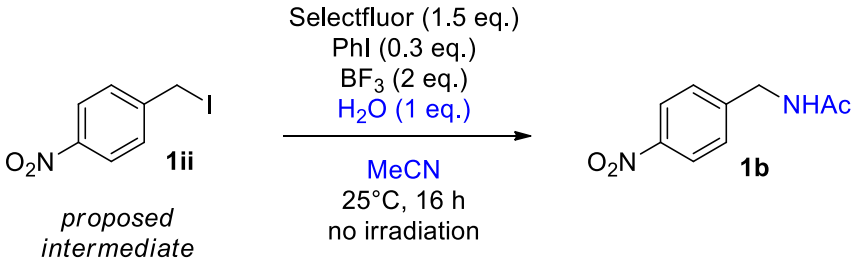

Entry	Selectfluor	PhI	BF_3	Ligand **1a** (1 eq.)	Yield [%]
A	-	-	yes	-	0
B	Yes	-	-	-	28
C	Yes	yes	-	-	34
D	Yes	yes	-	yes	41
E	Yes	-	yes	-	78
F	Yes	Yes	Yes	-	90
G	Yes	yes	yes	Yes	95
H	$PhI(OAc)_2$ (1.5 eq.)		-	-	4
I	$PhI(OAc)_2$ (1.5 eq.)		yes	-	95
J	$PhI(OOCCF_3)_2$ (1.5 eq.)		-	-	57
K	$PhI(OOCCF_3)_2$ (1.5 eq.)		yes	-	96

[1]H NMR yields determined by using acetanilide as internal standard.

The reaction mixtures were prepared by weighting the solid reagents in the reaction vials and adding 1 ml of a stock solution containing 0.1 mmol of **1ii** and 0.1 mmol of H_2O. The crimp vials with reagents were closed, degassed, and stirred at 25 °C (in the thermostated cooling blocks) for 16 hours without irradiation. The NMR yields were determined according to the standard procedure described in general procedures section.

2.6.4.4 Reaction starting from enantiomerically pure aliphatic iodide

For the synthesis of (R)-2-iodobutane, we used modified Appel reaction conditions which were developed and kindly shared with us ahead of the publication[32] by Alexander Kremsmair.

The aim of the experiment starting with enantiomerically pure alkyl iodide (Table S2.7) was to find out whether the reaction predominately proceeds via S_N1 (racemization) or S_N2 mechanism (inversion of chirality). We tested the developed conditions wherein iodine (III) reagents are formed *in situ* (conditions A) as well as the conditions where we start with the preformed commercially available $PhI(OAc)_2$ reagent (conditions B).

Table S2.7: Exposing enantiopure iodobutane to the developed reaction conditions.

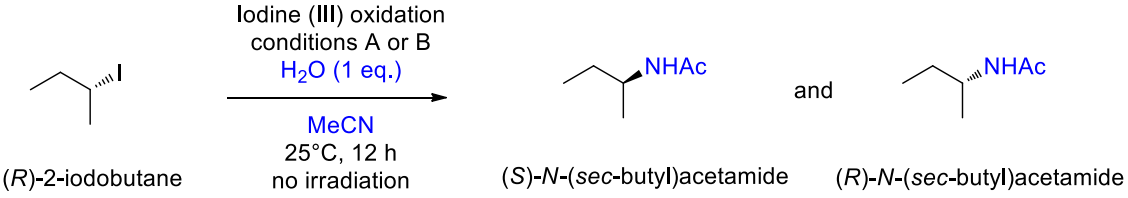

Sample	Oxidation conditions	GC yield	Specific rotation	ee
A	SF (1.5 eq.) / PhI (0.3 eq.) / BF_3 (2 eq.) / 2-methylbutanoic acid (1 eq.)	43%	$\alpha_D^{25} = 4.05\,°$, c = 1 in $CHCl_3$	40%
B	$PhI(OAc)_2$ (1.5 eq.) / BF_3 (2 eq.)	41%	not determined	37%

Isolation of the product mixture obtained in conditions A and measurement of the optical rotation revealed that the product mixture is not racemized and that the inversion product is present in excess ($\alpha_D^{25} = 4.05\,°$, for the S isomer). More accurate measurements by chiral GC revealed the exact ratios of isomers in both conditions. The results obtained are yield-wise and ee-wise very similar.

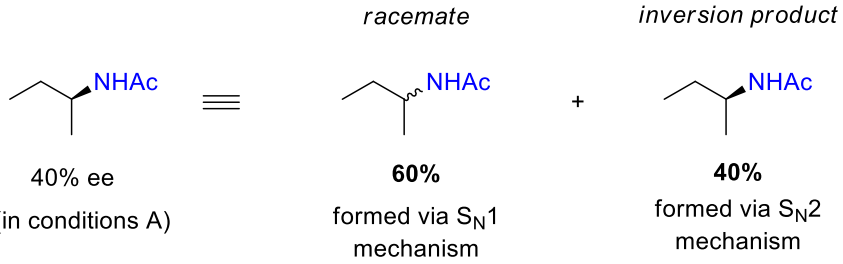

Scheme S2.3: Mechanistic interpretation of the obtained result

The reaction proceeds mostly via S_N1 mechanism, with a significant S_N2 component. The overall yield is relatively low due to side reactions which could also stem from the formation of carbenium intermediates (i.e., elimination and subsequent polymerization of olefins).

Table S2.8: Conditions for separation of racemate by chiral GC.

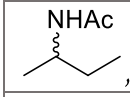 , N-Acetyl-2-butylamine (racemate)	
GC	Fisons 8000 series
Injection temperature	250 °C
Split ratio	1:20
Injection volume	0.5 µl, c = ca. 0.1 mol/l in ethylacetate
Detector	FID, 250 °C
Column	Varian CP-Chiralsil-Dex CB, 25 m x 0.25 mm x 0.39 mm, film 0.25 µm
Carrier gas	He, flow 1.25 ml/min
Temperature program	95 °C, Hold 3 min 95-105 °C, 0.5 °C/min

GC separation of the enantiomers on the chiral GC column

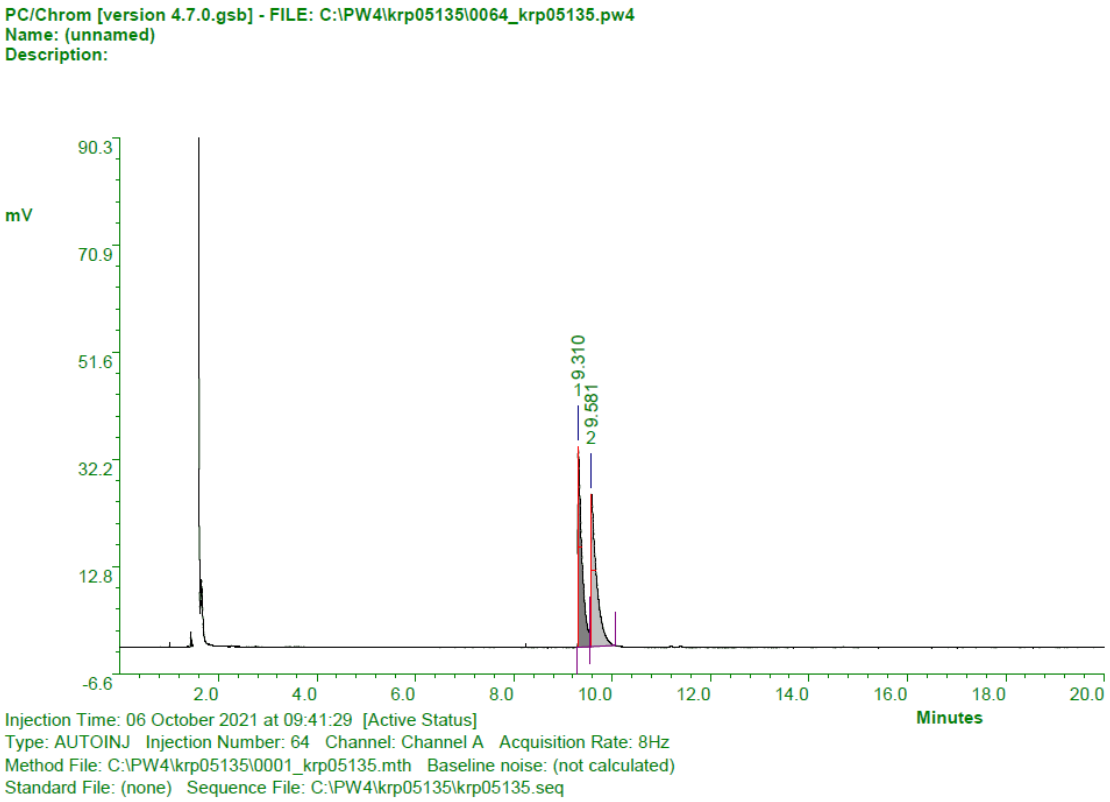

Peak	RT	Area	%Ar	Conc.(Ar)	Height	M	Units	Name
1	9.310	206.640	49.79	Not Calculated	36.312	1		
2	9.581	208.386	50.21	Not Calculated	27.535	1		

SAMPLE A

The product mixture was prepared by following isolation protocol described in general procedure B. The product was dissolved in EA and submitted for chiral GC analysis.

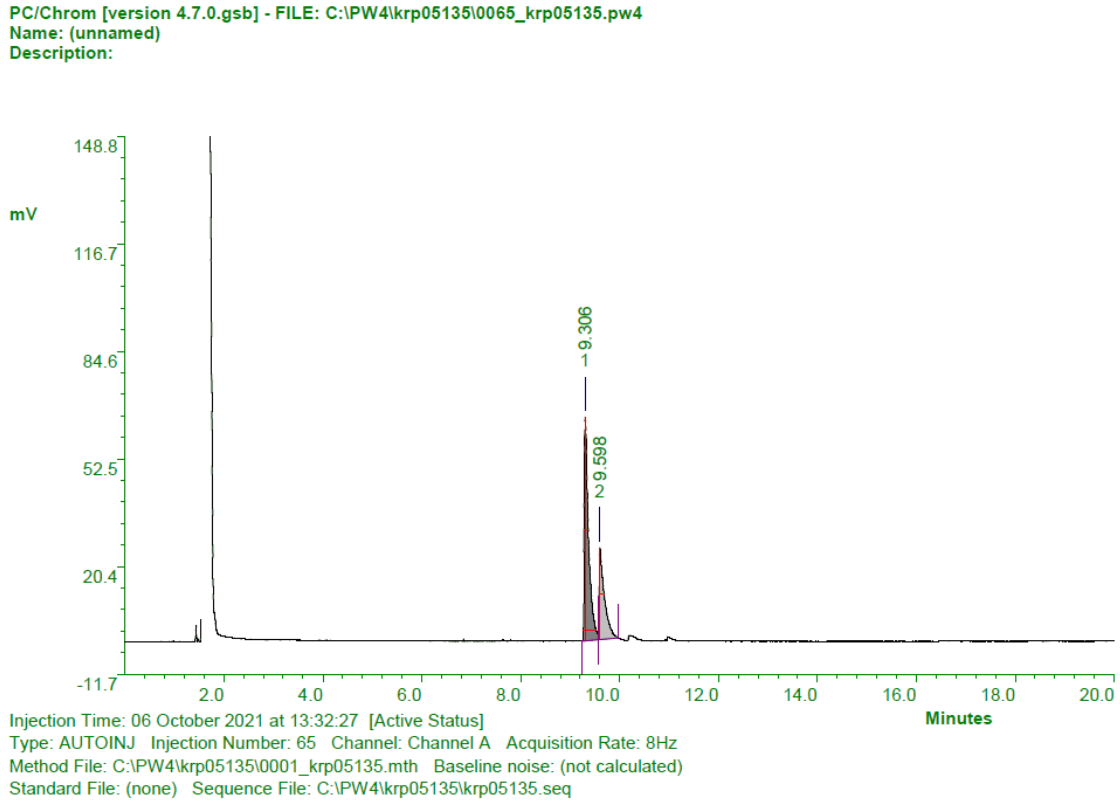

Peak	RT	Area	%Ar	Conc.(Ar)	Height	M	Units	Name
1	9.306	406.735	67.66	Not Calculated	66.648	1		
2	9.598	194.423	32.34	Not Calculated	27.305	1		

Figure S2.6: Chromatogram of isolated and purified mixture of product isomers obtained in conditions **A.**

SAMPLE B

The product mixture was prepared by following isolation protocol described in general procedure A. The product was dissolved in EA and submitted for chiral GC analysis. The sample contains also some iodobenzene, and mixture of *ortho*- and *para*-diiodobenzene.

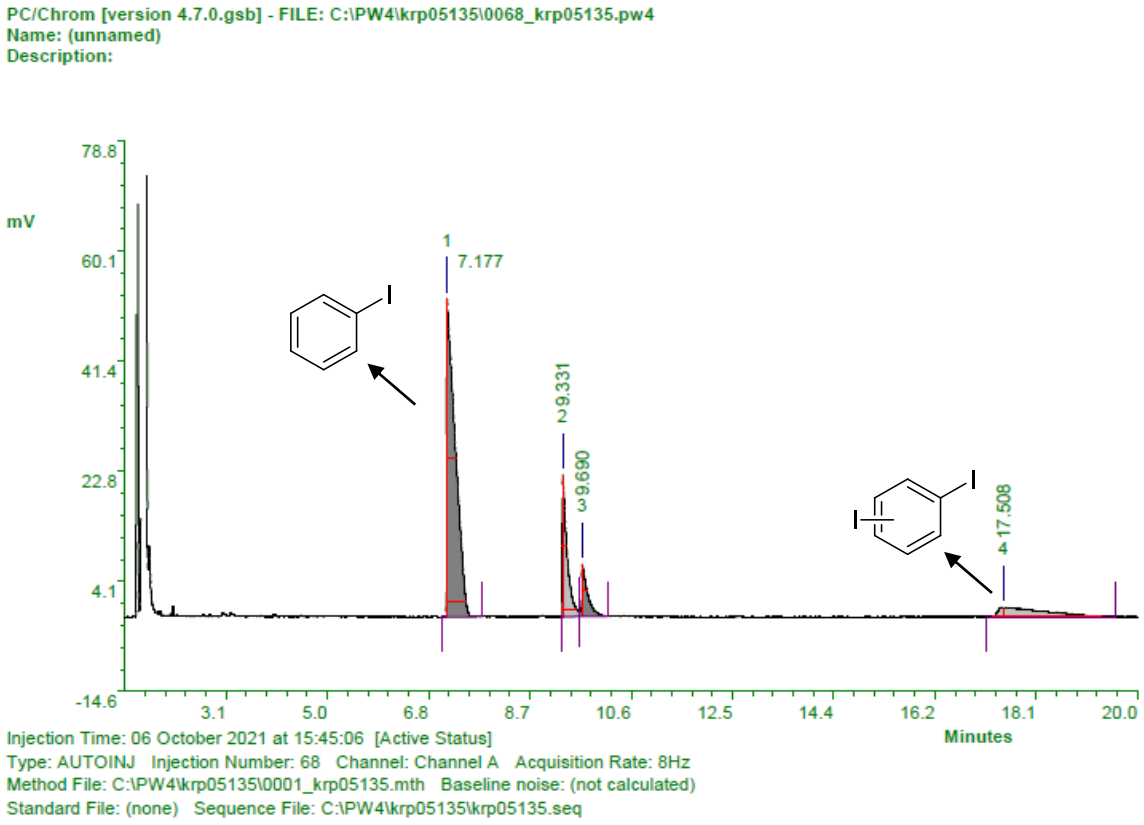

Peak	RT	Area	%Ar	Conc.(Ar)	Height	M	Units	Name
1	7.177	594.774	65.77	Not Calculated	53.993	0		
2	9.331	142.338	15.74	Not Calculated	24.047	0		
3	9.690	66.274	7.33	Not Calculated	8.835	0		
4	17.508	101.005	11.17	Not Calculated	1.645	0		

Figure S2.7: Chromatogram of isolated reaction mixture obtained in reaction conditions **B.**

2.6.5 Hammett kinetic plots analysis

Electronic effects of iodoarene

The reactions for kinetic studies were run on a 0.2 mmol scale. All reactions were prepared at the same time using the same freshly prepared stock solution (0.1 M **8a** and H_2O in dry MeCN) and they were all run in parallel to ensure high comparability within the series.

Selectfluor (92.0 mg, 0.26 mmol, 1.3 eq.) was weighed into each dry reaction vial of the series. Then, respective iodoarenes (0.06 mmol, 0.3 eq.) were added and 2.00 ml of a stock solution (**8a** and H_2O in dry MeCN, 0.1 M concentration of each component). The vials were closed and degassed using Ar. BF_3 (200 µl of 16% BF_3 in MeCN, 0.4 mmol, 2 eq.) and internal standard octane (16.3 µl, 0.1 mmol, 0.5 eq.) were added. The reaction vials were shaken briefly, put in the thermostated cooling block (25 °C), and irradiated with 400 nm LEDs. 100 µl aliquots were taken at indicated reaction times and processed by following the procedure for GC yield determination described in general procedures.

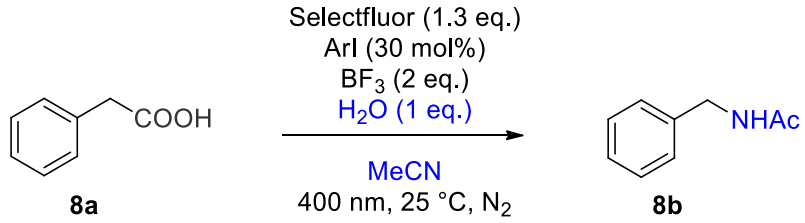

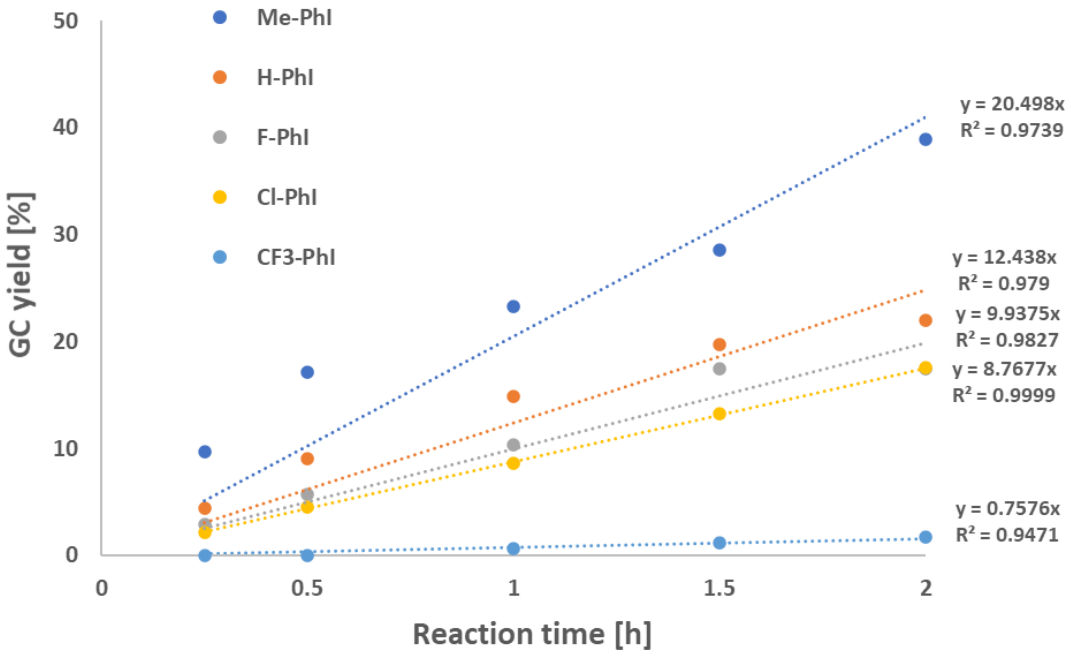

Graph S2.1: Kinetic profile of the reaction with differently substituted iodoarenes.

The reaction rate constants were approximated by reading the slope of the linear trendlines from the graphs of the first 2 hours of reaction kinetics monitoring.

Table S2.9: The data used to construct the Hammett plot for differently substituted iodoarenes.

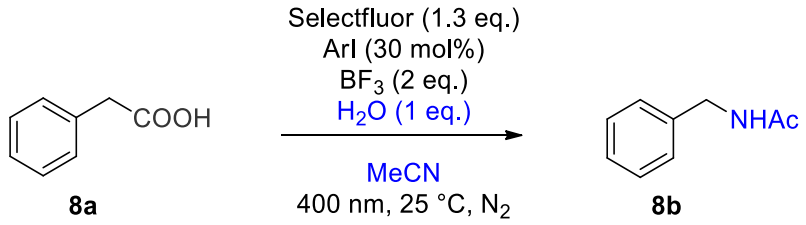

Entry	R group of ArI	σ_p^{-2}	k_R	$\log(k_R/k_H)$
1	$-CH_3$	-0.17	20.498	0.217
2	-H	0.00	12.438	0.000
3	-F	0.06	9.9375	-0.097
4	-Cl	0.23	8.7677	-0.152
5	$-CF_3$	0.54	0.7576	-1.215

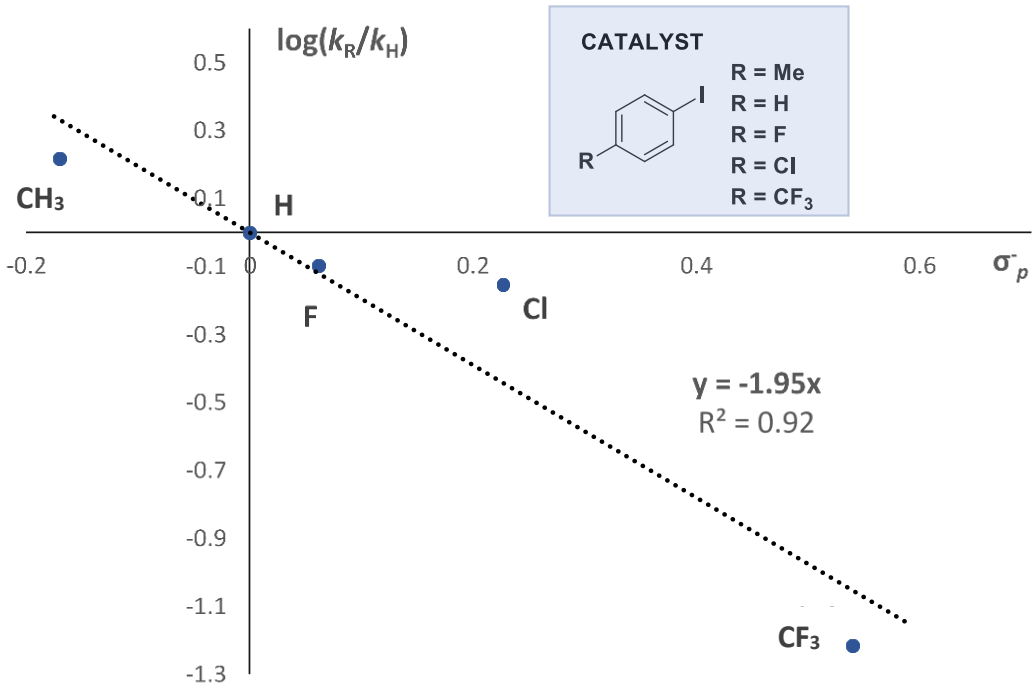

Graph S2.2: Hammett plot for differently substituted iodoarenes.

The obtained negative ρ value (-1.95) strongly indicates a buildup of positive charge at the iodine atom of iodoarene (oxidation) as the reaction's rate-determining step.

Electronic effects of substrate

Selectfluor (92.0 mg, 0.26 mmol, 1.3 eq.) was weighed into each dry reaction vial of the series. Then, respective phenylacetic acids (0.2 mmol, 1 eq.) were added and 2.00 ml of a stock solution containing 0.06 mmol PhI (0.03 M) and 0.2 mmol of H_2O (0.1 M) in MeCN. The vials were closed and degassed using Ar. BF_3 (200 µl of 16% BF_3 in MeCN, 0.4 mmol, 2 eq.) and internal standard benzonitrile (20.6 µl, 0.2 mmol, 1.0 eq.) were added. The reaction vials were shaken briefly, put in the thermostated cooling block (25 °C), and irradiated with 400 nm LEDs. 100 µl aliquots were taken at indicated reaction times and processed by following the procedure for GC yield determination described in general procedures.

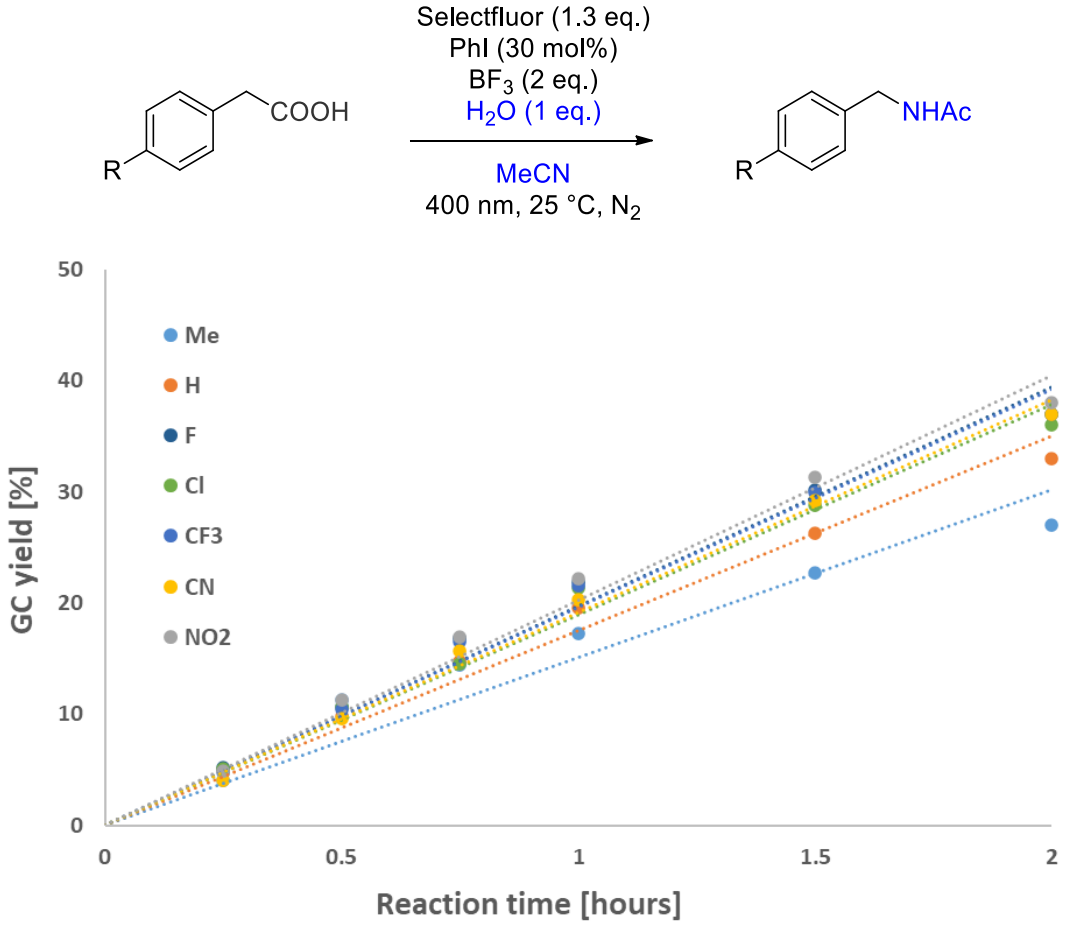

Graph S2.3: Kinetic profile of the reaction with differently substituted phenylacetic acids.

The reaction rate constants were approximated by reading the slope of the linear trendlines from the graphs of the first 2 hours of reaction kinetics monitoring. Note that the obtained absolute reaction rates in this experiment are comparable within the series but not with the previous series (wherein we used different iodobenzenes) because we used newer LEDs, which consume the same electrical power (3 W), but the optical output power is 6 times higher (ca. 20 mW compared to ca. 120 mW/per LED in the new setup.)

Table S2.10: The data used to construct the Hammett plot for differently substituted phenylacetic acids.

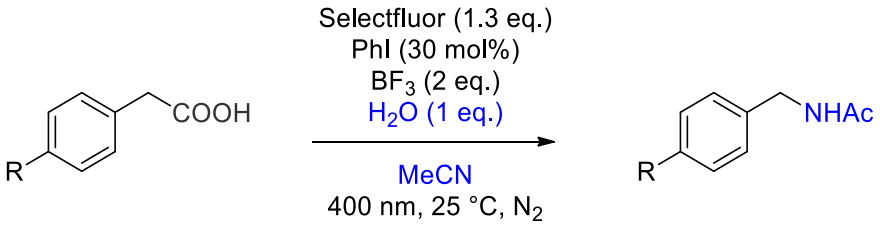

Entry	R group of SM	σ^{-}_{p} [2]	k_R	$\log(k_R/k_H)$
1	-CH_3	-0.17	15.10	-0.065
2	-H	0.00	17.52	0.000
3	-F	0.06	19.74	0.052
4	-Cl	0.23	18.96	0.035
5	-CF_3	0.54	19.62	0.049
6	-CN	0.66	19.17	0.039
7	-NO_2	0.78	20.26	0.063

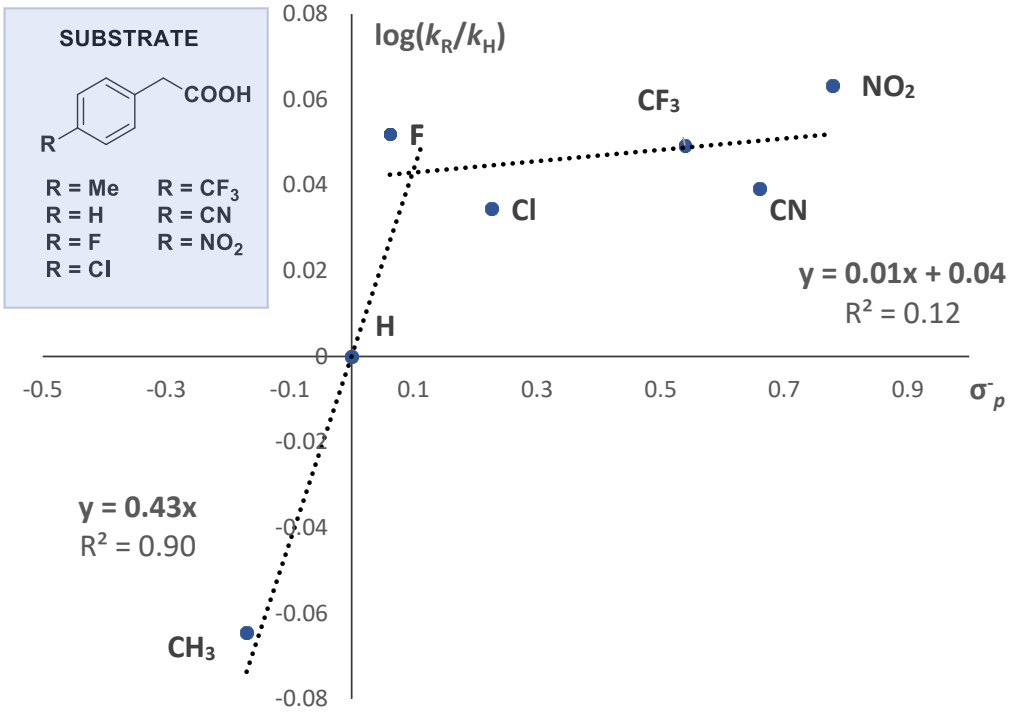

Graph S2.4: Hammett plot for differently substituted phenylacetic acids.

2.6.6 Inhibition of the reaction with excess of arene

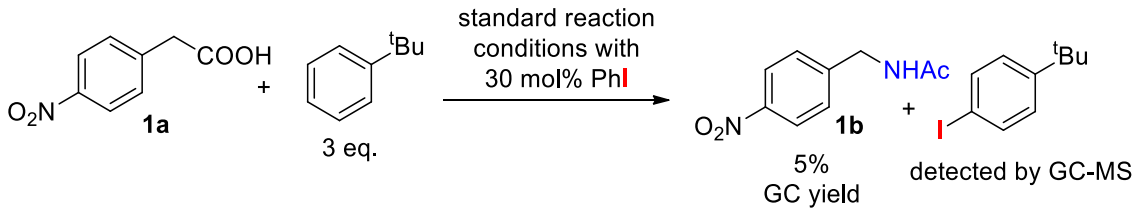

Scheme S2.4: Inhibition of the reaction with an excess of an electron-rich arene.

The reaction was set following the GP1 on a 0.1 mmol scale. After the degassing step, *tert*-butylbenzene (0.3 mmol, 3 eq.) was added. The GC yield was determined following the protocol described in general experimental procedures. The GC chromatogram showed formation of many side products which could not be accurately identified.

2.6.7 1,2-Hydride shift rearrangement

To probe whether the free carbocations are formed as intermediates, we performed the reaction on a substrate which has the possibility to undergo a 1,2-hydride shift to form a more stable carbocation intermediate.

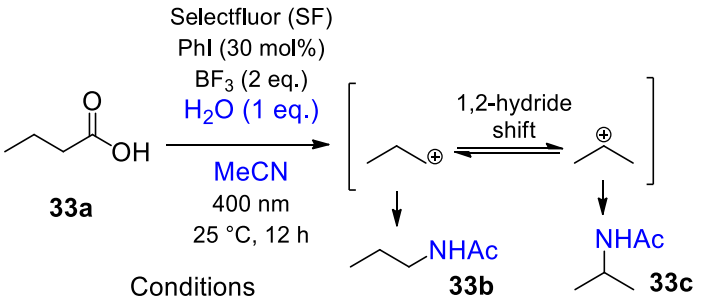

	Conditions	33b	33c
I	SF (1.3 eq.), no I_2	23%	28%
II	SF (2 eq.) + I_2 (10 mol%)	25%	30%

Scheme S2.5: 1,2-Hydride shift rearrangement in the reaction of *n*-butanoic acid (**33a**).

The reaction mixture was set according to GP1 and GP2, and the NMR yield was determined according to the general procedure for NMR yield determination described in General experimental procedures. See product characterization chapter for the GC-MS analysis and NMR spectra.

2.6.8 Reaction from a proposed hypervalent iodine (III) intermediate (1i)

The reaction from the iodine (III) intermediate (1ii) was run to see if the obtained yield is comparable to the yield obtained with the PhI/Selectfluor system.

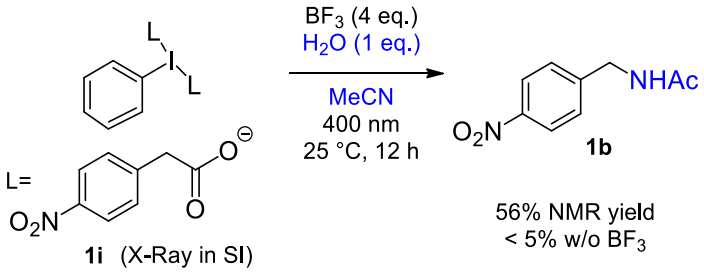

Scheme S2.6: Reaction starting from a proposed hypervalent iodine (III) intermediate (**1i**).

Hypervalent reagent 1i (56.4 mg, 0.1 mmol, 1 eq.) was weighed into the reaction vials. Then, 1 ml of a stock solution of H_2O (1.8 µl, 0.1 mmol, 1 eq.) in dry MeCN was added. The vials were closed and degassed via 4 nitrogen-vacuum cycles. In one case BF_3 (200 µl of 16% BF_3 in MeCN, 0.4 mmol, 4 eq.) was added. The samples were irradiated for 12 h at 400 nm. After the irradiation, the solvent was removed *in vacuo* and the samples were redissolved in *d*3-MeCN (0.7 ml/sample). Internal standard (4-tertbutylbenzonitrile) was added and the samples were submitted for ^{1}H NMR.

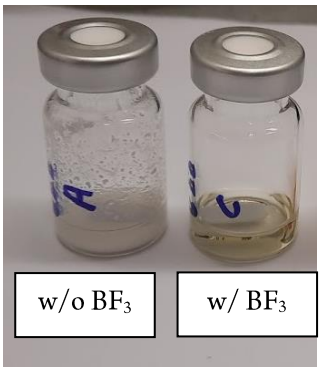

Before the reaction

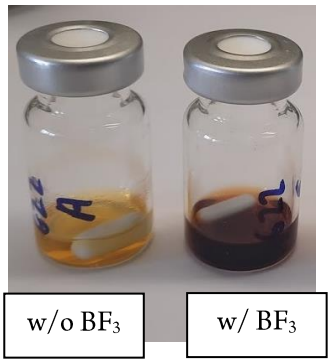

After irradiation

Figure S2.8: The reaction samples before and after irradiation.

The hypervalent iodine reagent is not well soluble in MeCN without the addition of BF_3. We have used more equivalents of BF_3 to mimic the acidity of the model reaction conditions (1 eq. of acidic starting material, 2 eq. of BF_3). Yields with 2 and 3 eq. of BF_3 were 41% and 53%, respectively. Additional iodine (10 mol%) when added to the reaction mixture, was found to have no effect on the reaction outcome.

2.6.9 "Light on/off" experiment

The reaction was set on a 0.2 mmol scale according to GP1 with internal standard (octane, 0.2 mmol) which was added after the degassing step. The samples were taken at indicated times and analyzed according to the general procedure for GC yield determination.

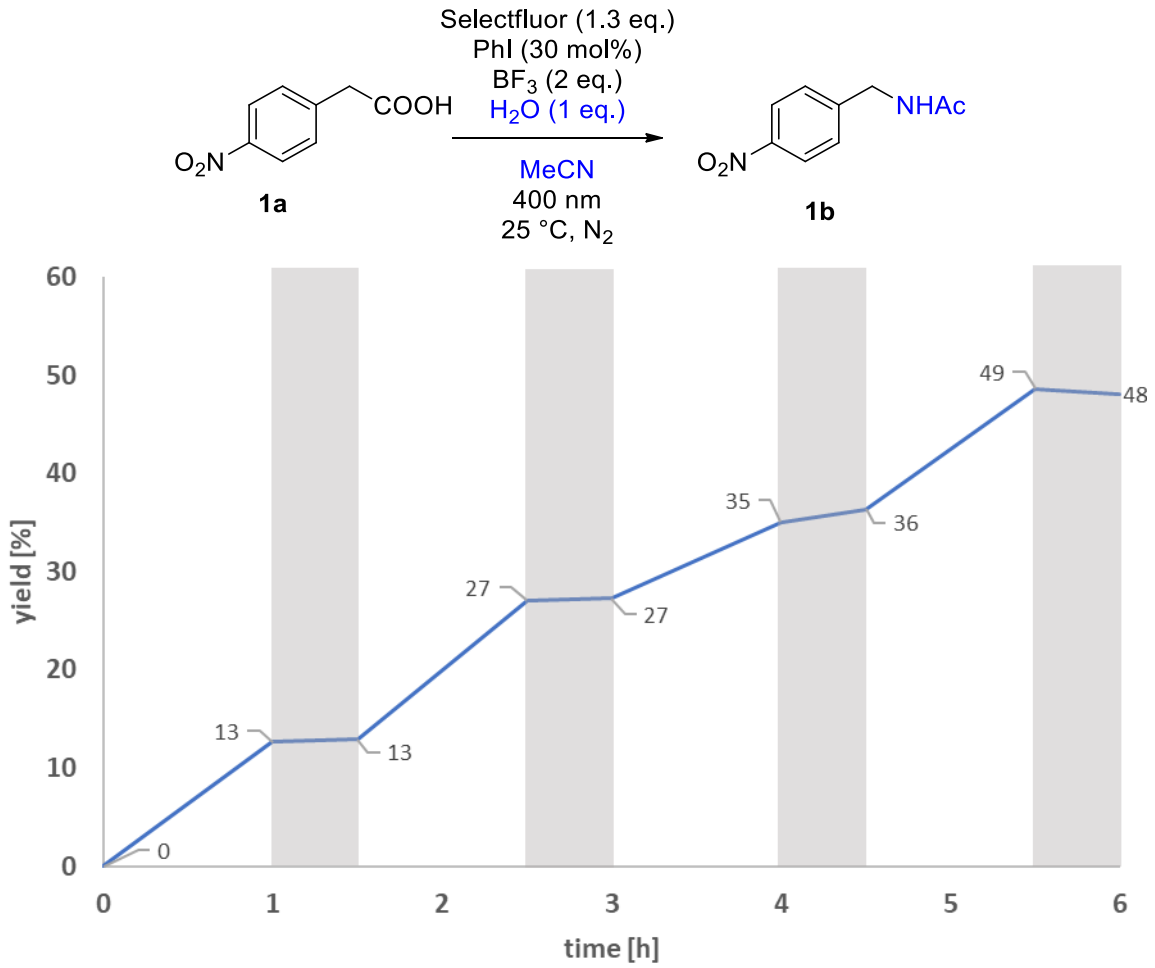

Graph S2.5: On/off experiment plot.

The reaction does not progress in the dark. We can safely exclude involvement of any long radical chains as a significant contribution to the reaction progress.

2.6.10 Quantum yield

Experimental Procedure for quantum yield determination

4-Nitrophenylacetic acid (18.1 mg,0.1 mmol, 1 eq.) and Selectfluor (46 mg, 0.13 mmol, 1.3 eq.) were weighed into a crimp reaction vial. Then, 1 ml of a stock solution containing iodobenzene (3.3 µl, 0.03 mmol, 0.3 eq.) and H_2O (1.8 µl, 0.1 mmol, 1 eq.) in dry MeCN were added. A stirring bar was added, and the vial was capped. The reaction mixture was degassed by 4 argon-vacuum cycles. Afterwards, BF_3 (100 µl of 16% BF_3 in MeCN, 0.2 mmol, 2 eq.) was added, and the reaction mixture was transferred into a degassed 0.4 × 10 mm fluorescence cuvette (see **Figure S2.3**). The reaction was run for ca. 6 hours and afterwards the NMR yield was determined following general procedure for NMR yield determination.

Table S2.11: Quantum yield determination of the reaction starting from carboxylic acid **1a**.

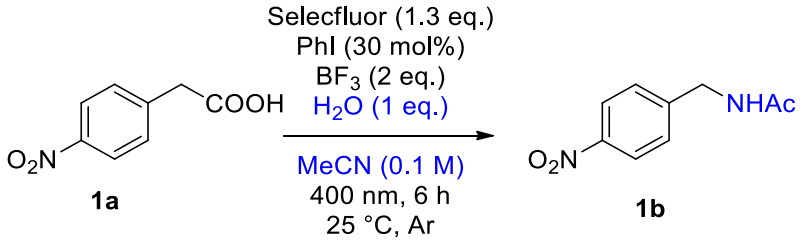

1a **1b**

$\Delta t\,[min]$	$P_{ref}[mW]$	$P_{sample}[mW]$	$P_{abs}[mW]$	NMR yield	φ
366	32.7	10.6	23.2	33%	**1.3 %**

Similarly, we have also measured the quantum yield from the proposed reaction intermediate **1i**. In this case, the reaction was performed at lower concentration (0.05 M) because of strong light absorption of the complex **1i**.

Table S2.12: Quantum yield of the reaction starting from the intermediate **1i**.

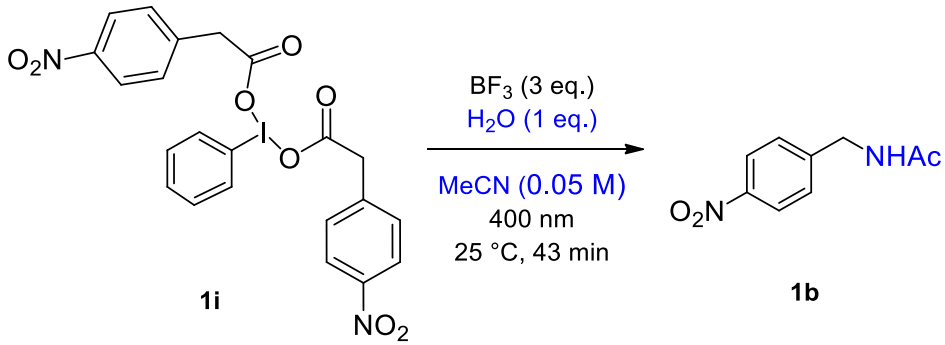

1i **1b**

$\Delta t\,[min]$	$P_{ref}[mW]$	$P_{sample}[mW]$	$P_{abs}[mW]$	NMR yield	φ
43	21.0	2.7	19.0	17 %	**5.2 %**

In both cases, the quantum yields are well below 100% which suggests that radical chain mechanism is not very likely.

More details on the calculation of the quantum yield (φ) of sample in Table S2.11.

Equation S2.1: Quantum yield calculation.

$$\Phi = \frac{N_{prod}}{N_{ph,abs}} = N_A \cdot h \cdot c \frac{c_{prod} \cdot V}{P_{abs} \cdot \Delta t \cdot \lambda_{LED}}$$

constants	
N_A= 6.02214 × 10^{23} mol^{-1}	*Avogadro constant*
h= 6.62607004 × 10^{-34} Js	*Planck constant*
c= 299792458 m/s	*Speed of light*

data for our system		
N_{prod}	*Number of product molecules*	
$N_{ph,abs}$	*Number of photons absorbed*	
c_{prod}	*Product concentration*	= 33 mmol/L
V	*Reaction volume*	= 1.00 mL
Δt	*Illumination time*	= 31962 s (6 h 6 min)
P_{abs}	*Absorbed power*	= 23.2 mW (calculated)
λ_{LED}	*Illumination wavelength*	= 401 nm

P_{abs} was calculated using the following equations:

Equation S2.2: Absorbed power calculation.

$$P_{abs} = (P_{ref} - P_{sample})f$$

Equation S2.3: Correction factor calculation.

$$f = \frac{1 + R\frac{P_{sample}}{P_{ref}}}{1 - R}$$

Data for our system		
P_{sample}	Average power during illumination	= 10.6 mW
P_{ref}	Reference power (solvent)	= 32.7 mW
f	Correction factor	= 1.049
R	Back reflection	= 0.0357 (parameter for fused silica cuvette)

2.6.11 Attempts of using I_2/PIDA system to functionalize benzylic positions

To demonstrate that the developed system can show reactivity which was not achievable by previously reported I_2/PIDA system, we performed reactions on two different substrates (Table S2.13 and Table S2.14).

Table S2.13: Ritter-type amination of challenging substrate **1a**.

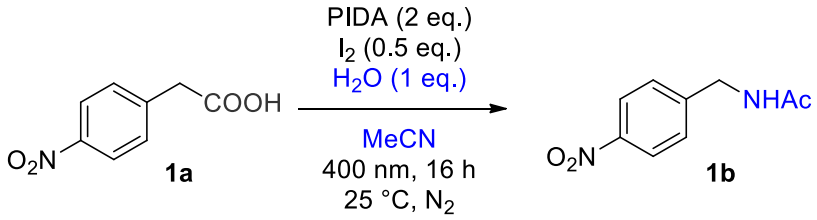

Entry	Deviation from standard conditions	BF_3	Yield (%)[a]
A	none	-	6
B	455 nm	-	7
C	CFL (ambient)	-	2
D	CFL (21 W, 10 cm from the vial)		3
E	400 nm	2 eq.	16
F	Our Selectfluor/PhI conditions	2 eq.	72 (63)

[a]Yields determined by ^{1}H NMR using 4-tertbutylbenzonitrile as internal standard.

Table S2.14: Ritter-type amination of substrate **8a**.

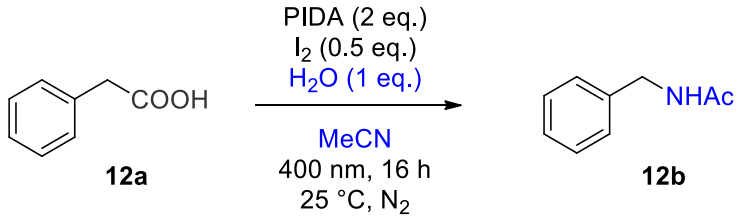

Entry	Deviation from standard conditions	BF_3	Yield (%)[a]	Note
A	none	-	32	
B	455 nm	-	20	
C	CFL (ambient)	-	24	
D	CFL (21 W, 10 cm from the vial)	-	23	
E	400 nm	2 eq.	15	iodination of the SM
F	Our Selectfluor/PhI conditions	2 eq.	62 (58)	

[a]Yields determined by ^{1}H NMR using 4-tertbutylbenzonitrile as internal standard.

2.6.12 Test of Brønsted acids for intermediates activation

Brønsted acids were found to be generally ineffective in the photocatalytic reaction of the carboxylic acid **1a** (Table S2.1). Nevertheless, we tested them on the proposed intermediate **1ii** and potential intermediate **1iii** to reassure they are not significantly contributing to the reactivity of the system. The benzyl alcohol intermediate **1iii** (potentially formed by substitution of benzyl iodide with water) is a known type of intermediate for Brønsted acid promoted Ritter-type amination.

The results in the Table S2.15 show that Brønsted acid activation is not important for neither of the intermediates under our conditions.

Table S2.15: Investigation of potential for Brønsted acid activation of potential intermediates

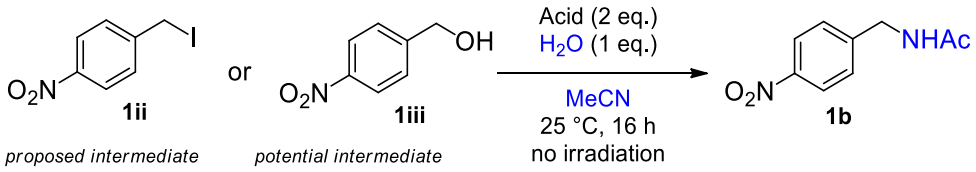

Entry	Intermediate	Acid (2 eq.)	Yield of 1b (%)
1	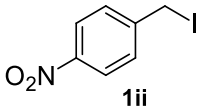	BF_3	0
2		HBF_4	0
3		CF_3SO_3H	0
4	*proposed intermediate*	H_2SO_4	trace
5	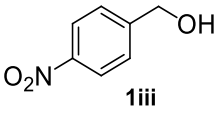	HBF_4	0
6		CF_3SO_3H	0
8	*potential intermediate*	H_2SO_4	0

2.6.13 Kinetic plots in the presence and absence of "I^+" sources.

We did the following kinetics investigations in order to find if the reactivity of the system comes from the photodecomposition of **1i** (or **1i** × BF_3 complex) to produce inorganic iodine. If the release of the iodine was a requirement for the successful progress of the reaction, we should be able to observe some specific traits in the kinetic profile of the reaction such as induction period and rate acceleration upon addition of iodine. The measurements were conducted with two different I^+ sources NIS and I_2, both used in 10 mol% quantity. This is enough to mimic the potential photodecomposition of **1i**. These two iodine sources were tested in different combinations with iodobenzene. PhI was used in 30 mol%, same as in the reaction conditions.

The reaction was set on a 0.2 mmol scale according to GP1 with internal standard (benzonitrile, 0.2 mmol) which was added after the degassing step. The samples were taken at indicated times and analyzed according to the general procedure for GC yield determination.

Surprisingly, the measurements revealed that the reaction catalyzed by "I^+" precursors I_2 and NIS is quite slow compared to the iodobenzene catalyzed reaction (Graph S2.6). Combination of iodobenzene with "I^+" sources also displayed a bit slower reaction rate. From these experiments we can conclude that iodine release is not required for the reaction to proceed. Even if small amount of iodine is released it is not significantly contributing to the overall reaction rate, because the direct radical oxidation pathway is a much faster process.

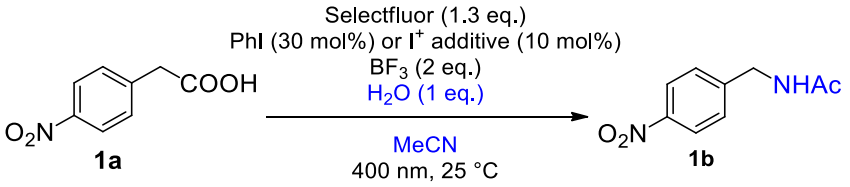

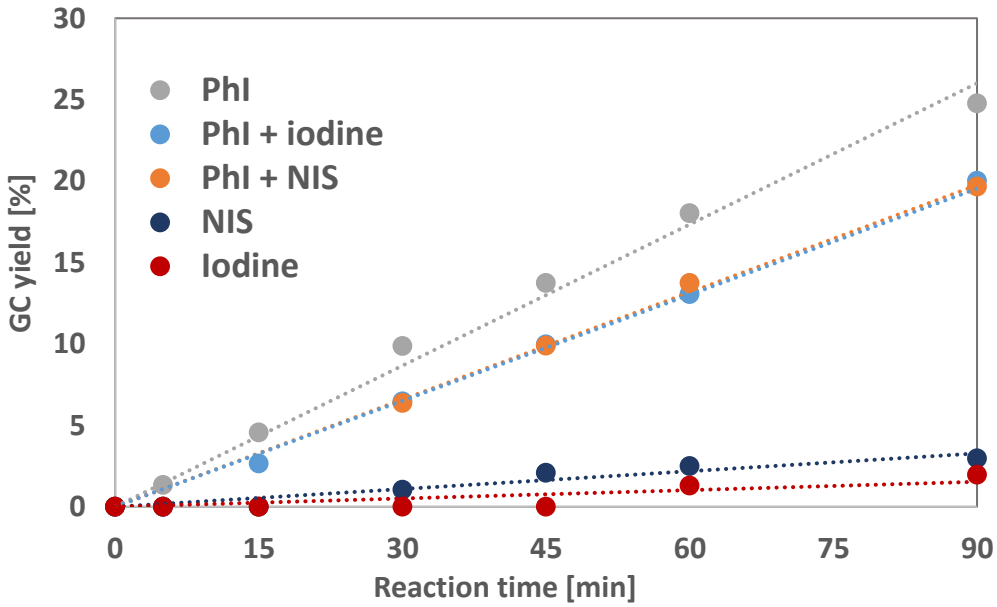

Graph S2.6: Kinetic profiles of reaction of **1a** in the presence of different I^+ sources.

Similarly, the effect of added iodine was tested also with the reaction of the hypervalent iodine (III) intermediate **1i-F** (Graph S2.7). The intermediate has a blocked *para* position, to prevent consumption of iodine for electrophilic

aromatic iodination under the reaction conditions. In this experiment, only I_2 was tested as a I^+ source because it was found in the previous experiment (Graph S2.6) that it behaves similarly as NIS. The kinetic profiles of the reactions with- and without iodine are almost overlaying, which additionally confirms that iodine is not required in the reaction and supports the direct oxidation of the radical as the main reaction mechanism.

The reaction was set on a 0.2 mmol scale according to GP1 with internal standard (benzonitrile, 0.2 mmol) which was added after the degassing step. The samples were taken at indicated times and analyzed according to the general procedure for GC yield determination.

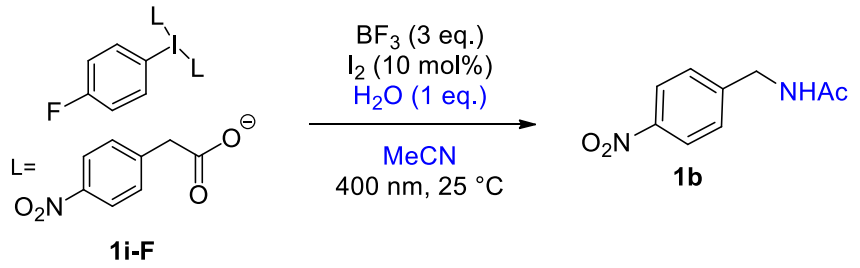

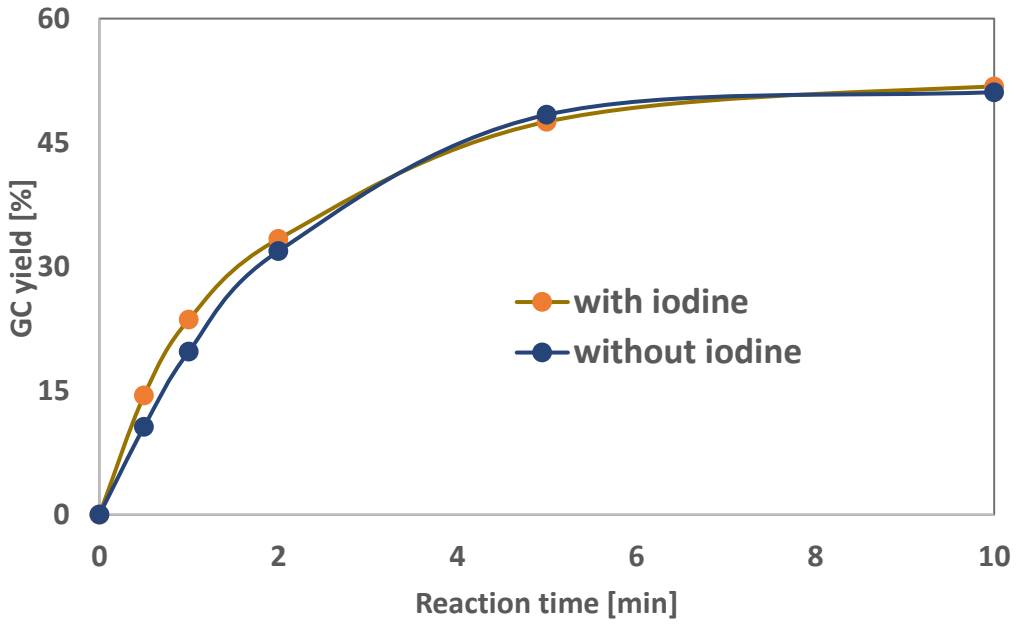

Graph S2.7:Kinetic plots from the intermediate **1i-F** in the presence of additional I_2.

2.7 Synthesis and characterization of compounds

2.7.1 Intermediates and starting materials

Synthesis of 1-(iodomethyl)-4-nitrobenzene (1i)

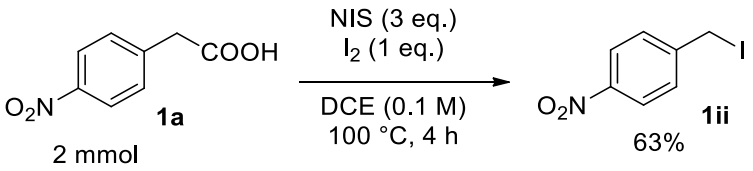

Compound **1ii** was synthesized according to a modified literature procedure.[3]

4-Nitrophenyl acetic acid (362 mg, 2 mmol, 1 eq.), NIS (1344 mg, 6 mmol, 3 eq.) and iodine (508 mg, 2 mmol, 1 eq.) where weighed into a 40 ml crimp cap reaction vial. 20 ml of DCE was added and the solution was degassed by 3 vacuum-nitrogen cycles. The reaction was heated to 100 °C. After 4 hours the heating was stopped, and the reaction was cooled down to room temperature. The reaction mixture was transferred into a separatory funnel and washed first with 10 ml of a saturated solution of $NaHCO_3$, and then with 5 ml of $Na_2S_2O_3$. The organic phase was dried over sodium sulphate and transferred into an RB flask. The dried organic phase was used to prepare a dry load for silica gel column chromatography. The dry load was used for the silica gel column chromatography (petrol ether/ethyl acetate). Pure product (330 mg, 63%) was obtained as a white solid.

1-(iodomethyl)-4-nitrobenzene (1ii)

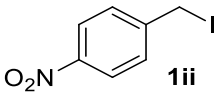

Yield	63%, white solid
^{1}H NMR	^{1}H NMR (300 MHz, $CDCl_3$) δ 8.16 (d, *J* = 8.5 Hz, 2H), 7.52 (d, *J* = 8.6 Hz, 2H), 4.48 (s, 2H).
^{13}C NMR	^{13}C NMR (75 MHz, $CDCl_3$) δ 145.1, 144.7, 127.5, 122.0, 0.0.

Synthesis of (R)-2-iodobutane (37ii-R)

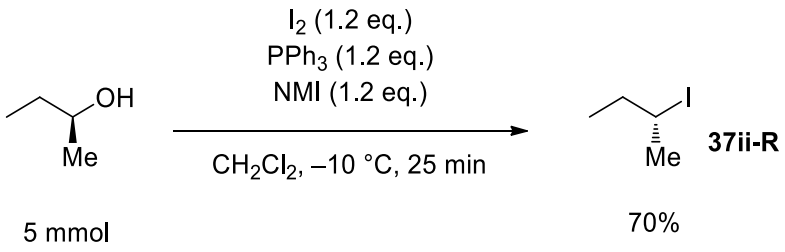

Compound 1i was synthesized according to a modified literature procedure.[1]

A dry and argon-flushed Schlenk-flask was charged with a solution of iodine (1.52 g, 6 mmol, 1.2 equiv.) in DCM (ca. 0.2 M solution) and cooled to −10 °C. Triphenylphosphine (1.57 g, 6 mmol, 1.2 equiv) was added in one portion and the resulting yellow suspension was stirred for 1 h at −10 °C. Then N-methylimidazole (0.49 g, 6 mmol, 1.2 equiv) was added dropwise. The reaction mixture was further stirred for 10 min after which the (S)-butan-2-ol (0.37 g, 5 mmol, dissolved in 10 ml DCM) was added over a period of 15 min. The reaction was stirred for further 10 min at −10 °C and then quenched with freshly prepared sat. aq. $NaHSO_3 \times Na_2S_2O_5$. The layers were separated, and the aqueous layer was extracted with dichloromethane (3 × 50 mL). The combined organic phases were dried over $MgSO_4$, and most of the solvent was removed under reduced pressure (700 mbar at 30 °C). Then, 50 ml of pentane was added and the byproduct triphenylphosphine oxide has crushed out. The resulting suspension was transferred on a silica column and washed with around 40 ml of pentane (2-3 column volumes) of the eluent. The collected solvents (pentane and DCM) have been removed using rotary evaporator (700 mbar at 30 °C), and the remaining traces of the solvents have been removed using Schlenk line vacuum (200 mbar at r.t. for 2 min). Pure product was obtained as a colorless oil (645 mg, 70%).

Analysis of the prepared 2-iodobutane by measuring optical rotation ($\alpha_D^{17} = 32.0$ °, c = 1 in $CHCl_3$, literature value[4] $\alpha_D^{17} = 31.98$ °) revealed that the product is sufficiently enantioenriched to be used in the following mechanistic studies.

(R)-2-iodobutane (37ii-R)

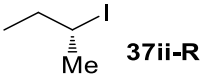

Yield	70%, colorless oil
^{1}H NMR	^{1}H NMR (400 MHz, $CDCl_3$) δ 4.25 – 4.07 (m, 1H), 1.92 (d, *J* = 6.8 Hz, 3H), 1.88 – 1.75 (m, 1H), 1.75 – 1.63 (m, 1H), 1.00 (t, *J* = 7.2 Hz, 3H).
^{13}C NMR	^{13}C NMR (101 MHz, CDCl3) δ 36.0, 32.9, 28.5, 14.2.
Specific rotation	$\alpha_D^{17} = 32.0$ °, c = 1 in $CHCl_3$ (literature: 31.98 °)[4]

Synthesis of 4-Fluoroiodobenzene diacetate (F-PIDA)

We synthesized fluorinated PIDA analogue by following a slightly modified protocol described in the literature.[5]

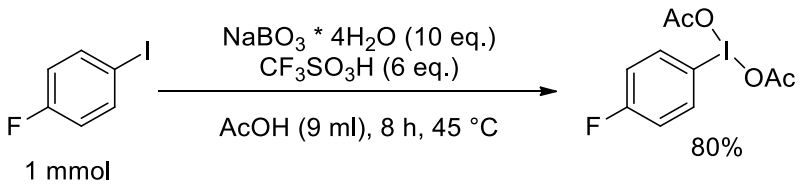

Sodium perborate tetrahydrate (10 mmol) was slowly added portionwise during 10 min to a stirred solution of iodobenzene (1 mmol) in glacial acetic acid (9 mL) with CF_3SO_3H (6 mmol) at 40-45 °C, and the mixture was stirred at this temperature until TLC analysis indicated completion of reaction. Reaction time needed 3 h. The solution was then concentrated to half its volume by evaporation of acetic acid under reduced pressure, and water (10 mL) was added. The product was obtained by extraction of the filtrate with dichloromethane (3 × 10 mL) followed by drying of the combined extracts (anhydrous Na_2SO_4), filtration, and removal of the solvent by evaporation under reduced pressure. The product was used without any further purification.

4-Fluoroiodobenzene diacetate (F-PIDA)

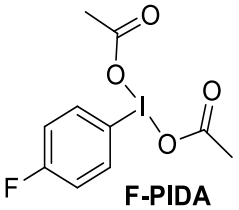

Yield	80% (270 mg, 0.80 mmol), white solid
^{1}H NMR	^{1}H NMR (300 MHz, $CDCl_3$) δ 8.14 – 7.99 (m, 2H), 7.25 – 7.11 (m, 2H), 2.01 (s, 6H).
^{13}C NMR	^{13}C NMR (75 MHz, $CDCl_3$) δ 176.5, 164.4 (d, *J* = 254.6 Hz), 137.6 (d, *J* = 8.8 Hz), 118.6 (d, *J* = 22.8 Hz), 115.6, 20.4.

Synthesis of (Di-4-nitrophenylacetoxyiodo) benzene (1ii) and other hypervalent iodine (III) reagents

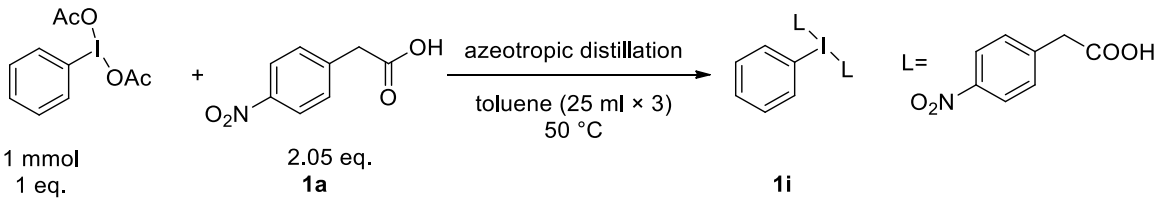

1 mmol
1 eq.

2.05 eq.
1a

1i

A 100 ml round-bottom flask was charged with phenyliodine(III) diacetate (PIDA) (322 mg, 1 mmol, 1 eq.), nitrophenylacetic acid (371 mg, 2.05 mmol, 2.05 eq.) and 25 ml of toluene. The solvent was removed using a rotary evaporator for ca. 15 min (bath temperature 50 °C). The solvent was added and removed two more times to completely remove acetic acid. The white residue was NMR-pure desired product obtained in quantitative yield. It was used in photochemical reactions without any additional purification.

Iodobenzene bis(4-nitrophenylacetate) (1i also HIR 5)

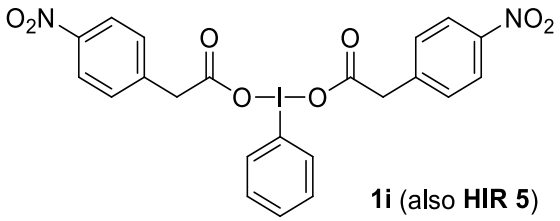

1i (also **HIR 5**)

Yield	Quant., white powder
^{1}H NMR	^{1}H NMR (300 MHz, CDCl3) δ 8.11 (d, J = 8.9 Hz, 4H), 8.02 – 7.94 (m, 2H), 7.62 (t, J = 7.5 Hz, 1H), 7.47 (t, J = 7.7 Hz, 2H), 7.34 (d, J = 8.8 Hz, 4H), 3.67 (s, 4H).
^{13}C NMR	^{13}C NMR (75 MHz, $CDCl_3$) δ 174.7, 147.0, 142.1, 134.8, 132.2, 131.1, 130.2, 123.6, 121.9, 40.6.
CRYSTAL STRUCTURE	CCDC 2091187

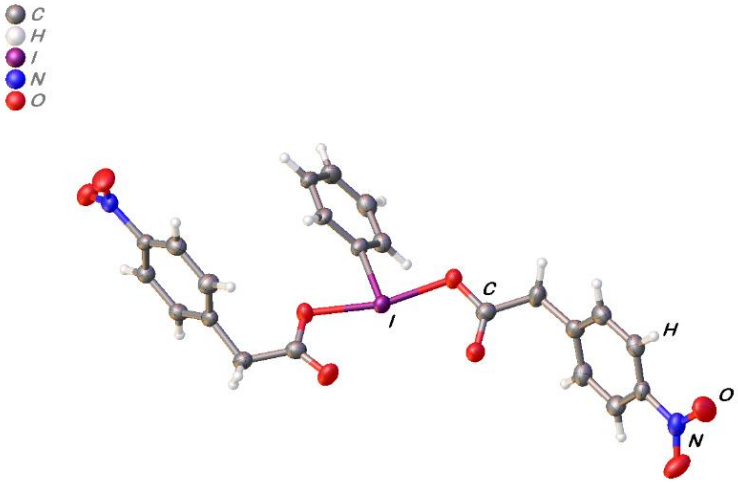

Crystallized from $CDCl_3$ (in the NMR tube)

Following the same procedure, we prepared also other hypervalent iodine reagents.

Iodobenzene dicylohexanecarboxylate (HIR 2)

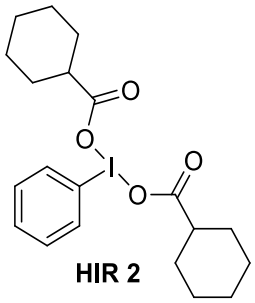

HIR 2

Yield	Quant., white powder
^{1}H NMR	^{1}H NMR (300 MHz, $CDCl_3$) δ 8.12 – 7.91 (m, 2H), 7.69 – 7.41 (m, 3H), 2.25 (tt, *J* = 11.1, 3.6 Hz, 2H), 1.86 – 1.52 (m, 10H), 1.44 – 1.06 (m, 10H).
^{13}C NMR	^{13}C NMR (75 MHz, $CDCl_3$) δ 181.2, 134.7, 131.5, 130.8, 121.9, 43.3, 29.6, 25.8, 25.6.

Iodobenzene bis(adamantane-1-carboxylate) (HIR 3)

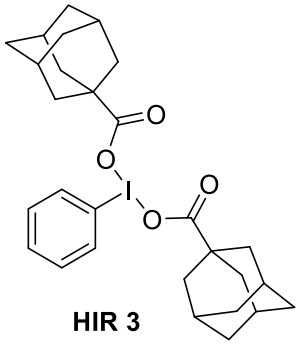

HIR 3

Yield	Quant., crystalline white solid
^{1}H NMR	^{1}H NMR (300 MHz, $CDCl_3$) δ 7.99 (d, *J* = 8.4 Hz, 2H), 7.58 – 7.42 (m, 3H), 1.94 (s, 6H), 1.80 (d, *J* = 2.9 Hz, 12H), 1.64 (s, 12H).
^{13}C NMR	^{13}C NMR (75 MHz, $CDCl_3$) δ 182.7, 134.3, 131.2, 130.6, 121.9, 41.1, 39.4, 36.5, 28.2.

Iodobenzene diphenylacetate (HIR 4)

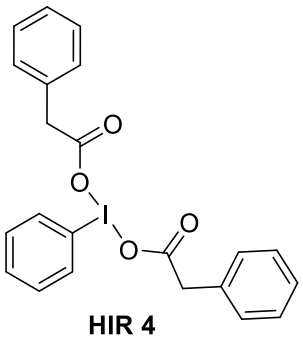

HIR 4

Yield	Quant., colorless oil
^{1}H NMR	^{1}H NMR (300 MHz, $CDCl_3$) δ 7.97 – 7.89 (m, 2H), 7.60 – 7.52 (m, 1H), 7.47 – 7.38 (m, 2H), 7.32 – 7.15 (m, 10H), 3.58 (s, 4H).
^{13}C NMR	^{13}C NMR (75 MHz, $CDCl_3$) δ 176.3, 134.8, 134.6, 131.7, 130.9, 129.2, 128.5, 126.9, 122.0, 41.1.

4-Fluoroiodobenzene bis(4-nitrophenylacetate) (1i-F)

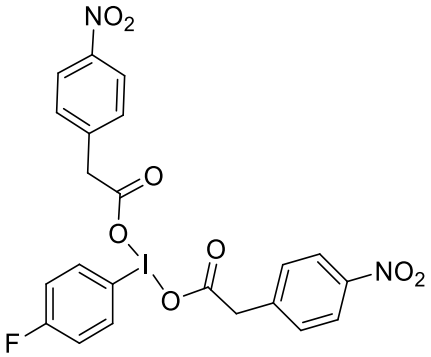

1i-F

Yield	Quant., white powder
^{1}H NMR	^{1}H NMR (400 MHz, $CDCl_3$) δ 8.12 (d, *J* = 8.7 Hz, 4H), 8.02 – 7.95 (m, 2H), 7.35 (d, *J* = 8.7 Hz, 4H), 7.20 – 7.11 (m, 2H), 3.67 (s, 4H).
^{13}C NMR	^{13}C NMR (101 MHz, $CDCl_3$) δ 174.8, 164.5 (d, *J* = 255.8 Hz), 147.1, 141.9, 137.5 (d, *J* = 8.9 Hz), 130.2, 123.7, 118.8 (d, *J* = 22.9 Hz), 115.7, 40.5.
^{19}F NMR	^{19}F NMR (376 MHz, $CDCl_3$) -104.79.

Synthesis of starting material 9a

Suzuki coupling conditions were adapted from the literature.[6]

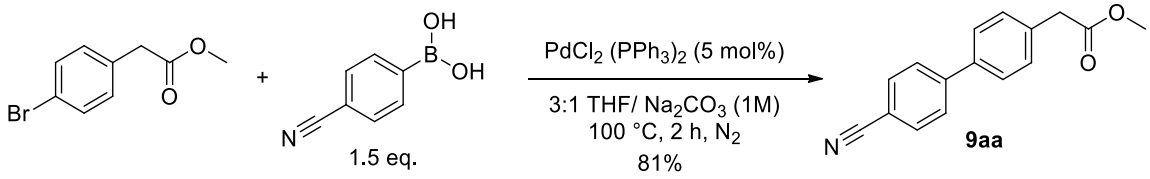

Aryl bromide (2.0 mmol, 460 mg) and the boronic acid (1.5 eq 441 mg) were weighted in a 60 ml glas crimp vial and dissolved in a mixture of 30 ml THF and 10 ml 1 M Na_2CO_3 (aq). Then, $PdCl_2(PPh_3)_2$ (5 mol%, 205 mg) was added, and the vial was closed and degassed. The reaction was heated for 2 h at 100 °C. Afterwards it was cooled and diluted with EtOAc (100 mL) and water (30 mL). The organic layer was dried over Na_2SO_4 and used to prepare a dry load for the column chromatography (eluent DCM/MeOH).

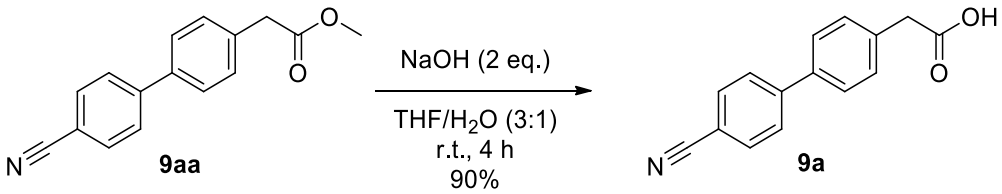

The compound **9aa** (1.5 mmol, 377 mg) and NaOH (2 eq., 120 mg) were dissolved in 5 ml of 3:1 THF/water mixture and stirred for 4 hours at room temperature. Then, the reaction mixture was acidified by the addition of 1M HCl to pH <1. The reaction mixture was extracted with 2× 20 ml EA. Organic layers were combined and dried over Na_2SO_4. Filtration of the drying agent and removal of the solvent gave us the desired product in **9a** in 90% yield.

methyl 2-(4′-cyano-[1,1′-biphenyl]-4-yl)acetate (9aa)

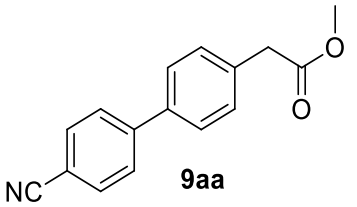

9aa

Yield	81% (407 mg, 1.62 mmol), White solid
^{1}H NMR	^{1}H NMR (300 MHz, $CDCl_3$) δ 7.75 – 7.63 (m, 4H), 7.56 (d, *J* = 8.4 Hz, 2H), 7.40 (d, *J* = 8.4 Hz, 2H), 3.72 (s, 3H), 3.70 (s, 2H).
^{13}C NMR	^{13}C NMR (75 MHz, $CDCl_3$) δ 171.8, 145.2, 138.1, 134.6, 132.7, 130.1, 127.7, 127.5, 119.0, 110.9, 52.2, 40.8.

2-(4′-cyano-[1,1′-biphenyl]-4-yl)acetic acid (9a)

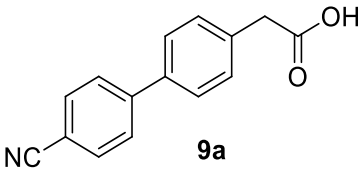

9a

Yield	90% (320 mg, 1.35 mmol), White solid
^{1}H NMR	^{1}H NMR (400 MHz, MeOD) δ 7.82 – 7.72 (m, 4H), 7.62 (d, *J* = 8.3 Hz, 2H), 7.41 (d, *J* = 8.3 Hz, 2H), 3.67 (s, 2H).
^{13}C NMR	^{13}C NMR (101 MHz, MeOD) δ 173.8, 145.3, 137.6, 135.5, 132.4, 129.9, 127.4, 126.9, 118.4, 110.4, 40.1.

2.7.2 Characterization of products

Characterization of the products which were not isolated

N-ethylacetamide (32b)

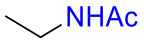

32b

Synthesized according to the GP2.

NMR yield 20%

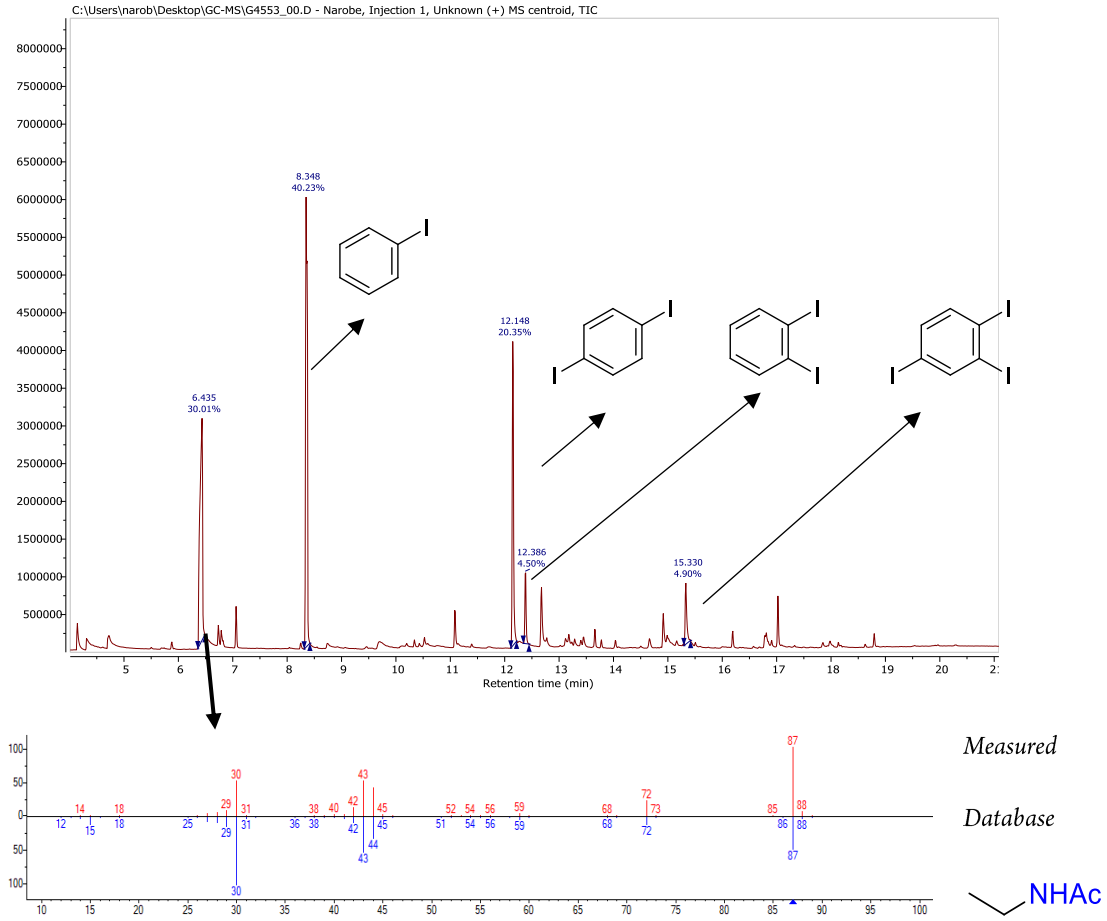

Figure S2.9: GC-MS chromatogram of the reaction mixture containing **32b**.

We tried to isolate N-ethylacetamide (**32b**), but we were not successful. The compound is miscible with water and a part of the compound is probably also lost by evaporation. Therefore, we think that the isolated yield (if we succeeded) would not be representative. We have ^{1}H NMR and GC-MS of the reaction mixture to confirm the identity and quantity.

N-propylacetamide (33b) and N-isopropylacetamide (33c)

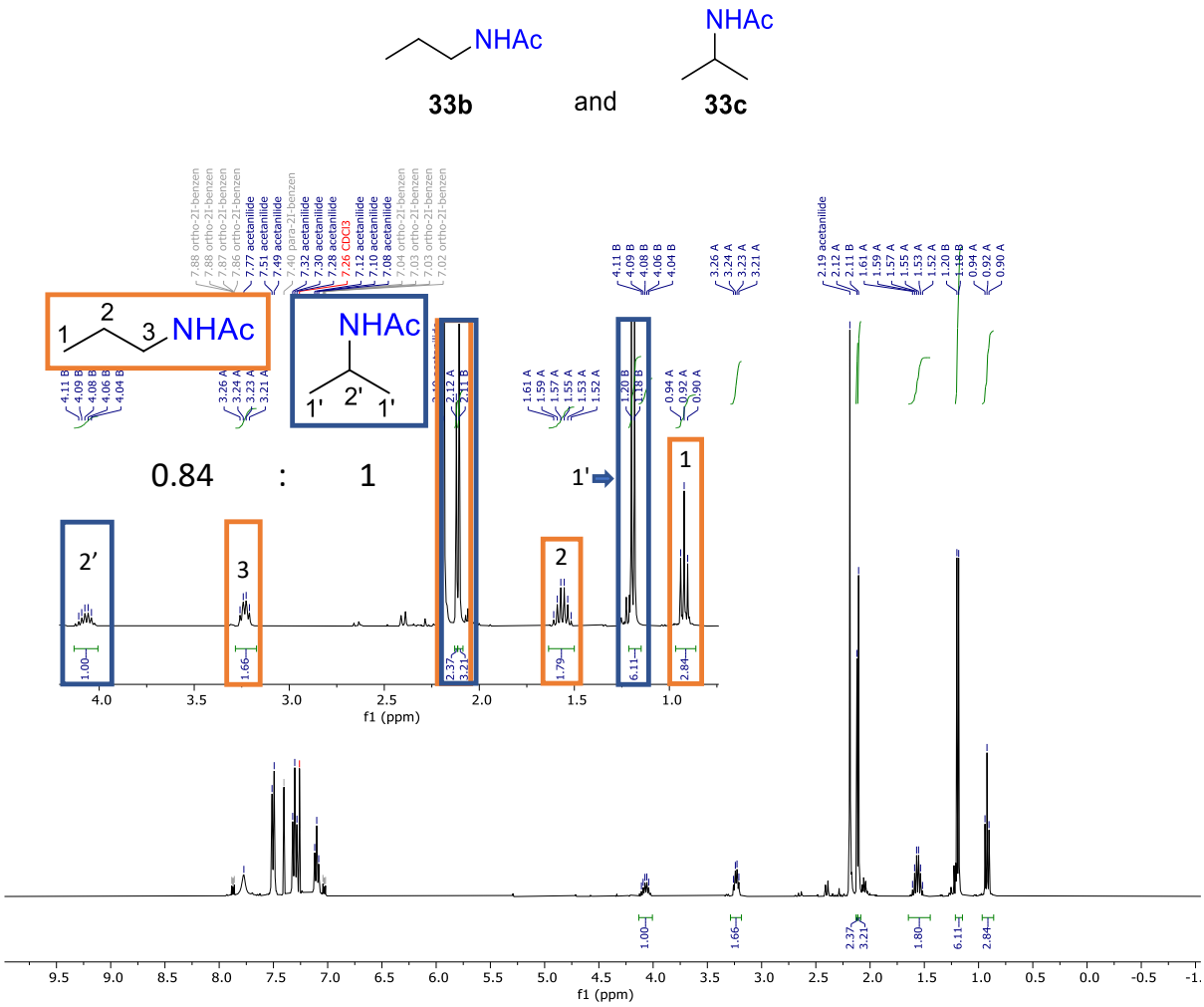

Figure S2.10: ^{1}H NMR spectrum (300 MHz in $CDCl_3$) of the reaction mixture II (see **Scheme S2.5**) with internal standard (acetanilide).

The NMR sample was then submitted also for GC-MS analysis.

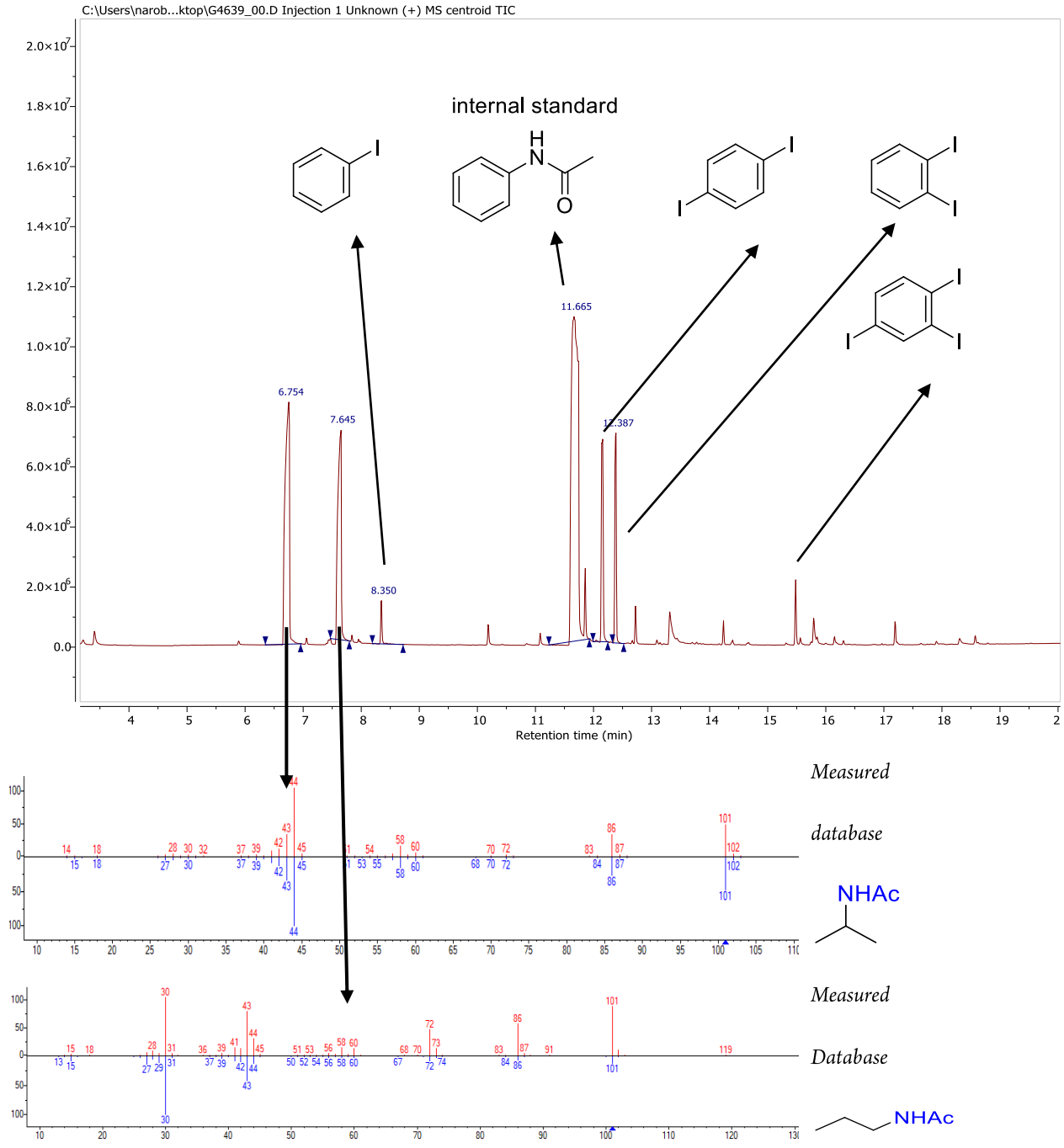

Figure S2.11: GC-MS chromatogram with fragmentation patterns of the reaction mixture II (see **Scheme S2.5**) with internal standard (acetanilide).

Characterization of products which were isolated.

N-(4-nitrobenzyl)acetamide (1b)

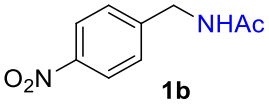

1b

Yield	63% (49 mg, 0.25 mmol), light yellow solid
^{1}H NMR	^{1}H NMR (400 MHz, $CDCl_3$) δ 8.11 (d, *J* = 8.7 Hz, 2H), 7.40 (d, *J* = 8.7 Hz, 2H), 6.42 (s, 1H), 4.49 (d, *J* = 6.1 Hz, 2H), 2.04 (s, 3H).
^{13}C NMR	^{13}C NMR (101 MHz, $CDCl_3$) δ 170.4, 147.1, 146.1, 128.2, 123.8, 42.9, 23.1.
HR-MS (ESI)	$(M+H)^+$: calc. 195.0764, found 195.0765
CRYSTAL STRUCTURE	CCDC 2091178

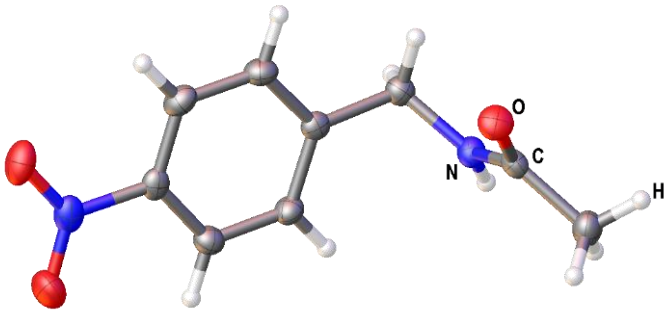

Crystalized from EtOH by slow evaporation of solvent at room temperature

N-(3-nitrobenzyl)acetamide (2b)

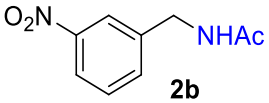

2b

Yield	67% (52 mg, 0.27 mmol), light yellow solid
^{1}H NMR	^{1}H NMR (400 MHz, $CDCl_3$) δ 8.13 – 8.03 (m, 2H), 7.60 (d, *J* = 7.5 Hz, 1H), 7.47 (t, *J* = 7.7 Hz, 1H), 6.52 (s, 1H), 4.49 (d, *J* = 6.1 Hz, 2H), 2.03 (s, 3H).
^{13}C NMR	^{13}C NMR (101 MHz, $CDCl_3$) δ 170.5, 148.4, 140.8, 133.9, 129.6, 122.4, 122.3, 42.8, 23.1.
HR-MS (ESI)	$(M+H)^+$: calc. 195.0764, found 195.0762

The compound was eluted with EA from the basic alumina column.

N-(4-cyanobenzyl)acetamide (3b)

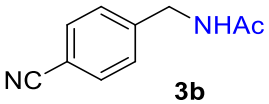

3b

Yield	49% (34 mg, 2.0 mmol), white solid
^{1}H NMR	^{1}H NMR (400 MHz, $CDCl_3$) δ 7.56 (d, *J* = 8.3 Hz, 2H), 7.35 (d, *J* = 8.3 Hz, 2H), 6.38 (s, 1H), 4.44 (d, *J* = 6.1 Hz, 2H), 2.02 (s, 3H).
^{13}C NMR	^{13}C NMR (101 MHz, $CDCl_3$) δ 170.4, 144.1, 132.4, 128.2, 118.7, 111.1, 43.1, 23.1.

HR-MS (ESI) $(M+H)^+$: calc. 175.0866, found 175.0865

N-(2-(trifluoromethyl)benzyl)acetamide (4b)

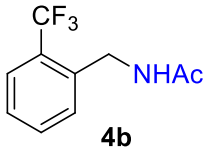

4b

Yield 74% (64 mg, 0.30 mmol), White solid

^{1}H NMR ^{1}H NMR (400 MHz, $CDCl_3$) δ 7.61 (d, *J* = 7.9 Hz, 1H), 7.55 – 7.44 (m, 2H), 7.37 – 7.30 (m, 1H), 6.28 (s, 1H), 4.55 (d, *J* = 6.0 Hz, 2H), 1.97 (s, 3H).

^{13}C NMR ^{13}C NMR (101 MHz, $CDCl_3$) δ 170.2, 139.3, 136.8 (d, *J* = 1.4 Hz), 132.3 (d, *J* = 0.6 Hz), 130.5, 127.5, 125.9 (q, *J* = 5.7 Hz), 121.7 (q, *J* = 274.8, 273.3 Hz), 40.1 (d, *J* = 2.3 Hz), 23.1.

^{19}F NMR ^{19}F NMR (376 MHz, $CDCl_3$) δ -60.01.

HR-MS (EI) $(M)^{+\cdot}$: calc. 217.07090, found 217.07047

N-(4-(trifluoromethyl)benzyl)acetamide (5b)

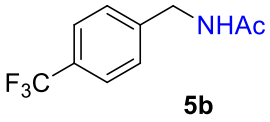

5b

Yield 59% (51 mg, 0.24 mmol), white solid

^{1}H NMR ^{1}H NMR (400 MHz, $CDCl_3$) δ 7.54 (d, *J* = 8.1 Hz, 2H), 7.34 (d, *J* = 8.0 Hz, 2H), 6.40 (s, 1H), 4.42 (d, *J* = 5.9 Hz, 2H), 1.99 (s, 3H).

^{13}C NMR ^{13}C NMR (101 MHz, $CDCl_3$) δ 170.3, 142.4, 129.7 (q, *J* = 32.5 Hz), 127.8, 125.5 (q, *J* = 3.8 Hz), 124.1 (q, *J* = 272.0 Hz), 43.1, 23.1.

^{19}F NMR ^{19}F NMR (377 MHz, $CDCl_3$) δ -63.1.

HR-MS (ESI) $(M+H)^+$: calc. 218.0787, found 218.0788

N-(4-(methylsulfonyl)benzyl)acetamide (6b)

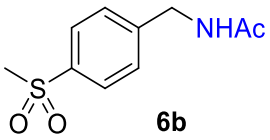

6b

Yield 65% (59 mg, 0.26 mmol), white solid

^{1}H NMR ^{1}H NMR (400 MHz, $CDCl_3$) δ 7.73 (d, *J* = 8.3 Hz, 2H), 7.37 (d, *J* = 8.2 Hz, 2H), 4.43 (d, *J* = 6.1 Hz, 2H), 2.98 (s, 3H), 2.01 (s, 3H).

^{13}C NMR ^{13}C NMR (101 MHz, $CDCl_3$) δ 170.6, 145.3, 139.1, 128.25, 127.5, 44.6, 42.8, 23.1.

HR-MS (EI) $(M)^{+\cdot}$: calc. 227.06107, found 227.06057

The compound was eluted with EA from the basic alumina column.

N-(3,5-bis(trifluoromethyl)benzyl)acetamide (7b)

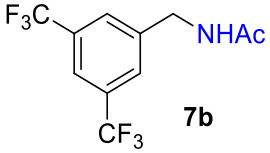

7b

Yield 73% (83 mg, 0.29 mmol), white solid

^{1}H NMR	^{1}H NMR (400 MHz, $CDCl_3$) δ 7.74 (s, 1H), 7.69 (s, 2H), 4.47 (d, *J* = 6.1 Hz, 2H), 2.00 (s, 3H).
^{13}C NMR	^{13}C NMR (101 MHz, $CDCl_3$) δ 170.7, 141.2, 131.9 (q, *J* = 33.3 Hz), 127.7 (d, *J* = 2.6 Hz), 123.2 (q, *J* = 272.6 Hz), 121.3 (p, *J* = 3.8 Hz), 42.7, 22.9.
^{19}F NMR	^{19}F NMR (376 MHz, $CDCl_3$) δ -63.5.
HR-MS (EI)	$(M)^{+\cdot}$: calc. 285.05828, found 285.05874

N-(4-(trifluoromethoxy)benzyl)acetamide (8b)

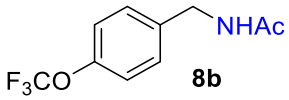

8b

Yield	80% (74 mg, 0.32 mmol), White solid
^{1}H NMR	^{1}H NMR (400 MHz, $CDCl_3$) δ 7.24 (d, *J* = 8.6 Hz, 2H), 7.12 (d, *J* = 8.1 Hz, 2H), 6.53 (s, 1H), 4.34 (d, *J* = 5.9 Hz, 2H), 1.95 (s, 3H).
^{13}C NMR	^{13}C NMR (101 MHz, $CDCl_3$) δ 170.3, 148.4 (d, *J* = 1.8 Hz), 137.3, 129.1, 121.1, 120.5 (q, *J* = 259.4 Hz), 42.8, 23.0.
^{19}F NMR	^{19}F NMR (376 MHz, $CDCl_3$) δ -58.49.
HR-MS (EI)	$(M)^{+\cdot}$: calc. 233.06581, found 233.06667

N-((4'-cyano-[1,1'-biphenyl]-4-yl)methyl)acetamide (9b)

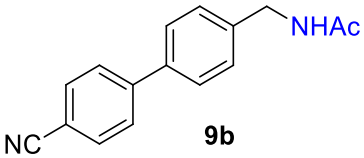

9b

Yield	77% (77 mg, 0.31 mmol), pale yellow solid
^{1}H NMR	^{1}H NMR (400 MHz, $CDCl_3$) δ 7.71 (d, *J* = 8.6 Hz, 2H), 7.65 (d, *J* = 8.6 Hz, 2H), 7.55 (d, *J* = 8.3 Hz, 2H), 7.39 (d, *J* = 8.3 Hz, 2H), 5.94 (s, 1H), 4.48 (d, *J* = 5.9 Hz, 2H), 2.05 (s, 3H).
^{13}C NMR	^{13}C NMR (101 MHz, $CDCl_3$) δ 170.1, 145.2, 139.1, 138.4, 132.7, 128.6, 127.7, 127.6, 118.9, 111.0, 43.3, 23.3.
HR-MS (EI)	$(M)^{+\cdot}$: calc. 250.11006, found 250.11010

The compound does not dissolve very well in EA or DCM. We used a bit more EA (5 ml) with a small amount of MeOH (ca. 10mol%) to completely dissolve the compound before filtration through the basic alumina column.

N-(1-(3-benzoylphenyl)ethyl)acetamide (10b)

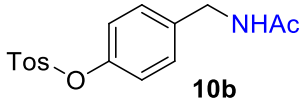

10b

Yield	55% (70.2 mg, 0.22 mmol), colorless oil
^{1}H NMR	^{1}H NMR (400 MHz, $CDCl_3$) δ 7.80 – 7.72 (m, 3H), 7.65 – 7.51 (m, 3H), 7.47 (t, *J* = 7.6 Hz, 2H), 7.41 (t, *J* = 7.7 Hz, 1H), 6.18 (d, *J* = 6.3 Hz, 1H), 5.16 (p, *J* = 7.1 Hz, 1H), 1.49 (d, *J* = 7.0 Hz, 3H).
^{13}C NMR	^{13}C NMR (101 MHz, $CDCl_3$) δ 196.7, 169.5, 143.9, 137.9, 137.5, 132.6, 130.7, 130.1, 129.3, 128.5, 128.4, 127.2, 48.8, 22.0.
HR-MS (ESI)	$(M+H)^+$: calc. 320.0951, found 320.0949

Remarks: EtOAc was used to completely wash the product from basic alumina column.

N-(4-methylbenzyl)acetamide (11b)

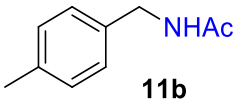

11b

Yield	26% (17 mg, 0.10 mmol), White solid
^{1}H NMR	^{1}H NMR (400 MHz, $CDCl_3$) δ 7.22 – 7.07 (m, 4H), 6.09 (s, 1H), 4.37 (d, *J* = 5.2 Hz, 2H), 2.33 (s, 3H), 2.01 (s, 3H).
^{13}C NMR	^{13}C NMR (101 MHz, $CDCl_3$) δ 170.1, 137.3, 135.1, 129.4, 127.9, 77.4, 43.6, 23.1, 21.1.
HR-MS (ESI)	$(M+H)^+$: calc. 164.1070, found 164.1068

N-benzylacetamide (12b)

12b

Yield	58% (34.6 mg, 0.23 mmol), White solid
^{1}H NMR	^{1}H NMR (300 MHz, $CDCl_3$) δ 7.40 – 7.20 (m, 5H), 6.18 (s, 1H), 4.38 (d, *J* = 5.7 Hz, 2H), 1.98 (s, 3H).
^{13}C NMR	^{13}C NMR (75 MHz, $CDCl_3$) δ 170.1, 138.3, 128.7, 127.8, 127.5, 43.7, 23.2.
HR-MS (ESI)	$(M+H)^+$: calc. 150.0913, found 150.0914

N-((perfluorophenyl)methyl)acetamide (13b)

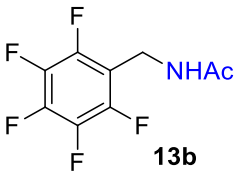

13b

Yield	48% (46 mg, 0.19 mmol), white solid
^{1}H NMR	^{1}H NMR (400 MHz, $CDCl_3$) δ 6.31 (s, 1H), 4.50 (d, *J* = 5.9 Hz, 2H), 1.97 (s, 3H).
^{13}C NMR	^{13}C NMR (101 MHz, $CDCl_3$): (except for C_6F_5) δ 170.0, 31.3, 22.9.
^{19}F NMR	NMR (376 MHz, $CDCl_3$) δ -143.5 (dd, *J* = 22.0, 8.2 Hz), -155.4 (t, *J* = 20.8 Hz), -162.5 (td, *J* = 22.2, 8.5 Hz).
HR-MS (EI)	$(M)^{+\cdot}$: calc. 239.03641, found 239.03586

N-(2-fluorobenzyl)acetamide (14b)

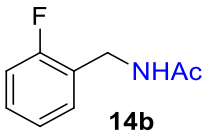

14b

Yield	51% (34 mg, 0.20 mmol) White solid
^{1}H NMR	^{1}H NMR (400 MHz, $CDCl_3$) δ 7.31 (td, *J* = 7.6, 1.7 Hz, 1H), 7.24 (tdd, *J* = 7.4, 5.3, 2.3 Hz, 1H), 7.08 (td, *J* = 7.5, 1.1 Hz, 1H), 7.02 (ddd, *J* = 9.5, 8.2, 1.0 Hz, 1H), 6.19 (s, 1H), 4.44 (d, *J* = 5.8 Hz, 2H), 1.98 (s, 3H).
^{13}C NMR	^{13}C NMR (101 MHz, $CDCl_3$) δ 170.2, 161.0 (d, *J* = 246.0 Hz), 130.3 (d, *J* = 4.3 Hz), 129.3 (d, *J* = 8.2 Hz), 125.2 (d, *J* = 14.8 Hz), 124.3 (d, *J* = 3.6 Hz), 115.3 (d, *J* = 21.3 Hz), 37.6 (d, *J* = 3.9 Hz), 23.1.
^{19}F NMR	^{19}F NMR (376 MHz, $CDCl_3$) δ -119.6.
HR-MS (ESI)	$(M+H)^+$: calc. 168.0819, found 168.0821

N-(3-fluorobenzyl)acetamide (15b)

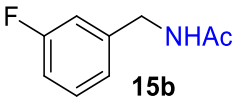

15b

Yield	52% (35 mg, 0.21 mmol), White solid
^{1}H NMR	^{1}H NMR (400 MHz, $CDCl_3$) δ 7.30 – 7.22 (m, 1H), 7.01 (d, *J* = 7.6 Hz, 1H), 6.99 – 6.89 (m, 2H), 6.31 (s, 1H), 4.37 (d, *J* = 5.9 Hz, 2H), 1.99 (s, 3H).
^{13}C NMR	^{13}C NMR (101 MHz, $CDCl_3$) δ 170.3, 163.0 (d, *J* = 246.3 Hz), 140.9 (d, *J* = 7.1 Hz), 130.2 (d, *J* = 8.2 Hz), 123.2 (d, *J* = 2.9 Hz), 114.5 (d, *J* = 19.7 Hz), 114.3 (d, *J* = 19.0 Hz), 43.1 (d, *J* = 1.7 Hz), 23.1.
^{19}F NMR	^{19}F NMR (376 MHz, $CDCl_3$) δ -113.4.
HR-MS (ESI)	$(M+H)^+$: calc. 168.0819, found 168.0820

N-(4-fluorobenzyl)acetamide (16b)

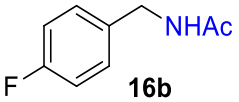

16b

Yield	59% (39 mg, 0.24 mmol), White solid
^{1}H NMR	^{1}H NMR (400 MHz, $CDCl_3$) δ 7.22 (dd, *J* = 8.7, 5.4 Hz, 2H), 6.98 (t, *J* = 8.7 Hz, 2H), 6.26 (s, 1H), 4.35 (d, *J* = 5.7 Hz, 2H), 1.98 (s, 3H).
^{13}C NMR	^{13}C NMR (101 MHz, $CDCl_3$) δ 170.1, 162.1 (d, *J* = 245.6 Hz), 134.1 (d, *J* = 3.2 Hz), 129.4 (d, *J* = 8.1 Hz), 115.5 (d, *J* = 21.5 Hz), 42.9, 23.1.
^{19}F NMR	^{19}F NMR (377 MHz, $CDCl_3$) δ -115.6.
HR-MS (ESI)	$(M+H)^+$: calc. 168.0819, found 168.0821

N-(4-chlorobenzyl)acetamide (17b)

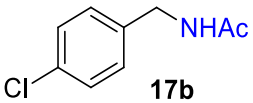

17b

Yield	63% (46 mg, 0.25 mmol), White solid
^{1}H NMR	^{1}H NMR (400 MHz, $CDCl_3$) δ 7.26 (d, *J* = 8.4 Hz, 2H), 7.16 (d, *J* = 8.6 Hz, 2H), 6.35 (s, 1H), 4.32 (d, *J* = 5.8 Hz, 2H), 1.97 (s, 3H).
^{13}C NMR	^{13}C NMR (101 MHz, $CDCl_3$) δ 170.3, 136.9, 133.2, 129.1, 128.8, 42.9, 23.1.
HR-MS (ESI)	$(M+H)^+$: calc. 184.0524, found 184.0524

N-(2-bromobenzyl)acetamide (18b)

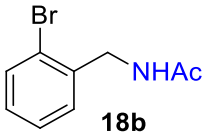

18b

Yield	54% (49 mg, 0.22 mmol) White solid
^{1}H NMR	^{1}H NMR (400 MHz, $CDCl_3$) δ 7.52 (dd, *J* = 8.0, 1.0 Hz, 1H), 7.34 (dd, *J* = 7.6, 1.6 Hz, 1H), 7.25 (td, *J* = 7.5, 1.1 Hz, 1H), 7.12 (td, *J* = 7.7, 1.7 Hz, 1H), 6.28 (s, 1H), 4.46 (d, *J* = 6.0 Hz, 2H), 1.99 (s, 3H).
^{13}C NMR	^{13}C NMR (101 MHz, $CDCl_3$) δ 170.1, 137.3, 132.8, 130.3, 129.2, 127.7, 123.7, 43.9, 23.2.
HR-MS (ESI)	$(M+H)^+$: calc. 228.0019, found 228.0017

N-(3-bromobenzyl)acetamide (19b)

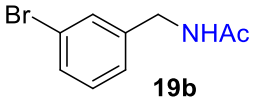

19b

Yield	52% (47 mg, 0.21 mmol), White solid
^{1}H NMR	^{1}H NMR (400 MHz, $CDCl_3$) δ 7.43 – 7.33 (m, 2H), 7.21 – 7.16 (m, 2H), 6.43 (s, 1H), 4.36 (d, *J* = 5.7 Hz, 2H), 2.02 (s, 3H).
^{13}C NMR	^{13}C NMR (101 MHz, $CDCl_3$) δ 170.4, 140.6, 130.7, 130.6, 130.3, 126.4, 122.7, 43.1, 23.1.
HR-MS (ESI)	$(M+H)^+$: calc. 228.0019, found 228.0017

N-(4-bromobenzyl)acetamide (20b)

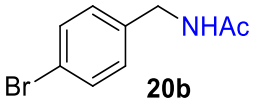

20b

Yield	35% (32 mg, 0.14 mmol) White solid
^{1}H NMR	^{1}H NMR (400 MHz, $CDCl_3$) δ 7.43 (d, *J* = 8.2 Hz, 1H), 7.13 (d, *J* = 8.2 Hz, 1H), 4.34 (d, *J* = 5.8 Hz, 1H), 2.00 (s, 2H).
^{13}C NMR	^{13}C NMR (101 MHz, $CDCl_3$) δ 170.1, 137.3, 131.8, 129.5, 121.4, 43.0, 23.2.
HR-MS (ESI)	$(M+H)^+$: calc. 228.0019, found 228.0018

N-(4-iodobenzyl)acetamide (21b)

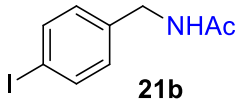

21b

Yield	65% (71.5 mg, 0.26 mmol), White solid
^{1}H NMR	^{1}H NMR (400 MHz, $CDCl_3$) δ 7.60 (d, *J* = 8.3 Hz, 2H), 6.97 (d, *J* = 8.3 Hz, 2H), 6.39 (s, 1H), 4.28 (d, *J* = 5.8 Hz, 2H), 1.96 (s, 3H).
^{13}C NMR	^{13}C NMR (101 MHz, $CDCl_3$) δ 170.2, 138.1, 137.7, 129.7, 92.8, 43.1, 23.1.
HR-MS (ESI)	$(M+H)^+$: calc. 275.9880, found 275.9883

N-(1-phenylethyl)acetamide (22b)

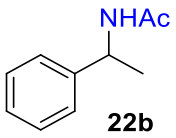

22b

Yield	57% (35 mg, 0.21 mmol), White solid
^{1}H NMR	^{1}H NMR (400 MHz, $CDCl_3$) δ 7.35 – 7.21 (m, 5H), 6.13 (s, 1H), 5.10 (p, *J* = 7.0 Hz, 1H), 1.95 (s, 3H), 1.46 (d, *J* = 6.9 Hz, 3H).
^{13}C NMR	^{13}C NMR (101 MHz, $CDCl_3$) δ 169.3, 143.3, 128.6, 127.3, 126.2, 48.8, 23.4, 21.8.
HR-MS (ESI)	$(M+H)^+$: calc. 164.1070, found 164.1070

2-acetamido-2-phenylethyl acetate (23b)

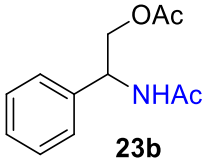

23b

Yield	55% (49 mg, 0.22 mmol), Oil which slowly crystalizes upon standing to give white solid
^{1}H NMR	^{1}H NMR (400 MHz, $CDCl_3$) δ 7.37 – 7.26 (m, 5H), 6.29 (d, *J* = 7.5 Hz, 1H), 5.28 (td, *J* = 7.8, 4.8 Hz, 1H), 4.39 (dd, *J* = 11.5, 7.3 Hz, 1H), 4.24 (dd, *J* = 11.5, 4.8 Hz, 1H), 2.03 (s, 3H), 2.00 (s, 3H).
^{13}C NMR	^{13}C NMR (101 MHz, $CDCl_3$) δ 171.2, 169.7, 138.4, 128.8, 128.0, 126.7, 66.1, 52.6, 23.3, 20.9.
HR-MS (ESI)	$(M+H)^+$: calc. 222.1125, found 222.1127

Remarks: EtOAc was used to completely wash the product from basic alumina column.

N-(bis(4-chlorophenyl)methyl)acetamide (24b)

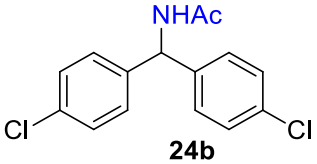

24b

Yield	65% (76 mg, 0.26 mmol), White solid
^{1}H NMR	^{1}H NMR (400 MHz, $CDCl_3$) δ 7.27 (d, *J* = 8.5 Hz, 4H), 7.10 (d, *J* = 8.4 Hz, 4H), 6.51 (d, *J* = 7.8 Hz, 1H), 6.11 (d, *J* = 7.9 Hz, 1H), 1.98 (s, 3H).
^{13}C NMR	^{13}C NMR (101 MHz, $CDCl_3$) δ 169.4, 139.6, 133.6, 128.9, 128.8, 55.9, 23.1.
HR-MS (ESI)	$(M+H)^+$: calc. 294.0447, found 294.0447

N-benzhydrylacetamide (25b)

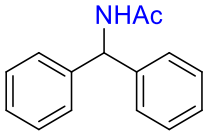

25b

Yield	67% (60 mg, 0.27 mmol), White solid
^{1}H NMR	^{1}H NMR (400 MHz, $CDCl_3$) δ 7.40 – 7.17 (m, 11H), 6.66 (d, *J* = 7.7 Hz, 1H), 6.26 (d, *J* = 8.1 Hz, 1H), 2.00 (s, 3H).
^{13}C NMR	^{13}C NMR (101 MHz, $CDCl_3$) δ 169.4, 141.6, 128.6, 127.5, 127.4, 57.0, 23.2.
HR-MS (ESI)	$(M+H)^+$: calc. 226.1226, found 226.1226

N-(1-(3-benzoylphenyl)ethyl)acetamide (26b)

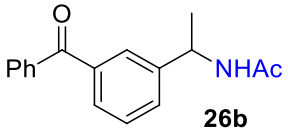

26b

Yield	67% (72 mg, 0.27 mmol), Colorless oil
^{1}H NMR	^{1}H NMR (400 MHz, $CDCl_3$) δ 7.78 – 7.71 (m, 3H), 7.64 – 7.49 (m, 3H), 7.45 (t, *J* = 7.6 Hz, 2H), 7.39 (t, *J* = 7.7 Hz, 1H), 6.46 (d, *J* = 7.4 Hz, 1H), 5.13 (p, *J* = 7.1 Hz, 1H), 1.95 (s, 3H), 1.45 (d, *J* = 7.1 Hz, 3H).
^{13}C NMR	^{13}C NMR (101 MHz, $CDCl_3$) δ 196.7, 169.6, 144.1, 137.8, 137.5, 132.6, 130.7, 130.1, 129.2, 128.5, 128.4, 127.2, 48.7, 23.2, 22.0.

HR-MS (ESI) $(M+H)^+$: calc. 268.1332, found 268.1333

N-(4-chlorobenzyl)acetamide (27b)

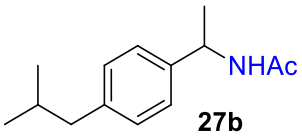

27b

Yield 22% (19 mg, 0.09 mmol), Light yellowish oil

^{1}H NMR ^{1}H NMR (400 MHz, $CDCl_3$) δ 7.21 (d, *J* = 8.0 Hz, 2H), 7.11 (d, *J* = 8.1 Hz, 2H), 5.89 (s, 1H), 5.10 (p, *J* = 7.0 Hz, 1H), 2.45 (d, *J* = 7.2 Hz, 2H), 1.97 (s, 3H), 1.84 (hept, *J* = 6.6 Hz, 1H), 1.48 (d, *J* = 6.9 Hz, 3H), 0.89 (d, *J* = 6.6 Hz, 7H).

^{13}C NMR ^{13}C NMR (101 MHz, $CDCl_3$) δ 169.2, 140.9, 140.3, 129.4, 126.0, 48.6, 45.0, 30.2, 23.4, 22.4, 21.6.

HR-MS (ESI) $(M+H)^+$: calc. 220.1696, found 220.1693

Remarks: TFA (2 eq.) was used instead of BF_3×MeCN

N-(1-(2-fluoro-[1,1'-biphenyl]-4-yl)ethyl)acetamide (28b)

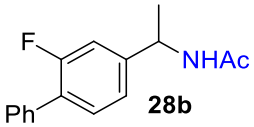

28b

Yield 34% (35 mg, 0.14 mmol), White solid

^{1}H NMR ^{1}H NMR (400 MHz, $CDCl_3$) δ 7.55 – 7.49 (m, 2H), 7.46 – 7.33 (m, 4H), 7.16 (dd, *J* = 7.9, 1.5 Hz, 1H), 7.11 (dd, *J* = 11.6, 1.5 Hz, 1H), 6.19 (d, *J* = 7.0 Hz, 1H), 5.13 (p, *J* = 7.1 Hz, 1H), 2.01 (s, 3H), 1.49 (d, *J* = 7.0 Hz, 3H).

^{13}C NMR ^{13}C NMR (101 MHz, $CDCl_3$) δ 169.5, 159.8 (d, *J* = 248.3 Hz), 145.1 (d, *J* = 7.1 Hz), 135.5, 131.0 (d, *J* = 3.9 Hz), 129.0 (d, *J* = 2.9 Hz), 128.5, 127.9 (d, *J* = 13.6 Hz), 127.7, 122.2 (d, *J* = 3.3 Hz), 113.8 (d, *J* = 23.6 Hz), 48.3 (d, *J* = 1.2 Hz), 23.3, 21.8.

^{19}F NMR ^{19}F NMR (376 MHz, $CDCl_3$) δ -118.0.

HR-MS (ESI) $(M+H)^+$: calc. 258.1289, found 258.1286

CRYSTAL STRUCTURE CCDC 2091186

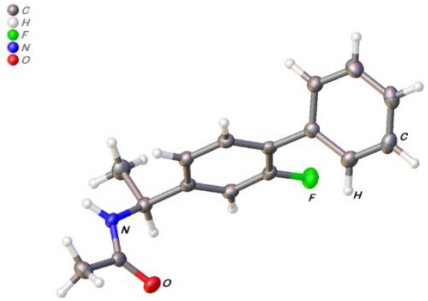

Crystalized from EtOH by slow evaporation of the solvent.

Remarks: TFA (2 eq.) was used instead of BF_3×MeCN

N-(1-(3-benzoylphenyl)ethyl)acetamide (29b)

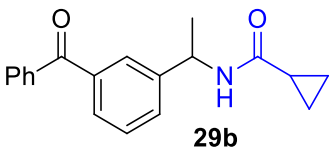

29b

Yield 41% (24 mg, 0.08 mmol), Colorless oil

^{1}H NMR	^{1}H NMR (400 MHz, $CDCl_3$) δ 7.80 – 7.72 (m, 3H), 7.65 – 7.51 (m, 3H), 7.47 (t, *J* = 7.6 Hz, 2H), 7.41 (t, *J* = 7.7 Hz, 1H), 6.18 (d, *J* = 6.3 Hz, 1H), 5.16 (p, *J* = 7.1 Hz, 1H), 1.49 (d, *J* = 7.0 Hz, 3H).
^{13}C NMR	^{13}C NMR (101 MHz, $CDCl_3$) δ 196.7, 169.5, 143.9, 137.9, 137.5, 132.6, 130.7, 130.1, 129.3, 128.5, 128.4, 127.2, 48.8, 22.0.
HR-MS (ESI)	$(M+H)^+$: calc. 294.1490, found 294.1489

Remarks: BF_3×Me_2O was used instead of BF_3×MeCN. Reaction was done on a 0.2 mmol scale

N-(1-(3-benzoylphenyl)ethyl)acetamide (30b)

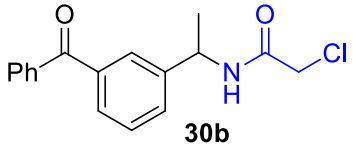

30b

Yield	56% (38 mg, 0.11 mmol), Colorless oil
^{1}H NMR	^{1}H NMR (400 MHz, $CDCl_3$) δ 7.80 – 7.72 (m, 3H), 7.65 – 7.51 (m, 3H), 7.47 (t, *J* = 7.6 Hz, 2H), 7.41 (t, *J* = 7.7 Hz, 1H), 6.18 (d, *J* = 6.3 Hz, 1H), 5.16 (p, *J* = 7.1 Hz, 1H), 1.49 (d, *J* = 7.0 Hz, 3H).
^{13}C NMR	^{13}C NMR (101 MHz, $CDCl_3$) δ 196.7, 169.5, 143.9, 137.9, 137.5, 132.6, 130.7, 130.1, 129.3, 128.5, 128.4, 127.2, 48.8, 22.0.
HR-MS (ESI)	$(M+H)^+$: calc. 302.0942, found 302.0941

Remarks: BF_3×Me_2O was used instead of BF_3×MeCN. Reaction was done on a 0.2 mmol scale

N-(1-(3-benzoylphenyl)ethyl)acetamide (31b)

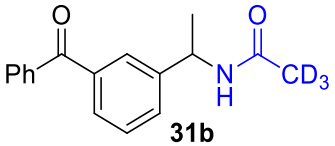

31b

Yield	27% (15 mg, 0.05 mmol), Colorless oil
^{1}H NMR	^{1}H NMR (400 MHz, $CDCl_3$) δ 7.80 – 7.72 (m, 3H), 7.65 – 7.51 (m, 3H), 7.47 (t, *J* = 7.6 Hz, 2H), 7.41 (t, *J* = 7.7 Hz, 1H), 6.18 (d, *J* = 6.3 Hz, 1H), 5.16 (p, *J* = 7.1 Hz, 1H), 1.49 (d, *J* = 7.0 Hz, 3H).
^{13}C NMR	^{13}C NMR (101 MHz, $CDCl_3$) δ 196.7, 169.5, 143.9, 137.9, 137.5, 132.6, 130.7, 130.1, 129.3, 128.5, 128.4, 127.2, 48.8, 22.0.
HR-MS (ESI)	$(M+H)^+$: calc.271.1520, found 271.1518

Remarks: BF_3×Me_2O was used instead of BF_3×MeCN. Reaction was done on a 0.2 mmol scale

N-cyclohexylacetamide (34b)

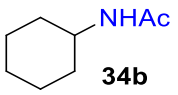

34b

Yield	50% (28.2 mg, 0.2 mmol), White solid
^{1}H NMR	^{1}H NMR (400 MHz, $CDCl_3$) δ 5.63 (s, 1H), 3.78 – 3.64 (m, 1H), 1.93 (s, 3H), 1.88 (dd, *J* = 12.4, 3.3 Hz, 2H), 1.68 (d, *J* = 13.6 Hz, 2H), 1.59 (d, *J* = 13.0 Hz, 1H), 1.33 (q, *J* = 12.3 Hz, 2H), 1.18 – 1.03 (m, 3H).
^{13}C NMR	^{13}C NMR (101 MHz, $CDCl_3$) δ 169.2, 48.3, 33.2, 25.5, 24.9, 23.5.
HR-MS (ESI)	$(M+H)^+$: calc. 142.1226, found 142.1227

N-cyclopentylacetamide (35b)

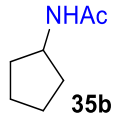

35b

Yield	32% (16 mg, 0.13 mmol), Light yellow oil
^{1}H NMR	^{1}H NMR (400 MHz, $CDCl_3$) δ 5.69 (s, 1H), 4.25 – 4.10 (m, 1H), 1.95 (s, 5H), 1.73 – 1.48 (m, 4H), 1.44 – 1.29 (m, 2H).
^{13}C NMR	^{13}C NMR (101 MHz, $CDCl_3$) δ 169.7, 51.3, 33.1, 23.7, 23.4.
HR-MS (ESI)	$(M+H)^+$: calc. 128.1070, found 128.1070

N-cyclobutylacetamide (36b)

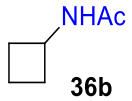

36b

Yield	31% (14 mg, 0.12 mmol), Light yellow oil
^{1}H NMR	^{1}H NMR (400 MHz, $CDCl_3$) δ 5.91 (s, 1H), 4.45 – 4.29 (m, 1H), 2.40 – 2.24 (m, 2H), 1.94 (s, 3H), 1.91 – 1.76 (m, 2H), 1.75 – 1.61 (m, 2H).
^{13}C NMR	^{13}C NMR (101 MHz, $CDCl_3$) δ 169.3, 44.8, 31.2, 23.2, 15.1.
HR-MS (ESI)	$(M+H)^+$: calc. 114.0913, found 114.0915

N-((3s,5s,7s)-adamantan-1-yl)acetamide (37b)

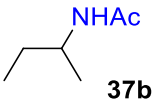

37b

Yield	44% (20 mg, 0.18 mmol), colorless oil
^{1}H NMR	^{1}H NMR (400 MHz, $CDCl_3$) δ 5.42 (s, 1H), 3.89 (dq, J = 8.4, 6.6 Hz, 1H), 1.96 (s, 3H), 1.44 (p, J = 7.3 Hz, 2H), 1.11 (d, J = 6.6 Hz, 3H), 0.89 (t, J = 7.5 Hz, 3H).
^{13}C NMR	^{13}C NMR (101 MHz, $CDCl_3$) δ 169.5, 46.7, 29.7, 23.5, 20.4, 10.3.

Remarks: EtOAc was used to completely wash the product from basic alumina column.

N-((3s,5s,7s)-adamantan-1-yl)acetamide (38b)

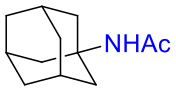

38b

Yield	52% (40 mg, 0.21 mmol), White solid
^{1}H NMR	^{1}H NMR (400 MHz, $CDCl_3$) δ 5.50 (s, 1H), 2.05 (s, 3H), 1.98 (d, J = 3.0 Hz, 6H), 1.93 (s, 3H), 1.66 (t, J = 2.9 Hz, 6H).
^{13}C NMR	^{13}C NMR (101 MHz, $CDCl_3$) δ 169.7, 52.2, 41.6, 36.3, 29.4, 24.5.
HR-MS (ESI)	$(M+H)^+$: calc. 194.1539, found 194.1539

N-((1r,3R,5S,7r)-3,5-dimethyladamantan-1-yl)acetamide (39b)

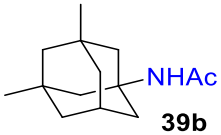

39b

Yield	54% (48 mg, 0.22 mmol), White solid

^{1}H NMR	^{1}H NMR (400 MHz, $CDCl_3$) δ 5.36 (s, 1H), 2.11 (p, *J* = 3.2 Hz, 1H), 1.89 (s, 3H), 1.80 (d, *J* = 2.9 Hz, 2H), 1.66 – 1.55 (m, 4H), 1.39 – 1.22 (m, 4H), 1.18 – 1.06 (m, 2H), 0.82 (s, 6H).
^{13}C NMR	^{13}C NMR (101 MHz, $CDCl_3$) δ 169.5, 53.5, 50.6, 47.6, 42.7, 40.1, 32.4, 30.1, 30.1, 24.6.
HR-MS (ESI)	$(M+H)^+$: calc. 222.1852, found 222.1854

N-(4-pentylbicyclo[2.2.2]octan-1-yl)acetamide (40b)

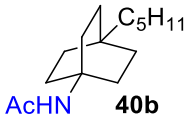

40b

Yield	51% (48 mg, 0.20 mmol), White solid
^{1}H NMR	^{1}H NMR (400 MHz, $CDCl_3$) δ 5.43 (s, 1H), 1.89 (s, 3H), 1.83 (dd, *J* = 9.7, 6.4 Hz, 6H), 1.42 (dd, *J* = 9.7, 6.3 Hz, 6H), 1.30 – 1.21 (m, 2H), 1.21 – 1.06 (m, 4H), 1.06 – 0.98 (m, 2H), 0.84 (t, *J* = 7.2 Hz, 3H).
^{13}C NMR	^{13}C NMR (101 MHz, $CDCl_3$) δ 169.8, 51.5, 41.2, 32.8, 31.1, 30.8, 30.2, 24.4, 23.4, 22.7, 14.1.
HR-MS (ESI)	$(M+H)^+$: calc. 238.2165, found 238.2164

methyl 4-acetamidobicyclo[2.2.2]octane-1-carboxylate (41b)

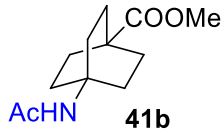

41b

Yield	84% (76 mg, 0.34 mmol), White solid
^{1}H NMR	^{1}H NMR (400 MHz, $CDCl_3$) δ 5.49 (s, 1H), 3.60 (s, 3H), 1.92 – 1.78 (m, 15H).
^{13}C NMR	^{13}C NMR (101 MHz, $CDCl_3$) δ 177.7, 169.9, 51.7, 51.1, 38.3, 29.9, 28.5, 24.3.
HR-MS (ESI)	$(M+H)^+$: calc. 226.1438, found 226.1435

2.8 Copies of NMR spectra

Dear reader, for the copies of the NMR spectra click on the URL below to open the full supporting information on the publisher's website (open access).

https://pubs.acs.org/doi/suppl/10.1021/acscatal.1c05077/suppl_file/cs1c05077_si_001.pdf

2.9 Notes and references

1. (a) Zhao, Y.; Xia, W. Recent advances in radical-based C–N bond formation via photo-/electrochemistry. *Chem. Soc. Rev.* **2018,** *47* (8), 2591-2608; (b) Yu, X.-Y.; Zhao, Q.-Q.; Chen, J.; Xiao, W.-J.; Chen, J.-R. When Light Meets Nitrogen-Centered Radicals: From Reagents to Catalysts. *Acc. Chem. Res.* **2020,** *53* (5), 1066-1083; (c) Murugesan, K.; Senthamarai, T.; Chandrashekhar, V. G.; Natte, K.; Kamer, P. C. J.; Beller, M.; Jagadeesh, R. V. Catalytic reductive aminations using molecular hydrogen for synthesis of different kinds of amines. *Chem. Soc. Rev.* **2020,** *49* (17), 6273-6328.

2. (a) Roughley, S. D.; Jordan, A. M. The Medicinal Chemist's Toolbox: An Analysis of Reactions Used in the Pursuit of Drug Candidates. *Journal of Medicinal Chemistry* **2011,** *54* (10), 3451-3479; (b) Froidevaux, V.; Negrell, C.; Caillol, S.; Pascault, J.-P.; Boutevin, B. Biobased Amines: From Synthesis to Polymers; Present and Future. *Chem. Rev.* **2016,** *116* (22), 14181-14224.

3. (a) Ritter, J. J.; Minieri, P. P. A New Reaction of Nitriles. I. Amides from Alkenes and Mononitriles1. *J. Am. Chem. Soc.* **1948,** *70* (12), 4045-4048; (b) Ritter, J. J.; Kalish, J. A New Reaction of Nitriles. II. Synthesis of *t*-Carbinamines. *J. Am. Chem. Soc.* **1948,** *70* (12), 4048-4050.

4. (a) Guérinot, A.; Reymond, S.; Cossy, J. Ritter Reaction: Recent Catalytic Developments. *Eur. J. Org. Chem.* **2012,** *2012* (1), 19-28; (b) Zhang, F.-M.; Chen, M.-E.; Chen, X.-W.; Hu, Y.-H.; Ye, R.; Lv, J.-W.; Li, B. Recent advances of Ritter reaction and its synthetic applications. *Org. Chem. Front.* **2021**.

5. Naredla, R. R.; Klumpp, D. A. Contemporary Carbocation Chemistry: Applications in Organic Synthesis. *Chem. Rev.* **2013,** *113* (9), 6905-6948.

6. (a) Li, Y.; Ge, L.; Muhammad, M. T.; Bao, H. Recent Progress on Radical Decarboxylative Alkylation for Csp^3–C Bond Formation. *Synthesis* **2017,** *49* (24), 5263-5284; (b) Zeng, Z.; Feceu, A.; Sivendran, N.; Gooßen, L. J. Decarboxylation-Initiated Intermolecular Carbon-Heteroatom Bond Formation. *Adv. Synth. Catal.* **2021,** *363* (11), 2678-2722; (c) Schwarz, J.; König, B. Decarboxylative reactions with and without light – a comparison. *Green Chem.* **2018,** *20* (2), 323-361.

7. (a) Pitzer, L.; Schwarz, J. L.; Glorius, F. Reductive radical-polar crossover: traditional electrophiles in modern radical reactions. *Chem. Sci.* **2019,** *10* (36), 8285-8291; (b) Donabauer, K.; König, B. Strategies for the Photocatalytic Generation of Carbanion Equivalents for Reductant-Free C–C Bond Formations. *Acc. Chem. Res.* **2021,** *54* (1), 242-252.

8. (a) Ramadoss, V.; Zheng, Y.; Shao, X.; Tian, L.; Wang, Y. Advances in Electrochemical Decarboxylative Transformation Reactions. *Chem. Eur. J.* **2021,** *27* (10), 3213-3228; (b) Xiang, J.; Shang, M.; Kawamata, Y.; Lundberg, H.; Reisberg, S. H.; Chen, M.; Mykhailiuk, P.; Beutner, G.; Collins, M. R.; Davies, A.; Del Bel, M.; Gallego, G. M.; Spangler, J. E.; Starr, J.; Yang, S.; Blackmond, D. G.; Baran, P. S. Hindered dialkyl ether synthesis with electrogenerated carbocations. *Nature* **2019,** *573* (7774), 398-402; (c) Sheng, T.; Zhang, H.-J.; Shang, M.; He, C.; Vantourout, J. C.; Baran, P. S. Electrochemical Decarboxylative *N*-Alkylation of Heterocycles. *Org. Lett.* **2020**.

9. Donabauer, K.; Maity, M.; Berger, A. L.; Huff, G. S.; Crespi, S.; König, B. Photocatalytic carbanion generation – benzylation of aliphatic aldehydes to secondary alcohols. *Chem. Sci.* **2019,** *10* (19), 5162-5166.

10. (a) Webb, E. W.; Park, J. B.; Cole, E. L.; Donnelly, D. J.; Bonacorsi, S. J.; Ewing, W. R.; Doyle, A. G. Nucleophilic (Radio)Fluorination of Redox-Active Esters via Radical-Polar Crossover Enabled by Photoredox Catalysis. *J. Am. Chem. Soc.* **2020,** *142* (20), 9493-9500; (b) Shibutani, S.; Kodo, T.; Takeda, M.; Nagao, K.;

Tokunaga, N.; Sasaki, Y.; Ohmiya, H. Organophotoredox-Catalyzed Decarboxylative C(sp^3)–O Bond Formation. *J. Am. Chem. Soc.* **2020,** *142* (3), 1211-1216.

11. (a) Li, P.; Zbieg, J. R.; Terrett, J. A. A Platform for Decarboxylative Couplings via Photoredox Catalysis: Direct Access to Carbocations from Carboxylic Acids for Carbon–Oxygen Bond Formation. *ACS Catal.* **2021,** *11* (17), 10997-11004; (b) Maeda, B.; Sakakibara, Y.; Murakami, K.; Itami, K. Photoredox-Catalyzed Benzylic Esterification via Radical-Polar Crossover. *Org. Lett.* **2021**.

12. Wayner, D. D. M.; McPhee, D. J.; Griller, D. Oxidation and reduction potentials of transient free radicals. *J. Am. Chem. Soc.* **1988,** *110* (1), 132-137.

13. Bosnidou, A. E.; Muñiz, K. Alkyliodines in High Oxidation State: Enhanced Synthetic Possibilities and Accelerated Catalyst Turn-Over. *Chem. Eur. J.* **2019,** *25* (60), 13654-13664.

14. Okuyama, T.; Takino, T.; Sueda, T.; Ochiai, M. Solvolysis of Cyclohexenyliodonium Salt, a New Precursor for the Vinyl Cation: Remarkable Nucleofugality of the Phenyliodonio Group and Evidence for Internal Return from an Intimate Ion-Molecule Pair. *J. Am. Chem. Soc.* **1995,** *117* (12), 3360-3367.

15. Kiyokawa, K.; Okumatsu, D.; Minakata, S. Hypervalent iodine(III)-mediated decarboxylative acetoxylation at tertiary and benzylic carbon centers. *Beilstein J. Org. Chem.* **2018,** *14*, 1046-1050.

16. Kiyokawa, K.; Watanabe, T.; Fra, L.; Kojima, T.; Minakata, S. Hypervalent Iodine(III)-Mediated Decarboxylative Ritter-Type Amination Leading to the Production of α-Tertiary Amine Derivatives. *J. Org. Chem.* **2017,** *82* (22), 11711-11720.

17. Examples of reactions using I_2/ PhI (III) catalytic system: (a) Bafaluy, D.; Georgieva, Z.; Muñiz, K. Iodine Catalysis for C(sp^3)–H Fluorination with a Nucleophilic Fluorine Source. *Angew. Chem. Int. Ed.* **2020,** *59* (34), 14241-14245; (b) Duhamel, T.; Martínez, M. D.; Sideri, I. K.; Muñiz, K. 1,3-Diamine Formation from an Interrupted Hofmann–Löffler Reaction: Iodine Catalyst Turnover through Ritter-Type Amination. *ACS Catal.* **2019,** *9* (9), 7741-7745; (c) Bosnidou, A. E.; Muñiz, K. Intermolecular Radical C(sp^3)–H Amination under Iodine Catalysis. *Angew. Chem. Int. Ed.* **2019,** *58* (22), 7485-7489; (d) Kiyokawa, K.; Takemoto, K.; Minakata, S. Ritter-type amination of C–H bonds at tertiary carbon centers using iodic acid as an oxidant. *Chem. Commun.* **2016,** *52* (89), 13082-13085; Selected related relevant literature: (e) Kohlhepp, S. V.; Gulder, T. Hypervalent iodine(iii) fluorinations of alkenes and diazo compounds: new opportunities in fluorination chemistry. *Chem. Soc. Rev.* **2016,** *45* (22), 6270-6288; (f) Murphy, G. K.; Gulder, T. Hypervalent Iodine Fluorination for Preparing Alkyl Fluorides (Stoichiometrically and Catalytically). In *Fluorination*, Hu, J.; Umemoto, T., Eds. Springer Singapore: Singapore, 2018; pp 1-32; (g) Arnold, A. M.; Ulmer, A.; Gulder, T. Advances in Iodine(III)-Mediated Halogenations: A Versatile Tool to Explore New Reactivities and Selectivities. *Chem. Eur. J.* **2016,** *22* (26), 8728-8739; (h) Zhdankin, V. V.; Stang, P. J. Chemistry of Polyvalent Iodine. *Chem. Rev.* **2008,** *108* (12), 5299-5358; (i) Chen, C.; Wang, X.; Yang, T. Recent Synthetic Applications of the Hypervalent Iodine(III) Reagents in Visible-Light-Induced Photoredox Catalysis. *Front Chem* **2020,** *8* (551159); (j) Wang, X.; Studer, A. Iodine(III) reagents in radical chemistry. *Acc. Chem. Res.* **2017,** *50* (7), 1712-1724; (k) Wirth, T. Hypervalent Iodine Chemistry in Synthesis: Scope and New Directions. *Angew. Chem. Int. Ed.* **2005,** *44* (24), 3656-3665; (l) Elsherbini, M.; Wirth, T. Hypervalent Iodine Reagents by Anodic Oxidation: A Powerful Green Synthesis. *Chem. Eur. J.* **2018,** *24* (51), 13399-13407; (m) Yusubov, M. S.; Zhdankin, V. V. Iodine catalysis: A green alternative to transition metals in organic chemistry and technology. *Resource-Efficient Technologies* **2015,** *1* (1), 49-67.

18. Izquierdo, S.; Essafi, S.; del Rosal, I.; Vidossich, P.; Pleixats, R.; Vallribera, A.; Ujaque, G.; Lledós, A.; Shafir, A. Acid Activation in Phenyliodine Dicarboxylates: Direct Observation, Structures, and Implications. *J. Am. Chem. Soc.* **2016,** *138* (39), 12747-12750.

19. (a) Dasgupta, A.; Thiehoff, C.; Newman, P. D.; Wirth, T.; Melen, R. Reactions Promoted by Hypervalent Iodine Reagents and Boron Lewis Acids. *Org. Biomol. Chem.* **2021**; (b) Ochiai, M.; Takeuchi, Y.; Katayama, T.; Sueda, T.; Miyamoto, K. Iodobenzene-Catalyzed α-Acetoxylation of Ketones. In Situ Generation of Hypervalent (Diacyloxyiodo)benzenes Using *m*-Chloroperbenzoic Acid. *J. Am. Chem. Soc.* **2005,** *127* (35), 12244-12245.

20. Liteature about direct excitation of hypervalent iodine (III) reagents: (a) Nakajima, M.; Nagasawa, S.; Matsumoto, K.; Kuribara, T.; Muranaka, A.; Uchiyama, M.; Nemoto, T. A Direct $S_0 \rightarrow T_n$ Transition in the Photoreaction of Heavy-Atom-Containing Molecules. *Angew. Chem. Int. Ed.* **2020,** *59* (17), 6847-6852; (b) Amos, S. G. E.; Cavalli, D.; Le Vaillant, F.; Waser, J. Direct Photoexcitation of Ethynylbenziodoxolones: An Alternative to Photocatalysis for Alkynylation Reactions. *Angew. Chem. Int. Ed.* **2021,** *60* (44), 23827-23834.

21. Previously reported methods work best for tertiary positions. Some methods can also be used for stabilized benzylic positions (secondary or tertiary with electron-donating groups on the phenyl moiety), especially in a combination with stronger nucleophiles like acetate or sulfonamides.

22. (a) Zagulyaeva, A. A.; Banek, C. T.; Yusubov, M. S.; Zhdankin, V. V. Hofmann Rearrangement of Carboxamides Mediated by Hypervalent Iodine Species Generated in Situ from Iodobenzene and Oxone: Reaction Scope and Limitations. *Org. Lett.* **2010,** *12* (20), 4644-4647; (b) Saikia, I.; Borah, A. J.; Phukan, P. Use of Bromine and Bromo-Organic Compounds in Organic Synthesis. *Chem. Rev.* **2016,** *116* (12), 6837-7042; (c) Hofmann, A. W. Über die Einwirkung des Broms in alkalischer Lösung auf Amide. *Berichte der deutschen chemischen Gesellschaft* **1881,** *14* (2), 2725-2736.

23. Ghosh, A. K.; Brindisi, M.; Sarkar, A. The Curtius Rearrangement: Applications in Modern Drug Discovery and Medicinal Chemistry. *ChemMedChem* **2018,** *13* (22), 2351-2373.

24. (a) Ye, C.; Twamley, B.; Shreeve, J. n. M. Straightforward Syntheses of Hypervalent Iodine(III) Reagents Mediated by Selectfluor. *Org. Lett.* **2005,** *7* (18), 3961-3964; (b) Sarie, J. C.; Thiehoff, C.; Mudd, R. J.; Daniliuc, C. G.; Kehr, G.; Gilmour, R. Deconstructing the Catalytic, Vicinal Difluorination of Alkenes: HF-Free Synthesis and Structural Study of *p*-TolIF$_2$. *J. Org. Chem.* **2017,** *82* (22), 11792-11798.

25. (a) Stavber, S.; Kralj, P.; Zupan, M. Progressive Direct Iodination of Sterically Hindered Alkyl Substituted Benzenes. *Synthesis* **2002,** *2002* (11), 1513-1518; (b) Narobe, R.; Düsel, S. J. S.; Iskra, J.; König, B. Photocatalytic Oxidative Iodination of Electron-Rich Arenes. *Adv. Synth. Catal.* **2019,** *361* (17), 3998-4004.

26. The yields of aliphatic carboxylic acids are lower presumably due to formation of eliminaiton products which undergo decomposition under the reaction conditions.

27. Iodo compounds stick to the baseline, because they are in their oxidized iodine (III) form.

28. (a) Merritt, E. A.; Olofsson, B. Diaryliodonium Salts: A Journey from Obscurity to Fame. *Angew. Chem. Int. Ed.* **2009,** *48* (48), 9052-9070; (b) Interestingly, the reaction progress of the model substrate **1a** is completely inhibited with excess of an electron-rich arene (Scheme S2.3).

29. Neufeld, J.; Daniliuc, C. G.; Gilmour, R. Fluorohydration of alkynes via I(I)/I(III) catalysis. *Beilstein J. Org. Chem.* **2020,** *16*, 1627-1635.

30. Concepcion, J. I.; Francisco, C. G.; Freire, R.; Hernandez, R.; Salazar, J. A.; Suarez, E. Iodosobenzene diacetate, an efficient reagent for the oxidative decarboxylation of carboxylic acids. *J. Org. Chem.* **1986,** *51* (3), 402-404.

31. (a) Zhu, J.; Pérez, M.; Stephan, D. W. C–C Coupling of Benzyl Fluorides Catalyzed by an Electrophilic Phosphonium Cation. *Angew. Chem. Int. Ed.* **2016,** *55* (29), 8448-8451; (b) Vuković, V. D.; Richmond, E.; Wolf, E.; Moran, J. Catalytic Friedel–Crafts Reactions of Highly Electronically Deactivated Benzylic Alcohols. *Angew. Chem. Int. Ed.* **2017,** *56* (11), 3085-3089.

32. Kremsmair, A.; Wilke, H. R.; Simon, M. M.; Schmidt, Q.; Karaghiosoff, K.; Knochel, P. General stereoretentive preparation of chiral secondary mixed alkylmagnesium reagents and their use for enantioselective electrophilic aminations. *Chem. Sci.* **2021**. DOI: 10.1039/d1sc05315a

33. The overall yield is relatively low due to side reactions which could also stem from the formation of carbenium intermediates (i.e., elimination and subsequent polymerization of the olefins).

34. Leffler, J. E.; Story, L. J. The decomposition of aryl iodine diacetates. *J. Am. Chem. Soc.* **1967,** *89* (10), 2333-2338.

35. Released iodine (I_2 or RCOOI) reacts in an electrophilic iodination with iodobenzene. The diiodinated products can also be rationalized by the formation of diarlyiodonium salts and their hydrolysis during the workup.

Chapter 3

3 C(sp³)–H Ritter Amination by Excitation of *in situ* Generated Iodine (III) - BF_3 Complexes

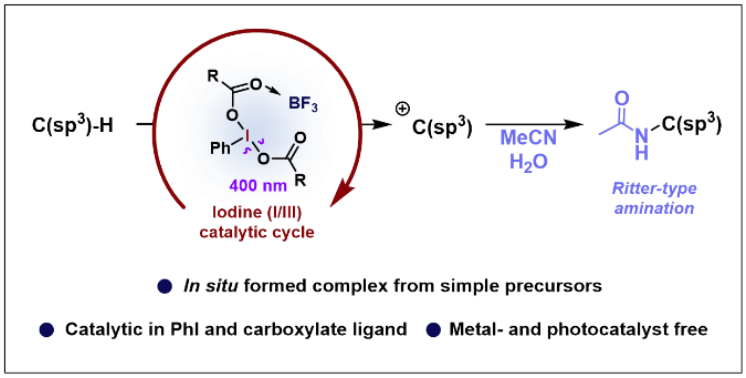

Abstract: Visible light excitation of Iodine (III) - BF_3 complex enables the formation of carbocations from C(sp³)–H bonds. The complexes are generated catalytically from iodoarene, carboxylate ligand, oxidizing agent Selectfluor, and Lewis acid BF_3. This modular catalytic system allows formation of synthetically valuable amine derivatives without metal- or photocatalyst.

This chapter has been published. For reference see:
Narobe, R.; Murugesan, K.; Haag, C.; Schirmer, T. E.; König, B., C(sp³)–H Ritter amination by excitation of in situ generated iodine(III)–BF_3 complexes. *Chem. Commun.* **2022,** *58* (63), 8778-8781. Reproduced with permission from the Royal Society of Chemistry.

Author contribution
RN designed the reaction, performed the optimization, synthesized the scope, and carried out the mechanistic investigations. KM and CH helped with the isolation of products. TES prepared a few potential substrates. RN wrote the manuscript with the input of all authors. BK supervised the project and is the corresponding author.

3.1 Introduction

Efficient C–H functionalization of abundant chemical precursors to value-added chemicals is of great interest in modern organic chemistry.[1] Over the past years, many methods have been developed for functionalization of C(sp^3)–H bonds relying on alkyl radical or metal-alkyl intermediates, while methods involving carbocation intermediates remain less developed.[2] These versatile polar intermediates are highly desired as they can be used in different transformations such as rearrangements, eliminations, or reactions with different weak nucleophiles.[3] The reaction scope of the reactions with nucleophiles involves etherification, halogenation, arylation, and Ritter-type amination reactions.[4] When starting from a C(sp^3)–H bond, a formal hydride (H^-) transfer is required to access carbocations. Typically, this is achieved as a sequence of elementary steps *e.g.*, hydrogen ($H^\cdot$) abstraction followed by a fast oxidation of the resulting carbon radical (Scheme 3.1a). In these net oxidative processes, iodine (III) based terminal oxidizing agents are often used, and the electron transfers are generally mediated by a ruthenium- or iridium-based photocatalyst.[5]

Recently, we found that visible light excitation of phenyliodine(III) dicarboxylate - BF_3 complexes leads to a decarboxylative Ritter amination via carbenium intermediates (Scheme 3.1b).[6] The strategy is quite unique in a sense that it does not require any photocatalyst to mediate the electron transfers to obtain the charged intermediates.[7] Moreover, it is based on simple commercial reagents, without the need for any sophisticated oxidizing agents. Based on our previous report, we considered using different carboxylate ligands which do not undergo fast decarboxylation but instead serve as hydrogen atom transfer (HAT) catalysts. This opens the possibility to expand the applicability of our iodine (III) based catalytic system to activation of more challenging C(sp^3)–H substrates. In this communication, we analyze the influence of the structure of the iodine (III) - BF_3 complexes on the reaction outcome and demonstrate the developed method's synthetic potential.

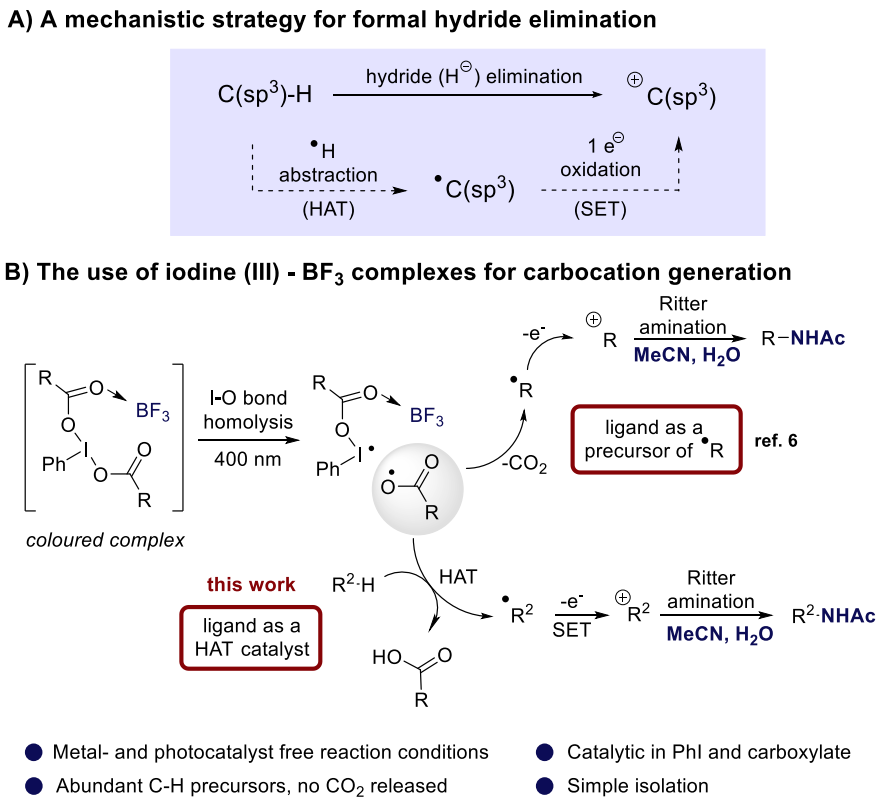

Scheme 3.1. Application of hypervalent iodine (III) - BF_3 complexes for generation of carbenium ions.

3.2 Reaction development

We started our investigation by using the established system for *in situ* generation of hypervalent iodine species from iodobenzene using Selectfluor as stoichiometric oxidizing agent.[8] Benzoic acid was selected as a ligand because its corresponding carboxyl radical is known to act as a very potent hydrogen abstracting agent while the rate of decarboxylation is reportedly relatively slow.[9] After minor adjustments to the original conditions, our envisioned process proved feasible and yielded Ritter type amination product **1b** of our model substrate *para*-fluorotoluene in 77% yield (Table 3.1, entry 1). Other acids or bases are not effective in this transformation due to absence of strong interactions with the formed iodine (III) reagents.[10] The control experiments confirmed the essential roles of light and iodobenzene as organocatalyst (entries 6 and 7). Also, the reaction from commercially available iodine (III) reagents as combined precatalyst and terminal oxidant gave lower product yields (entries 8 and 9).

Table 3.1. Screening of the conditions for the C(sp³)–H amination.[a]

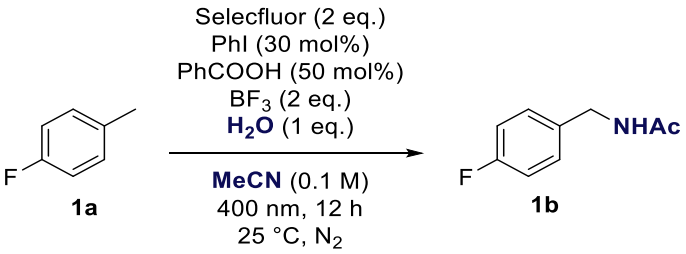

Entry	Deviation	Yield [%]
1	-	77
2	No BF_3	14
3	Cs_2CO_3 (2 eq.) instead of BF_3	0
4	TFA (2 eq.) instead of BF_3	15
5	HFIP (2 eq.) instead of BF_3	13
6	No light	0
7	No iodobenzene	0
8[b]	$PhI(OAc)_2$ (2 eq.)	19
9[b]	$PhI(OC(O)CF_3)_2$ (2 eq.)	8

[a]Reaction conditions: 0.1 mmol substrate, 2 eq. Selectfluor, 30 mol% PhI, 50 mol% benzoic acid, 2 eq. Lewis acid ($BF_3 \times MeCN$ unless otherwise noted), 1 eq. H_2O, 1 ml MeCN (0.1 M) under N_2 atmosphere, 25 °C, 12 h. Yields were determined by ^{19}F NMR using trifluorotoluene as internal standard. [b]The indicated iodine (III) reagent instead of a combination of Selectfluor and PhI.

The approach by *in situ* generation of iodine (III) reagents from iodoarene and a ligand allows convenient tunability of the formed reagent.[8a] Building on the promising results with benzoic acid as HAT we sought to improve the performance of our system by investigating performance of different ligands, which can act as precursors to both oxygen and nitrogen centred radicals (Scheme 3.2). The reaction works in low 22% yield also without any additional ligand, because the DABCO moiety from Selectfluor can also take a role of the ligand capable of abstracting hydrogen atoms. Screening of the differently *para*-substituted benzoic acids revealed a correlation of Hammett σ substituent constants and the reaction yield (Table S3.2). The more electron-withdrawing substituents decreased the yield of the transformation, and slightly electron-donating groups seemed to have beneficial effect on the overall reactivity. This is presumably due to higher electron density and thus better binding with Lewis acid BF_3. The yield with the most electron-donating substituent -OMe is nevertheless low because it undergoes decomposition under the reaction conditions. The examples with ortho and meta substituted benzoic acids follow the previously observed trend of lower yields with more electron-deficient substituents. Similar complexes of iodine (III) with (sulfon)amides as ligands are less effective in the transformation with the exception of saccharin, which yielded **1b** in 65%. Despite the considerable

nucleophilicities of the tested (sulfon)amide moieties, we never observed any coupling products with the electrophilic cationic intermediates. Alcohols as ligands showed only low reactivity (<40% yield) in this transformation.

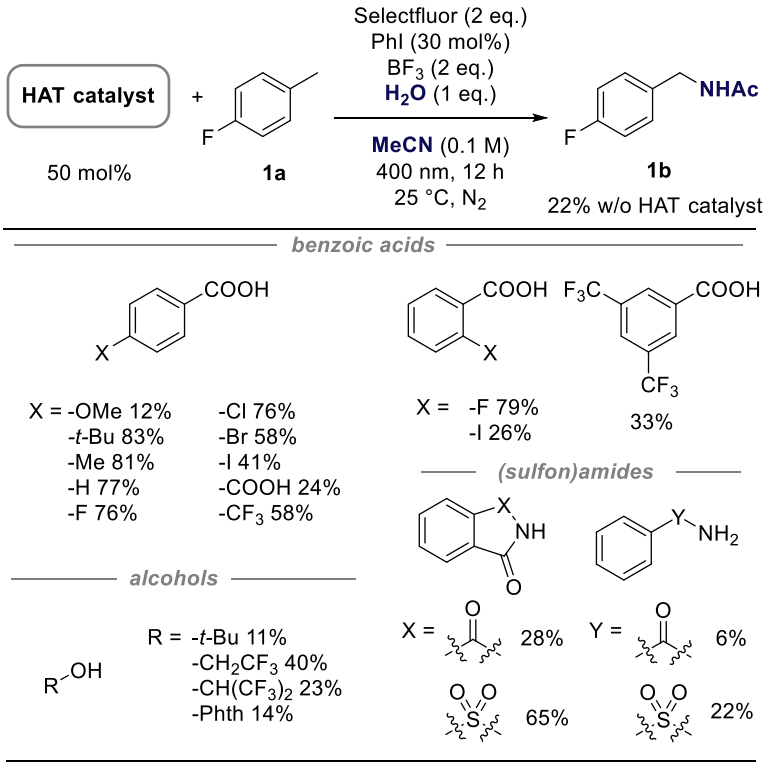

Scheme 3.2. Optimization of the ligand of the hypervalent iodine (III) reagent for hydrogen abstraction. [a] 0.1 mmol substrate, 2 eq. Selectfluor, 30 mol% PhI, 50 mol% of the indicated HAT reagent, 2 eq. $BF_3 \times MeCN$, 1 eq. H_2O, 1 ml MeCN (0.1 M) under N_2 atmosphere, 25 °C, 12 h. Yields were determined by ^{19}F NMR using trifluorotoluene as internal standard. Phth. = phthalimide moiety.

The variations in the structure of the iodoarenes revealed that very electron-rich iodoarenes (naphthyl, -OMe substituted) are not suitable catalysts for this transformation as they undergo decomposition under the reaction conditions. The yields obtained with less electron-rich iodoarenes are all very similar (Scheme S3.1), and therefore, we decided to proceed with the simplest iodoarene representative - iodobenzene.

3.3 Synthetic application

With the optimized conditions in hand, we continued with the application of the method to different C(sp^3)–H precursors (Scheme 3.3). In general, the method performs well with differently *para*-substituted toluene derivatives (**1-18a**) giving moderate to good yields. Differently protected phenols or aniline, as well as biphenyl derivatives were all found to be suitable substrates for the C(sp^3)–H amination. However, we noticed a high sensitivity to the electronic properties of the aromatic moiety. When the aromatic moiety is too electron-deficient (**12a**) the reaction does not work, presumably due to a higher energetic barrier associated with a polarity mismatched hydrogen abstraction.[11] Nevertheless, this reactivity preference can also be exploited to achieve selectivity between different primary benzylic positions within the molecule as demonstrated in examples **15**-**18b**. Interestingly, in the case of **17b**, we observed a small amount of ortho functionalized product, which may indicate that the sulfone group can also serve as a ligand for the hypervalent iodine (III) intermediate directing the 1,5-hydrogen abstraction. In other examples with multiple potential reaction sites, only the benzylic positions undergo functionalization in the presence of C–H bonds in alpha position to oxygen (**8** and **9b**) or nitrogen (**18b**). Noteworthy, primary benzylic substrates cannot be functionalized by most of the previously reported methods as the corresponding primary radicals are short lived and

difficult to oxidize.[12] Some (photo)electrochemical methods[13] can overcome these limitations, but they are operationally more demanding.

The yield of the ethyl benzene derivatives (**19**-**29b**) is less sensitive to acceptors substituents compared to the toluene ones. The method works surprisingly well also with some very electron-deficient systems, such as **24**-**26a**. For some poorly performing substrates, an increase in light intensity proved beneficial. Possibly due to the reversible character of I–O bond cleavage[14] and consequently higher concentration of the hydrogen abstracting carboxylate radicals in the reaction mixture at higher light intensities. Lastly, we applied the developed method to cyclohexane (**30a**) and obtained low 30% yield.

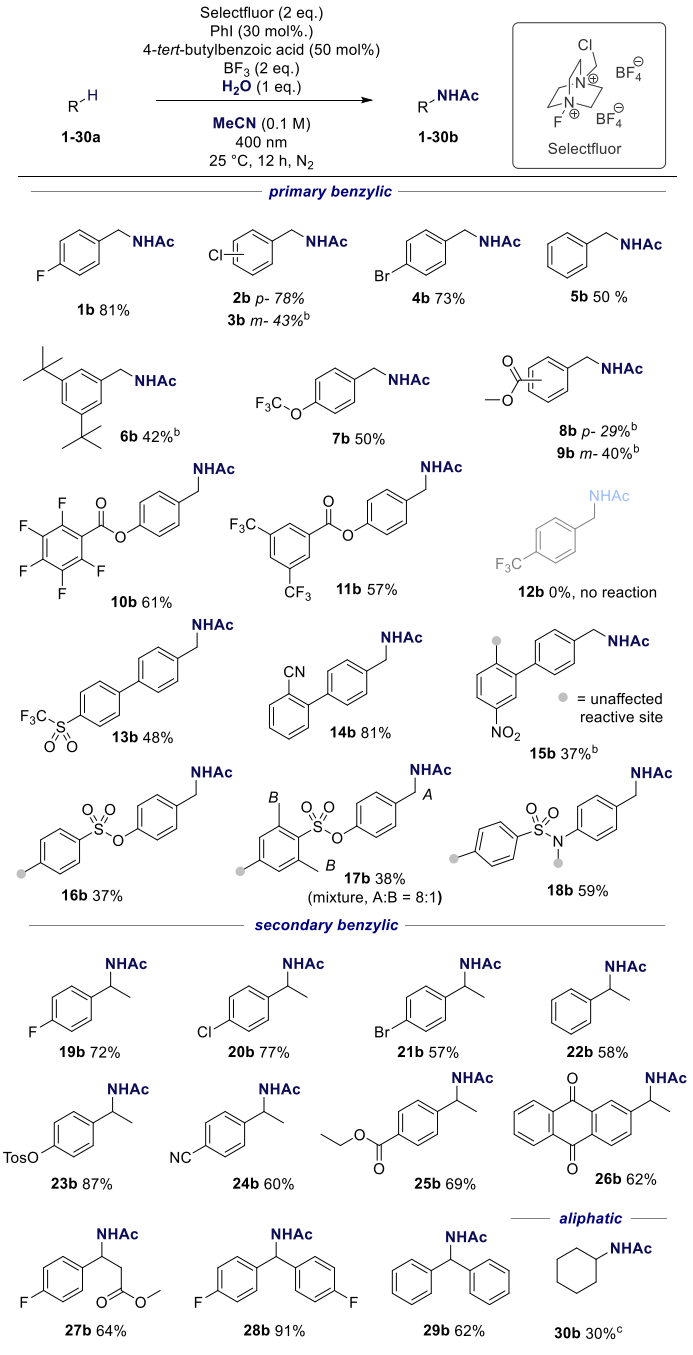

Scheme 3.3. Synthetic scope of the transformation. [a]Reaction conditions: 0.4 mmol substrate, 2 eq. Selectfluor, 30 mol% PhI, 50 mol% 4-*tert*-butlybenzoic acid, 2 eq. $BF_3 \times MeCN$, 1 eq. H_2O, 4 ml MeCN (0.1 M) under N_2 atmosphere, 25 °C, 16 h, isolated yields. [b]High power 400 nm LEDs were used (see SI). [c]In parenthesis is ^1H NMR yield using acetanilide as internal standard.

3.4 Mechanistic proposal

To support our initial mechanistic hypothesis on the *in situ* formation of a hypervalent iodine (III) species with benzoate ligands and its essential role as catalytic species, we performed an experiment with a stoichiometric amount of the preformed iodine (III) reagent **1i** (Scheme 3.4a). In the iodine (III) reagent, 4-*tert*-butylbenzoate ligands were used and the reaction was performed with an excess of BF_3 and without Selectfluor. The obtained 66% reaction yield indeed supports the involvement of such or alike iodine (III) intermediates.

Based on our experimental data and previous investigations,[6a] we propose the following mechanism (Scheme 3.4b). In the first step, Selectfluor oxidizes iodobenzene to iodine (III) compound in which 4-*tert*-butylbenzoic acid acts as a ligand.[8a] Complexation with BF_3 shifts the absorption maximum towards higher wavelengths (Figure S3.2) and enhances the oxidation properties of the complex A.[10a] After a visible light-induced homolysis of iodine-oxygen bond,[7a] 4-*tert*-butylbenzyloxy radicals are formed, which abstract a hydrogen atom from substrate B. The formed carbon radical is oxidized by the remaining part of the iodine complex (C) to give a reactive carbocation. The carbocation readily reacts with the solvent acetonitrile yielding Ritter amination product D. Iodobenzene, 4-*tert*-butylbenzoic acid and BF_3 are released back in the system and can enter a new catalytic cycle. However, BF_3 still has to be used as a stoichiometric additive, as it is also acting as a scavenger of other nucleophiles in the system such as Selectfluor oxidation byproducts.

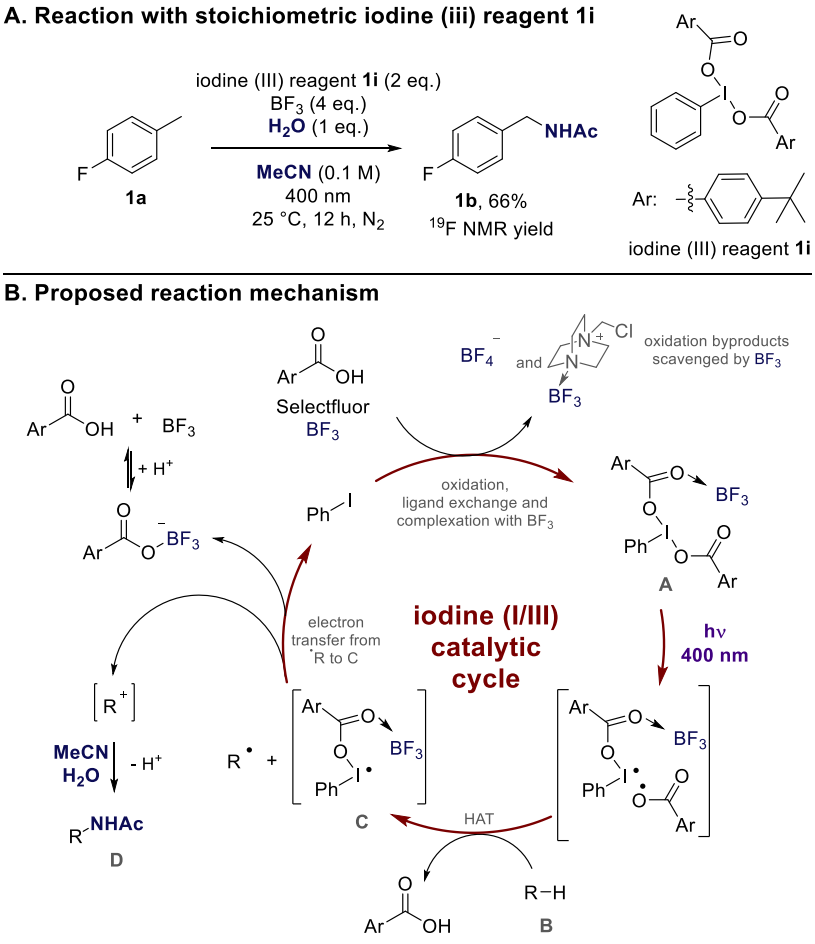

Scheme 3.4. Non-catalytic reaction with preformed iodine (III) reagent (A) and plausible reaction mechanism (B).

3.5 Conclusion

In conclusion, we have expanded the scope of the transformations relying on direct excitation of hypervalent iodine (III) - BF_3 complexes also to functionalization of abundant C(sp^3)–H precursors. We optimized the performance of the *in situ* formed iodine (III) - BF_3 complex for a Ritter-type amination by screening different ligands and iodoarenes. The developed method complements existing methods for carbenium ions generation by allowing functionalization of certain more challenging substrates (e.g., primary benzylic). Moreover, the method is practically simple and based on readily available chemicals.

3.6 Experimental information

3.6.1 General information

Starting materials and reagents were purchased from commercial suppliers (Sigma Aldrich, Alfa Aesar, Acros or Fluka) and were used without further purification. Solvents were used as p.a. grade. Reactions were monitored by analytic thin layer chromatography (TLC) using Fluka silica gel or NH2-Modified Silica Plates with a fluorescent indicator. Visualization of the developed TLC chromatogram was performed using 254 nm UV light source. Organic solutions were concentrated using Büchi rotary evaporator. Flash column chromatography was performed either by hand in filled Pasteour pipettes or on a Biotage® IsoleraTM Spektra. The columns were filled either with Silica gel (60-200 μm) or basic alumina (50-200 μm).

NMR spectroscopy
All NMR spectra were recorded at room temperature using a Bruker Avance 300 (300 MHz for ^{1}H, 75 MHz for ^{13}C, 282 MHz for ^{19}F) or a Bruker Avance 400 (400 MHz for ^{1}H, 101 MHz for ^{13}C, 376 MHz for ^{19}F) NMR spectrometer. All chemical shifts are reported in δ-scale as parts per million [ppm]c (multiplicity, coupling constant J, number of protons), relative to the solvent residual peaks as the internal standard. Coupling constants J are given in Hertz [Hz]. Abbreviations used for signal multiplicity: ^{1}H-NMR: br = broad, s = singlet, d = doublet, t = triplet, q = quartet, dd = doublet of doublets, dt = doublet of triplets, and m = multiplet.

Gas chromatography
GC measurements were performed on a GC 7890 from Agilent Technologies system coupled to a FID. The system was equipped with a capillary column (HP-5ms UI, length 30 m, diam. 0.25 mm, film 0.25 μm) and worked with H_2 as carrier gas. GC program: The initial temperature of the GC was set to 40 °C and kept for 1.5 minutes. Subsequently, the oven temperature was increased at a rate of 25 °C/min. until reaching 280 °C, which was maintained for 3 min. Then, temperature was further increased (42 °C/min) until reaching 300 °C and final temperature was hold for 5 minutes. Injector temperature was set to 280 °C and temperature of the detecting unit to 310 °C. A split ratio of 30:1 (split flow 42 mL/min) was applied, and the column flow was set to 1.4 mL/min. Data acquisition and evaluation was done with Agilent ChemStation Rev.C.01.04.

Mass spectrometry
High resolution mass spectrometry (HRMS) was performed at the Central Analytical Laboratory of the University of Regensburg. Mass spectra were measured on a Finnigan MAT 95, ThermoQuest Finnigan TSQ 7000, Finnigan MAT SSQ 710 A or Agilent Q-TOF 6540 UHD instrumenta and a Waters Acquity UPLC system equipped with Waters PDA, sample manager, sample organiser, column oven and Waters Xevo QTOF mass spectrometer.

UV-Vis
Absorption spectra were measured on an Agilent Cary 100 UV/Vis spectrometer in a 10 mm × 10 mm quartz cuvette at 25.0 °C under air atmosphere.

Photochemical setups
Photochemical reactions were performed in sealed reaction vials, placed approximately 2 cm above a 400 nm LED array and stirred under irradiation (Figure S3.1). The reaction temperature was controlled by a thermostated (25 °C) metal cooling block. The reactor setup is a custom-made device (University of Regensburg workshop) and is not a commercially available product.

A) regular 400 nm setup (optical power 100-120 mW/ LED spot)

B) Higher power 400 nm setup (optical power 600-800 mW/ LED spot)

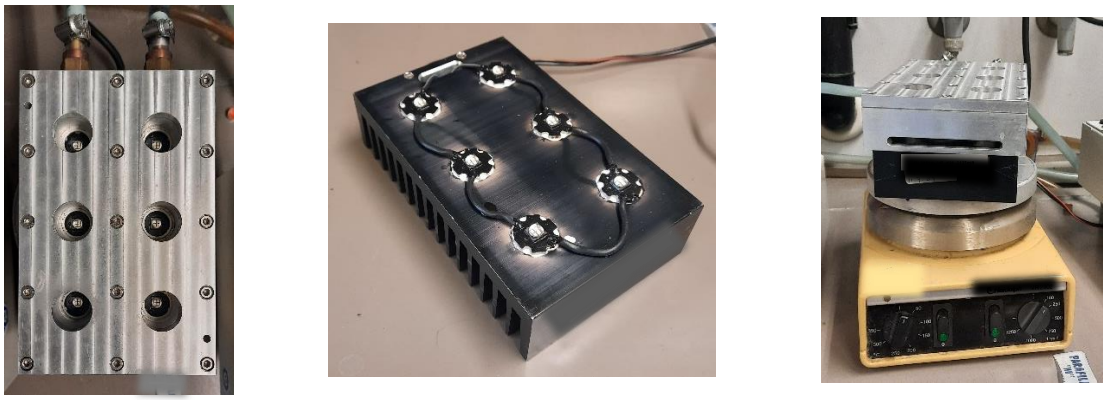

Figure S3. 1: Photochemical setups used in this work from different perspectives.

General experimental procedures

General procedure for preparative scale reactions

The reactions were set in 2 parallel vials, each containing 0.2 mmol of the substrate. A C(sp³)–H precursor (0.2 mmol, 1 eq.), 4-tertbutylbenzoic acid (17.8 mg, 0.1 mmol, 0.5 eq.) and Selectfluor (142 mg, 0.40 mmol, 2 eq.) were weighed into a crimp reaction vial. Then, 2 ml of a stock solution containing iodobenzene (6.7 µl, 0.06 mmol, 0.3 eq.) and H_2O (3.6 µl, 0.2 mmol, 1 eq.) in dry MeCN were added. A stirring bar was added, and the vial was capped. The reaction mixture was degassed by 4 nitrogen-vacuum cycles. Afterwards BF_3 (200 µl of 16% BF_3 in MeCN, 0.4 mmol, 2 eq.) was added, and the vial was placed in a thermostated cooling block (25 °C) and irradiated through the plane bottom side of the vial by a 400 nm LED for 16 hours (see Figure S3. 1). After the completion, the two reaction batches were combined, and the solvent was removed *in vacuo*. The solid residue was dissolved in 2 ml H_2O and 4 ml EtOAc and transferred into a separatory funnel containing 2 ml of brine. The aqueous layer was washed two times with 5 ml of EtOAc. Combined organic phases were concentrated *in vacuo* to ca 0.5 ml solvent volume. The sample was filtered through a small basic alumina column (packed in a Pasteur pipette). The column was then washed with approximately 5 ml of EtOAc. In that way, we remove remaining hypervalent iodine species, 4-tertbutylbenzoic acid and polymeric side products. The obtained eluent always contained only the product and some remaining substrate. The solvent was removed in vacuo and the product mixture was redissolved in a minimal amount of DCM and applied on silica gel column (packed in a Pasteur pipette). The column was first washed with DCM (5 ml) to elute the remaining substrate, and then with EtOAc (5 ml) to elute the product. Removal of the solvent afforded analytical pure samples of the products. In some cases, we were able to skip the second (silica gel) column. The decision was based on the TLC of the eluent after the first column.

General procedure for screening and optimization studies

Selectfluor (typically 71 mg, 0.2 mmol, 2 eq.) was weighed into a crimp reaction vial together with any other solid materials (different ligands, Lewis acids/bases, PIDA, PIFA, …). Then, 1 ml of a stock solution containing, 4-fluorotoluene (11.0 µl, 0.1 mmol, 1 eq.), iodobenzene (3.3 µl, 0.03 mmol, 0.3 eq.) and H_2O (1.8 µl, 0.1 mmol, 1 eq.) in dry MeCN were added. A stirring bar was added, and the vial was capped. The reaction mixture was degassed by 4 nitrogen-vacuum cycles. Afterwards, BF_3 (100 µl of 16% BF_3 in MeCN, 0.2 mmol, 2 eq.) or any other liquids (Lewis acids) were added, and the vial was placed in a thermostated cooling block (25 °C) and irradiated through the plane bottom side of the vial by a 400 nm LED for 16 hours (see Figure S3. 1: **Photochemical setups used in this work from different perspectives.**
). After the completion, the analysis was done following the typical procedure for 19F NMR yield determination (*vide infra*).

Note: The reaction is a bit sensitive (Table S3.3) to the amount of water in the reaction mixture. Stock solutions containing 4-fluorotoluene, H_2O and PhI were always used in order to have all the entries within the series (optimization table) comparable.

Procedure for NMR yield determination

The screening and optimization reactions were all performed on a 0.1 mmol scale following the above-described general procedure. After the reaction completion, internal standard trifluorotoluene (12.3 µl, 0.1 mmol) was added into the vial. The reaction vial was well shaken before we took out 0.4 ml of the reaction mixture and transferred it into a 2 ml conical bottom Eppendorf vial. Then 0.4 ml $CDCl_3$ was added to precipitate the remaining Selectfluor and quench the reaction. The vials were centrifuged, and the clean solution was submitted for ^{19}F NMR analysis.

3.6.2 UV-Vis of hypervalent iodine (III)-BF_3 complex of 1i

The absorption increases upon addition of BF_3 to the hypervalent iodine reagent **1i** due to the formation of the complex **1i-BF_3**.[10a]

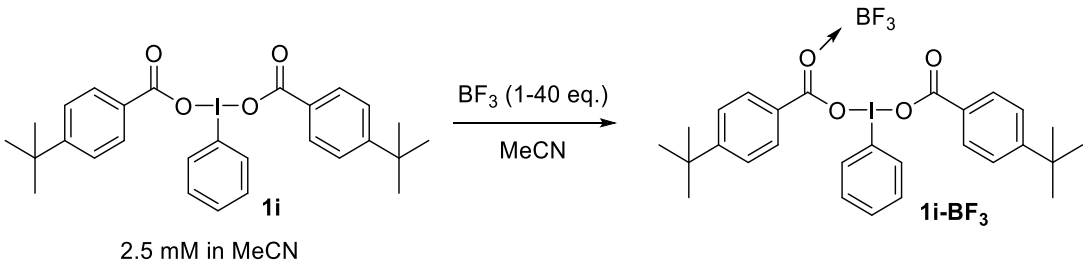

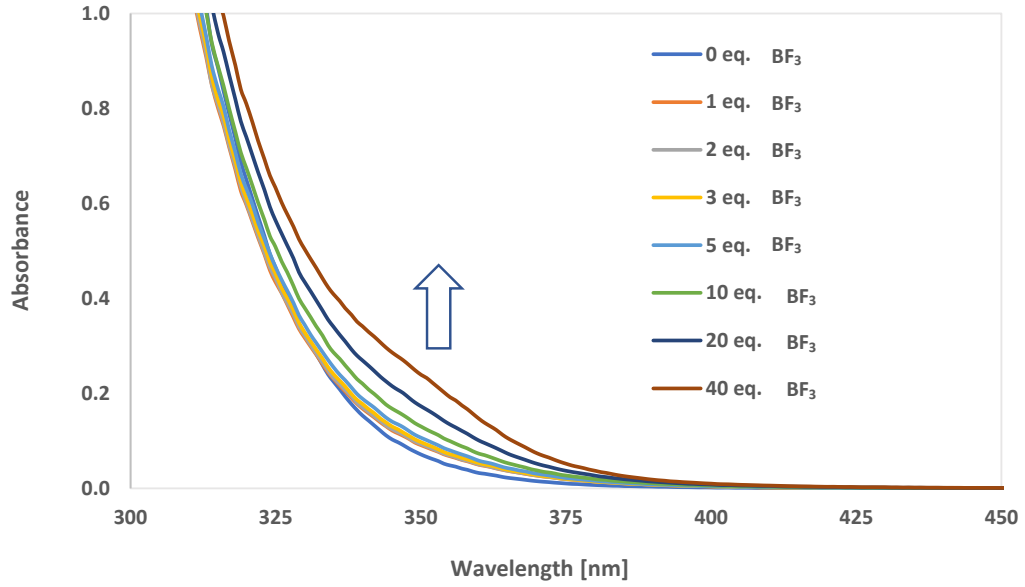

Figure S3. 2: Spectral changes upon addition of BF_3 to **1i**.

3.6.3 Optimization tables

3.6.3.1 Screening of different Lewis acids

Different acids have been screened for the C-H Ritter type amination. Most of the tested acids are ineffective supporting our previously disclosed findings about necessity of complexation of the hypervalent iodine reagent with BF_3.[6a]

Table S3. 1: Screening of different Lewis acids.

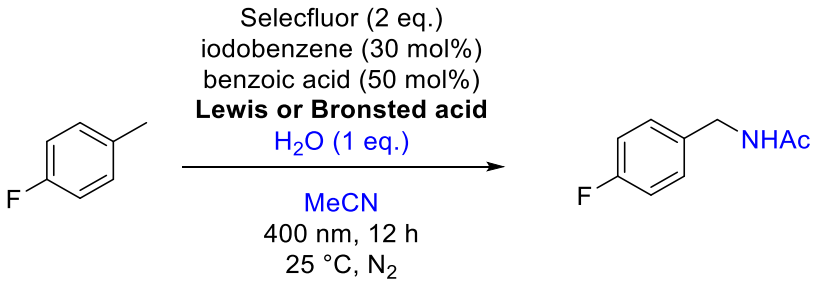

Entry	Acid/base	Yields [%]
A	-	14
B	Cs_2CO_3 (2 eq.)	0
C	TFA (2 eq.)	15
D	H_2SO_4 (2 eq.)	48
E	$HClO_4$ (70%, 2 eq.)	36
F	HFIP (2 eq.)	13
G	**BF_3 (16% in MeCN, 2 eq.)**	77
H	$BF_3 \times 2H_2O$ (2 eq.)	21
I	$B(OH)_3$ (2 eq.)	18
J	HBF_4 (32% in water, 2 eq.)	26
K	$LiBF_4$ (2 eq.)	13
L	$Zn(OTf)_2$ (0.5 eq.)	20
M	$Sc(OTf)_3$ (0.5 eq.)	28

0.1 mmol substrate, 30 mol% of the PhI, 50 mol% benzoic acid, 2 eq. Selectfluor, 2 eq. or 0.5 eq. of the indicated Lewis acid, 1 eq. H_2O, 1 ml MeCN (0.1 M) under N_2 atmosphere, 25 °C, 12 h. Yields were determined by ^{19}F NMR using trifluorotoluene as internal standard.

3.6.3.2 Screening of different iodoarenes

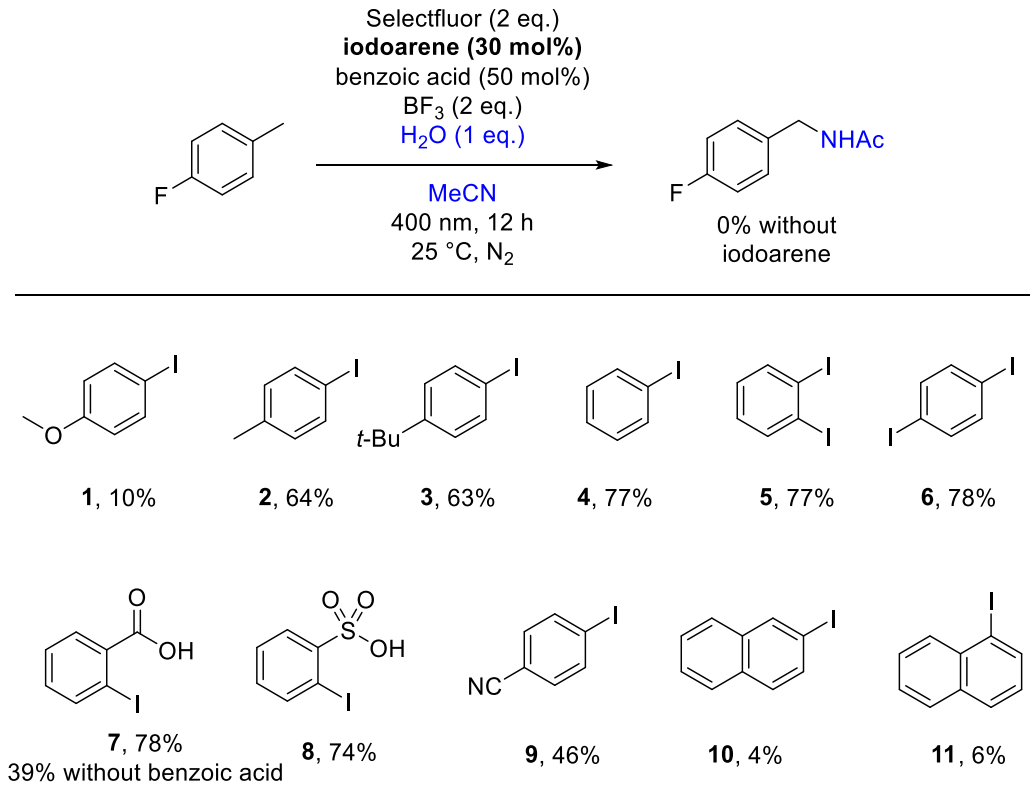

Scheme S3. 1: Screening of different iodoarenes, precursors of the *in situ* formed hypervalent iodine (III) reagent. [a] 0.1 mmol substrate, 30 mol% of the indicated ArI, 50 mol% benzoic acid, 2 eq. Selectfluor, 2 eq. $BF_3 \times MeCN$, 1 eq. H_2O, 1 ml MeCN (0.1 M) under N_2 atmosphere, 25 °C, 12 h. Yields were determined by ^{19}F NMR using trifluorotoluene as internal standard.

Iodoarenes **10** and **11** underwent decomposition after the addition of BF_3 even without light irradiation.

3.6.3.3 Screening of different HAT catalysts

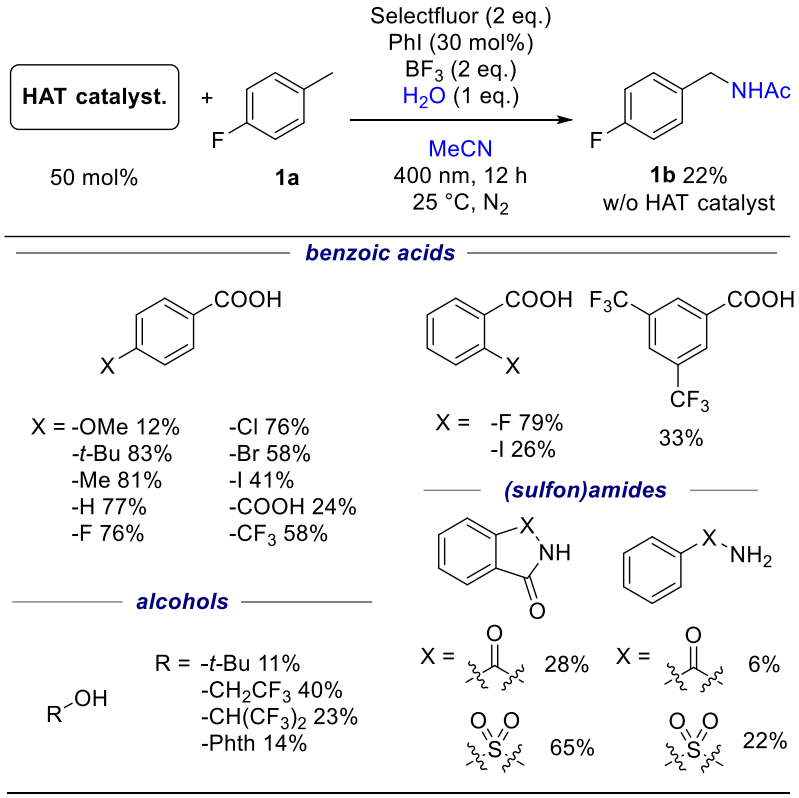

Scheme S3. 2: Optimization of the ligand of the hypervalent iodine (III) reagent for hydrogen abstraction. [a] 0.1 mmol substrate, 30 mol% PhI, 50 mol% of the indicated HAT reagent, 2 eq. Selectfluor, 2 eq. $BF_3 \times MeCN$, 1 eq. H_2O, 1 ml MeCN (0.1 M) under N_2 atmosphere, 25 °C, 12 h. Yields were determined by ^{19}F NMR using trifluorotoluene as internal standard.

Table S3. 2: Correlation of substituent electronic properties of the benzoic acid with the reaction yield.

Substituent	Hammet constant σ_p[15]	Reaction yield	Note
-OMe	-0.27	12%	Decomposition
-*t*-Bu	-0.20	83%	
-Me	-0.17	81%	
-H	0.00	77%	
-F	0.06	76%	
-I	0.18 or 0.88 for -I(OAc)$_2$	41%	4-Iodobenzoic gets oxidized under the reaction conditions.
-Cl	0.22	76%	
-Br	0.23	58%	
-COOH	0.45	24%	Solubility issue. The iodine (III) reagent is not dissolved even after addition of BF_3.
-CF_3	0.54	58%	

3.6.3.4 Optimization of catalysts loadings and reagent quantities

Table S3. 3: Effect of catalysts loadings and reagent quantities.

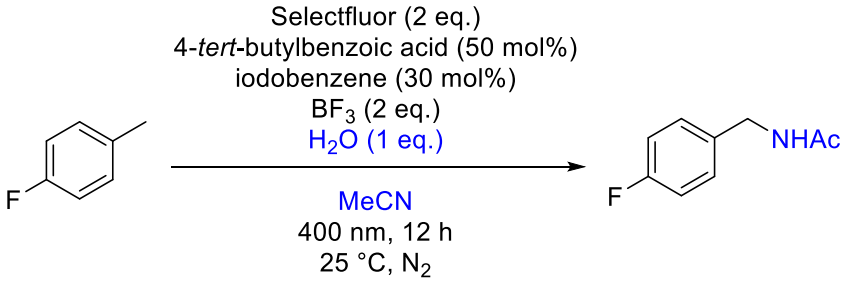

Entry	Selectfluor [eq.]	*4-tert*-butylbenzoic acid [mol%]	PhI [mol%]	BF_3 [eq.]	H_2O [eq.]	λ [nm]	Yield [%]
A	1	50	30	2	1	400	57
B	1.3	50	30	2	1	400	69
C	1.5	50	30	2	1	400	77
D	**2**	**50**	**30**	**2**	**1**	**400**	**83**
E	2	30	30	2	1	400	71
F	2	10	30	2	1	400	32
G	2	50	20	2	1	400	77
H	2	50	10	2	1	400	74
I	2	50	30	1	1	400	35
J	2	50	30	3	1	400	80
K	2	50	30	2	5	400	21
L	2	50	30	2	1	455	79
M	2	50	30	2	1	525	21

[a] All the entries are deviations of the entry D: 0.1 mmol substrate, 30 mol% PhI, 50 mol% of the 4-*tert*-butylbenzoic acid, 2 eq. Selectfluor, 2 eq. $BF_3 \times MeCN$, 1 eq. H_2O, 1 ml MeCN (0.1 M) under N_2 atmosphere, 25 °C, 12 h. Yields were determined by ^{19}F NMR using trifluorotoluene as internal standard.

3.6.3.5 Control experiments with different iodine (III) sources and additives

Table S3.4: Control experiments with preformed iodine (lll) reagents and different additives.

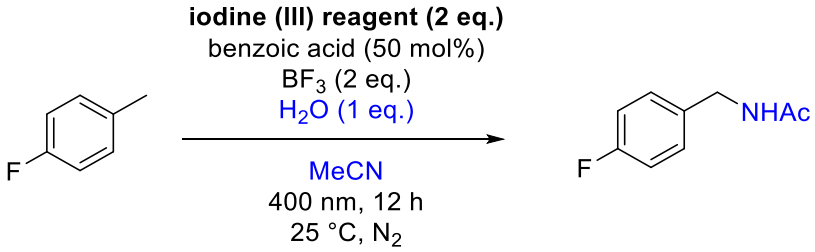

Entry	Iodine (lll) reagent	BF_3	Additive	Yield [
A	$PhI(OAc)_2$ (2 eq.)	Yes	-	19
B	$PhI(OAc)_2$ (2 eq.)	-	-	3
C	$PhI(OC(O)CF_3)_2$ (2 eq.)	Yes	-	8
D	$PhI(OC(O)CF_3)_2$ (2 eq.)	-	-	7
E	Selectfluor (2 eq.) + PhI (0.3 eq.)	Yes	-	77
F	Selectfluor (2 eq.) + PhI (0.3 eq.)	Yes	AcOH (4 eq.)	73
G	Selectfluor (2 eq.) + PhI (0.3 eq.)	Yes	TFA (4 eq.)	77

The approach by *in situ* generation of aryl iodine (lll) reagent gives higher yield than the use of commercially available aryliodine (lll) reagents. A possible reason could be competitive decarboxylation of (trifluroo)acetate ligands in the reaction conditions. This parasitic reaction leads to unproductive consumption of the hypervalent iodine (III) reagent.

3.6.4 Synthesis and characterization of starting materials, intermediates and products

3.6.4.1 Synthesis and characterization data of substrates and intermediates

Synthesis of hypervalent iodine reagent **1i**

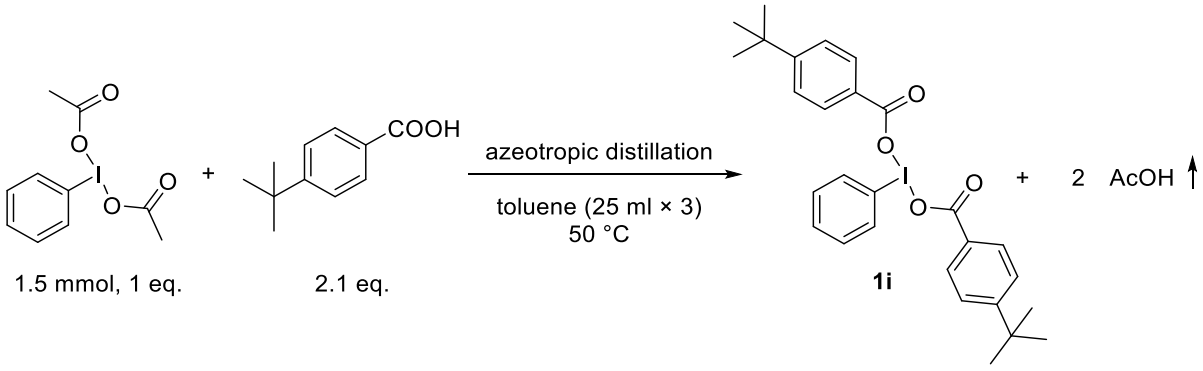

The reagent was prepared following adapted literature procedure.[16] Phenyliodine (III) diacetate (PIDA, 482 mg, 1.50 mmol, 1.0 eq.) and 4-*tert*-butylbenzoic acid (547 mg, 3.08 mmol, 2.1 eq.) were dissolved in toluene (25 mL) and the toluene was removed with a rotary evaporator (50 °C) over 10 minutes. After its removal, toluene (25 mL) was added again and removed with the rotary evaporator. This process was repeated three times in total. After drying *in vacuo*, the remaining solid material was dissolved in $CDCl_3$ and submitted for ^{1}H- and ^{13}C-NMR measurements. The reagent was used in the mechanistic experiments without any additional purification.

Iodobenzene bis(4-tert-butylbenzoate) (1i)

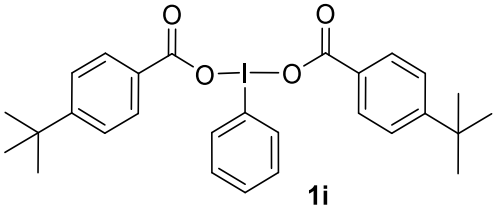

1i

Yield	Quant, White powder
^{1}H NMR	^{1}H NMR (400 MHz, $CDCl_3$) δ 8.23 (d, *J* = 7.6 Hz, 2H), 7.89 (d, *J* = 8.4 Hz, 4H), 7.60 (t, *J* = 7.4 Hz, 1H), 7.52 (t, *J* = 7.6 Hz, 2H), 7.39 (d, *J* = 8.4 Hz, 4H), 1.32 (s, 18H).
^{13}C NMR	^{13}C NMR (101 MHz, $CDCl_3$) δ 171.4, 156.1, 134.8, 131.6, 130.9, 130.0, 127.5, 125.2, 122.6, 35.1, 31.2.

Synthesis of **10a** and **11a**

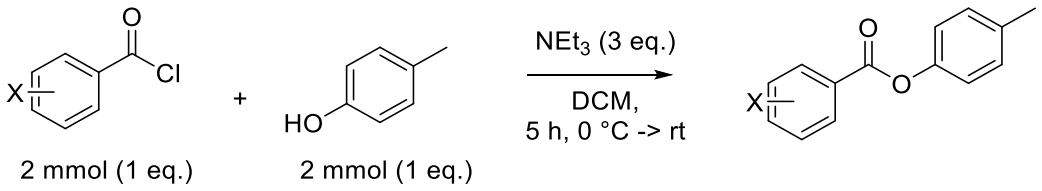

p-Cresol (2 mmol, 216 µl) and triethylamine (6 mmol, 835 µl) were dissolved in DCM (3 ml) in a 10 ml reaction vial and cooled down to 0 °C. Substituted benzoyl chloride (2 mmol) was dissolved in DCM (3 ml) in another vial and slowly added (ca. 5 min) to the reaction mixture in the first vial. After addition, the ice bath was removed, and the reaction mixture was stirred for 5 h at rt. After the reaction completion, the reaction mixture was transferred into a separatory funnel, diluted with DCM (20 ml), and quenched with HCl (10 ml; 0.1 M). The organic layer was washed again with a base NaOH (10 ml; 0.1 M) to remove any remaining benzoyl chloride or substrate, and then once again with HCl (10 ml; 0.1 M). The organic fraction was then dried over Na_2SO_4, filtered, and concentrated in vacuo. The products were analyzed by NMR spectroscopy and used without any additional purification.

p-tolyl 2,3,4,5,6-pentafluorobenzoate (10a)

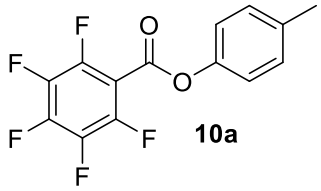

10a

Yield	77%, White solid
^{1}H NMR	1H NMR (400 MHz, CDCl3) δ 7.24 (d, J = 8.3 Hz, 2H), 7.12 (d, J = 8.5 Hz, 2H), 2.38 (s, 3H).
^{13}C NMR	13C NMR (101 MHz, CDCl3) (except for C6F5) δ 157.7, 147.9, 136.6, 130.2, 120.9, 20.9.
^{19}F NMR	19F NMR (376 MHz, CDCl3) δ -137.8 – -137.9 (m), -148.0 (tt, J = 20.9, 4.8 Hz), -160.4 – -160.6 (m).
HR-MS (EI)	$(M)^{+\cdot}$: calc. 302.0361, found 302.0355

p-tolyl 3,5-bis(trifluoromethyl)benzoate (11a)

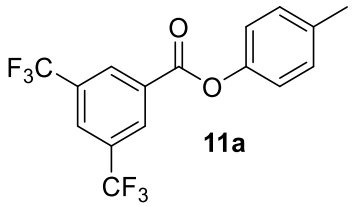

11a

Yield	72%, colourless oil
^{1}H NMR	^{1}H NMR (400 MHz, $CDCl_3$) δ 8.65 (s, 2H), 8.14 (s, 1H), 7.26 (d, *J* = 8.2 Hz, 2H), 7.15 – 7.06 (m, 2H), 2.40 (s, 3H).
^{13}C NMR	^{13}C NMR (101 MHz, $CDCl_3$) δ 162.8, 148.2, 136.3, 132.6 (q, *J* = 34.0 Hz), 132.0, 130.3 (bs), 126.9 (p, *J* = 3.8 Hz), 122.8 (q, *J* = 273.0 Hz), 121.0, 20.9.
^{19}F NMR	^{19}F NMR (376 MHz, $CDCl_3$) δ -63.4.
HR-MS (EI)	$(M)^{+\cdot}$: calc. 348.0579, found 348.0574

Synthesis of **13a** and **15a**

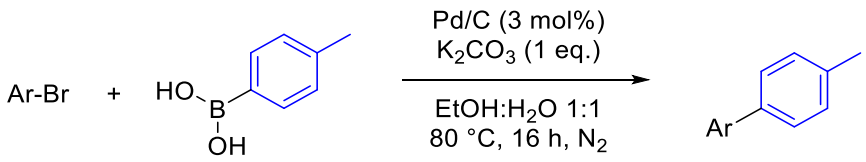

The Suzuki cross-coupling reactions[17] were performed by dissolving the 4-Methylphenylboronic acid (204 mg, 1.50 mmol, 1.5 eq.) and sodium bicarbonate (138 mg, 1.00 mmol, 1.0 eq.) as a base in a mixture of ethanol and water (1:1, 8 mL) inside a 10 mL crimp vial. To each vial, an aryl bromide and Pd/C as catalyst (31.8 mg corresponding to 0.03 mmol, 0.03 eq. of pure Pd) was added before it was closed, degassed and set under N_2 atmosphere. The reaction mixtures were stirred overnight at elevated temperature (16 h, 80 °C). After the completion, most of the ethanol was removed *in vacuo*, and the products were isolated by extraction (ethyl acetate/brine 1:1, 15 mL each). The product-containing organic phases were dried over sodium sulfate and after filtration, a spoon-full of flush silica gel (60M, Ø 0.04 – 0.036 mm) was added to prepare a dry load for a column chromatography. The dry load was transferred onto a silica gel column and the products were eluted with ethyl acetate as eluent (a single fraction collected). Products were analyzed by NMR spectroscopy.

4-methyl-4′-((trifluoromethyl)sulfonyl)-1,1′-biphenyl (13a)

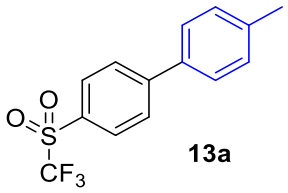

13a

Yield	48%, white solid
^{1}H NMR	^{1}H NMR (400 MHz, $CDCl_3$) δ 8.08 (d, *J* = 8.4 Hz, 2H), 7.85 (d, *J* = 8.5 Hz, 2H), 7.55 (d, *J* = 8.1 Hz, 2H), 7.33 (d, *J* = 7.9 Hz, 2H), 2.44 (s, 3H).
^{13}C NMR	^{13}C NMR (101 MHz, $CDCl_3$) δ 149.6, 139.7, 135.5, 131.3, 130.0, 129.1, 128.1, 127.4, 119.9 (q, *J* = 325.8 Hz), 21.3.
^{19}F NMR	^{19}F NMR (376 MHz, $CDCl_3$) δ -78.9.

2,4′-dimethyl-5-nitro-1,1′-biphenyl (15a)

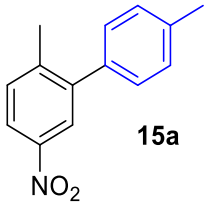

15a

Yield	94%, orange oil
^{1}H NMR	^{1}H NMR (400 MHz, $CDCl_3$) δ 8.12 – 8.05 (m, 2H), 7.44 – 7.36 (m, 1H), 7.27 (d, *J* = 8.2 Hz, 2H), 7.23 – 7.18 (m, 2H), 2.43 (s, 3H), 2.37 (s, 3H).
^{13}C NMR	^{13}C NMR (101 MHz, $CDCl_3$) δ 146.3, 143.6, 143.1, 137.7, 136.7, 131.1, 129.2, 128.8, 124.7, 121.9, 21.2, 20.9.
HR-MS (EI)	$(M)^+$: calc. 227.0941, found 227.0945

Synthesis of **16a, 17a** and **23a**

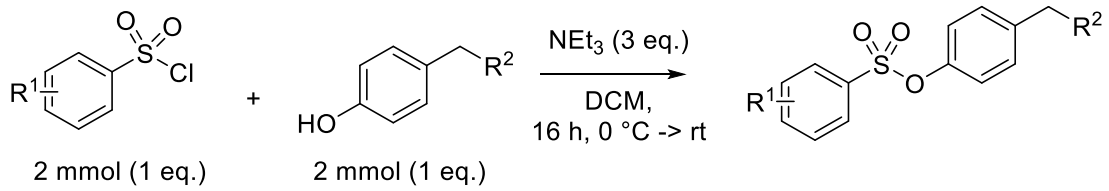

The corresponding phenol (2 mmol) and triethylamine (6 mmol, 835 µl) were dissolved in DCM (3 ml) in a 10 ml reaction vial and cooled down to 0 °C. Sulfonyl chloride (2 mmol) was dissolved in DCM (3 ml) in another vial and slowly added (ca. 5 min) to the reaction mixture in the first vial. After addition, the ice bath was removed, and the reaction mixture was stirred overnight (16 h) at rt. After the reaction completion, the reaction mixture was transferred into a separatory funnel, diluted with DCM (20 ml), and quenched with HCl (10 ml; 0.1 M). The organic layer was washed again with a base NaOH (10 ml; 0.1 M) to remove any remaining substrate, and then once again with HCl (10 ml; 0.1 M). The organic fraction was then dried over Na_2SO_4, filtered, and concentrated in vacuo. The products were analyzed by NMR spectroscopy and used without any additional purification.

p-tolyl 4-methylbenzenesulfonate (16a)

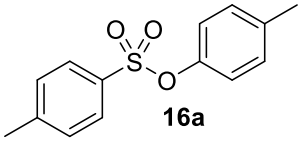

Yield	87%, White solid
^{1}H NMR	^{1}H NMR (400 MHz, $CDCl_3$) δ 7.76 – 7.61 (m, 2H), 7.30 (d, *J* = 8.0 Hz, 2H), 7.09 – 7.02 (m, 2H), 6.88 – 6.80 (m, 2H), 2.44 (s, 3H), 2.30 (s, 3H).
^{13}C NMR	^{13}C NMR (101 MHz, $CDCl_3$) δ 147.5, 145.2, 137.0, 132.6, 130.1, 129.7, 128.6, 122.1, 21.7, 20.9.
HR-MS (ESI)	$(M+H)^+$: calc. 263.0736, found 263.0736

p-tolyl 2,4,6-trimethylbenzenesulfonate (17a)

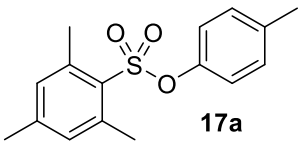

Yield	78%, White solid
^{1}H NMR	^{1}H NMR (400 MHz, $CDCl_3$) δ 7.05 (d, *J* = 8.2 Hz, 2H), 6.96 (s, 2H), 6.86 – 6.81 (m, 2H), 2.55 (s, 6H), 2.32 (s, 3H), 2.29 (s, 3H).
^{13}C NMR	^{13}C NMR (101 MHz, $CDCl_3$) δ 147.3, 143.7, 140.5, 136.8, 131.7, 130.7, 130.1, 122.0, 22.8, 21.1, 20.9.
HR-MS (ESI)	$(M+H)^+$: calc. 291.1049, found 291.1051

4-ethylphenyl 4-methylbenzenesulfonate (23a)

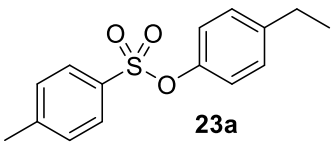

Yield	83%, colorless oil

^{1}H NMR	^{1}H NMR (400 MHz, $CDCl_3$) δ 7.71 (d, *J* = 8.6 Hz, 2H), 7.30 (d, *J* = 8.0 Hz, 2H), 7.13 – 7.04 (m, 2H), 6.94 – 6.81 (m, 2H), 2.60 (q, *J* = 7.6 Hz, 2H), 2.45 (s, 3H), 1.20 (t, *J* = 7.6 Hz, 3H).
^{13}C NMR	^{13}C NMR (101 MHz, $CDCl_3$) δ 147.6, 145.2, 143.2, 132.6, 129.7, 128.9, 128.6, 122.1, 28.3, 21.7, 15.4.
HR-MS (ESI)	$(M+H)^+$: calc. 277.0893 , found 277.0896

Synthesis of **18a**

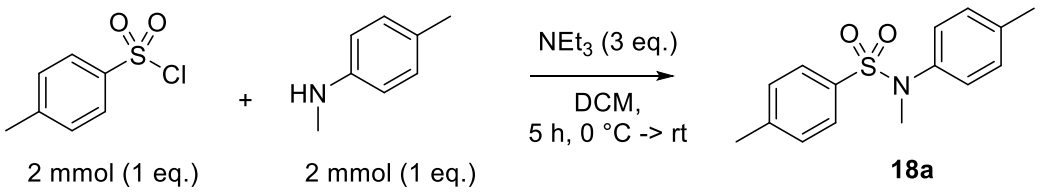

N,4-dimethylaniline (2 mmol, 242 mg) and triethylamine (6 mmol, 835 µl) were dissolved in DCM (3 ml) in a 10 ml reaction vial and cooled down to 0 °C. Tosyl chloride (2 mmol, 380 mg) was dissolved in DCM (3 ml) in another vial and slowly added (ca. 5 min) to the reaction mixture in the first vial. After addition, the ice bath was removed, and the reaction mixture was stirred for 5 h at rt. After the reaction completion, the reaction mixture was transferred into a separatory funnel, diluted with DCM (20 ml), and quenched with HCl (10 ml; 0.1 M). The organic layer was washed again with a base NaOH (10 ml; 0.1 M) to remove any remaining tosyl chloride, and then once again with HCl (10 ml; 0.1 M). The organic fraction was then dried over Na_2SO_4, filtered, and concentrated in vacuo. The products were analyzed by NMR spectroscopy and used without any additional purification.

N,4-dimethyl-N-(p-tolyl)benzenesulfonamide (18a)

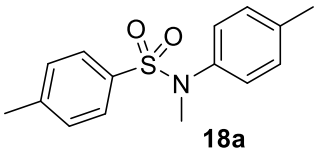

Yield	85%, slightly brownish oil
^{1}H NMR	^{1}H NMR (400 MHz, $CDCl_3$) δ 7.46 – 7.40 (m, 2H), 7.24 (d, *J* = 8.0 Hz, 2H), 7.09 (d, *J* = 8.1 Hz, 2H), 6.99 – 6.93 (m, 2H), 3.13 (s, 3H), 2.42 (s, 3H), 2.33 (s, 3H).
^{13}C NMR	^{13}C NMR (101 MHz, $CDCl_3$) δ 143.5, 139.0, 137.3, 133.7, 129.5, 129.3, 128.0, 126.6, 38.2, 21.6, 21.1.
HR-MS (ESI)	$(M+H)^+$: calc. 276.1053, found 276.1052

Synthesis of **27a**

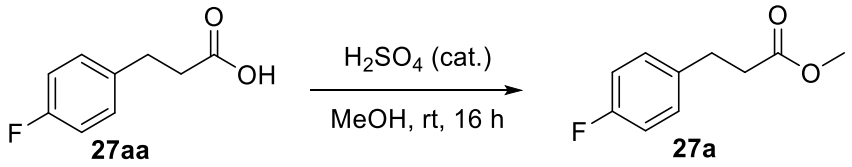

The carboxylic acid **27aa** (1.68 g, 10.00 mmol, 1.0 eq.) was dissolved in methanol (50 mL) inside a 250 mL round-bottom flask and five drops of conc. H_2SO_4 were added as an acid catalyst. The reaction mixture was stirred overnight (~16 h, r.t.) and after the completion of the reaction, the methanol was removed by a rotary evaporator. The remaining oil was dissolved in ethyl acetate (20 mL) and washed twice with saturated brine (20 mL each). The organic phase was dried over Na_2SO_4 and after filtrating the drying agent off, the ethyl acetate was removed *in vacuo to obtain* a pure product **27a**.

N-(4-(trifluoromethoxy)benzyl)acetamide (27a)

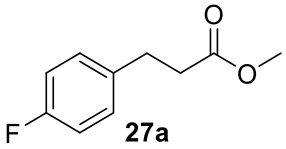

Yield	81%, colourless oil
^{1}H NMR	^{1}H NMR (400 MHz, $CDCl_3$) δ 7.20 – 7.09 (m, 2H), 6.96 (t, *J* = 8.7 Hz, 2H), 3.66 (s, 3H), 2.92 (t, *J* = 7.7 Hz, 2H), 2.61 (t, *J* = 7.7 Hz, 2H).
^{13}C NMR	^{13}C NMR (101 MHz, $CDCl_3$) δ 173.2, 161.5 (d, *J* = 244.0 Hz), 136.2 (d, *J* = 3.2 Hz), 129.7 (d, *J* = 7.8 Hz), 115.3 (d, *J* = 21.2 Hz), 51.7, 35.8, 30.1.
^{19}F NMR	^{19}F NMR (376 MHz, $CDCl_3$) δ -117.5.
HR-MS (EI)	$(M)^{+\cdot}$: calc. 182.0738, found 182.0741

3.6.4.2 Characterization of the products of photochemical reactions

N-(4-fluorobenzyl)acetamide (1b)[13b]

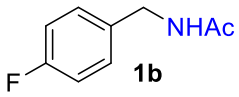

1b

Yield	81% (54 mg, 0.32 mmol), White solid
^{1}H NMR	^{1}H NMR (400 MHz, $CDCl_3$) δ 7.25 – 7.13 (m, 2H), 7.07 – 6.89 (m, 2H), 6.33 (s, 1H), 4.32 (d, *J* = 5.8 Hz, 2H), 1.96 (s, 3H).
^{13}C NMR	^{13}C NMR (101 MHz, $CDCl_3$) δ 170.2, 162.1 (d, *J* = 245.5 Hz), 134.2 (d, *J* = 3.2 Hz), 129.4 (d, *J* = 8.1 Hz), 115.5 (d, *J* = 21.5 Hz), 42.9, 23.1.
^{19}F NMR	^{19}F NMR (376 MHz, $CDCl_3$) δ -115.7.

N-(4-chlorobenzyl)acetamide (2b)[13b]

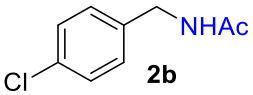

2b

Yield	78% (57 mg, 0.31 mmol), White solid
^{1}H NMR	^{1}H NMR (400 MHz, $CDCl_3$) δ 7.25 (d, *J* = 8.5 Hz, 2H), 7.15 (d, *J* = 8.4 Hz, 2H), 6.37 (s, 1H), 4.31 (d, *J* = 5.9 Hz, 2H), 1.96 (s, 3H).
^{13}C NMR	^{13}C NMR (101 MHz, $CDCl_3$) δ 170.3, 136.9, 133.2, 129.1, 128.8, 42.9, 23.1.

N-(3-chlorobenzyl)acetamide (3b)[18]

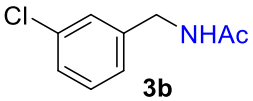

3b

Yield	43% (31 mg, 0.17 mmol), White solid
^{1}H NMR	^{1}H NMR (400 MHz, $CDCl_3$) δ 7.26 – 7.20 (m, 3H), 7.17 – 7.10 (m, 1H), 6.19 (s, 1H), 4.36 (d, *J* = 5.9 Hz, 2H), 2.00 (s, 3H).
^{13}C NMR	^{13}C NMR (101 MHz, $CDCl_3$) δ 170.2, 140.4, 134.5, 130.0, 127.8, 127.6, 125.9, 43.1, 23.2.

N-(4-bromobenzyl)acetamide (4b)[13b]

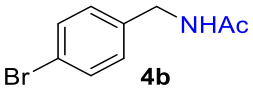

4b

Yield	73% (67 mg, 0.29 mmol), White solid
^{1}H NMR	^{1}H NMR (400 MHz, $CDCl_3$) δ 7.41 (d, *J* = 8.5 Hz, 2H), 7.11 (d, *J* = 8.5 Hz, 2H), 6.26 (s, 1H), 4.31 (d, *J* = 5.9 Hz, 2H), 1.97 (s, 3H).
^{13}C NMR	^{13}C NMR (101 MHz, $CDCl_3$) δ 170.2, 137.4, 131.7, 129.5, 121.3, 43.0, 23.2.

N-benzylacetamide (5b)[13b]

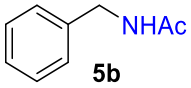

5b

Yield	50% (30 mg, 0.20 mmol), White solid
^{1}H NMR	^{1}H NMR (400 MHz, $CDCl_3$) δ 7.39 – 7.17 (m, 5H), 6.04 (s, 1H), 4.39 (d, *J* = 5.7 Hz, 2H), 1.99 (s, 3H).
^{13}C NMR	^{13}C NMR (101 MHz, $CDCl_3$) δ 170.1, 138.3, 128.7, 127.9, 127.5, 43.7, 23.2.

N-(4-(trifluoromethoxy)benzyl)acetamide (7b)[6a]

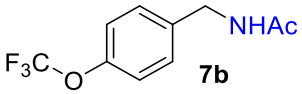

7b

Yield	50% (47 mg, 0.20 mmol), White solid
^{1}H NMR	^{1}H NMR (400 MHz, $CDCl_3$) δ 7.28 (d, *J* = 8.7 Hz, 2H), 7.15 (d, *J* = 8.0 Hz, 2H), 6.14 (s, 1H), 4.39 (d, *J* = 5.9 Hz, 2H), 1.99 (s, 3H).
^{13}C NMR	^{13}C NMR (101 MHz, $CDCl_3$) δ 170.2, 148.5 (d, *J* = 1.8 Hz), 137.2, 129.2, 121.7 (q, *J* = 258.6 Hz), 121.2, 42.9, 23.2.
^{19}F NMR	^{19}F NMR (376 MHz, $CDCl_3$) δ -58.4.

methyl 4-(acetamidomethyl)benzoate (8b)

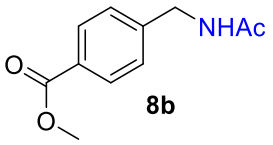

8b

Yield	29% (24 mg, 0.12 mmol), White solid
^{1}H NMR	^{1}H NMR (400 MHz, $CDCl_3$) δ 7.96 (d, 2H), 7.31 (d, *J* = 8.5 Hz, 2H), 6.12 (s, 1H), 4.45 (d, *J* = 5.9 Hz, 2H), 3.89 (s, 3H), 2.03 (s, 3H).
^{13}C NMR	^{13}C NMR (101 MHz, $CDCl_3$) δ 170.17, 166.9, 143.6, 123.0, 129.3, 127.5, 52.2, 43.3, 23.2.
HR-MS (EI)	$(M)^{+\cdot}$: calc. 207.0890, found 207.0891

methyl 3-(acetamidomethyl)benzoate (9b)

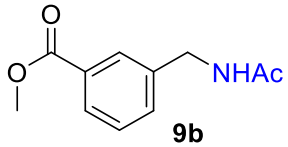

9b

Yield	40% (33 mg, 0.16 mmol), White solid
^{1}H NMR	^{1}H NMR (400 MHz, $CDCl_3$) δ 7.97 – 7.84 (m, 2H), 7.49 – 7.42 (m, 1H), 7.37 (t, *J* = 7.9 Hz, 1H), 6.16 (s, 1H), 4.44 (d, *J* = 5.9 Hz, 2H), 3.88 (s, 3H), 2.01 (s, 3H).
^{13}C NMR	^{13}C NMR (101 MHz, $CDCl_3$) δ 170.2, 166.9, 138.8, 132.4, 130.5, 128.8, 128.7, 52.2, 43.3, 23.2.
HR-MS (EI)	$(M)^{+\cdot}$: calc. 207.0890, found 207.0887

4-(acetamidomethyl)phenyl 2,3,4,5,6-pentafluorobenzoate (10b)

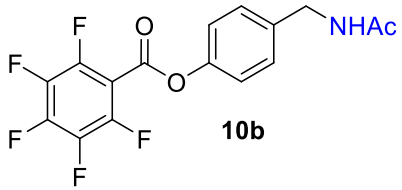

10b

Yield	61% (88 mg, 0.24 mmol), White solid
^{1}H NMR	^{1}H NMR (400 MHz, $CDCl_3$) δ 7.33 (d, *J* = 8.5 Hz, 2H), 7.16 (d, *J* = 8.7 Hz, 2H), 6.37 (s, 1H), 4.40 (d, *J* = 5.7 Hz, 2H), 2.00 (s, 3H).
^{13}C NMR	^{13}C NMR (101 MHz, $CDCl_3$): (except for C_6F_5) δ 170.4, 157.6, 149.2, 137.1, 129.2, 121.5, 43.0, 23.1.
^{19}F NMR	^{19}F NMR (376 MHz, $CDCl_3$) δ -137.6 – -137.8 (m), -147.5 (tt, *J* = 21.3, 5.4 Hz), -160.2 – -160.4 (m).
HR-MS (ESI)	$(M+H)^{+}$: calc. 360.0654 , found 360.0656

4-(acetamidomethyl)phenyl 3,5-bis(trifluoromethyl)benzoate (11b)

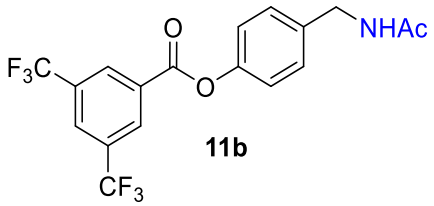

11b

Yield	57% (92 mg, 0.23 mmol), White solid
^{1}H NMR	^{1}H NMR (400 MHz, $CDCl_3$) δ 8.61 (s, 2H), 8.13 (s, 1H), 7.35 (d, *J* = 8.5 Hz, 2H), 7.22 – 7.12 (m, 2H), 6.45 (s, 1H), 4.42 (d, *J* = 5.8 Hz, 2H), 2.01 (s, 3H).
^{13}C NMR	^{13}C NMR (101 MHz, $CDCl_3$) δ 170.4, 162.7, 149.6, 136.9, 132.5 (q, *J* = 34.2 Hz), 131.7, 130.3 (d, *J* = 3.1 Hz), 129.2, 127.0 (p, *J* = 3.6 Hz), 122.8 (q, *J* = 272.9 Hz), 121.6, 43.0, 23.1.
^{19}F NMR	^{19}F NMR (376 MHz, $CDCl_3$) δ -63.5.
HR-MS (ESI)	$(M+H)^+$: calc. 406.0872 , found 406.0876

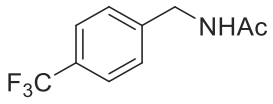

12b

12b was not obtained according to ^{1}H NMR. SM remained unreacted.

N-((4'-((trifluoromethyl)sulfonyl)-[1,1'-biphenyl]-4-yl)methyl)acetamide (13b)

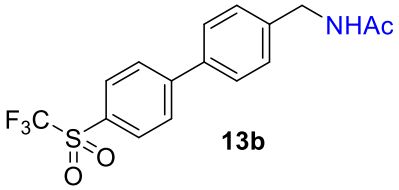

13b

Yield	48% (35 mg, 0.1 mmol), White solid
^{1}H NMR	^{1}H NMR (400 MHz, $CDCl_3$) δ 8.06 (d, *J* = 8.4 Hz, 2H), 7.92 – 7.72 (m, 2H), 7.65 – 7.53 (m, 2H), 7.42 (d, *J* = 8.2 Hz, 2H), 6.06 (s, 1H), 4.49 (d, *J* = 5.9 Hz, 2H), 2.05 (s, 3H).
^{13}C NMR	^{13}C NMR (101 MHz, $CDCl_3$) δ 149.1, 139.9, 137.5, 131.4, 128.6, 128.3, 127.8, 119.9 (q, *J* = 325.8 Hz), 43.2, 23.3.
^{19}F NMR	^{19}F NMR (376 MHz, $CDCl_3$) δ -78.9.
HR-MS (ESI)	$(M+H)^+$: calc. 358.0719 , found 358.0723

Experiment was performed on a 0.2 mmol scale (only one reaction vial).

N-((2'-cyano-[1,1'-biphenyl]-4-yl)methyl)acetamide (14b)

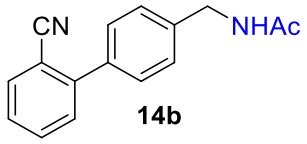

14b

Yield	81% (81 mg, 0.32 mmol), White solid
^{1}H NMR	^{1}H NMR (400 MHz, $CDCl_3$) δ 7.73 (dd, *J* = 7.8, 1.4 Hz, 1H), 7.62 (td, *J* = 7.7, 1.4 Hz, 1H), 7.50 – 7.39 (m, 4H), 7.39 – 7.33 (m, 2H), 6.47 (s, 1H), 4.43 (d, *J* = 5.7 Hz, 2H), 1.99 (s, 3H).
^{13}C NMR	^{13}C NMR (101 MHz, $CDCl_3$) δ 170.4, 145.1, 139.1, 137.3, 133.7, 133.0, 130.1, 129.0, 128.2, 127.7, 118.8, 111.1, 43.3, 23.1.
HR-MS (EI)	$(M)^{+\cdot}$: calc. 250.1101, found 250.1098

N-((2'-methyl-5'-nitro-[1,1'-biphenyl]-4-yl)methyl)acetamide (15b)

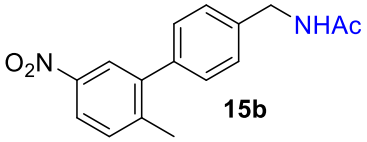

15b

Yield	37% (42 mg, 0.15 mmol), White solid
^{1}H NMR	^{1}H NMR (400 MHz, $CDCl_3$) δ 8.15 – 7.97 (m, 2H), 7.45 – 7.33 (m, 3H), 7.28 – 7.21 (m, 2H), 6.14 (s, 1H), 4.48 (d, *J* = 5.9 Hz, 2H), 2.33 (s, 3H), 2.05 (s, 3H).
^{13}C NMR	^{13}C NMR (101 MHz, $CDCl_3$) δ 170.2, 146.2, 143.6, 142.7, 138.8, 138.2, 131.2, 129.3, 127.9, 124.6, 122.2, 43.4, 23.3, 20.8.
HR-MS (EI)	$(M)^{+\cdot}$: calc. 284.1155, found 284.1157

4-(acetamidomethyl)phenyl 4-methylbenzenesulfonate (16b)[6a]

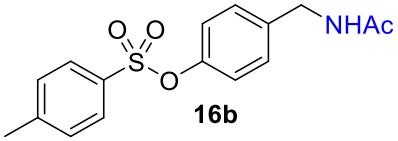

16b

Yield	37% (47 mg, 0.15 mmol), White solid
^{1}H NMR	^{1}H NMR (400 MHz, $CDCl_3$) δ 7.69 (d, *J* = 8.4 Hz, 2H), 7.31 (d, *J* = 7.7 Hz, 2H), 7.18 (d, *J* = 8.7 Hz, 2H), 6.92 (d, *J* = 8.6 Hz, 2H), 5.92 (s, 1H), 4.37 (d, *J* = 5.9 Hz, 2H), 2.45 (s, 3H), 2.00 (s, 3H).
^{13}C NMR	^{13}C NMR (101 MHz, $CDCl_3$) δ 170.0, 148.8, 145.5, 137.5, 132.4, 129.9, 129.0, 128.5, 122.6, 42.9, 23.3, 21.8.

4-(acetamidomethyl)phenyl 2,4,6-trimethylbenzenesulfonate (17b - major)

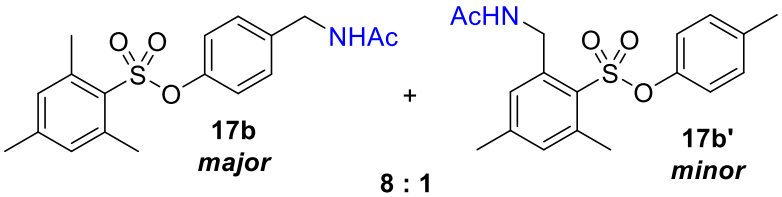

17b ***major*** **8 : 1** **17b'** ***minor***

Yield	38% (51 mg, 0.15 mmol), slightly brownish oil
^{1}H NMR (major)	^{1}H NMR (400 MHz, $CDCl_3$) δ 7.15 (d, *J* = 8.6 Hz, 2H), 6.96 (s, 2H), 6.89 (d, *J* = 8.6 Hz, 2H), 6.15 (s, 1H), 4.34 (d, *J* = 5.9 Hz, 2H), 2.53 (s, 6H), 2.37 – 2.26 (m, 4H), 1.98 (s, 3H).

^{13}C NMR (major)	^{13}C NMR (101 MHz, $CDCl_3$) δ 170.2, 148.7, 144.0, 140.4, 137.3, 131.9, 128.9, 122.4, 42.9, 23.1, 22.7, 21.1.
HR-MS (ESI)	$(M+H)^+$: calc. 348.1264 , found 348.1267 (major), 348.1265 (minor) (the isomers separate well in LC-QTOF instrument)

See the end of this chapter for more detailed information about the identification of the minor isomer.

N-(4-((N,4-dimethylphenyl)sulfonamido)benzyl)acetamide (18b)

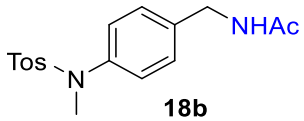

18b

Yield	59% (78 mg, 0.23 mmol), White solid
^{1}H NMR	^{1}H NMR (400 MHz, $CDCl_3$) δ 7.39 (d, *J* = 8.3 Hz, 2H), 7.22 (d, *J* = 8.0 Hz, 2H), 7.17 (d, *J* = 8.4 Hz, 2H), 7.01 (d, *J* = 8.3 Hz, 2H), 6.33 (s, 1H), 4.36 (d, *J* = 5.8 Hz, 2H), 3.09 (s, 3H), 2.39 (s, 3H), 1.98 (s, 3H).
^{13}C NMR	^{13}C NMR (101 MHz, $CDCl_3$) δ 170.3, 143.8, 140.8, 137.7, 133.5, 129.5, 128.2, 127.9, 126.8, 43.0, 38.1, 23.2, 21.6.
HR-MS (ESI)	$(M+H)^+$: calc. 333.1267 , found 333.1268

N-(1-(4-fluorophenyl)ethyl)acetamide (19b)[19]

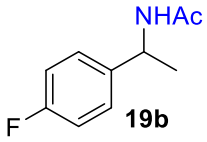

19b

Yield	72% (52 mg, 0.29 mmol), White solid
^{1}H NMR	^{1}H NMR (400 MHz, $CDCl_3$) δ 7.26 (dd, *J* = 8.7, 5.2 Hz, 2H), 6.99 (t, *J* = 8.7 Hz, 2H), 6.19 (s, 1H), 5.07 (p, *J* = 7.1 Hz, 1H), 1.97 (s, 3H), 1.45 (d, *J* = 6.9 Hz, 3H).
^{13}C NMR	^{13}C NMR (101 MHz, $CDCl_3$) δ 169.4, 162.0 (d, *J* = 245.6 Hz), 139.0 (d, *J* = 3.2 Hz), 127.8 (d, *J* = 8.0 Hz), 115.4 (d, *J* = 21.4 Hz), 48.3, 23.2, 21.8.
^{19}F NMR	^{19}F NMR (377 MHz, $CDCl_3$) δ -115.9.

N-(1-(4-chlorophenyl)ethyl)acetamide (20b)[19]

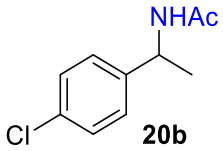

20b

Yield	77% (61 mg, 0.31 mmol), White solid
^{1}H NMR	^{1}H NMR (400 MHz, $CDCl_3$) δ 7.30 – 7.24 (m, 2H), 7.24 – 7.19 (m, 2H), 6.26 (d, *J* = 7.7 Hz, 1H), 5.04 (p, *J* = 7.1 Hz, 1H), 1.95 (s, 3H), 1.43 (d, *J* = 7.0 Hz, 3H).
^{13}C NMR	^{13}C NMR (101 MHz, $CDCl_3$) δ 169.4, 142.0, 132.9, 128.7, 127.6, 48.2, 23.3, 21.8.

N-(1-(4-bromophenyl)ethyl)acetamide (21b)[19]

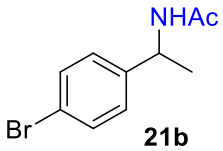

21b

Yield	57% (55 mg, 0.23 mmol), White solid

^{1}H NMR	^{1}H NMR (400 MHz, $CDCl_3$) δ 7.50 – 7.39 (m, 2H), 7.22 – 7.14 (m, 2H), 5.75 (s, 1H), 5.07 (p, *J* = 7.1 Hz, 1H), 1.98 (s, 3H), 1.46 (d, *J* = 6.9 Hz, 3H).
^{13}C NMR	^{13}C NMR (101 MHz, $CDCl_3$) δ 169.2, 142.3, 131.8, 128.0, 121.2, 48.3, 23.4, 21.7.

N-(1-phenylethyl)acetamide (22b)[6a]

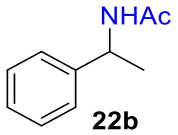

22b

Yield	58% (38 mg, 023 mmol), White solid
^{1}H NMR	^{1}H NMR (400 MHz, $CDCl_3$) δ 7.37 – 7.22 (m, 5H), 5.94 (s, 1H), 5.11 (p, *J* = 7.0 Hz, 1H), 1.96 (s, 3H), 1.47 (d, *J* = 6.9 Hz, 3H).
^{13}C NMR	^{13}C NMR (101 MHz, $CDCl_3$) δ 169.2, 143.2, 128.7, 127.4, 126.2, 48.8, 23.4, 21.8.

4-(1-acetamidoethyl)phenyl 4-methylbenzenesulfonate (23b)

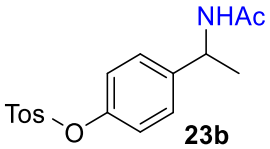

23b

Yield	87% (116 mg, 0.35 mmol), White solid
^{1}H NMR	^{1}H NMR (400 MHz, $CDCl_3$) δ 7.68 (dd, *J* = 8.3, 1.4 Hz, 2H), 7.30 (d, *J* = 8.3 Hz, 2H), 7.20 (d, *J* = 8.5 Hz, 2H), 6.89 (dd, *J* = 8.6, 2.0 Hz, 2H), 6.21 (s, 1H), 5.04 (p, *J* = 7.1 Hz, 1H), 2.43 (s, 3H), 1.93 (d, *J* = 2.8 Hz, 3H), 1.40 (dd, *J* = 6.9, 2.2 Hz, 3H).
^{13}C NMR	^{13}C NMR (101 MHz, $CDCl_3$) δ 169.5, 148.6, 145.5, 142.4, 132.4, 129.9, 128.4, 127.5, 122.4, 48.1, 23.2, 21.8, 21.7.
HR-MS (ESI)	$(M+H)^+$: calc. 334.1108, found 334.1106

N-(1-(4-cyanophenyl)ethyl)acetamide (24b)[20]

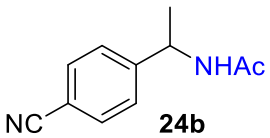

24b

Yield	60% (45 mg, 0.24 mmol), White solid
^{1}H NMR	^{1}H NMR (400 MHz, $CDCl_3$) δ 7.61 (d, *J* = 8.4 Hz, 2H), 7.41 (d, *J* = 8.1 Hz, 2H), 5.91 (s, 1H), 5.11 (p, *J* = 7.1 Hz, 1H), 2.00 (s, 3H), 1.47 (d, *J* = 7.0 Hz, 3H).
^{13}C NMR	^{13}C NMR (101 MHz, $CDCl_3$) δ 169.4, 148.9, 132.5, 126.9, 118.8, 111.1, 48.7, 23.3, 21.8.

ethyl 4-(1-acetamidoethyl)benzoate (25b)

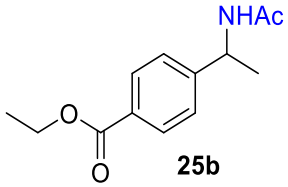

25b

Yield	69% (65 mg, 0.28 mmol), White solid
^{1}H NMR	^{1}H NMR (400 MHz, $CDCl_3$) δ 7.95 (d, *J* = 8.4 Hz, 2H), 7.33 (d, *J* = 8.2 Hz, 2H), 6.47 (d, *J* = 7.5 Hz, 1H), 5.10 (p, *J* = 7.1 Hz, 1H), 4.33 (q, *J* = 7.1 Hz, 2H), 1.96 (s, 3H), 1.43 (d, *J* = 7.0 Hz, 3H), 1.35 (t, *J* = 7.1 Hz, 4H).

^{13}C NMR	^{13}C NMR (101 MHz, $CDCl_3$) δ 169.5, 166.4, 148.6, 129.9, 129.4, 126.1, 70.0, 48.7, 23.2, 21.8, 14.3.
HR-MS (EI)	$(M)^{+\cdot}$: calc. 235.1203, found 235.1202

N-(1-(9,10-dioxo-9,10-dihydroanthracen-2-yl)ethyl)acetamide (26b)

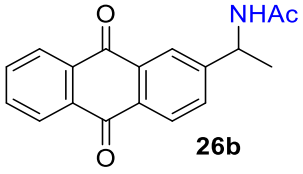

26b

Yield	62% (73 mg, 0.25 mmol), lightly yellowish solid
^{1}H NMR	^{1}H NMR (400 MHz, $CDCl_3$) δ 8.31 – 8.27 (m, 2H), 8.25 (d, *J* = 8.0 Hz, 1H), 8.21 (d, *J* = 1.6 Hz, 1H), 7.87 – 7.75 (m, 2H), 7.73 (dd, *J* = 8.0, 1.7 Hz, 1H), 6.06 (d, *J* = 6.6 Hz, 1H), 5.23 (p, *J* = 7.1 Hz, 1H), 2.06 (s, 3H), 1.55 (d, *J* = 7.0 Hz, 3H).
^{13}C NMR	^{13}C NMR (101 MHz, $CDCl_3$) δ 183.2, 182.8, 169.6, 150.4, 134.2, 134.1, 133.8, 133.5, 132.6, 132.4, 127.9, 127.3, 124.1, 49.0, 23.4, 22.1.
HR-MS (EI)	$(M)^{+\cdot}$: calc. 293.1046, found 293.1041

methyl 3-acetamido-3-(4-fluorophenyl)propanoate (27b)

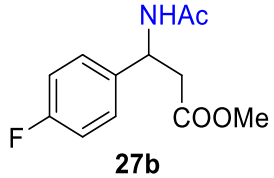

27b

Yield	64% (61 mg, 0.26 mmol), White solid
^{1}H NMR	^{1}H NMR (400 MHz, $CDCl_3$) δ 7.29 – 7.18 (m, 2H), 7.01 – 6.87 (m, 3H), 5.43 – 5.29 (m, 1H), 3.58 (s, 3H), 2.86 (dd, *J* = 15.8, 6.2 Hz, 1H), 2.76 (dd, *J* = 15.7, 6.2 Hz, 1H), 1.95 (s, 3H).
^{13}C NMR	^{13}C NMR (101 MHz, $CDCl_3$) δ 171.5, 169.5, 162.1 (d, *J* = 246.0 Hz), 136.5 (d, *J* = 3.2 Hz), 128.0 (d, *J* = 8.1 Hz), 115.5 (d, *J* = 21.5 Hz), 51.9, 49.1, 39.9, 23.2.
^{19}F NMR	^{19}F NMR (376 MHz, $CDCl_3$) δ -115.4.
HR-MS (EI)	$(M)^{+\cdot}$: calc. 239.0952, found 239.0947

N-(bis(4-fluorophenyl)methyl)acetamide (28b)[19]

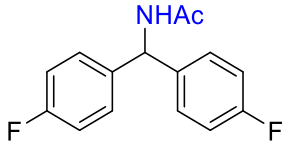

28b

Yield	91% (95 mg, 0.36 mmol), White solid
^{1}H NMR	^{1}H NMR (400 MHz, $CDCl_3$) δ 7.18 – 7.08 (m, 4H), 7.03 – 6.93 (m, 4H), 6.60 (d, *J* = 7.7 Hz, 1H), 6.14 (d, *J* = 8.0 Hz, 1H), 1.96 (s, 3H).
^{13}C NMR	^{13}C NMR (101 MHz, $CDCl_3$) δ 169.4, 162.1 (d, *J* = 246.5 Hz), 137.2 (d, *J* = 3.2 Hz), 129.1 (d, *J* = 8.1 Hz), 115.6 (d, *J* = 21.5 Hz), 55.7, 23.1.
^{19}F NMR	^{19}F NMR (376 MHz, $CDCl_3$) δ -115.3.

N-benzhydrylacetamide (29b)[13b]

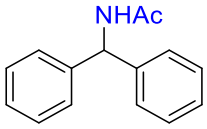

29b

Yield	62% (56 mg, 0.25 mmol), White solid
^{1}H NMR	^{1}H NMR (400 MHz, $CDCl_3$) δ 7.39 – 7.13 (m, 10H), 6.59 (d, *J* = 7.6 Hz, 1H), 6.23 (d, *J* = 8.1 Hz, 1H), 1.98 (s, 3H).
^{13}C NMR	^{13}C NMR (101 MHz, $CDCl_3$) δ 169.4, 141.6, 128.7, 127.6, 127.5, 57.1, 23.2.

Characterization of the minor isomer in reaction mixture 17b

The isomers cannot be separated on a silica TLC plate. The identification of the structure of the minor isomer was done by the ^{1}H NMR (Figure S3. 3 and Figure S3. 4). The ortho isomer **17b'** shows 3 different benzylic signals, while isomer **17b"** is more symmetric and should show only 2 different benzylic protons. The ratio of integrals of the aliphatic NMR signals (1:1:1:1) additionally supports the structure of **17b'** as a minor isomer in the product mixture.

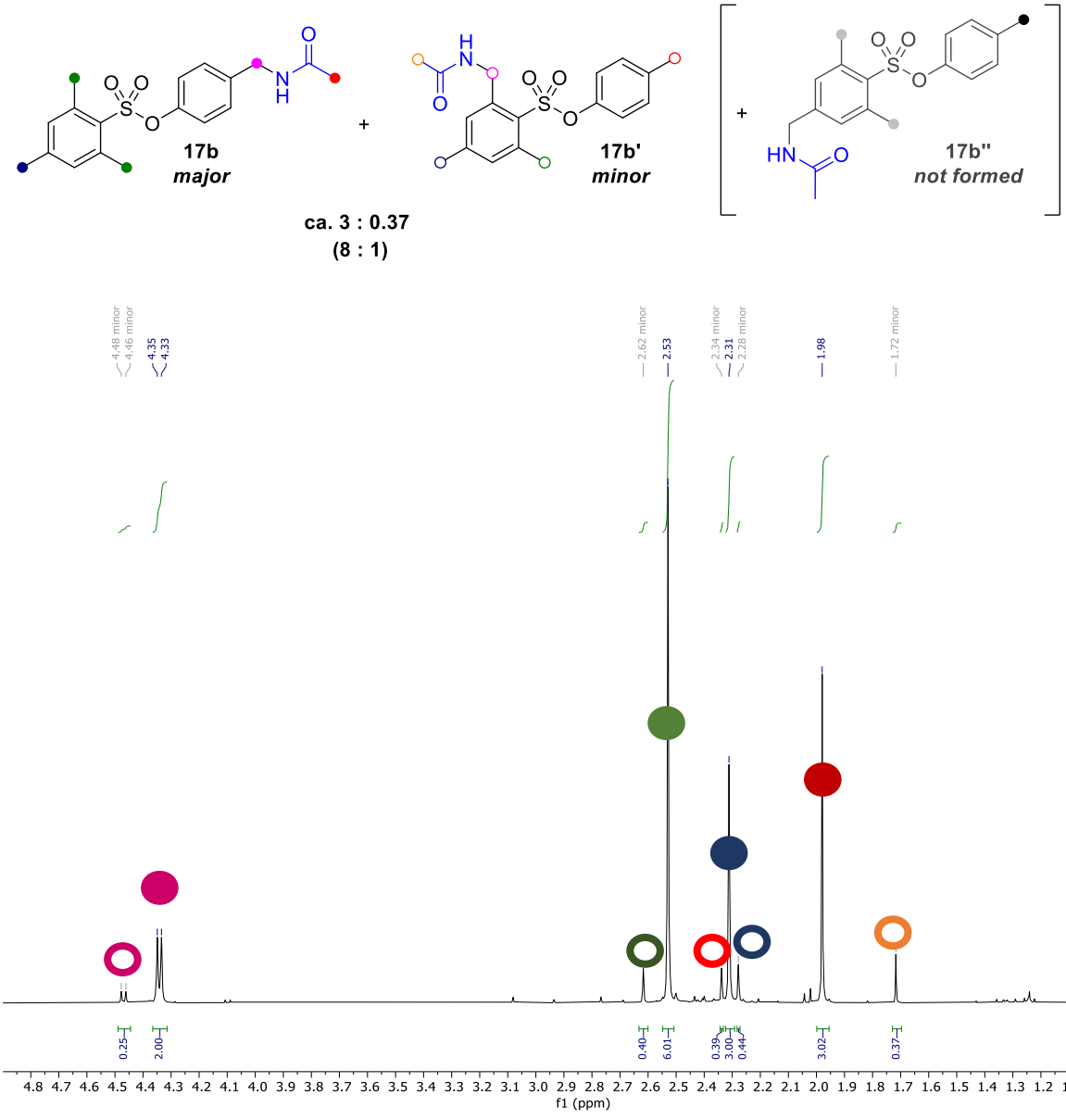

Figure S3. 3: Identification of the minor isomer in the product mixture **17b** – aliphatic region.

The assignments of the signals were done with the help of the ChemDraw NMR predictor. The only signal which is significantly different from the predicted value is signal of acetyl group of **17b'** at 1.72 ppm. The reason for the shift could be the proximity of magnetic field inducing π-systems.

The aromatic region of the ^{1}H NMR (Figure S3. 4) shows quite complex pattern of signals which would fit better to the structure **17b'** than the symmetric molecule **17b''**.

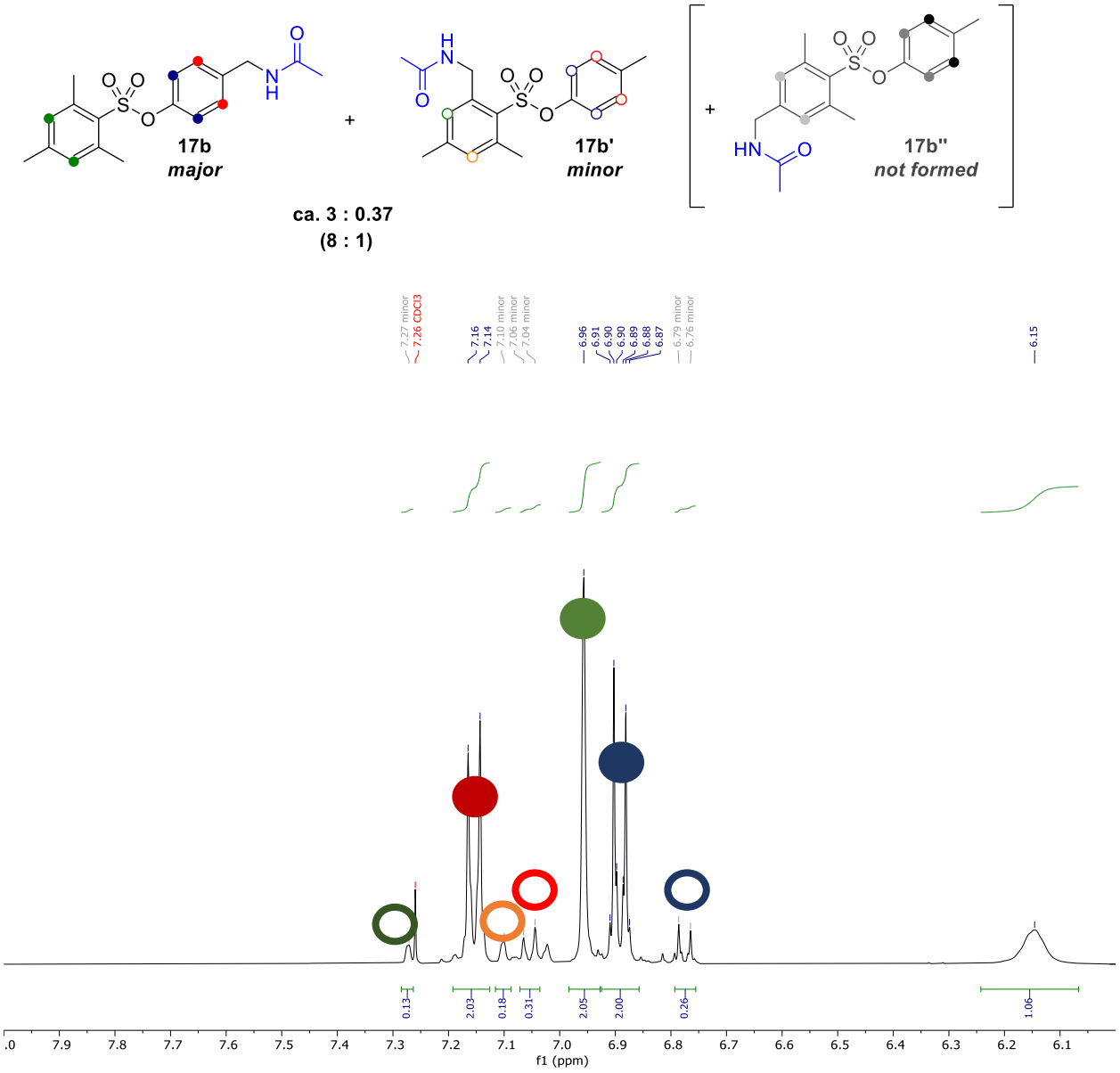

Figure S3. 4: Identification of the minor isomer in the product mixture **17b** – aromatic region.

3.7 Copies of NMR Spectra

Dear reader, for the copies of the NMR spectra click on the URL below to open the full supporting information on the publisher's website (open access).

https://www.rsc.org/suppdata/d2/cc/d2cc03283j/d2cc03283j1.pdf

3.8 Notes and references

1. Abrams, D. J.; Provencher, P. A.; Sorensen, E. J., Recent applications of C–H functionalization in complex natural product synthesis. *Chem. Soc. Rev.* **2018,** *47* (23), 8925-8967.

2. (a) Protti, S.; Fagnoni, M.; Ravelli, D., Photocatalytic C-H Activation by Hydrogen-Atom Transfer in Synthesis. *ChemCatChem* **2015,** *7* (10), 1516-1523; (b) Capaldo, L.; Ravelli, D., Hydrogen Atom Transfer (HAT): A Versatile Strategy for Substrate Activation in Photocatalyzed Organic Synthesis. *Eur. J. Org. Chem.* **2017,** *2017* (15), 2056-2071.

3. Naredla, R. R.; Klumpp, D. A., Contemporary Carbocation Chemistry: Applications in Organic Synthesis. *Chem. Rev.* **2013,** *113* (9), 6905-6948.

4. (a) Zhang, Y.; Fitzpatrick, N. A.; Das, M.; Bedre, I. P.; Yayla, H. G.; Lall, M. S.; Musacchio, P. Z., A photoredox-catalyzed approach for formal hydride abstraction to enable Csp^3–H functionalization with nucleophilic partners (F, C, O, N, and Br/Cl). *Chem Cat.* **2022,** *2* (2), 292-308; (b) Leibler, I. N.-M.; Tekle-Smith, M. A.; Doyle, A. G., A general strategy for C(sp3)–H functionalization with nucleophiles using methyl radical as a hydrogen atom abstractor. *Nat. Commun.* **2021,** *12* (1), 6950; (c) Zhang, F.-M.; Chen, M.-E.; Chen, X.-W.; Hu, Y.-H.; Ye, R.; Lv, J.-W.; Li, B., Recent advances of Ritter reaction and its synthetic applications. *Org. Chem. Front.* **2021**; (d) Jiang, D.; He, T.; Ma, L.; Wang, Z., Recent developments in Ritter reaction. *RSC Adv.* **2014,** *4* (110), 64936-64946; (e) Kiyokawa, K.; Takemoto, K.; Minakata, S., Ritter-type amination of C–H bonds at tertiary carbon centers using iodic acid as an oxidant. *Chem. Commun.* **2016,** *52* (89), 13082-13085; (f) Kiyokawa, K.; Minakata, S., Iodine-Based Reagents in Oxidative Amination and Oxygenation. *Synlett* **2020,** *31* (09), 845-855; (g) Michaudel, Q.; Thevenet, D.; Baran, P. S., Intermolecular Ritter-Type C–H Amination of Unactivated sp^3 Carbons. *J. Am. Chem. Soc.* **2012,** *134* (5), 2547-2550.

5. (a) Reed, N. L.; Yoon, T. P., Oxidase reactions in photoredox catalysis. *Chem. Soc. Rev.* **2021,** *50* (5), 2954-2967; (b) Li, G.-X.; Morales-Rivera, C. A.; Gao, F.; Wang, Y.; He, G.; Liu, P.; Chen, G., A unified photoredox-catalysis strategy for C(sp3)–H hydroxylation and amidation using hypervalent iodine. *Chem. Sci.* **2017,** *8* (10), 7180-7185; (c) Chen, C.; Wang, X.; Yang, T., Recent Synthetic Applications of the Hypervalent Iodine(III) Reagents in Visible-Light-Induced Photoredox Catalysis. *Front. Chem.* **2020,** *8* (551159); (d) Li, P.; Zbieg, J. R.; Terrett, J. A., A Platform for Decarboxylative Couplings via Photoredox Catalysis: Direct Access to Carbocations from Carboxylic Acids for Carbon–Oxygen Bond Formation. *ACS Catal.* **2021,** *11* (17), 10997-11004; (e) Maeda, B.; Sakakibara, Y.; Murakami, K.; Itami, K., Photoredox-Catalyzed Benzylic Esterification via Radical-Polar Crossover. *Org. Lett.* **2021.**

6. (a) Narobe, R.; Murugesan, K.; Schmid, S.; König, B., Decarboxylative Ritter-Type Amination by Cooperative Iodine (I/III)—Boron Lewis Acid Catalysis. *ACS Catal.* **2022,** *12* (1), 809-817; (b) Robert, E. G. L.; Le Du, E.; Waser, J., Synthesis of polycyclic aminal heterocycles via decarboxylative cyclisation of dipeptide derivatives. *Chem. Commun.* **2022,** *58* (21), 3473-3476.

7. (a) Nakajima, M.; Nagasawa, S.; Matsumoto, K.; Kuribara, T.; Muranaka, A.; Uchiyama, M.; Nemoto, T., A Direct $S_0 \rightarrow T_n$ Transition in the Photoreaction of Heavy-Atom-Containing Molecules. *Angew. Chem. Int. Ed.* **2020,** *59* (17), 6847-6852; (b) Amos, S. G. E.; Cavalli, D.; Le Vaillant, F.; Waser, J., Direct Photoexcitation of Ethynylbenziodoxolones: An Alternative to Photocatalysis for Alkynylation Reactions. *Angew. Chem. Int. Ed.* **2021,** *60* (44), 23827-23834; (c) Singh, F. V.; Wirth, T., Hypervalent iodine chemistry and light: photochemical reactions involving hypervalent iodine chemistry. *ARKIVOC* **2021,** *2021* (7), 12-47; (d) Wei, Y.; Zhou, Q.-Q.; Tan, F.; Lu, L.-

Q.; Xiao, W.-J., Visible-Light-Driven Organic Photochemical Reactions in the Absence of External Photocatalysts. *Synthesis* **2019,** *51* (16), 3021-3054.

8. (a) Ye, C.; Twamley, B.; Shreeve, J. n. M., Straightforward Syntheses of Hypervalent Iodine(III) Reagents Mediated by Selectfluor. *Org. Lett.* **2005,** *7* (18), 3961-3964; (b) Sarie, J. C.; Thiehoff, C.; Mudd, R. J.; Daniliuc, C. G.; Kehr, G.; Gilmour, R., Deconstructing the Catalytic, Vicinal Difluorination of Alkenes: HF-Free Synthesis and Structural Study of p-TolIF2. *J. Org. Chem.* **2017,** *82* (22), 11792-11798; (c) Schäfer, M.; Stünkel, T.; Daniliuc, C. G.; Gilmour, R., Regio- and Enantioselective Intermolecular Aminofluorination of Alkenes via Iodine(I)/Iodine(III) Catalysis. *Angew. Chem. Int. Ed.* **2022,** *n/a* (n/a).

9. Fokin, A. A.; Schreiner, P. R., Selective Alkane Transformations via Radicals and Radical Cations: Insights into the Activation Step from Experiment and Theory. *Chem. Rev.* **2002,** *102* (5), 1551-1594.

10. (a) Izquierdo, S.; Essafi, S.; del Rosal, I.; Vidossich, P.; Pleixats, R.; Vallribera, A.; Ujaque, G.; Lledós, A.; Shafir, A., Acid Activation in Phenyliodine Dicarboxylates: Direct Observation, Structures, and Implications. *J. Am. Chem. Soc.* **2016,** *138* (39), 12747-12750; (b) Dasgupta, A.; Thiehoff, C.; Newman, P. D.; Wirth, T.; Melen, R. L., Reactions promoted by hypervalent iodine reagents and boron Lewis acids. *Org. Biomol. Chem.* **2021,** *19* (22), 4852-4865.

11. P. Roberts, B., Polarity-reversal catalysis of hydrogen-atom abstraction reactions: concepts and applications in organic chemistry. *Chem. Soc. Rev.* **1999,** *28* (1), 25-35.

12. Wayner, D. D. M.; McPhee, D. J.; Griller, D., Oxidation and reduction potentials of transient free radicals. *J. Am. Chem. Soc.* **1988,** *110* (1), 132-137.

13. (a) Kabeshov, M. A.; Musio, B.; Ley, S. V., Continuous direct anodic flow oxidation of aromatic hydrocarbons to benzyl amides. *React. Chem. Eng.* **2017,** *2* (6), 822-825; (b) Shen, T.; Lambert, T. H., C–H Amination via Electrophotocatalytic Ritter-type Reaction. *J. Am. Chem. Soc.* **2021,** *143* (23), 8597-8602.

14. Hyun, S.-M.; Yuan, M.; Maity, A.; Gutierrez, O.; Powers, D. C., The Role of Iodanyl Radicals as Critical Chain Carriers in Aerobic Hypervalent Iodine Chemistry. *Chem* **2019,** *5* (9), 2388-2404.

15. Hansch, C.; Leo, A.; Taft, R. W., A survey of Hammett substituent constants and resonance and field parameters. *Chem. Rev.* **1991,** *91* (2), 165-195.

16. Liang, Y.; Zhang, X.; MacMillan, D. W. C., Decarboxylative sp^3 C–N coupling via dual copper and photoredox catalysis. *Nature* **2018,** *559* (7712), 83-88.

17. Liu, C.; Rao, X.; Zhang, Y.; Li, X.; Qiu, J.; Jin, Z., An Aerobic and Very Fast Pd/C-Catalyzed Ligand-Free and Aqueous Suzuki Reaction Under Mild Conditions. *Eur. J. Org. Chem.* **2013,** *2013* (20), 4345-4350.

18. Rao, S. N.; Mohan, D. C.; Adimurthy, S., l-Proline: An Efficient Catalyst for Transamidation of Carboxamides with Amines. *Org. Lett.* **2013,** *15* (7), 1496-1499.

19. Sanz, R.; Martínez, A.; Guilarte, V.; Álvarez-Gutiérrez, J. M.; Rodríguez, F., The Ritter Reaction under Truly Catalytic Brønsted Acid Conditions. *Eur. J. Org. Chem.* **2007,** *2007* (28), 4642-4645.

20. Yamamoto, Y.; Hasegawa, H.; Yamataka, H., Dynamic Path Bifurcation in the Beckmann Reaction: Support from Kinetic Analyses. *J. Org. Chem.* **2011,** *76* (11), 4652-4660.

CHAPTER 4

4 Synthetic Application of Bismuth LMCT Photocatalysis in Radical Coupling Reactions

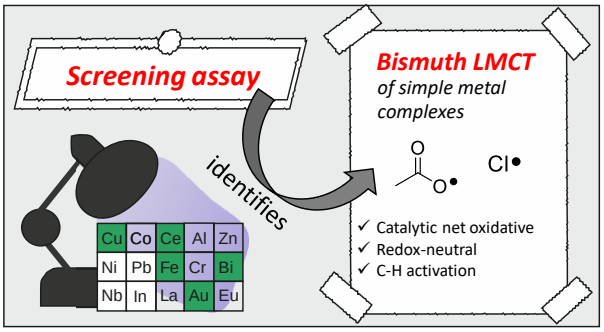

Abstract: Ligand-to-metal charge transfer (LMCT) photocatalysis allows the activation and synthetic utilization of halides and other heteroatoms in metal complexes. Many metals are known to undergo LMCT, but so far remain underutilized in the field of catalysis. A screening assay identifying LMCT activity helped us to expand this catalysis concept to application of bismuth LMCT in organic radical coupling reactions. We demonstrate its application for generation of two different radicals (chlorine and carboxyl) in net-oxidative as well as redox-neutral photochemical reactions. Detailed investigation of the model Giese-type coupling revealed $BiCl_4^-$ and $BiCl_5^{2-}$ as catalytically active bismuth species under 385 nm irradiation. Combined cyclovoltammetry and UV-vis studies gave insight into the reactivity of the highly reactive bismuth(II) catalyst fragment.

This chapter has been published. For reference see:
Birnthaler, D.;[+] Narobe, R.;[+] Lopez-Berguno, E.; Haag, C.; König, B., Synthetic Application of Bismuth LMCT Photocatalysis in Radical Coupling Reactions. *ACS Catal.* **2023**, 1125-1132. ([+]= equal contribution). Reproduced with permission from the American Chemical Society.

Author contribution
DB and RN contributed equally to the work. Both were involved in all the stages of the project; LMCT activity assay design, screening and optimization of Giese coupling, synthetic scope investigations and mechanistic studies. CH and ELP assisted in the screening and optimizations. CH also helped to obtain presentable UV-vis spectra and LMCT screening assay data. The manuscript was written by DB and RN with the input of all authors. BK supervised the project and is the corresponding author.

4.1 Introduction

Ligand-to-metal charge transfer (LMCT) photocatalysis has emerged into a powerful tool to easily access reactive electrophilic radicals from abundant and inexpensive metal complexes enabling diverse reactivity.[1] Light absorption by a LMCT band induces a homolytic cleavage of a metal-ligand bond resulting in a reduced metal complex and an oxidized ligand radical.[2] Even though these photophysical principles were never restricted to certain metals,[3] modern synthetic applications have been limited mostly to cerium and its alkoxy[4] and carboxyl[5] radical chemistry. The recent utilisation of chlorine radicals generated from copper[6] and iron salts[7] serving as hydrogen atom abstractors expanded the portfolio of LMCT applications to C–H bond functionalisation of various hydrocarbons. In these transformations, the bond homolysis of a catalyst complex circumvents the requirements for long excited state lifetimes and matching redox potentials between substrate and catalyst thus allowing complementary reactivity patterns to classical single electron transfer (SET) catalysis.[1c] Comparing the different LMCT complexes it becomes clear that metal character is crucially influencing, enabling and disabling certain reactivity modes. Benzoic acids, for example, while being utilized as fully recoverable ligands in synergistic cerium catalysis,[8] readily undergo decarboxylation as copper-substrate complexes yielding phenyl radicals after excitation.[9] Moreover, unique reaction outcomes are achieved when a single metal fulfils multiple roles besides LMCT activation. Of course, this behaviour is linked to specific elements - as an example efficient photocatalytic radical oxidation enabling cross-nucleophile coupling has so far only been achieved with copper.[10] Furthermore, Doyle group demonstrated an intriguing combination of LMCT with multiple transition metal catalysis steps orchestrated by a single nickel catalyst.[11] Despite these impressive developments, this research field is still in its infancy and new synthetic opportunities are to be discovered by exploring LMCT of different underutilized metals.

4.2 Development of an LMCT activity screening assay

To unlock access to the synthetic potential different elements may offer, we sought to design a systematic, rational screening assay for accelerated identification of LMCT activity across the periodic table. To begin, we focused on establishing a suitable test system allowing a conclusive qualitative readout. The reaction of choice should produce an easily detectable product without any major side reactions. The only essential requirement for product formation should be a LMCT step of the metal catalyst. Leveraging net oxidative reactions with oxygen as terminal oxidant, using a 96-well plate setup becomes a simple choice for fast high-throughput screening (see Figure S4.1). Out of reported aerobic decarboxylative oxidation,[12] benzylic C(sp^3)-H oxidation,[12b] oxidative cleavage of diols,[13] and dehydrogenative lactonization of 2-arylbenzoic acids,[14] the lastly mentioned transformation caught our attention. Cerium[14a] and iron[14b] based systems are described in literature to give the respective coumarin **1b** under diverse reaction conditions. In this reaction, the key intermediate - highly reactive carboxylate radical - undergoes rapid intramolecular addition to the tethered phenyl ring which then gets quickly oxidized and rearomatized.

We started to investigate the potential of simple bench stable metal chlorides available in our laboratories (Figure 4.1). A relatively high metal chloride loading (35 mol%) was selected to spot also minor LMCT activity. A set of differently coordinating solvents was used as their coordination has been proven to be beneficial in some cases (e.g., copper).[6, 10] One set of conditions used additional chloride ligand to allow the formation of highly coordinated carboxylate, or mixed carboxylate-chloride complexes. Higher coordination generally improves absorption properties as demonstrated in the case of copper and cerium (e.g., $CuCl_3^-$,[6] $FeCl_4^-$[7a]). Based on previous reports,[1] 375 nm LEDs were used, because they excite synthetically useful LMCT absorption bands. These bands typically appear higher than 300 nm and tail towards the visible region. To verify the developed screening assay, cerium and iron chlorides were used as positive controls. Indeed, the positive outcome of these two metals made us confident that the selected parameters cover a correct range of conditions enabling LMCT. Moreover, an expected rediscovery of carboxyl

radicals from copper complexes[10, 12a] in a new transformation gave additional validity to the assay. Taking advantage of the experimental simplicity of this screening, also improbable metal chlorides like $AlCl_3$, $ZnCl_2$, $NbCl_3$, $CdCl_2$, $InCl_3$ and $PbCl_2$ were tested, and some gave product in detectable amounts. $NiCl_2$ and $CoCl_2$ showed no conversion even though their photophysical properties for LMCT were described before.[15] The reason for inactivity is probably that higher oxidation state (III) was not achieved by oxidation with oxygen. Remarkable is the LMCT activity of gold across multiple reaction conditions. We did not further investigate this observation but hope that the reactivity and synthetic use of these complexes will be further investigated in a different context.

For us, the biggest surprise and opportunity of the screening was the discovery of the exceptional performance of bismuth chloride in the lactonization. In all conditions we got significant amount of product **1b**, and in some cases, we even observed a complete consumption of the carboxylic acid **1a**. An additional experiment with a lower bismuth chloride loading (5 mol%) and TBACl ligand (15 mol%) in MeCN revealed high 78% yield of **1b** implicating that simple bismuth salts can act as a catalyst in this reaction (Scheme S4.3).

Knowing the right keywords, focused review of old photophysical literature brought us to the pioneering studies of Vogler.[16] Therein, the photolysis of $BiCl_3$ in benzene was studied which resulted in a formation of chlorobenzene and bismuth metal under 290 nm irradiation.[16c] Over the years, investigations on photochemical[17] and photoluminescent[18] behaviour of different bismuth complexes have followed. However, it is important to note that the observed photochemical reactions were reported in the context of photodecomposition which have not been transferred to catalytic applications in organic synthesis.

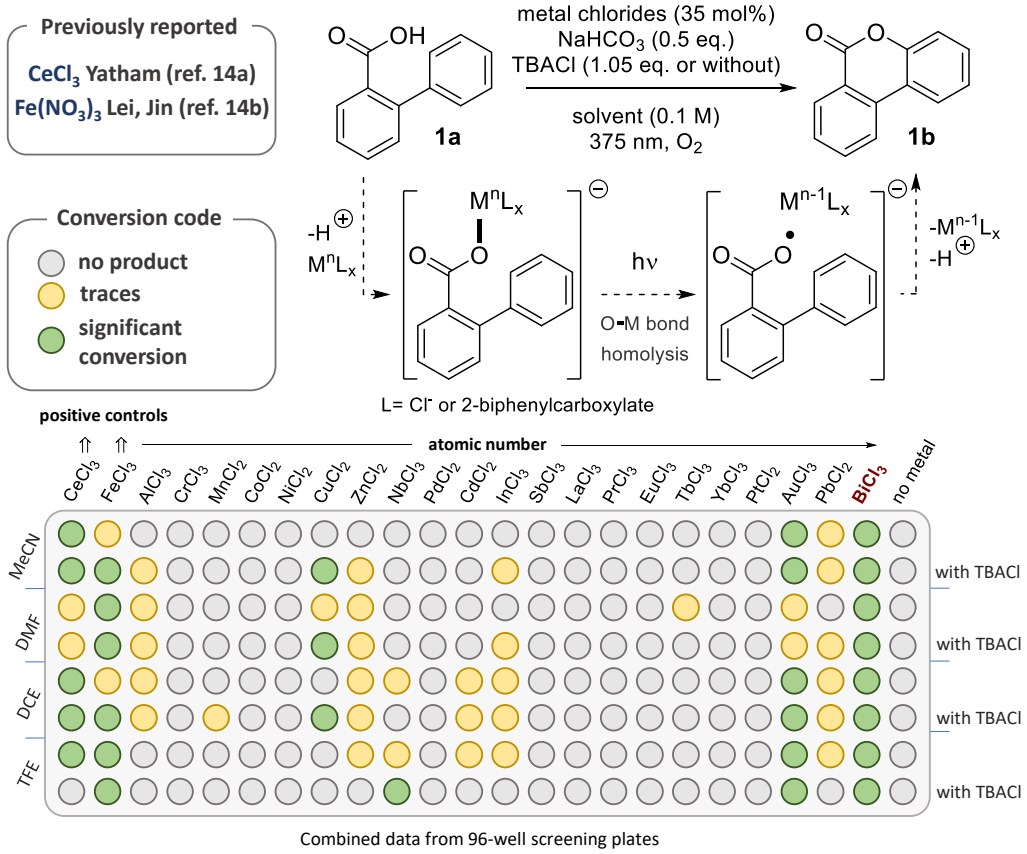

Figure 4.1: The developed LMCT reactivity assay along with combined screening results. 96-Well plate was analysed by qualitative TLC. TBACl = tetrabutylammonium chloride. For further experimental details of the screening see Supporting Information.

4.3 LMCT catalysis of bismuth

Rare examples of homogenous bismuth(II/III) catalysis are represented in the reactions of radical polymerizations,[19] dehydrocouplings of TEMPO or phenol and hydrosilane,[20] and radical cycloisomerization of δ-iodo-olefins.[21] A plausible reason for the limited number of catalytic examples might be that bismuth(II) is a radical species.[22] Seemingly the reactivity of such radicals is hard to control as they tend to undergo undesired side reactions. The catalytically active bismuth complexes in these reports contain carefully selected organic ligands and the reactions mostly proceed under thermal activation. An exception is light-initiated dehydrocoupling reported by Lichtenberg which has been performed under harsh mercury lamp irradiation.[20b, c] In this transformation, the role of light is to generate an active bismuth(II) catalyst fragment, which interacts with stable oxygen radicals (TEMPO or phenoxy radicals) and initiates bismuth(II/III) catalytic cycle. While using TEMPO in the presence of the bismuth(II) radical is a unique and thoughtful strategy, such an approach is difficult to expand to reactions involving carbon-centered radicals. Such a persistent radical would actively interfere productive turnover, as they are commonly applied to trap carbon centered radical intermediates.[23]

Building on our initial discovery of catalytic performance of simple bismuth salts in a net oxidative reaction, where an active stabilization strategy was not required, we sought to generalize the use of simple bismuth salts as a homogenous photocatalysts in a redox-neutral Giese-type coupling reaction.[24] In this reaction, no external oxidizing agent is added and therefore bismuth has to get reoxidzied by transient organic radicals, before undergoing side reactions. This step is challenging and requires addition of a cocatalyst in some LMCT systems.[4b, 25] With reports of Vogler[16c] in mind, we considered chlorine radical generation from bismuth chlorides for activation of aliphatic C(sp^3)-H bonds relying on hydrogen atom transfer (HAT) strategy.[26]

To avoid mercury lamp irradiation, we utilized highly coordinated bismuth polychloride complexes which have absorption shifted towards higher, synthetically more appealing wavelengths. As an initial model reaction, we selected coupling of cyclohexane with acrylonitrile (Table 4.1). Gratifyingly, a combination of $BiCl_3$ and TBACl (1:2) in a relatively low 5% loading gave the desired coupling product **2c** in 72% yield under 385 nm LEDs irradiation (entry 1). Interestingly, heterogenous materials Bi_2O_3 and BiOCl lead to unproductive degradation of the alkene (entries 2 and 3) despite being established photocatalysts in environmental applications[27] and in some synthetic procedures.[28] Control experiments without $BiCl_3$ and in the absence of light confirmed essential role of both in this transformation (entries 4 and 5).

Table 4.1: Evaluation of the reaction conditions and control experiments for the C(sp^3)-H functionalization of alkanes.[a]

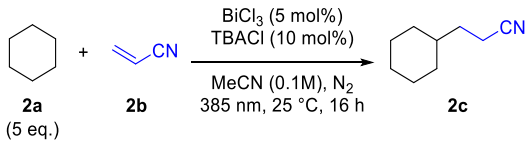

entry	deviation from optimized	yield 2c
1	none	72 %
2	BiOCl instead of $BiCl_3$	<5 %
3	Bi_2O_3 instead of $BiCl_3$	0 %
4	without $BiCl_3$	0 %
5	no light, 80 °C	0 %

[a]Reaction conditions: 0.2 mmol acrylonitrile, 5 mol% of bismuth salt, 10 mol% tetrabutylammonium chloride, 5 eq. cyclohexane, 2 ml MeCN (0.1 M) under N_2 atmosphere, 385 nm, 25 °C, 16 h. Yields were determined by GC-FID using benzotrifluoride as internal standard.

During optimization of the ratio of $BiCl_3$ to TBACl ligand, an interesting reactivity pattern was observed (Figure 4.2). *In situ* formed $BiCl_4^-$ and $BiCl_5^{2-}$ are competent catalysts when irradiated at 385 nm giving comparable yields of **2c**, whereas at 400 nm only $BiCl_5^{2-}$ is active. We followed the observation by performing UV-vis titration studies. [17d]The sequential addition of one equivalent TBACl to $BiCl_3$ resulted in a bathochromic shift, which increased upon adding a second equivalent, and the third chloride addition led to less significant changes of absorption properties. This suggests that $BiCl_5^{2-}$ is indeed the preferred coordination mode of bismuth chlorides. Consistent with this finding are Gibbs free energy calculations performed by the Hunt group. These show that Bi^{3+} ions favour a square pyramidal coordination in excess of chloride over other structures.[29]

4.4 Synthetic application

The synthetic scope of this photocatalytic bismuth mediated Giese-type coupling was explored to showcase its generality (Scheme 4.1). Differently substituted electron-deficient alkenes bearing nitrile, carboxyl and sulfone groups were viable coupling partners (**2-8b**). Nitrile group containing radical traps gave best product yields. Less steric hindrance around the radical trap seemed to be beneficial, hinting at close interactions of reaction intermediates and bismuth catalyst. The free carboxylic acid functional group of **6c** and **7c** are tolerated under the pH neutral conditions of this coupling. This shows that coordination of carboxylic acid to bismuth without base is unlikely to happen. The protocol was successfully upscaled to gram scale(**8c**) without any significant loss of efficiency at higher irradiation wavelength of 400 nm (Scheme S4.5).

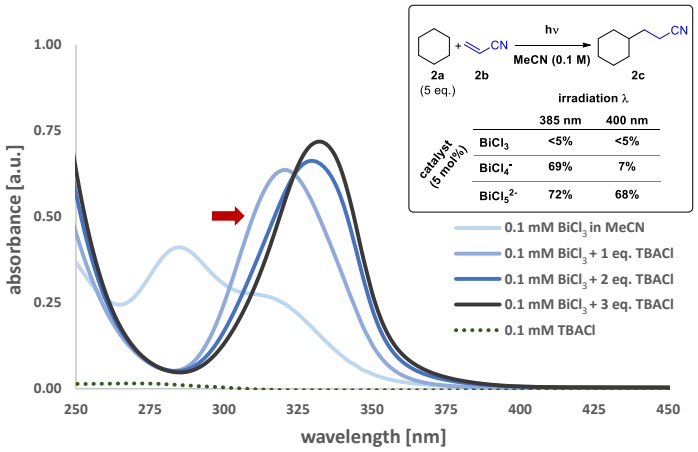

Figure 4.2: UV-vis spectra of different bismuth(III) chloride complexes in MeCN and display of their reactivity in the inset.

The chlorine radical-mediated HAT allows the C–H bond activation of a broad range of starting materials. The selectivity of abstraction is steered to the most hydric hydrogen atoms – an established abstraction pattern of the electrophilic chlorine radical.[30] Compounds **12c** and **18c** illustrate the described selectivity. The benzylic -CH_3 group of 4-methylanisol (**12a**) is functionalized in the presence of -OCH_3 moiety which remains intact. In the case of more functionalized anisole derivative **18a**, the electron-withdrawing ester group deactivates the benzylic position enough that HAT is happening exclusively at the previously untouched aromatic -OCH_3 group. Similarly, the α-keto-CH_3 group of benzodioxol **17a** is deactivated enough, that functionalisation occurs only at the dioxol motive. In general, α- to heteroatom C–H bond containing precursors are high-yielding. Particularly, **19a** gave an excellent yield of 98%. Tetrahydrothiophene (**20a**) was converted to the desired product **20c** without any noticeable oxidation of the sulfide moiety. Diastereomeric products were obtained in 1:1 diastereomeric ratio.

Scheme 4.1: Synthetic scope of the bismuth-catalysed Giese-type coupling reaction.[a]

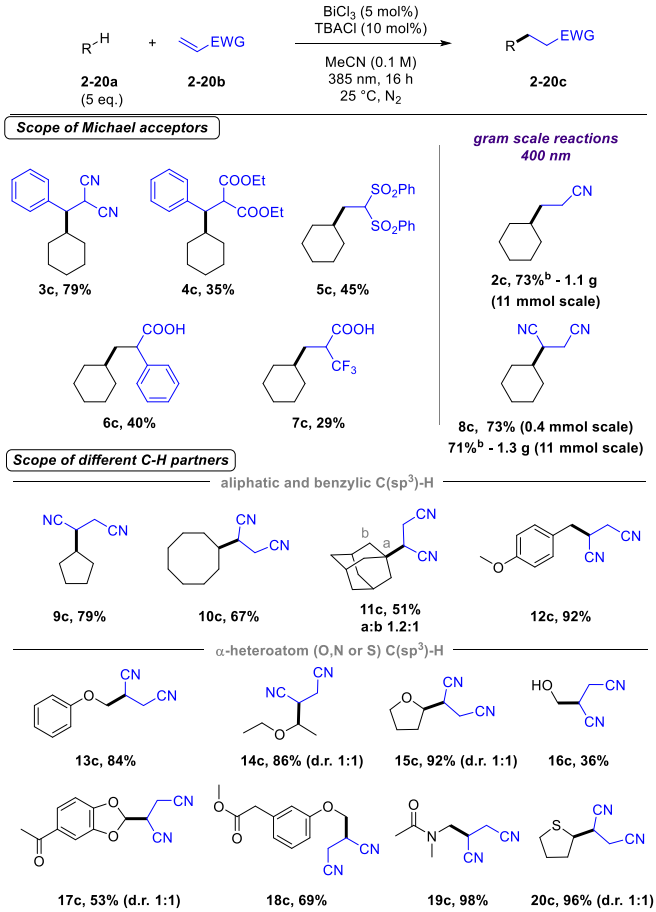

[a]Reaction conditions: 0.4 mmol of the radical trap, 5 mol% of $BiCl_3$, 10 mol% tetrabutylammonium chloride, 5 eq. of alkane in 4 ml MeCN (0.1 M) under N_2 atmosphere, 385 nm, 25 °C, 16 h. [b]Reaction performed on a 11 mmol scale in a different setup with irradiation at 400 nm. See SI for details.

4.5 Mechanistic investigation

In the synthetic scope investigation, a black precipitate was observed after the reaction, which did not appear under oxidative conditions. It is reasonable to assume that this precipitate originates from the decompositions of reduced bismuth(II) radical species.[16c, 22, 31]To get additional insight into the behaviour of bismuth(II) in our catalytic system, we performed cyclic voltammetry (CV) studies. Electroreduction serves as a complementary approach to photochemical reduction offering us the opportunity to study bismuth(II) radical behaviour. The cyclic voltammogram of $BiCl_5^{2-}$ revealed reversible behaviour (Figure 4.3A), whereas voltammogram of $BiCl_3$ showed an additional irreversible reduction peak (Figure 4.3A-I) indicating some chemical reaction.

Gratifyingly, this reaction could be identified by monitoring the bismuth species interconversions during the electrochemical reduction by UV-vis spectroscopy (Figures 4.3B and C). These combined spectro-electrochemical measurements displayed the shift of the absorption maximum of $BiCl_3$ from 280 nm to 340 nm in the first reduction step (Figure 4.3C-I). This behaviour is mimicking the observation of the UV-vis titration studies (Figure 4.2) making evident that the newly formed species is $Bi^{III}Cl_5^{2-}$.[32] Finding this newly formed bismuth species, still in oxidation state III is counterintuitive at the first sight. However, this suggests that the unstable bismuth(II) radical rapidly undergoes disproportionation to bismuth(III) and to a further reduced bismuth species without any absorption features. Hereby, the released chlorine is transferred to bismuth(III) to eventually form $BiCl_5^{2-}$ as observed by UV-Vis. Indeed,

the absorption and electrochemical behaviour of *in situ* generated $BiCl_5^{2-}$ and preformed $BiCl_5^{2-}$ is the same. Further reduction of $BiCl_5^{2-}$ results in a complete disappearance of all absorption features (Figures 4.3B-II and 4.3C-II), likely indicating its complete reduction.[33] Upon oxidation, the absorption features of $BiCl_5^{2-}$ reappear (Figures 4.3B-III and 4.3C-III). Upon further oxidation, the concentration of Bi^{3+} ions increases, and in the absence of free chloride ions, Bi^{3+} ions start taking chloride atoms from $BiCl_5^{2-}$. As a consequence, we observed reappearance of the $BiCl_3$ signal at 280 nm (Figure 4.3C-IV). Interestingly, during these investigations we observed the black deposit again, this time on the electrode.

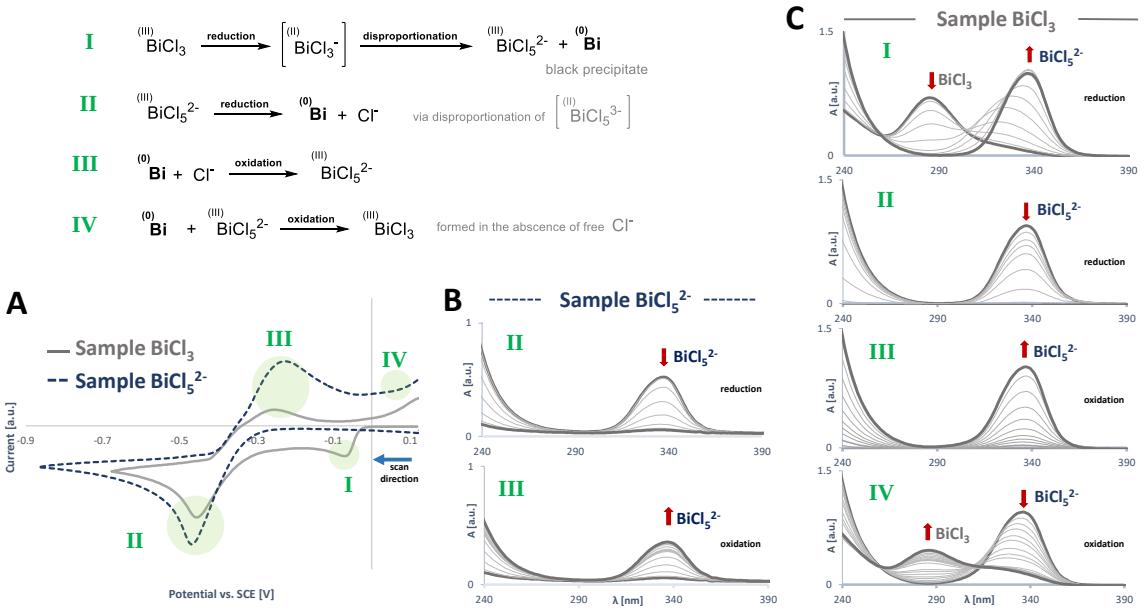

Figure 4.3: Cyclic voltammograms of two different bismuth(III) chlorides ($BiCl_3$ and $BiCl_5^{2-}$) (**A**), and on-line UV-vis spectra showing interconversions of the bismuth species during the CV measurements of two samples - $BiCl_5^{2-}$ (**B**) and $BiCl_3$ (**C**). Each UV-vis spectrum corresponds to the change in the potential by 50 mV

To better characterize the formed black solid, we conducted a direct photochemical synthesis by irradiating concentrated $BiCl_5^{2-}$ solution without any reactants (Scheme S4.3). The analysis by powder diffraction identified the black precipitate as elemental bismuth (Figure S4.18) which was obtained in 51 % yield. In the context of our C–H activation protocol this disproportionation to bismuth(0) poses a loss of active catalyst and therefore termination of the reaction. However, judging on the high Giese coupling product yields (up to 98%) it seems that the disproportionation process is successfully interfered by much faster kinetics of the productive reaction. Reaction kinetic monitoring within the first hour gave a linear profile showing six catalyst turnovers (Figure S4.16). To determine whether the reaction is light initiated or light-driven, we measured the quantum yield (Table S4.6). The obtained quantum yield of 1.5%, makes a radical chain pathway to the coupling product unlikely. These two measurements suggest, that the active catalytic species continuously catalyses the reaction and remains intact as long as reactants are present.

A plausible explanation for the efficiency of this catalytic system and neglectable disproportionation is an interaction of the open shell bismuth(II) radical fragment with carbon centred radicals. Such a rebound mechanism would stabilize the highly reactive bismuth(II), and at the same time assemble reaction partners for a fast turnover. Similar effects have been postulated for bismuth polymerisation catalysts.[19c] Additionally, in a seminal report of the Cornella group on the nature of such bismuth(II) - carbon radical equilibria have been studied in detail in SET oxidative additions of redox active esters to bismuth(I).[34]

Based on our mechanistic experiments and previous abovementioned studies on low valent bismuth, the following mechanism is proposed (Scheme 4.2). The addition of two equivalents of TBACl to $BiCl_3$ generates the active $BiCl_5^{2-}$

catalyst. Under 385 nm irradiation this catalyst undergoes bismuth – chlorine bond homolysis releasing an electrophilic chlorine radical. This radical abstracts a hydrogen atom from the C–H bond precursor. The resulting carbon centred radical can recombine with bismuth(II). After radical addition of the cyclohexyl radical to an electron-deficient alkene, a reduction event gives the desired coupling product and regenerates photoactive bismuth(III). This can be either facilitated by an inner-sphere protodemetallation step or by an outer-sphere SET event followed by protonation. The regenerated bismuth(III) then perpetuates the bismuth(II/III) catalytic cycle.

Scheme 4.2: Plausible reaction mechanism.

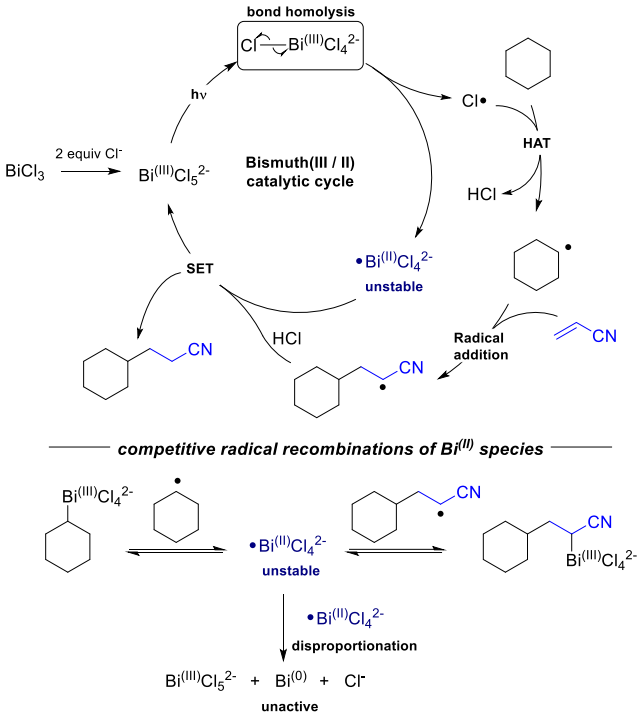

4.6 Conclusion

In summary, we developed a screening assay which enables quick identification of dissociative LMCT activity. The developed assay revealed LMCT activity of simple bismuth(III) salts in a net oxidative lactonization reaction which turned out to be catalytic. The concept of photoinduced bismuth (II/III) LMCT catalysis was successfully extended to more challenging redox neutral Giese-type coupling. In these reactions, simple bismuth polychloride species were used as a source of chlorine radicals, which enabled the functionalization of different C(sp^3)-H precursors. In the latter model reaction system we investigated the fate of bismuth(II) radical intermediates by combined cyclovoltammetry and spectro-electrochemical measurements. In the absence of organic substrates, we observed a pronounced bismuth(II) disproportionation which is not affecting catalytic applicability. In summary our findings are establishing bismuth as a generally working LMCT photocatalyst and present important mechanistic ground and considerations for more advanced catalytic applications in organic synthesis.

4.7 Experimental information

General information

Starting materials and reagents were purchased from commercial suppliers (Sigma Aldrich, Alfa Aesar, Acros or Fluka) and were used without further purification. Solvents were used as p.a. grade. Reactions were monitored by analytic thin layer chromatography (TLC) using Fluka silica gel plates with a fluorescent indicator. Visualization of the developed TLC chromatogram was performed using 254 nm UV light source or potassium permanganate stain. Organic solutions were concentrated using Büchi rotary evaporator. Flash column chromatography was performed either on a Biotage® IsoleraTM Spektra or by hand for non-UV absorbing products. In both cases we used columns filled with Silica gel (60-200 μm). For non-UV-Vis absorbing product we used permanganate TLC stain for the visualization of the TLC spots.

NMR spectroscopy

All NMR spectra were recorded at room temperature using a Bruker Avance 300 (300 MHz for ^{1}H, 75 MHz for ^{13}C, 282 MHz for ^{19}F) or a Bruker Avance 400 (400 MHz for ^{1}H, 101 MHz for ^{13}C, 376 MHz for ^{19}F) NMR spectrometer. All chemical shifts are reported in δ-scale as parts per million [ppm] (multiplicity, coupling constant J, number of protons), relative to the solvent residual peaks as the internal standard. Coupling constants J are given in Hertz [Hz]. Abbreviations used for signal multiplicity: ^{1}H-NMR: br = broad, s = singlet, d = doublet, t = triplet, q = quartet, dd = doublet of doublets, dt = doublet of triplets, and m = multiplet.

Gas chromatography

GC measurements were performed on a GC 7890 from Agilent Technologies system coupled to a FID. The system was equipped with a capillary column (HP-5ms UI, length 30 m, diam. 0.25 mm, film 0.25 μm) and worked with H_2 as carrier gas. GC program: The initial temperature of the GC was set to 40 °C and kept for 1.5 minutes. Subsequently, the oven temperature was increased at a rate of 25 °C/min. until reaching 280 °C, which was maintained for 3 min. Then, temperature was further increased (42 °C/min) until reaching 300 °C and final temperature was hold for 5 minutes. Injector temperature was set to 280 °C and temperature of the detecting unit to 310 °C. A split ratio of 30:1 (split flow 42 mL/min) was applied, and the column flow was set to 1.4 mL/min. Data acquisition and evaluation was done with Agilent ChemStation Rev.C.01.04.

Mass spectrometry

High resolution mass spectrometry (HRMS) was performed at the Central Analytical Laboratory of the University of Regensburg. Mass spectra were measured on a Finnigan MAT 95, ThermoQuest Finnigan TSQ 7000, Finnigan MAT SSQ 710 A or Agilent Q-TOF 6540 UHD instrument and a Waters Acquity UPLC system equipped with Waters PDA, sample manager, sample organizer, column oven and Waters Xevo QTOF mass spectrometer.

UV-Vis

Absorption spectra were measured on an Agilent Cary 100 UV/Vis spectrometer in a 10 mm × 10 mm quartz cuvette at 25.0 °C under air atmosphere.

Cyclic voltammetry

Cyclic voltammetry was conducted using a three-electrode setup consisting of a glassy carbon disc working electrode 'WE' (d = 3.0 mm, BASi MF-2012), an Ag wire reference electrode 'RE' and a platinum wire counter-electrode 'CE'. Electrochemical measurements were carried out using an Metrohm Autolab PGSTAT 302N potentiostat at room temperature (298 K). Before use and between measurements, the working electrode was mechanically cleaned by polishing (Buehler Metadi Diamond polishing 1 Micron) and rinsed with distilled water repeatedly until its surface was reflective by eye, then allowed to air dry. The reference electrode was washed with electrolyte solution and

distilled water and stored in 3.0 M aq. KCl when not in use/between measurements. The counter electrode was cleaned by soaking in 2.0 M HCl for 1-2 h, then rinsed with distilled water and allowed to air dry. Ferrocene was recrystallized twice from n-hexane prior to use. *n*-Bu_4NBF_4 (TBAB) was used as supplied commercially from TCI (98%+). Unless otherwise stated, all solutions were prepared at 10.0 mM concentration (in 0.1 M TBAB that had been bubbled for 5 min with Ar prior to the analyte being added) and were purged with Ar bubbling for 5 min prior to recording CV. After measuring one CV scan, Ferrocene (2.2 mg, 12 μmol) was added and the mixture purged with Ar bubbling for 5 min prior to recording CV again. Data acquisition and processing were performed with Metrohm Autolab Nova 42 1.10.4.

Spectro-electrochemical measurements

Chrono amperometry was measured in an Ottle Cell (optically transparent thin-layer electrochemical cell) with Pt mini grid as working and counter electrode. A silver wire was used as a pseudo-reference electrode. The optical path length of the cell is 0.02 cm. The potentials were controlled by Metrohm Autolab PGSTAT 302N potentiostat at room temperature (298 K). UV-Vis spectra were measured during the measurements by using Agilent 8453 spectrometer. Data acquisition and processing were performed with Metrohm Autolab Nova 42 1.10.4.

For further details about Ottle Cell, see:
https://research.reading.ac.uk/spectroelectrochemistry/opticallytransparent-thin-layer-electrochemical-cells/room-temperature-ottle-cell/

X-ray powder diffraction

For X-ray powder diffraction analysis, the samples were measured on a STADI P diffractometer (STOE & Cie GmbH, Darmstadt, Germany) in transmission geometry with Mo K alpha1 radiation. The software package WinXPOW (STOE & Cie GmbH, Version 3.10, Darmstadt, Germany) was used for visualization and the software MATCH! (Match! - Phase Analysis using Powder Diffraction, Version 3.x, Crystal Impact - Dr. H. Putz & Dr. K. Brandenburg GbR, Kreuzherrenstr. 102, 53227 Bonn, Germany) for phase analysis.

Microscopy

The photos were taken with a modified microscope Swift SW380T equipped with a 15MP Swiftcam. The modified version has illumination from the top side, whereas the original had illumination from the bottom side.

Photochemical setups

Screenings of different metal chlorides for LMCT activity have been performed on 96-well plates (PP, 400 µl well volume with flat bottom). Typically, a 96-well plate containing reaction mixtures was covered with a transparent foil and placed on a thermostated cooling block (Figure S4.1). The plate was irradiated from the top side with a LED array containing 96 LEDs (above each individual well). The reactor setup is a custom-made device (University of Regensburg workshop) and is not a commercially available product.

LED specifications: 375 nm Nichia NSSU100DT. Manufacturer optical power: 9.9 mW, measured: 6.4 mW, maximum current 20 mA, max voltage 3.3 V/LED.

Figure S4.1: Equipment for 96-well plate irradiation.

Photochemical reactions were performed in closed crimp reaction vials, placed approximately 2 cm above a 385 nm LED array (Figure S4.2). The reactions were stirred under irradiation by magnetic stirrer under each reaction well. The reaction temperature was controlled by a thermostated (25 °C) metal cooling block. The reactor setup is a custom-made device (University of Regensburg workshop) and is not a commercially available product.

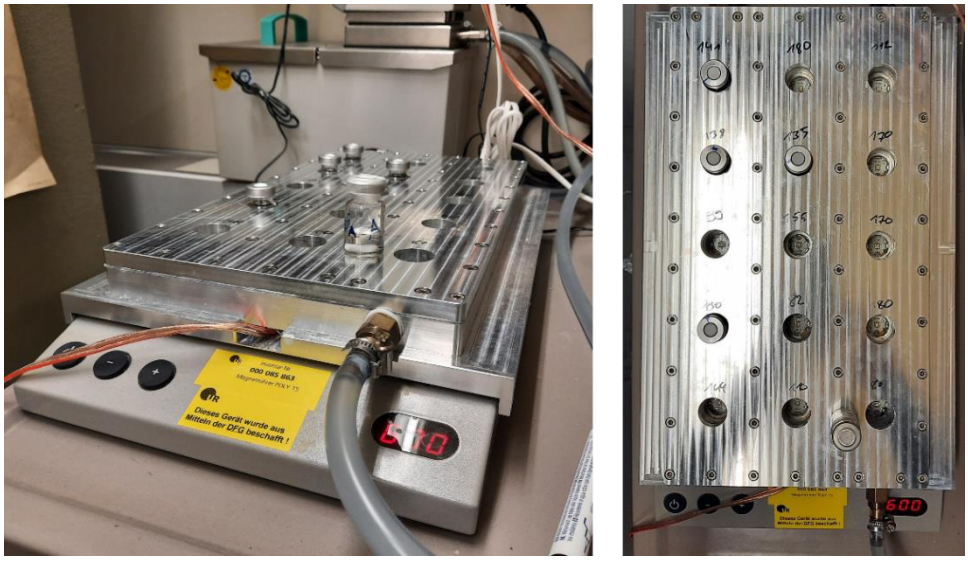

Figure S4.2: Equipment for screening and synthetic scope reactions.

Gram-scale reaction was performed in a custom build glass photoreactor which was irradiated from the sides by 18 LEDs (400 nm, 3 W electrical power each). The temperature of the inner part of the glass photoreactor was actively controlled by a thermostat (25 °C).

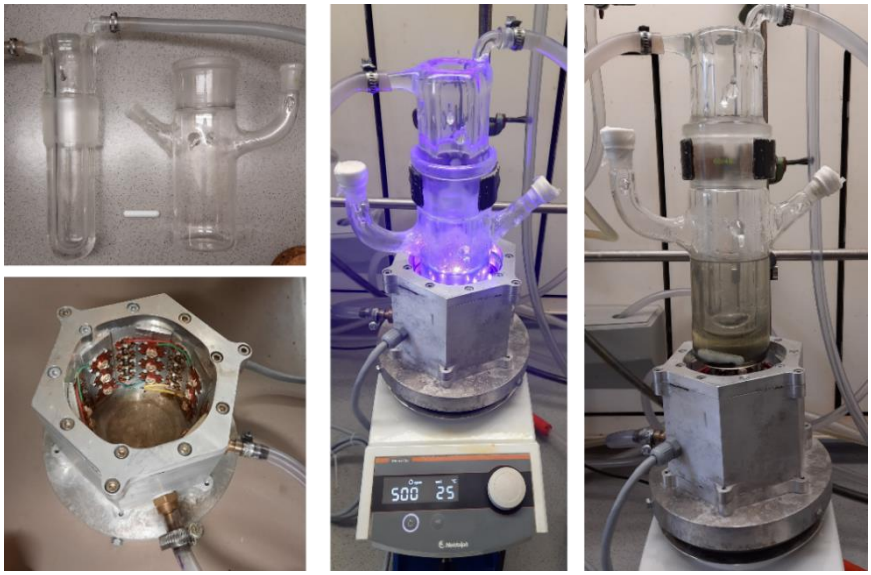

Figure S4.3: Gram-scale reactor before, during and after the photochemical reaction.

Quantum yield measurement was performed in a setup developed by Prof. Riedle.[35] For the sample we have used 10×10 mm fluorescence cuvette.

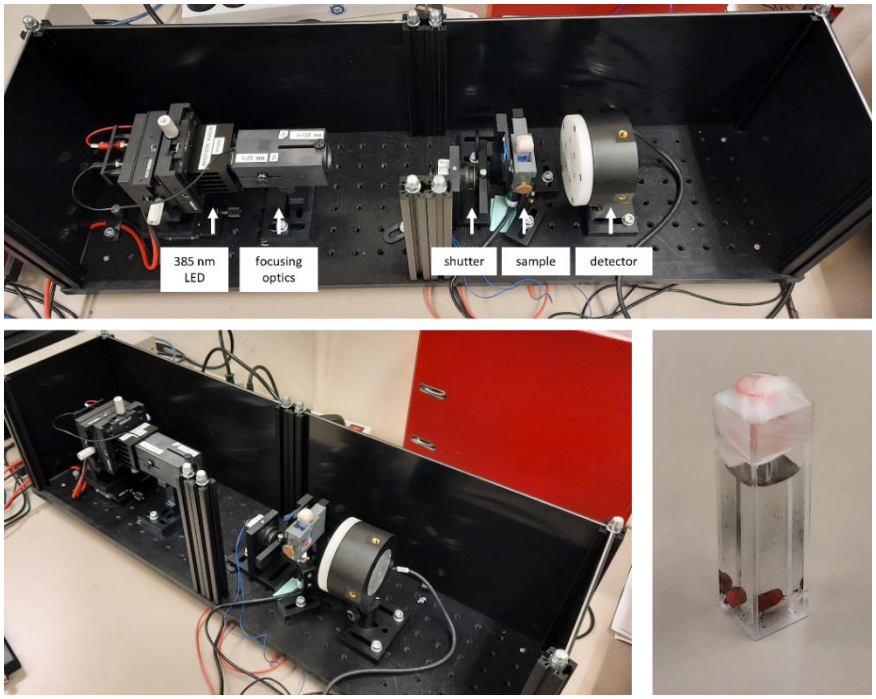

Figure S4.4: Quantum yield determination setup and the sample after completion of the reaction.

4.7.1 General experimental procedures

General procedure for the preparative scale reactions

The preparative scale reactions were set in 2 parallel vials, each containing 0.2 mmol of a radical trap as the limiting reagent. If solid, radical trap (0.2 mmol, 1 eq.) and C–H substrate (1.0 mmol, 5 eq.) were weighed into a 5 ml crimp reaction vial. Then, 2.0 ml of a stock solution containing $BiCl_3$ (0.01 mmol, 3.2 mg, 10 mol%) and TBACl (0.02 mmol, 5.5 mg, 10 mol%) in dry MeCN were added and the vial was capped. The reaction mixture was degassed by 4 nitrogen-vacuum cycles. Afterwards any liquid reagents (radical trap or a C–H substrate) were added with syringe through the septum, and the vial was placed in a thermostated cooling block (25 °C) and irradiated through the plane bottom side of the vial by a 385 nm LED for 16 hours (see Figure S4.2). After the completion, the two reaction batches were combined in a 100 ml round bottom flask to which a spoon of silica was added before removing the solvent *in vacuo*. So prepared dry load was purified on the automatic column machine (Biotage® IsoleraTM Spektra) or by hand column for non-UV absorbing products using a mixture of petrol ether and EtOAc. For non-UV-Vis absorbing product permanganate TLC stain was used for the visualization of the TLC spots.

General procedure for screening and optimization studies:

Bismuth precursors and tetrabutylammonium chloride were weighed into a crimp reaction vial together with any other solid materials. Then, 2 ml of an indicated solvent were added, and the vial was capped. The reaction mixture was degassed by 4 nitrogen-vacuum cycles. Afterwards, degassed acrylonitrile (13.1 µl, 0.2 mmol, 1 eq.) and degassed cyclohexane (108 µl, 1.0 mmol, 5 eq.) together with and any other liquids were added through septum, and the vial was placed in a thermostated cooling block (25 °C) and irradiated through the plane bottom side of the vial by a 385 nm LED for 12 hours After the reaction completion, internal standard benzotrifluoride (22.5 µl, 0.2 mmol) was added into the reaction vial. The sample was briefly shaken, filtered, and submitted for GC-FID analysis.

4.7.2 96-well plate screening of different metals for LMCT reactivity

The screening experiments were performed on a 0.01 mmol scale (0.1 M concentration in 100 µl of the solvent) on 96-well plates (material: transparent PP). The compounds were applied on the 96-well plate by distributing them as stock solutions in volatile solvents which were later evaporated. First, sodium bicarbonate was added as a stock solution in water and the plate was left overnight in the oven to dry completely. Next, the substrate (stock solution in EtOAc) and metal chlorides were added. Some of the metal chlorides dissolved well in ethyl acetate and in the cases when they did not dissolve, we prepared fine suspensions by putting them on the ultrasound bath for 30 min. The organic solvents were evaporated in the flow of air in the fume hood (ca. 1 hour). Due to its hygroscopicity, TBACl was added as the last compound dissolved in a small amount of DCM which was evaporated within minutes after being put on the plate. Then, 100 µl of each indicated reaction solvent was added. The plate was purged with oxygen and immediately closed with a transparent sticker foil. The plate was irradiated from the top site in a custom-built setup (Figure S4.1) for 12 hours. To analyse the reaction mixtures, we filled the wells to 200 µl with EtOAc and transferred 25 µl of each reaction mixture onto another 96-well plate and diluted them to 225 µl. With the TLC capillaries, we applied 3 drops of each so-prepared sample on the TLC plate. For the spotting, we used fresh, brand new TLC capillaries. TLCs were developed using petrol ether/ EtOAc 3:1 solvent mixture containing a few drops of AcOH. The photos of the developed TLC plates in the Figure S4. 5 Figure S4.1 were taken in a dark lab under UV light irradiation.

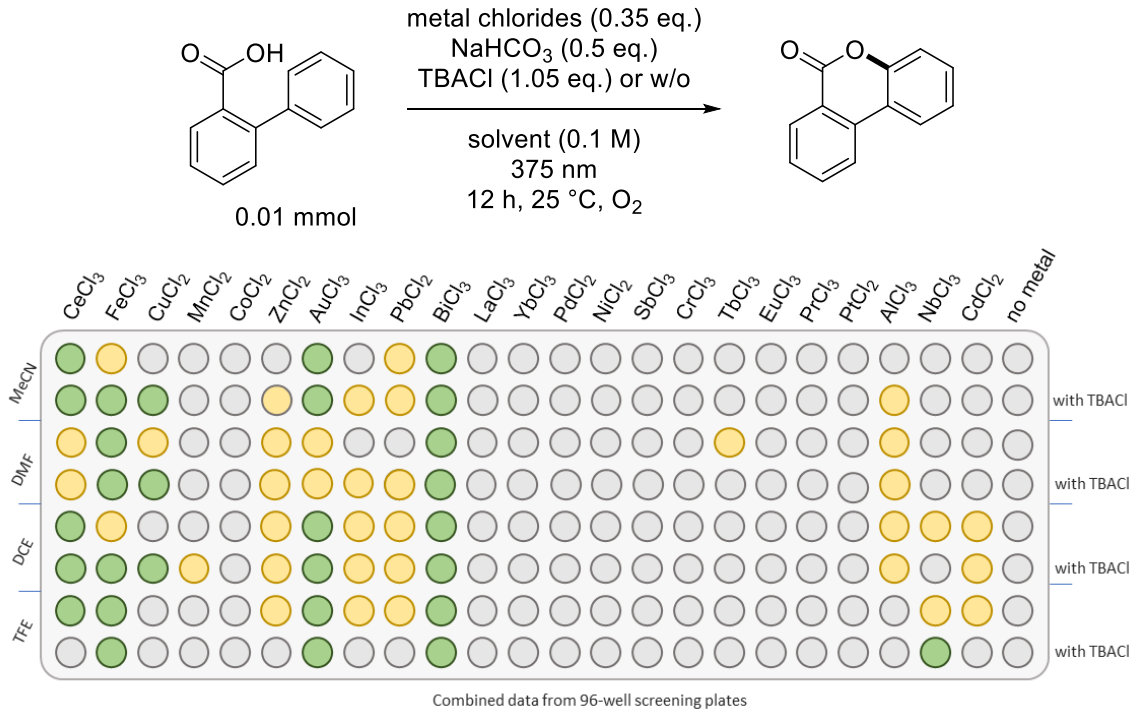

Scheme S4.1: Summarized results of the 96-well plate screenings.

An important note: Care should be taken when using this reaction to probe for the LMCT reactivity because we observed some product formation without any metal at higher light intensities over extended time periods. Therefore, suitable negative control (without metal) and positive control (with known LMCT metals) experiments have to be carried out before screening any new reaction conditions.

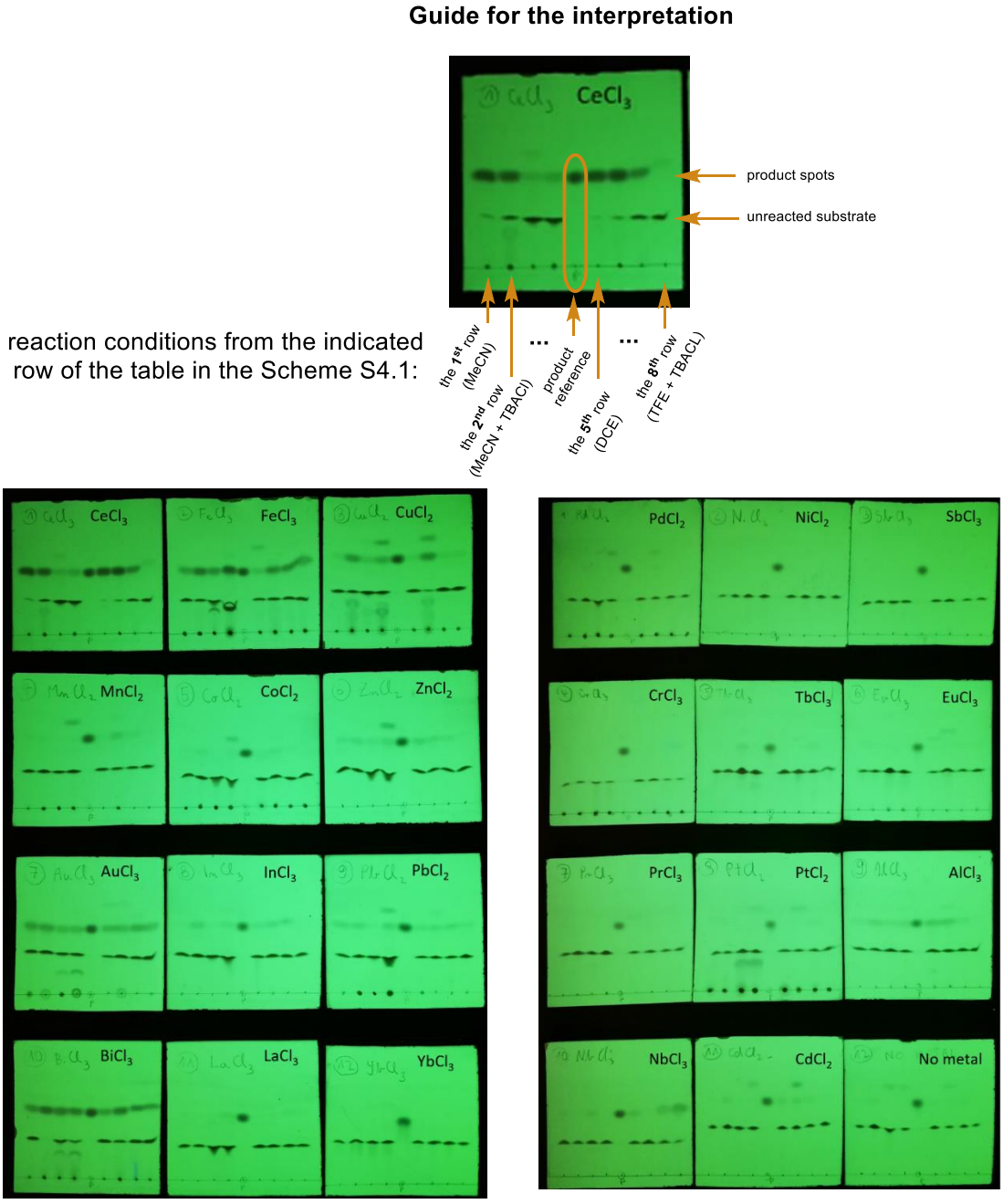

Figure S4. 5: Raw data of the TLC analysis.

To additionally confirm the screening results obtained in 96-well plates, we repeated the reaction with $BiCl_3$ in conditions 2 (MeCN, additional TBACl ligand) also on a normal scale (0.2 mmol) and isolated the product **1b**.

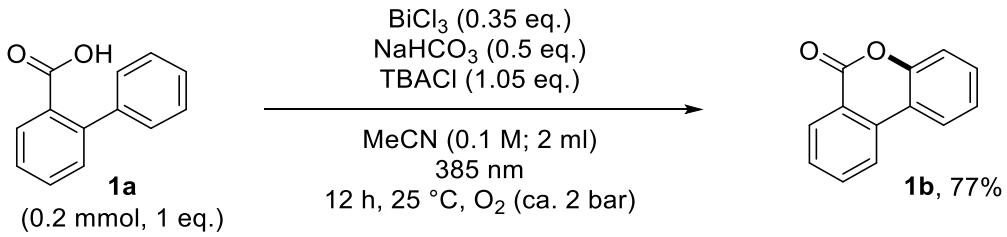

Scheme S4. 2: Synthesis of the lactone **1b** on a normal 0.2 mmol scale.

2-phenylbenzoic acid (**1a**, 39.6 mg, 0.2 mmol, 1 eq.), $NaHCO_3$ (8.4 mg, 0.1 mmol, 0.5 eq.), tetrabutylammonium chloride (29 mg, 0.21 mmol, 1.05 eq.), and $BiCl_3$ (22 mg, 0.07 mmol, 0.35 eq.) were weighed in a 5 ml reaction vial. Then, 2 ml of dry MeCN were added and the vial was closed with a crimp cap with a septum. Then an oxygen balloon was attached to the vial and the atmosphere inside the vial was exchanged by pumping out 20 ml three times. At the end we removed the balloon and pumped additional 5 ml of oxygen into the vial with a syringe to create approximately 2 bar oxygen overpressure. The reaction mixture was shaken briefly, and the vial was placed approximately 2 cm above a 385 nm LED and stirred under irradiation at 25 °C for 12 hours. After completion of the reaction, the solvent was evaporated, and the suspension of the reaction mixture was in DCM was prepared. Then we filtered the crude reaction mixture through a short basic alumina column (ca. 4 cm of basic alumina filled in a Pasteur pipette) to remove insoluble salts and any leftover carboxylic acid. We washed the column with more DCM (ca. 5 ml) to elute all the product. After evaporation of the organic solvent, 30 mg of the product **1b** (77% yield) was obtained as a white solid. The purity and identity were confirmed by ^{1}H-NMR and GC-FID analysis.

Following a similar procedure, we performed the same reaction as well with lower (5 mol%) bismuth catalyst loading. The reaction gave almost the same product yield.

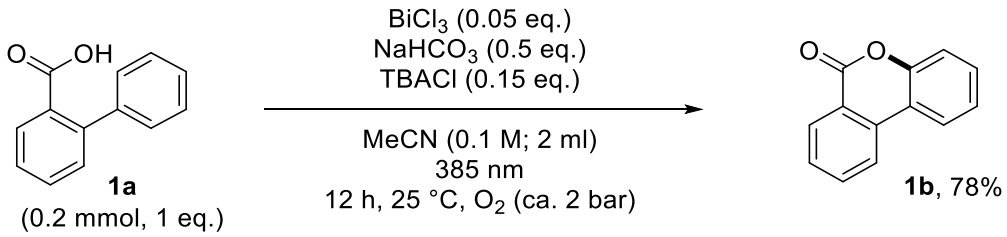

Scheme S4.3: Synthesis of the lactone **1b** on a normal 0.2 mmol scale using lower catalyst loading.

4.7.3 Optimization tables of C-H functionalization

4.7.3.1 Screening of bismuth precursors

We screened different simple and easily available bismuth sources as catalysts for our model reaction.

Table S4.1: Screening of different bismuth sources.

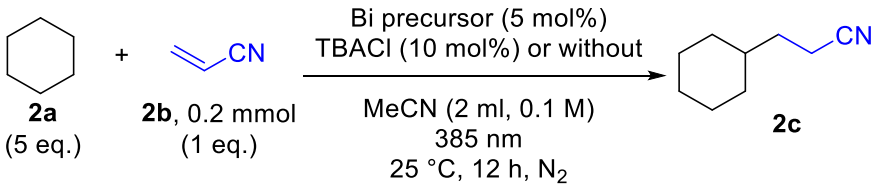

entry	Bi precursors	TBACl	GC Yield (%)
A	BiF_3	10 mol%	0
B	$BiCl_3$	10 mol%	72
C	$BiBr_3$	10 mol%	1
D	$Bi(OAc)_3$	10 mol%	0
E	BiOCl	10 mol%	0
F	BiOCl	-	0
G	Bi_2O_3	10 mol%	0
H	Bi_2O_3	-	0
I	Bismuth powder	10 mol%	4

GC yields determined by using benzotrifluoride as internal standard.

Bismuth chloride is the only one which showed significant catalytic activity. Importantly, heterogenous bismuth oxychloride and bismuth oxide which are frequently used in material/inorganic chemistry are completely inactive in our transformation.

4.7.3.2 Solvent screening and effect of water content

Table S4. 2: Screening of different solvents.

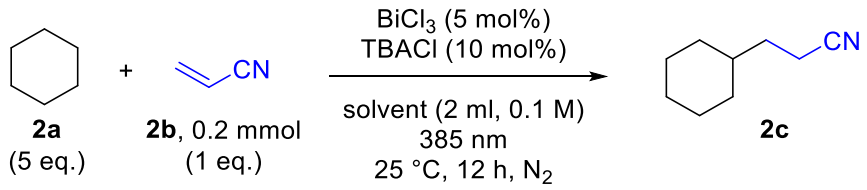

entry	reaction solvent	GC Yields (%)
A	MeCN	72
B	DMF	7
C	DMSO	0
D	TFE	4
E	DCE	14
F	PhCN	44
G	MeCN/H_2O (5 eq)	31
H	MeCN/H_2O (1:1)	0

GC yields determined by using benzotrifluoride as internal standard.

4.7.3.3 Screening of wavelengths for excitation of different bismuth chloride complexes

Table S4.3: Excitation of different complexes.

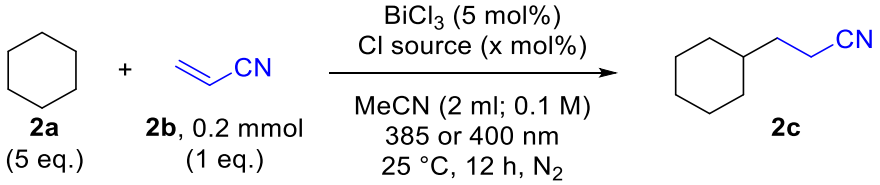

entry	TBACl (mol%)	Ratio $BiCl_3$: TBACl	385 nm	400 nm	GC Yield (%)
A	-	0	X		1
B	5	1 - 1	X		69
C	5	1 - 1		X	7
D	10	1 - 2	X		72
E	10	1 - 2		X	68
F	15	1 - 3	X		61
G	50	1 - 10	X		50

GC yields determined by using benzotrifluoride as internal standard.

A part of the data from this table is included also in the **Figure S4.6**.

4.7.3.4 Catalyst loading and estimation of TON

Table S4.16: Attempts changing the catalyst loading

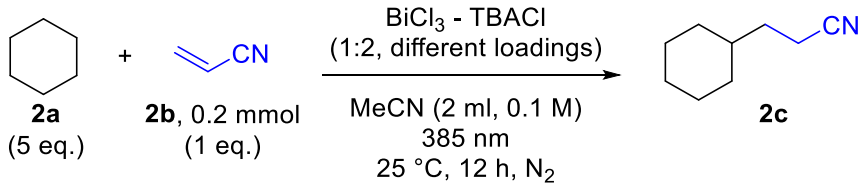

entry	$BiCl_3$ (mol%)	TBACl (mol%)	GC Yield (%)
A	1	2	15
B	5	10	72
C	10	20	74
D	20	40	70

GC yields determined by using benzotrifluoride as internal standard.

From these entries we can estimate that each catalytic unit of bismuth can do approximately 14 catalytic turnovers before it loses its activity.

4.7.3.5 Control experiments

The performed control experiments show that indeed bismuth source in combination with UV irradiation are required for the reaction to proceed. Importantly, the reaction cannot be performed at elevated temperature instead of irradiation.

Table S4.17: Control experiments.

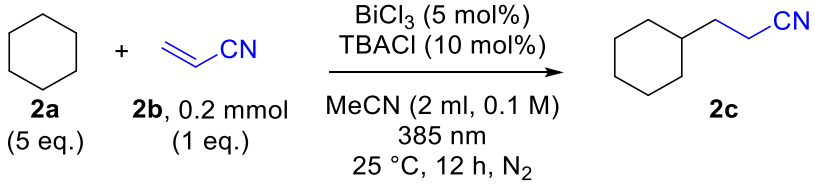

entry	deviation	GC yield (%)
A	no $BiCl_3$	0
B	no light	0
C	80 °C, no light	0

GC yields determined by using benzotrifluoride as internal standard.

We continued with the investigation of the absorbing species in the reaction system.

4.7.4 Mechanistic experiments

4.7.4.1 UV-VIS of bismuth (III) chloride complexes

4.7.4.1.1 $BiCl_3$ titration with chloride anions

Upon addition of chloride anions to $BiCl_3$, new bismuth polychloride complexes are formed. These complexes have different spectral properties (Figure S4. 6) and only sufficiently coordinated species are active reaction catalysts at 385 nm or 400 nm irradiation wavelength (Figure S4. 6, in the inset).

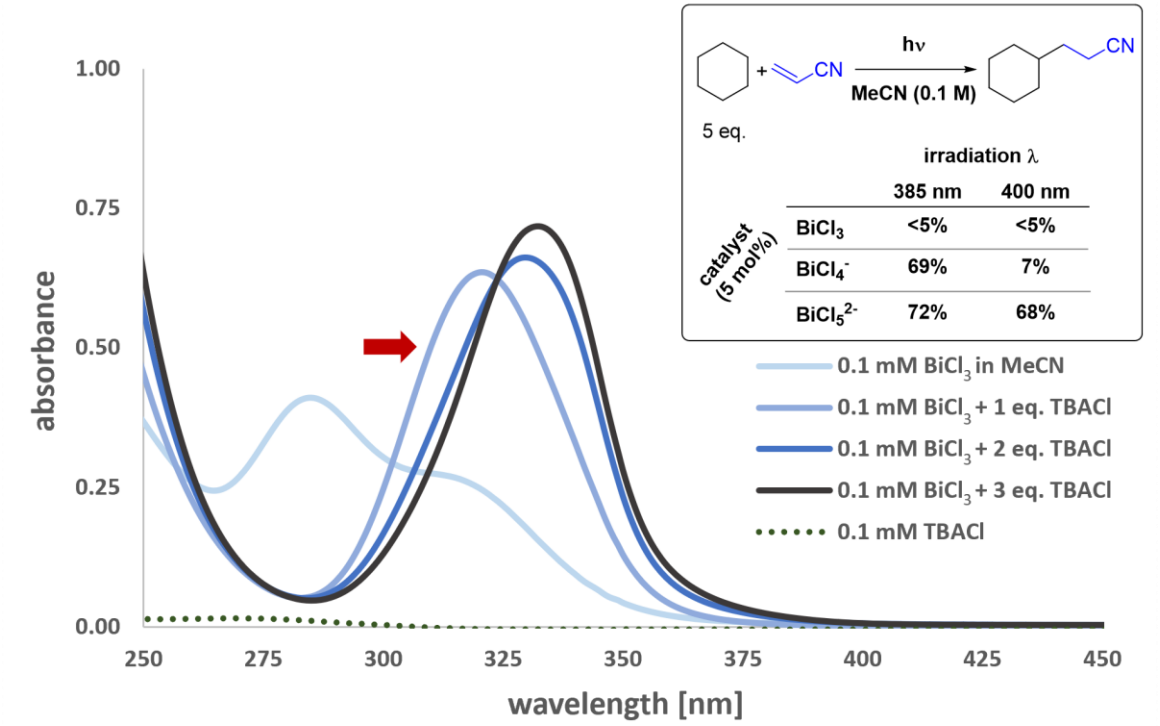

Figure S4. 6: UV-Vis spectra of different bismuth (III) chloride complexes in acetonitrile and display of their reactivity in the inset.

4.7.4.1.2 $BiCl_3$ titration with water

When water was gradually added to the solution of $BiCl_3$ in MeCN, we noticed significant blue shift in the light absorption (Figure S4. 7). However, we did not observe any significant difference in the reactivity between dried and non-dried $BiCl_3$ from the commercial bottle. In general, small amount of water (e.g., from a wet TBACl) is well tolerated in the reaction conditions despite the possibly of coordination to $BiCl_3$.

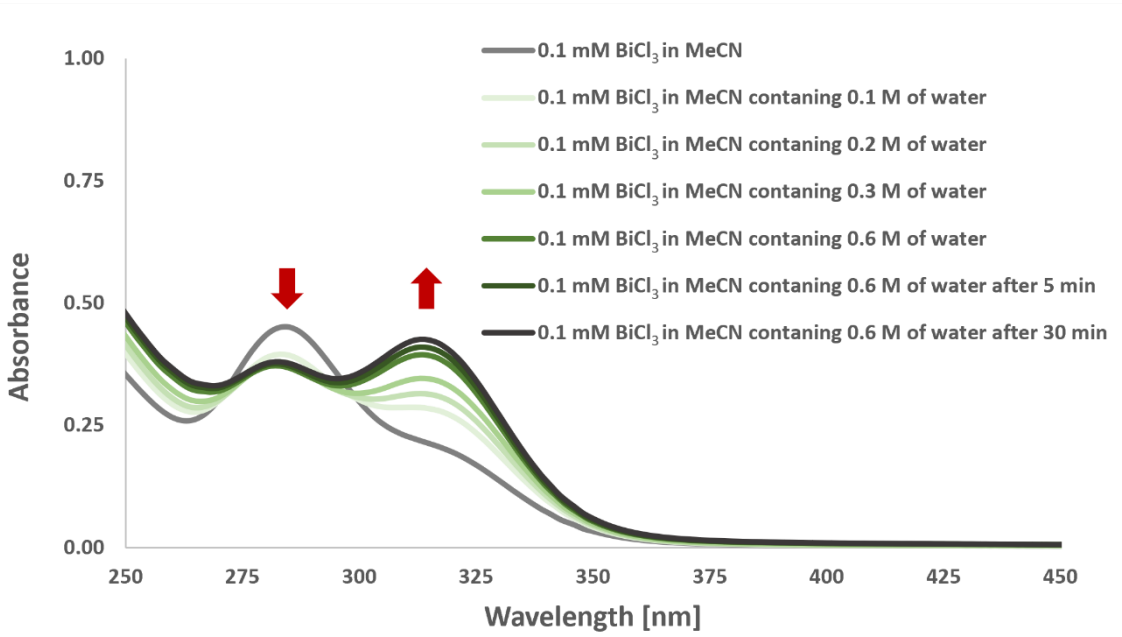

Figure S4. 7: UV-Vis spectra of bismuth (III) chloride in acetonitrile upon gradual addition of water.

4.7.4.2 Cyclovoltammetry of bismuth chlorides

The potentials were measured against the potential of the ferrocene/ferrocenium couple and were corrected with the conversion constant of +0.38 V to saturated calomel electrode (vs. SCE).

4.7.4.2.1 Cyclovoltammetry of $BiCl_5^{2-}$

Solutions were prepared by adding 1 mL of a 0.1 M $BiCl_5^{2-}$ stock solution in MeCN to 6 mL of a 0.1 M conducting $TBABF_4$ salt in MeCN. The measurement was started in oxidative direction to get the ferrocene reference peaks and then were run in reductive direction for two cycles. However, starting directly in the reductive direction does not change the cyclic voltammogram. The ferrocene is overlapping with additional oxidation peaks. We do not want to speculate on the nature of these additional peaks as bismuth has five different possible oxidation states (0, I, II, III, V) and additional chemical reactions are possible. The CV peaks relevant for bismuth LMCT are the first reduction (Bi(III) to Bi(0)) and the first oxidation peak (Bi(0) to Bi(III). The first and second CV cycle show a slightly altered curve. Presumably this change is caused by the deposition of an elemental bismuth film on the carbon working electrode.

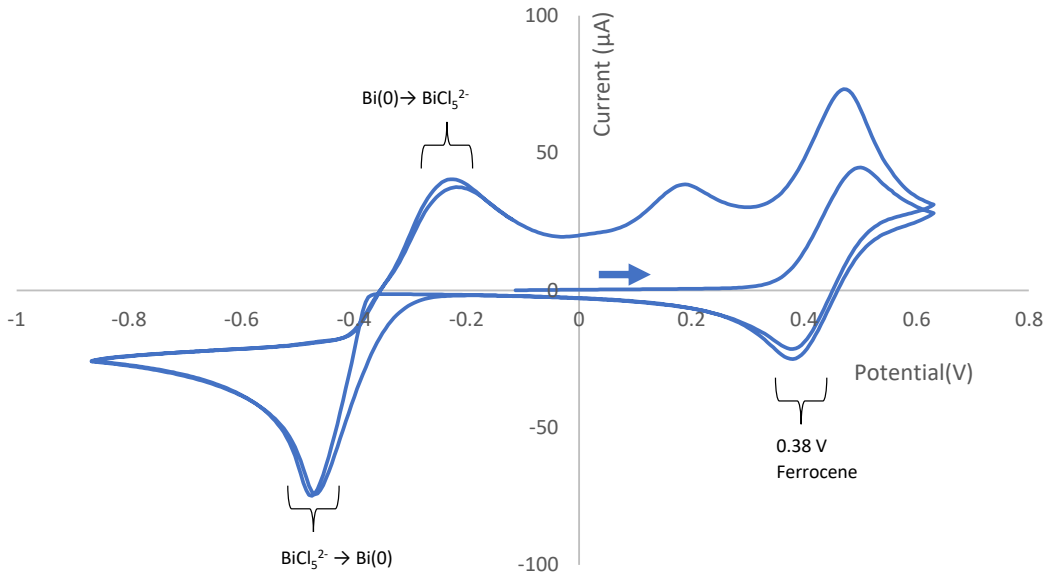

Figure S4. 8: Cyclic voltammogram of $BiCl_5^{2-}$ in MeCN.

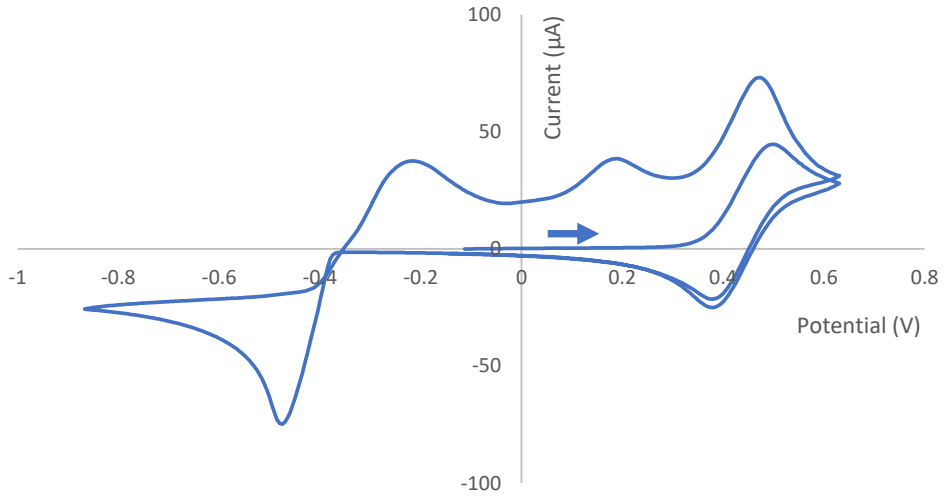

Figure S4. 9: Only the first cycle of cyclic voltammogram of $BiCl_5^{2-}$ in MeCN.

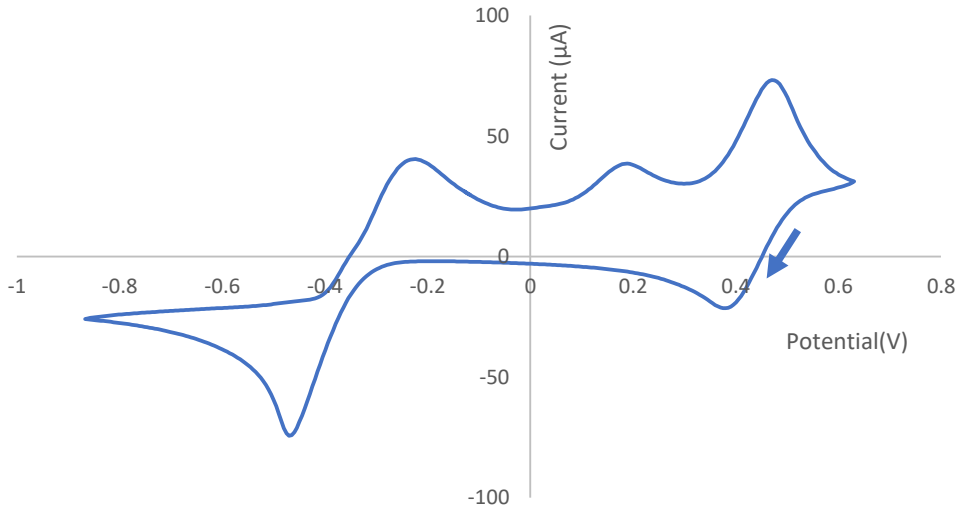

Figure S4. 10: Only the second cycle of cyclic voltammogram of $BiCl_5^{2-}$ in MeCN.

4.7.4.2.2 Cyclovoltammetry of $BiCl_3$

The measurement was performed similarly as with $BiCl_5^{2-}$. The only difference was that we started the measurements in reductive direction.

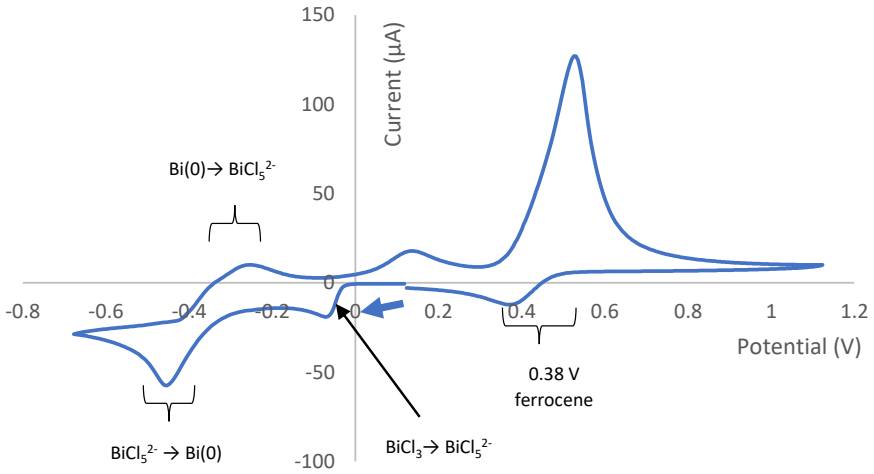

Figure S4. 11: Cyclic voltammogram of $BiCl_3$ in MeCN.

4.7.4.2.3 Cyclovoltammetry of $BiCl_4^-$

We performed this measurement to support our spectro-electrochemical investigation. The measurement shows only a small reduction peak (at -0.2 V) for $BiCl_4^-$, indicating that the released chloride immediately reacts with the remaining $BiCl_4^-$ to form $BiCl_5^{2-}$.

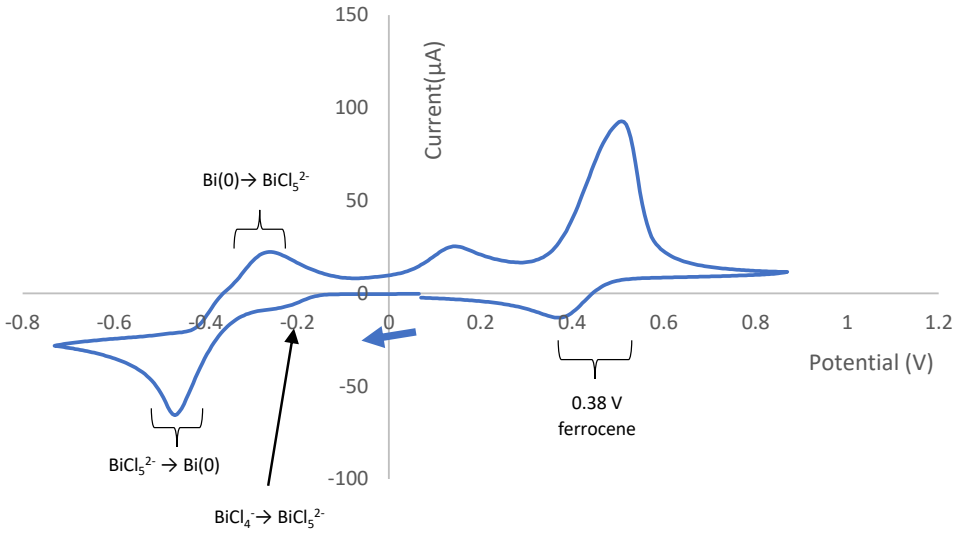

Figure S4. 12: Cyclovoltammetry of $BiCl_4^-$ in MeCN.

4.7.4.3 Spectro-electrochemical experiments

The samples dissolved in MeCN were purged with argon for 5 min before they were transferred in the Ottle cell. During the measurements, the potential was being changed slowly at rate 5 mV/s. The UV-Vis spectra were measured after each change of potential for 50 mV (corresponds to 10 seconds).

4.7.4.3.1 Cyclovoltammetry of $BiCl_5^{2-}$

The absorption maximum peak of $BICl_5^{2-}$ at 340 nm disappears upon reduction (Figure S4. 13A), and upon oxidation reappears without any noticeable intermediates or side reactions (Figure S4. 13B).

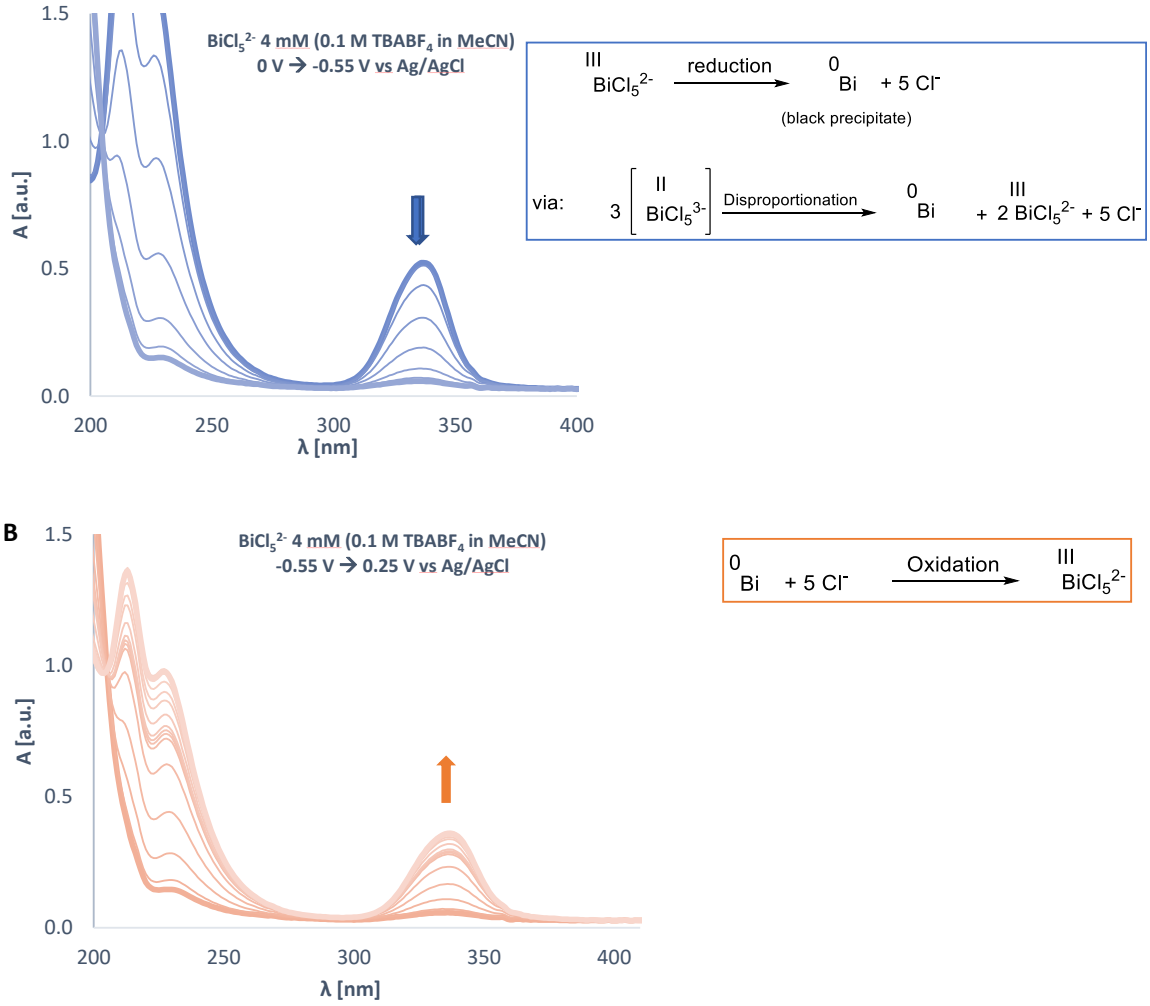

Figure S4. 13: UV-vis monitoring of the reduction (**A**) and subsequent oxidation of $BiCl_5^{2-}$ (**B**).

The reduction of $Bi^{(III)}Cl_5^{2-}$ and oxidation of $Bi^{(0)}$ are complex processes. In both cases 3 electrons are transferred, but we could only observe a single peak in CV. This likely indicates that after the initial electron transfer, a fast series of disproportionations is triggered which results in Bi (III) and Bi (0).

4.7.4.3.2 Cyclovoltammetry of UV-vis monitoring of the reduction and oxidation of $BiCl_3$

The reduction of $BiCl_3$ (Figure S4. 14) is a two-step process. In the first step $BiCl_3$ is reduced to $BiCl_5^{2-}$. The absorption maximum of $BiCl_3$ at 280 nm disappears, and a new peak at 340 nm appears indicating formation of $BiCl_5^{2-}$ (Figure S4. 14A). In principle, the disproportionation should generate both $BiCl_5^{2-}$ and $BiCl_4^-$ (otherwise it is impossible to balance the chemical equation) but we observed only $BiCl_5^{2-}$. This could be explained by the onset of the reduction of the $BiCl_4^-$ (Figure S4. 12) which releases some chloride. The released chloride reacts with $BiCl_4^-$ to form $BiCl_5^{2-}$. In the second step (Figure S4. 14B), when the reduction potential is further decreased, *in situ* generated $BiCl_5^{2-}$ undergoes reduction - similarly as in Figure S4. 13A.

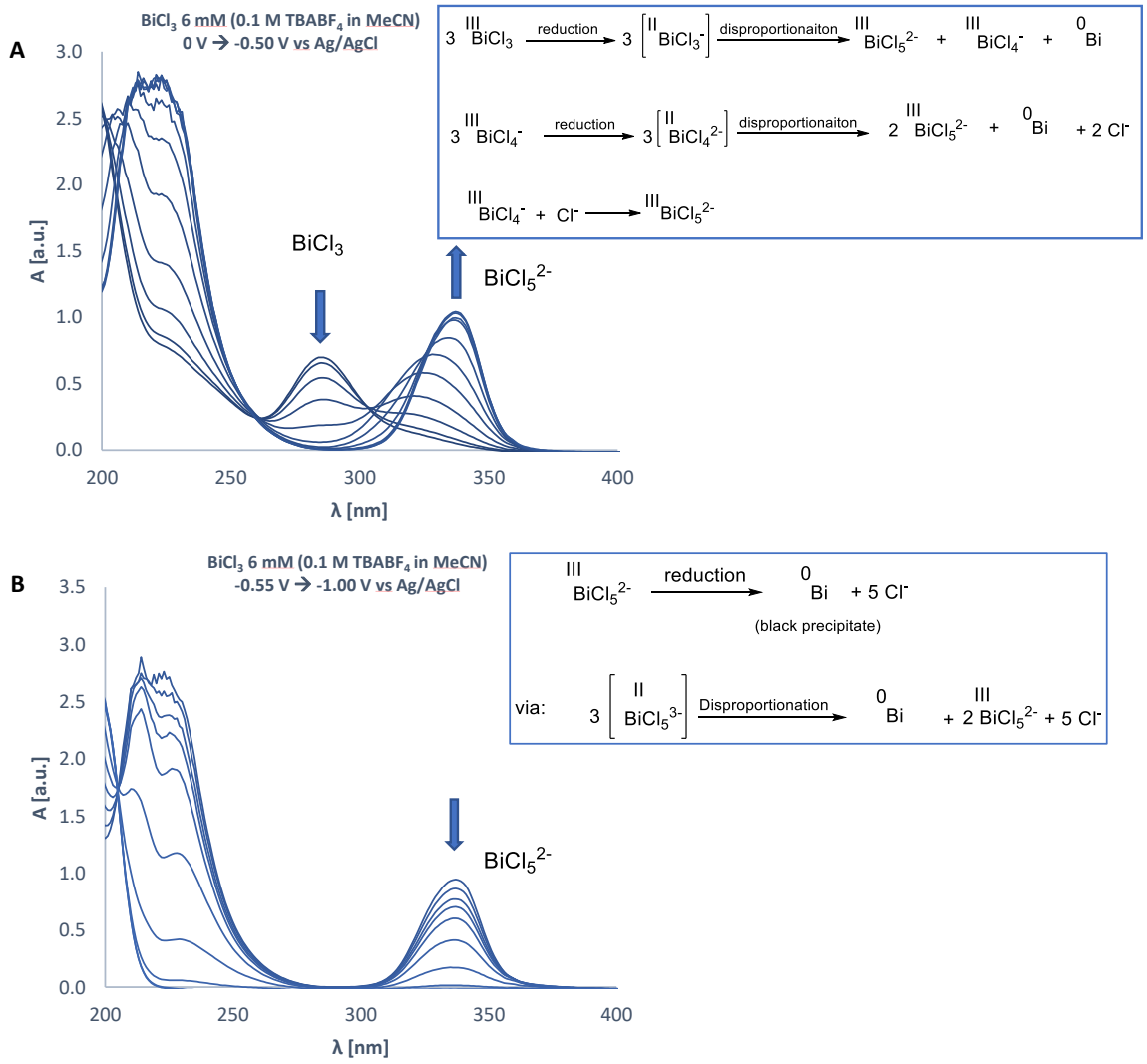

Figure S4. 14: UV-vis monitoring of the reduction of $BiCl_3$ (A) and $BiCl_5^{2-}$ (B).

In the first step of oxidation of Bi(0) (Figure S4. 15A), absorption maximum of $BiCl_5^{2-}$ at 340 nm reappears – similarly as in Figure S4. 13B. During further oxidation of bismuth (0) (Figure S4. 15B), the disappearance of the band at 340 nm and formation of a new absorption maximum at 280 nm was observed. We can explain that by looking at the concentration of the chloride ions. Once, when the free Cl^- ions are used up, the newly formed Bi^{3+} ions start taking the chloride ions from $BiCl_5^{2-}$ leading to formation of $BiCl_3$.

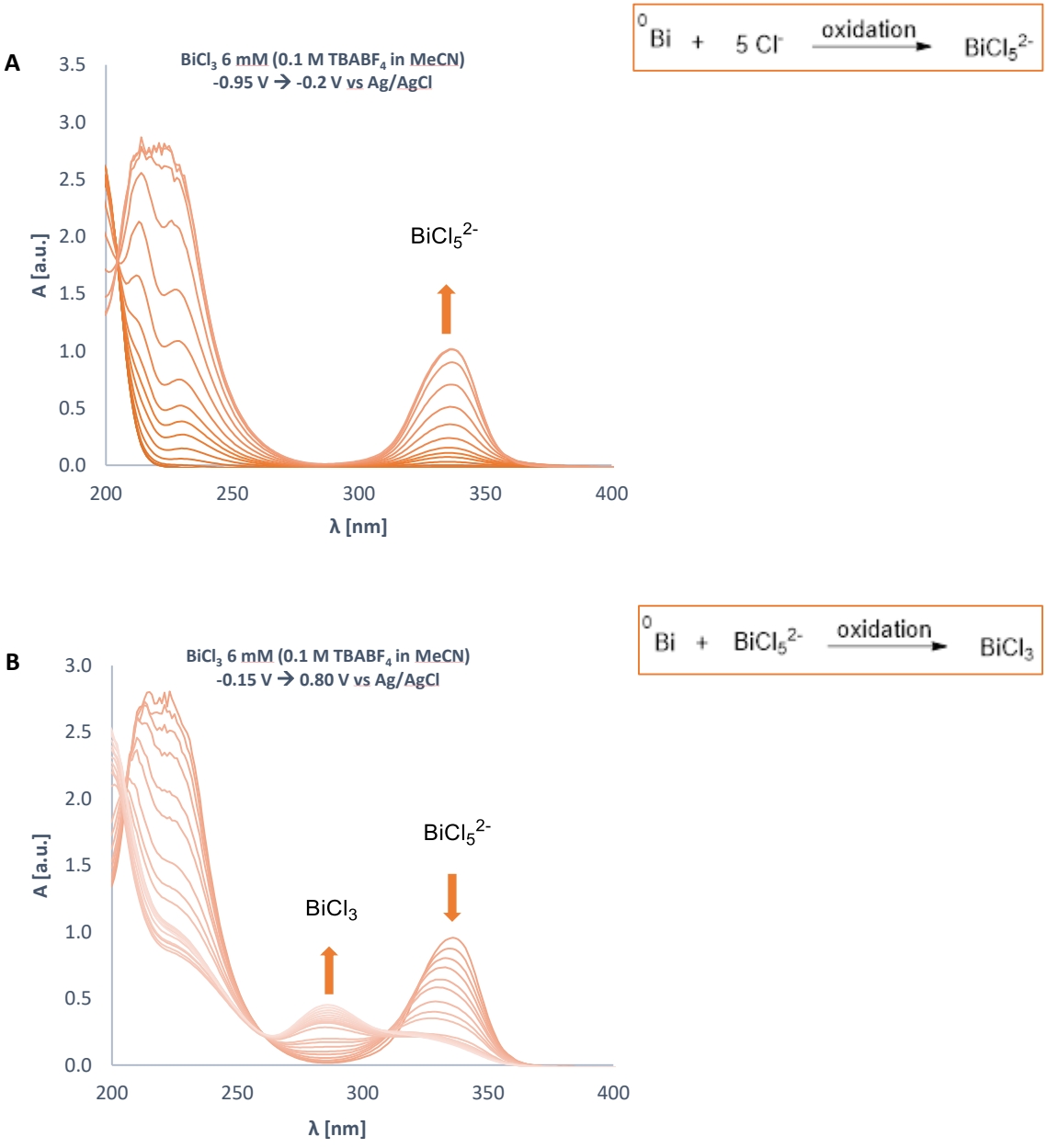

Figure S4. 15: UV-vis monitoring of the oxidation of the previously reduced $BiCl_3$ sample.

4.7.4.4 Powder diffraction and microscopy of the black precipitate

The black powder which forms in redox neutral reactions corresponds to some reduced bismuth species. The main question we had, was whether we are getting bismuth in oxidation sate (I), (so-called complex bismuth subchlorides) or is it elemental bismuth (0). The black precipitate was prepared by two different means. In one case, we analyzed the solid residue which was formed in large scale reaction between acrylonitrile and cyclohexane (Scheme S4. 6). In the other case, we directly prepared the black precipitate by irradiation of the solution of the $BiCl_5^{2-}$ complex in the absence of any reactants (Scheme S4. 4 on the next page).

The powder X-ray diffraction analysis unambiguously identified the black precipitate as elemental bismuth (0) in both cases (Figure S4. 16). The unidentified peak areas were less than 4% in both samples. We estimate the purity of the samples to be 92+ %.

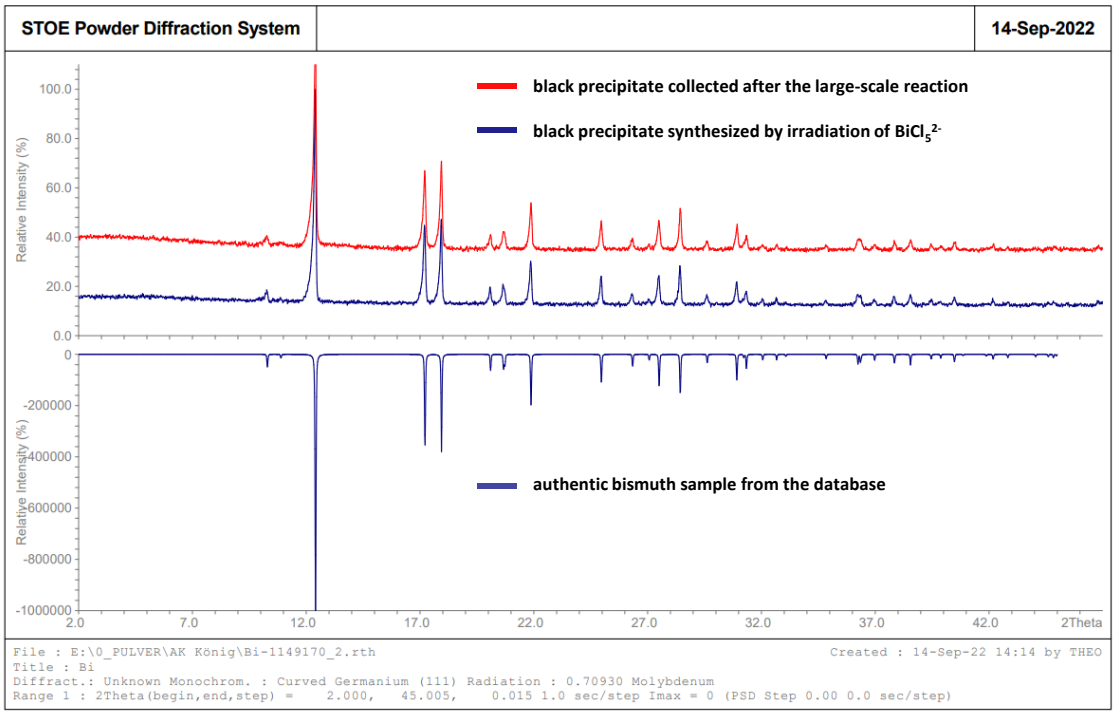

Figure S4. 16: Comparison of the measured powder X-Ray diffractograms to the database bismuth reference.[36]

Experimental procedure for preparation of Bi(0) by irradiation of $BiCl_5^{2-}$.

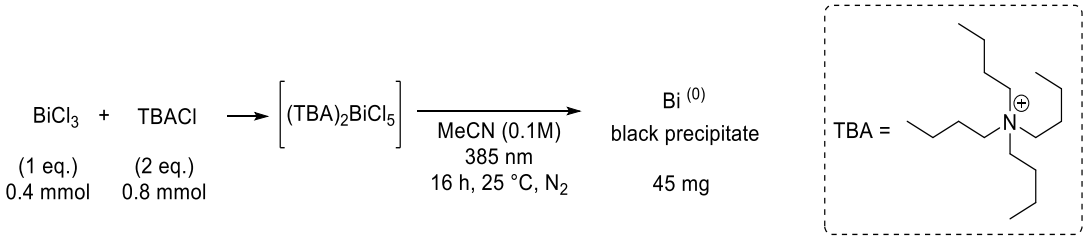

Scheme S4. 4: Preparation of the black precipitate by irradiation of bismuth chloride in the presence of tetrabutylammonium chloride.

$BiCl_3$ (132 mg, 0.4 mmol, 1 eq.) and TBACl (222 mg, 0.8 mmol, 2 eq.) were weight into a reaction vial. We added 4 ml of dry MeCN and closed the vial. The solution was degassed by three vacuum-nitrogen cycles and irradiated at 25 °C with 385 nm for 16 hours. After the irradiation, the sample was transferred into a conical Eppendorf vial (2 ml) and washed three times with fresh MeCN. The obtained powder was dried under low pressure, before being submitted for powder X-Ray diffraction analysis. The mass of the dry powder was 45 mg, corresponding to 51% yield. We also looked for any crystals in the sample using a microscope. We observed shiny, amorphous solid agglomerates of different sizes.

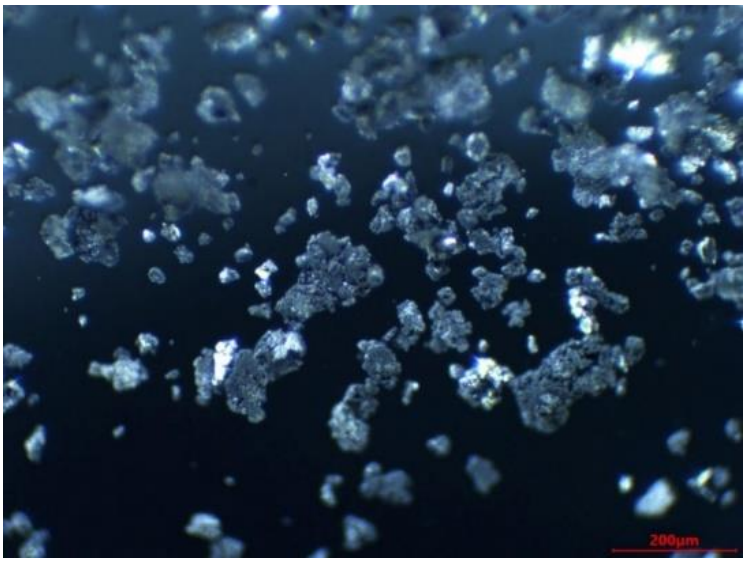

Figure S4. 17: Magnified photo of the black precipitate.

4.7.4.5 Kinetics of the model reaction

The yield after one hour, 26% corresponds to 5 catalytic turnovers of the bismuth catalyst (5 mol% loading). The reaction profile in the first one hour is linear, likely indicating that the active catalytic species is not changing over time.

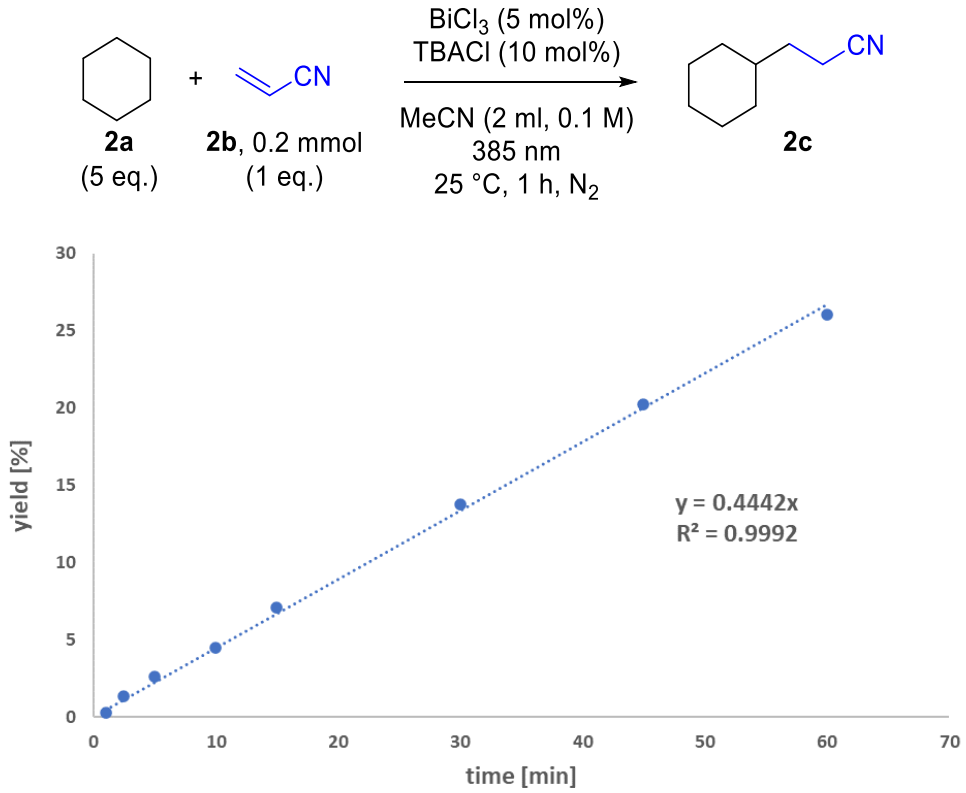

Figure S4. 18: Initial kinetics of the model reaction.

4.7.4.6 Quantum yield of the model reaction

Experimental procedure for quantum yield determination

The method and instrument which we used was originally developed by Prof. Riedle.[35]

$BiCl_3$ (6.3 mg, 0.02 mmol, 5 mol%) and TBACl (11.1 mg, 0.04 mmol, 10 mol%) were weighed into a crimp reaction vial. 4 ml of dry MeCN was added and the vial was closed. The reaction mixture was stirred for a few minutes and degassed by 4 argon-vacuum cycles. Then, 3.0 ml of the so-prepared reaction mixture was transferred using air-free techniques into a 10×10 mm fluorescence cuvette equipped with a stirring bar (see Figure S4.4). Afterwards, degassed internal standard benzotrifluoride (36.8 µl, 0.3 mmol, 1 eq.) and liquid reactants acrylonitrile (19.7 µl, 0.3 mmol, 1 eq.) and cyclohexane (162 µl, 1.5 mmol, 5 eq.) were added. The reaction mixture was irradiated with a single spot 385 nm LED in a quantum yield determination setup for 12 hours. 50 µl aliquots of the reaction mixture were and taken analysed by GC-FID after approximately 4, 8 and 12 hours of irradiation.

Table S4. 4: Quantum yield determination.

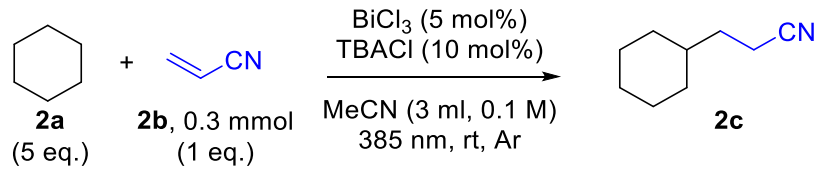

Entry	Δt $[min]$	$P_{ref\ (solvent)}$ $[mW]$	P_{sample} $[mW]$	P_{abs} $[mW]$	GC yield	Quantum yield φ
1	265	50.7	13.9	38.5	11 %	1.6 %
2	455	50.7	13.5	38.9	17 %	1.5 %
3	715	50.7	11.9	40.6	25 %	1.3 %
						average = **1.5 %**

More details on the calculation of the quantum yield (φ) of the Entry 1.

$$\Phi = \frac{N_{prod}}{N_{ph,abs}} = N_A \cdot h \cdot c \frac{c_{prod} \cdot V}{P_{abs} \cdot \Delta t \cdot \lambda_{LED}}$$

constants	
N_A= 6.02214 × 10^{23} mol^{-1}	Avogadro constant
h= 6.62607004 × 10^{-34} Js	Planck constant
c= 299792458 m/s	Speed of light

data for our system		
N_{prod}	Number of product molecules	
$N_{ph,abs}$	Number of photons absorbed	
c_{prod}	Product concentration	= 10.5 mmol/L
V	Reaction volume	= 3.00 mL
Δt	Illumination time	= 15908 s (4 h 25 min)
P_{abs}	Absorbed power	= 13.9 mW (calculated)
λ_{LED}	Illumination wavelength	= 385 nm

P_{abs} was calculated using the following equations:

$$P_{abs} = (P_{ref} - P_{sample})f \qquad f = \frac{1 + R\frac{P_{sample}}{P_{ref}}}{1 - R}$$

Data for our system		
P_{sample}	Average power during illumination	= 13.9 mW
P_{ref}	Reference power (solvent)	= 50.7 mW
f	Correction factor	= 1.049
R	Back reflection	= 0.0357 (parameter for fused silica cuvette)

4.7.5 Gram-scale reactions

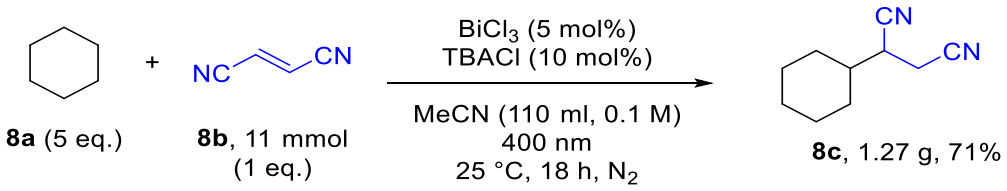

Scheme S4.5: Gram-scale reaction for preparation of **8c**.

Fumaronitrile (858 mg, 11 mmol, 1 eq.), $BiCl_3$ (173 mg, 0.55 mmol, 5 mol%) and tetrabutylammonium chloride (305 mg, 1.1 mmol, 10 mol%) were weighed in a reaction vessel (see Figure S4.3 for pictures of the setup). Then, dry MeCN (110 ml) was added, and the reaction vessel was closed and degassed by 4 nitrogen-vacuum cycles. Afterwards, degassed cyclohexane (5.9 ml, 55 mmol, 5 eq.) was added through a septum and the reaction mixture was stirred under irradiation for 18 hours at 25 °C. The conversion of the fumaronitrile was monitored by GC-FID. After the completion, the reaction mixture was transferred into a round bottom flask, 2 spoons of silica gel were added, and the solvent was removed by a rotary evaporator to prepare a dry load for the column. 5-20 % ethyl acetate/petrol ether solvent mixture was used as an eluent for the column. The spots on the TLC were visualized by permanganate stain. After the column and pentane wash, the product was obtained as a white crystalline solid in 71% yield.

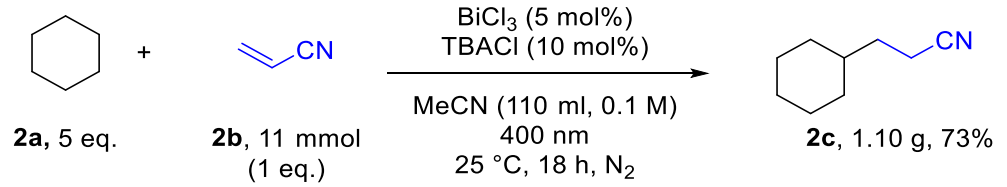

Scheme S4.6: Gram-scale reaction for preparation of **2c**.

Gram-scale reaction for preparation of **2c** was done similarly as in above-described procedure (Figure S4.3). Acrylonitrile **2b** was degassed in a separate reaction vial before it was added to the degassed reaction mixture. After the completion, the reaction mixture was transferred into a round bottom flask and the solvent was removed under reduced pressure. The crude reaction mixture was purified by Kugelrohr distillation. The purified product was obtained as a colorless oil in 73% yield.

4.7.6 Characterization data

6H-benzo[c]chromen-6-one (1b)

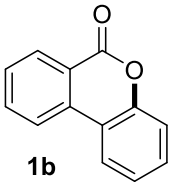

1b

Yield	77% (30 mg, 0.15 mmol), White solid
^{1}H NMR	^{1}H NMR (400 MHz, $CDCl_3$) δ 8.35 (dd, *J* = 8.1, 1.0 Hz, 1H), 8.06 (d, *J* = 8.1 Hz, 1H), 8.00 (dd, *J* = 7.9, 1.3 Hz, 1H), 7.79 (ddd, *J* = 8.1, 6.9, 1.3 Hz, 1H), 7.54 (ddd, *J* = 8.1, 6.9, 0.9 Hz, 1H), 7.44 (ddd, *J* = 8.3, 6.9, 1.3 Hz, 1H), 7.37 – 7.27 (m, 2H).
^{13}C NMR	^{13}C NMR (101 MHz, $CDCl_3$) δ 161.2, 151.3, 134.8, 134.7, 130.5, 130.4, 128.9, 124.6, 122.8, 121.7, 121.2, 118.0, 117.7.

3-cyclohexylpropanenitrile (2c)

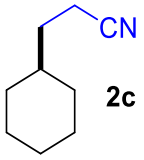

2c

Yield	large scale (11 mmol): 73% (1.10 g, 8.0 mmol), colorless oil.
^{1}H NMR	^{1}H NMR (400 MHz, $CDCl_3$) δ 2.33 (t, *J* = 7.3 Hz, 2H), 1.75 – 1.60 (m, 5H), 1.53 (dt, *J* = 7.3, 7.3 Hz, 2H), 1.44 – 1.29 (m, 1H), 1.30 – 1.04 (m, 3H), 0.97 – 0.80 (m, 2H).
^{13}C NMR	^{13}C NMR (101 MHz, $CDCl_3$) δ 120.1, 36.6, 32.6, 32.5, 26.3, 26.0, 14.7.
HR-MS (EI)	$(M^{+\cdot}\text{-}H^{\cdot})^{+}$: calc. 136.1121, found 136.1120

The compound is too volatile to be isolated on a normal scale (0.4 mmol) in a representative yield.

2-(cyclohexyl(phenyl)methyl)malononitrile (3c)

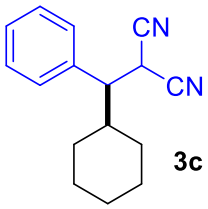

3c

Yield	79% (75 mg, 0.32 mmol), colorless oil
^{1}H NMR	^{1}H NMR (400 MHz, $CDCl_3$) δ 7.46 – 7.28 (m, 5H), 4.20 (d, *J* = 5.5 Hz, 1H), 2.89 (dd, *J* = 9.8, 5.5 Hz, 1H), 2.10 – 1.97 (m, 1H), 1.97 – 1.89 (m, 1H), 1.89 – 1.77 (m, 1H), 1.77 – 1.60 (m, 2H), 1.53 – 1.29 (m, 2H), 1.29 – 0.96 (m, 3H), 0.90 – 0.76 (m, 1H).
^{13}C NMR	^{13}C NMR (101 MHz, $CDCl_3$) δ 136.8, 129.1, 128.7, 128.4, 112.4, 112.1, 52.3, 39.3, 31.2, 30.6, 27.2, 25.9, 25.9, 25.8.
HR-MS (EI)	$(M)^{+\cdot}$: calc. 238.1465, found 238.1459

diethyl 2-(cyclohexyl(phenyl)methyl)malonate (4c)

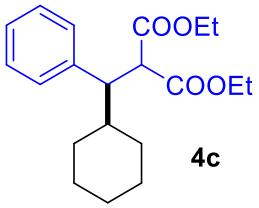

4c

Yield	35% (47 mg, 0.14 mmol), colorless oil
^{1}H NMR	^{1}H NMR (400 MHz, $CDCl_3$) δ 7.26 – 7.08 (m, 5H), 4.30 – 4.16 (2H), 3.97 (d, *J* = 11.3 Hz, 1H), 3.91 – 3.78 (2H), 3.37 (dd, *J* = 11.3, 5.0 Hz, 1H), 1.74 – 1.48 (m, 6H), 1.35 – 1.04 (m, 5H), 1.01 – 0.75 (m, 6H).
^{13}C NMR	^{13}C NMR (101 MHz, $CDCl_3$) δ 168.9, 168.1, 139.0, 129.5, 127.7, 126.7, 61.5, 61.1, 55.4, 51.1, 40.9, 32.1, 28.4, 26.7, 26.5, 26.2, 14.1, 13.7.
HR-MS (ESI)	$(M+H)^+$: calc. 333.2060 , found 333.2067

(2-cyclohexylethane-1,1-diyldisulfonyl)dibenzene (5c)

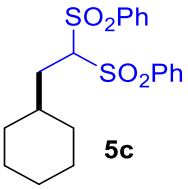

5c

Yield	45% (71 mg, 0.18 mmol), White solid
^{1}H NMR	^{1}H NMR (400 MHz, $CDCl_3$) δ 7.95 (dt, *J* = 8.6, 1.6 Hz, 4H), 7.75 – 7.64 (m, 2H), 7.64 – 7.51 (m, 4H), 4.46 (t, *J* = 5.6 Hz, 1H), 1.99 (dd, *J* = 6.9, 5.7 Hz, 2H), 1.70 – 1.54 (m, 5H), 1.50 – 1.37 (m, 1H), 1.20 – 1.00 (m, 3H), 0.80 – 0.67 (m, 2H).
^{13}C NMR	^{13}C NMR (101 MHz, $CDCl_3$) δ 137.9, 134.6, 129.7, 129.2, 81.4, 35.7, 32.6, 32.5, 26.1, 25.8.
HR-MS (ESI)	$(M+H)^+$: calc. 393.1197, found 393.1189

3-cyclohexyl-2-phenylpropanoic acid (6c)

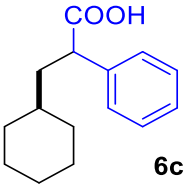

6c

Yield	40% (37 mg, 0.16 mmol), colorless oil
^{1}H NMR	^{1}H NMR (400 MHz, $CDCl_3$) δ 10.34 (s, 1H), 7.36 – 7.24 (m, 5H), 3.71 (t, *J* = 7.8 Hz, 1H), 2.02 – 1.94 (m, 1H), 1.80 – 1.56 (m, 6H), 1.26 – 1.10 (m, 4H), 0.97 – 0.84 (m, 2H)
^{13}C NMR	^{13}C NMR (101 MHz, $CDCl_3$) δ 180.7, 138.8, 128.7, 128.1, 127.4, 48.8, 40.6, 35.2, 33.3, 33.0, 26.5, 26.1, 26.1.
HR-MS (EI)	$(M)^{+\cdot}$: calc. 232.1458, found 232.1462

2-(cyclohexylmethyl)-3,3,3-trifluoropropanoic acid (7c)

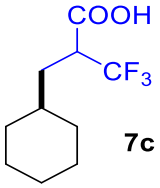

7c

Yield	29% (26 mg, 0.12 mmol), colorless oil
^{1}H NMR	^{1}H NMR (400 MHz, $CDCl_3$) δ 7.52 (bs, 1H), 3.42 – 3.03 (m, 1H), 2.05 – 1.52 (m, 7H, overlap with water), 1.44 – 1.07 (m, 5H), 1.07 – 0.80 (m, 2H).
^{13}C NMR	^{13}C NMR (101 MHz, $CDCl_3$) δ 173.5, 124.7 (q, *J* = 276.7 Hz), 47.8 (q, *J* = 28.0 Hz), 34.9, 33.5, 33.4, 32.1, 26.3, 26.0, 25.8.
^{19}F NMR	^{19}F NMR (376 MHz, $CDCl_3$) δ -68.9.
HR-MS (EI)	$(M\text{-}HF)^{+\cdot}$: calc. 204.0956, found 204.0957

A similar complex ^{13}C NMR pattern was observed for a related methyl ester compound.[37]

2-cyclohexylsuccinonitrile (8c)

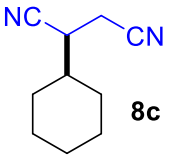

8c

Yield	Normal scale (0.4 mmol): 73% (47 mg, 0.29 mmol), white solid Large scale (11 mmol): 71% (1.27 g, 7.8 mmol), white solid
^{1}H NMR	^{1}H NMR (400 MHz, $CDCl_3$) δ 2.81 – 2.73 (m, 1H), 2.73 – 2.59 (m, 2H), 1.92 – 1.56 (m, 6H), 1.35 – 1.02 (m, 5H).
^{13}C NMR	^{13}C NMR (101 MHz, $CDCl_3$) δ 118.5, 116.4, 38.5, 34.6, 30.8, 29.0, 25.6, 25.6, 25.5, 18.7.
HR-MS (EI)	$(M^{+\cdot}\text{-}H^{\cdot})^{+}$: calc. 161.1073, found 161.1073

2-cyclopentylsuccinonitrile (9c)

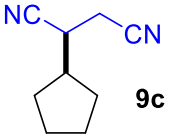

9c

Yield	79% (47 mg, 0.32 mmol), colorless oil
^{1}H NMR	^{1}H NMR (400 MHz, $CDCl_3$) δ 2.95-2.87 (m, 1H), 2.80 – 2.61 (m, 2H), 2.28 – 2.10 (m, 1H), 2.05 – 1.81 (m, 2H), 1.81 – 1.51 (m, 4H), 1.51 – 1.19 (m, 2H).
^{13}C NMR	^{13}C NMR (101 MHz, $CDCl_3$) δ 118.5, 115.9, 41.0, 33.6, 30.9, 29.7, 25.2, 25.0, 20.5.
HR-MS (ESI)	$(M+NH_4)^{+}$: calc. 166.1339, found 166.1338

2-cyclooctylsuccinonitrile (10c)

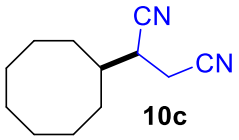

10c

Yield	67% (51 mg, 0.27 mmol), colorless oil
^{1}H NMR	^{1}H NMR (400 MHz, $CDCl_3$) δ 2.90 – 2.63 (m, 3H), 2.05 – 1.89 (m, 1H), 1.87 – 1.40 (m, 14H).
^{13}C NMR	^{13}C NMR (101 MHz, $CDCl_3$) δ 118.6, 116.0, 38.3, 35.8, 31.6, 28.9, 26.5, 26.3, 26.2, 25.6, 25.0, 19.2.
HR-MS (EI)	$(M^{+\cdot}\text{-}H^{\cdot})^+$: calc. 189.1386, found 189.1391

2-((3r,5r,7r)-adamantan-1-yl)succinonitrile / 2-((1r,3r,5r,7r)-adamantan-2-yl)succinonitrile (11c)

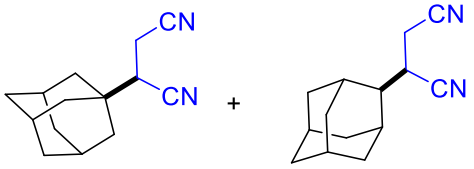

11c
1.2:1 mixture
(GC FID)

Yield	51% (44 mg, 0.20 mmol), white solid
^{1}H NMR (mixture)	^{1}H NMR (400 MHz, $CDCl_3$) δ 3.25 – 3.16 (m, 1H), 2.87 – 2.74 (m, 1H), 2.69 – 2.58 (m, 4H), 2.20 (s, 1H), 2.13 – 1.99 (m, 4H), 1.98 – 1.90 (m, 3H), 1.90 – 1.57 (m, 22H).
^{13}C NMR (mixture)	^{13}C NMR (101 MHz, $CDCl_3$) δ 118.9, 117.8, 116.9, 115.8, 45.2, 41.1, 39.4, 38.2, 38.1, 37.5, 36.2, 35.0, 31.5, 30.9, 30.8, 30.2, 28.2, 28.1, 27.3, 27.2, 19.0, 15.4.
HR-MS (ESI)	$(M+NH_4)^+$: calc. 232.1808, found 232.1809
GC-FID	

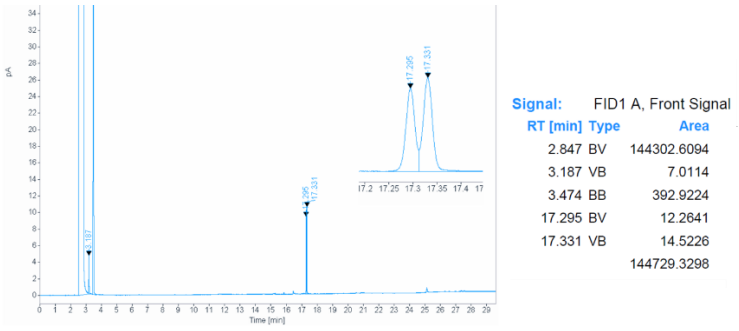

Ratio of the two isomers was determined from the GC-FID analysis. The isomers in the sample are not easy to separate on the column and therefore, we used very low concentration to minimize the overlap.

2-(4-methoxybenzyl)succinonitrile (12c)

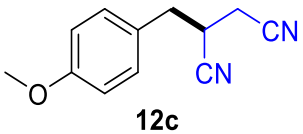

12c

Yield	92% (74 mg, 0.37 mmol), yellowish oil
^{1}H NMR	^{1}H NMR (400 MHz, $CDCl_3$) δ 7.18 (d, J = 8.7 Hz, 2H), 6.89 (d, J = 8.7 Hz, 2H), 3.79 (s, 3H), 3.14 – 2.92 (m, 3H), 2.63 (dd, *J* = 6.3, 1.4 Hz, 2H).
^{13}C NMR	^{13}C NMR (101 MHz, $CDCl_3$) δ 159.4, 130.3, 126.5, 118.8, 115.8, 114.6, 55.4, 36.2, 30.3, 20.0.
HR-MS (EI)	$(M)^{+\cdot}$: calc. 200.0944, found 200.0941

2-(phenoxymethyl)succinonitrile (13c)

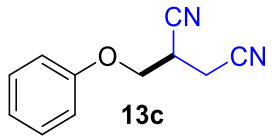

13c

Yield	84% (63 mg, 0.34 mmol), yellowish oil
^{1}H NMR	^{1}H NMR (400 MHz, $CDCl_3$) δ 7.33 (dd, *J* = 8.7, 7.3 Hz, 2H), 7.06 (t, *J* = 7.3 Hz, 1H), 6.93 (d, *J* = 8.7, 2H), 4.30 – 4.18 (m, 2H), 3.40 – 3.32 (m, 1H), 2.94 (dd, *J* = 6.7, 1.1 Hz, 2H).
^{13}C NMR	^{13}C NMR (101 MHz, $CDCl_3$) δ 157.3, 129.9, 122.5, 116.9, 115.5, 114.8, 65.4, 29.0, 18.1.
HR-MS (EI)	$(M)^{+\cdot}$: calc. 186.0788, found 186.0789

2-(1-ethoxyethyl)succinonitrile (14c)

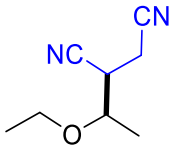

14c
1:1 mixture of diasteromers

Yield	86% (52 mg, 0.34 mmol), colorless oil
^{1}H NMR	^{1}H NMR (400 MHz, $CDCl_3$) δ 3.76 – 3.57 (m, 2H), 3.52 – 3.33 (m, 1H), 3.07 – 2.69 (m, 3H), 1.35 (dd, *J* = 7.9, 6.2 Hz, 3H), 1.27 – 1.14 (m, 3H).
^{13}C NMR	^{13}C NMR (101 MHz, $CDCl_3$) δ 117.6, 117.1, 116.2, 116.0, 73.3, 72.1, 65.1, 64.8, 35.2, 35.1, 17.7, 17.7, 17.5, 17.4, 15.2, 15.2.
HR-MS (EI)	$(M^{+\cdot}\text{-}H^{\cdot})^+$: calc. 151.0866, found 151.0866

2-(tetrahydrofuran-2-yl)succinonitrile (15c)

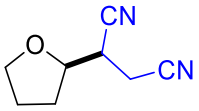

15c
1:1 mixture of diasteromers

Yield	92% (55 mg, 0.37 mmol), colorless oil
^{1}H NMR	^{1}H NMR (400 MHz, $CDCl_3$) δ 4.15 – 3.73 (m, 3H), 3.13 – 2.69 (m, 3H), 2.35 – 1.75 (m, 4H).
^{13}C NMR	^{13}C NMR (101 MHz, $CDCl_3$) δ 117.3, 117.2, 116.0, 115.7, 77.2, 76.4, 69.4, 69.1, 34.6, 34.3, 30.1, 29.9, 25.9, 25.5, 18.8, 18.5.
HR-MS (EI)	$(M^{+\cdot}\text{-}H^{\cdot})^+$: calc. 149.0709, found 149.0711

2-(hydroxymethyl)succinonitrile (16c)

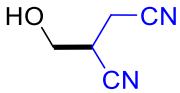

16c

Yield	36% (16 mg, 0.14 mmol), yellowish oil
^{1}H NMR	^{1}H NMR (400 MHz, $CDCl_3$) δ 3.96 (dd, *J* = 5.2, 1.4 Hz, 2H), 3.11 (tt, *J* = 6.8, 5.2 Hz, 1H), 2.87 (dd, *J* = 6.8, 1.4 Hz, 2H), 2.44 (bs, 1H).
^{13}C NMR	^{13}C NMR (101 MHz, $CDCl_3$) δ 117.5, 115.6, 60.8, 31.1, 17.5.
HR-MS (EI)	$(M)^{+\cdot}$: calc. 110.0475, found 110.0473

2-(5-acetylbenzo[d][1,3]dioxol-2-yl)succinonitrile (17c)

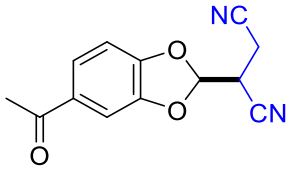

17c
1:1 mixture of diasteromers

Yield	53% (51 mg, 0.21 mmol), slightly brownish oil
^{1}H NMR	^{1}H NMR (400 MHz, $CDCl_3$) δ 7.61 (dd, *J* = 8.2, 1.7 Hz, 1H), 7.50 (t, *J* = 1.8 Hz, 1H), 6.95 (dd, *J* = 8.2, 1.9 Hz, 1H), 6.45 (dd, *J* = 3.7, 2.4 Hz, 1H), 3.59 – 3.51 (m, 1H), 2.95 (dd, *J* = 7.0, 1.4 Hz, 2H), 2.54 (s, 3H).
^{13}C NMR	^{13}C NMR (101 MHz, $CDCl_3$) δ 196.2, 150.1, 146.9, 146.9, 133.1, 125.6, 114.7, 114.6, 114.1, 114.1, 108.7, 108.7, 107.2, 107.2, 34.2, 34.2, 26.6, 16.0, 15.9.
HR-MS (EI)	$(M)^{+\cdot}$: calc. 242.0686, found 242.0691

methyl 2-(3-(2,3-dicyanopropoxy)phenyl)acetate (18c)

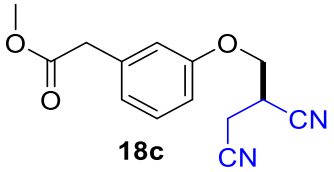

18c

Yield	69% (71 mg, 0.28 mmol), yellowish oil
^{1}H NMR	^{1}H NMR (400 MHz, $CDCl_3$) δ 7.27 (dd, *J* = 7.9, 7.9 Hz, 1H), 6.94 (d, *J* = 7.9 Hz, 1H), 6.89 – 6.85 (m, 1H), 6.84 – 6.80 (m, 1H), 4.28 – 4.15 (m, 2H), 3.69 (s, 3H), 3.61 (s, 2H), 3.41 – 3.30 (m, 1H), 2.93 (d, *J* = 6.6 Hz, 2H).
^{13}C NMR	^{13}C NMR (101 MHz, $CDCl_3$) δ 171.8, 157.4, 136.0, 130.0, 123.4, 116.9, 115.9, 115.5, 113.4, 65.4, 52.2, 41.0, 29.0, 18.1
HR-MS (EI)	$(M)^{+\cdot}$: calc. 258.0999, found 258.1001

N-(2,3-dicyanopropyl)-N-methylacetamide (19c)

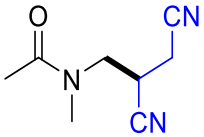

19c

Yield	98% (65 mg, 0.39 mmol), yellowish oil
^{1}H NMR	^{1}H NMR (400 MHz, $CDCl_3$) δ 3.82 – 3.74 (m, 1H), 3.53 – 3.35 (m, 2H), 3.15 (s, 3H), 2.82 – 2.63 (m, 2H), 2.09 (s, 3H).
^{13}C NMR	^{13}C NMR (101 MHz, $CDCl_3$) δ 172.3, 118.3, 115.8, 49.4, 38.2, 27.2, 21.8, 18.9.
HR-MS (EI)	$(M)^{+\cdot}$: calc. 165.0897, found 165.0896

2-(tetrahydrothiophen-2-yl)succinonitrile (20c)

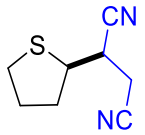

20c
1:1 mixture of diasteromers

Yield	96% (combined yield of both diastereomers, 64 mg, 0.38 mmol), yellowish oil
^{1}H NMR	isomer #1 (less polar, eluted first from the column) ^{1}H NMR (400 MHz, $CDCl_3$) δ 3.70 – 3.49 (m, 1H), 3.02 – 2.74 (m, 5H), 2.39 – 2.22 (m, 1H), 2.15 – 1.95 (m, 3H). isomer #2 ^{1}H NMR (400 MHz, $CDCl_3$) δ 3.76 – 3.63 (m, 1H), 3.31 – 3.20 (m, 1H), 3.09 – 2.90 (m, 2H), 2.90 – 2.69 (m, 2H), 2.38 – 2.24 (m, 2H), 2.09 – 1.92 (m, 1H), 1.92 – 1.77 (m, 1H).
^{13}C NMR	isomer #1 ^{13}C NMR (101 MHz, $CDCl_3$) δ 117.6, 115.4, 48.8, 35.7, 35.3, 33.2, 30.1, 20.8. isomer #2 ^{13}C NMR (101 MHz, $CDCl_3$) δ 117.5, 115.5, 48.4, 35.9, 35.2, 33.3, 30.9, 20.8.
HR-MS (EI)	$(M)^{+\cdot}$: calc. 166.0559, found 16.0561

4.7.7 Copies of NMR spectra

Dear reader, for the copies of the NMR spectra click on the URL below to open the full supporting information on the publisher's website (open access).

https://pubs.acs.org/doi/suppl/10.1021/acscatal.2c05631/suppl_file/cs2c05631_si_001.pdf

4.7.8 Notes and references

1. (a) Abderrazak, Y.; Bhattacharyya, A.; Reiser, O., Visible-Light-Induced Homolysis of Earth-Abundant Metal-Substrate Complexes: A Complementary Activation Strategy in Photoredox Catalysis. *Angew. Chem. Int. Ed.* **2021,** *60* (39), 21100-21115; (b) Li, C.; Kong, X. Y.; Tan, Z. H.; Yang, C. T.; Soo, H. S., Emergence of ligand-to-metal charge transfer in homogeneous photocatalysis and photosensitization. *Chem. phys. rev.* **2022,** *3* (2), 021303; (c) Juliá, F., Ligand-to-Metal Charge Transfer (LMCT) Photochemistry at 3d-Metal Complexes: An Emerging Tool for Sustainable Organic Synthesis. *ChemCatChem* **2022,** *n/a* (n/a), e202200916.

2. Vogler, A.; Kunkely, H., Charge Transfer Excitation of Coordination Compounds. Generation of Reactive Intermediates. In *Photosensitization and Photocatalysis Using Inorganic and Organometallic Compounds,* Kalyanasundaram, K.; Grätzel, M., Eds. Springer Netherlands: Dordrecht, 1993; pp 71-111.

3. (a) Vogler, A.; Nikol, H., Photochemistry and photophysics of coordination compounds of the main group metals. *Pure Appl. Chem.* **1992,** *64* (9), 1311-1317; (b) Vogler, A.; Paukner, A.; Kunkely, H., Photochemistry of coordination compounds of the main group metals. *Coord. Chem. Rev.* **1990,** *97*, 285-297; (c) Sheldon, R. A.; Kochi, J. K., Photochemical and thermal reduction of cerium(IV) carboxylates. Formation and oxidation of alkyl radicals. *J. Am. Chem. Soc.* **1968,** *90* (24), 6688-6698; (d) Inoue, H.; Tamaki, K.; Komakine, N.; Imoto, E., The Photochemical Reaction of Ethylene Glycol with Ferric Chloride-Pyridine Complex. *Bull. Chem. Soc. Jpn.* **1967,** *40* (4), 875-880; (e) Bacha, J. D.; Kochi, J. K., Oxidation of alkyl radicals from decarboxylation of acids by lead(IV) and copper(II). *J. Org. Chem.* **1968,** *33* (1), 83-93.

4. (a) Hu, A.; Guo, J.-J.; Pan, H.; Zuo, Z., Selective functionalization of methane, ethane, and higher alkanes by cerium photocatalysis. *Science* **2018,** *361* (6403), 668-672; (b) An, Q.; Wang, Z.; Chen, Y.; Wang, X.; Zhang, K.; Pan, H.; Liu, W.; Zuo, Z., Cerium-Catalyzed C–H Functionalizations of Alkanes Utilizing Alcohols as Hydrogen Atom Transfer Agents. *J. Am. Chem. Soc.* **2020,** *142* (13), 6216-6226.

5. Yatham, V. R.; Bellotti, P.; König, B., Decarboxylative hydrazination of unactivated carboxylic acids by cerium photocatalysis. *Chem. Commun.* **2019,** *55* (24), 3489-3492.

6. Treacy, S. M.; Rovis, T., Copper Catalyzed C(sp^3)–H Bond Alkylation via Photoinduced Ligand-to-Metal Charge Transfer. *J. Am. Chem. Soc.* **2021,** *143* (7), 2729-2735.

7. (a) Dai, Z.-Y.; Zhang, S.-Q.; Hong, X.; Wang, P.-S.; Gong, L.-Z., A practical $FeCl_3$/HCl photocatalyst for versatile aliphatic C–H functionalization. *Chem Cat.* **2022,** *2* (5), 1211-1222; (b) Kang, Y. C.; Treacy, S. M.; Rovis, T., Iron-Catalyzed Photoinduced LMCT: A 1° C–H Abstraction Enables Skeletal Rearrangements and C(sp3)–H Alkylation. *ACS Catal.* **2021,** *11* (12), 7442-7449.

8. Chen, Y.; Wang, X.; He, X.; An, Q.; Zuo, Z., Photocatalytic Dehydroxymethylative Arylation by Synergistic Cerium and Nickel Catalysis. *J. Am. Chem. Soc.* **2021,** *143* (13), 4896-4902.

9. (a) Xu, P.; López-Rojas, P.; Ritter, T., Radical Decarboxylative Carbometalation of Benzoic Acids: A Solution to Aromatic Decarboxylative Fluorination. *J. Am. Chem. Soc.* **2021,** *143* (14), 5349-5354; (b) Chen, T. Q.; Pedersen, P. S.; Dow, N. W.; Fayad, R.; Hauke, C. E.; Rosko, M. C.; Danilov, E. O.; Blakemore, D. C.; Dechert-Schmitt, A.-M.; Knauber, T.; Castellano, F. N.; MacMillan, D. W. C., A Unified Approach to Decarboxylative Halogenation of (Hetero)aryl Carboxylic Acids. *J. Am. Chem. Soc.* **2022,** *144* (18), 8296-8305.

10. Li, Q. Y.; Gockel, S. N.; Lutovsky, G. A.; DeGlopper, K. S.; Baldwin, N. J.; Bundesmann, M. W.; Tucker, J. W.; Bagley, S. W.; Yoon, T. P., Decarboxylative cross-nucleophile coupling via ligand-to-metal charge transfer photoexcitation of Cu(ii) carboxylates. *Nat. Chem.* **2022,** *14* (1), 94-99.

11. Kariofillis, S. K.; Doyle, A. G., Synthetic and Mechanistic Implications of Chlorine Photoelimination in Nickel/Photoredox C(sp3)–H Cross-Coupling. *Acc. Chem. Res.* **2021,** *54* (4), 988-1000.

12. (a) Reichle, A.; Sterzel, H.; Kreitmeier, P.; Fayad, R.; Castellano, F. N.; Rehbein, J.; Reiser, O., Copper(ii)-photocatalyzed decarboxylative oxygenation of carboxylic acids. *Chem. Commun.* **2022,** *58* (28), 4456-4459; (b) Wang, Y.-H.; Yang, Q.; Walsh, P. J.; Schelter, E. J., Light-mediated aerobic oxidation of C(sp3)–H bonds by a Ce(iv) hexachloride complex. *Org. Chem. Front.* **2022,** *9* (10), 2612-2620.

13. Schwarz, J.; König, B., Visible-light mediated C–C bond cleavage of 1,2-diols to carbonyls by cerium-photocatalysis. *Chem. Commun.* **2019,** *55* (4), 486-488.

14. (a) Wadekar, K.; Aswale, S.; Yatham, V. R., Cerium photocatalyzed dehydrogenative lactonization of 2-arylbenzoic acids. *Org. Biomol. Chem.* **2020,** *18* (5), 983-987; (b) Xia, S.; Hu, K.; Lei, C.; Jin, J., Intramolecular Aromatic C–H Acyloxylation Enabled by Iron Photocatalysis. *Org. Lett.* **2020,** *22* (4), 1385-1389; The same intermediate can also be obtained by outersphere SET as described in the following works. However, such mechanism is very unlikely when using single metal chloride salts. (c) Luo, Z.; Gao, Z.-H.; Song, Z.-Y.; Han, Y.-F.; Ye, S., Visible light mediated oxidative lactonization of 2-methyl-1,1′-biaryls for the synthesis of benzocoumarins. *Org. Biomol. Chem.* **2019,** *17* (17), 4212-4215; (d) Ramirez, N. P.; Bosque, I.; Gonzalez-Gomez, J. C., Photocatalytic Dehydrogenative Lactonization of 2-Arylbenzoic Acids. *Org. Lett.* **2015,** *17* (18), 4550-4553.

15. (a) Hwang, S. J.; Anderson, B. L.; Powers, D. C.; Maher, A. G.; Hadt, R. G.; Nocera, D. G., Halogen Photoelimination from Monomeric Nickel(III) Complexes Enabled by the Secondary Coordination Sphere. *Organometallics* **2015,** *34* (19), 4766-4774; (b) Weit, S. K.; Kutal, C., Contrasting reactivities of ligand-to-metal charge transfer excited states in ammine and methylamine complexes of cobalt(III). *Inorg. Chem.* **1990,** *29* (8), 1455-1456.

16. (a) Oldenburg, K.; Vogler, A., Electronic Spectra and Photochemistry of Tin(II), Lead(II), Antimony(III), and Bismuth(III) Bromide Complexes in Solution. *Z. Naturforsch.* **1993,** *48b,* 1519-1523; (b) Oldenburg, K.; Vogler, A.; Mikó, I.; Horváth, O., Photoredox decomposition of tin(II), lead(II), antimony(III) and bismuth(III) iodide complexes in solution. *Inorganica Chim. Acta* **1996,** *248* (1), 107-110; (c) Oldenburg, K.; Vogler, A., Photoredox chemistry of bismuth trichloride in benzene. *J. Organomet. Chem.* **1996,** *515* (1), 245-248.

17. (a) Choi, E. H.; Ahn, D.-S.; Park, S.; Kim, C.; Ahn, C. W.; Kim, S.; Choi, M.; Yang, C.; Kim, T. W.; Ki, H.; Choi, J.; Pedersen, M. N.; Wulff, M.; Kim, J.; Ihee, H., Structural Dynamics of Bismuth Triiodide in Solution Triggered by Photoinduced Ligand-to-Metal Charge Transfer. *J. Phys. Chem. Lett.* **2019,** *10* (6), 1279-1285; (b) Maurer, A. B.; Hu, K.; Meyer, G. J., Light Excitation of a Bismuth Iodide Complex Initiates I–I Bond Formation Reactions of Relevance to Solar Energy Conversion. *J. Am. Chem. Soc.* **2017,** *139* (24), 8066-8069; (c) Maurer, L. A.; Pearce, O. M.; Maharaj, F. D. R.; Brown, N. L.; Amador, C. K.; Damrauer, N. H.; Marshak, M. P., Open for Bismuth: Main Group Metal-to-Ligand Charge Transfer. *Inorg. Chem.* **2021,** *60* (14), 10137-10146; (d) Mason, W. R., Electronic Absorption and MCD Spectra for BiX63-, X = Cl-, Br-, and I-, in Acetonitrile Solution: Metal-Centered vs Ligand-to-Metal Charge-Transfer Assignments. *Inorg. Chem.* **1999,** *38* (11), 2742-2745; (e) Warren, S. C.; Jackson, A. C.; Cater-Cyker, Z. D.; DiSalvo, F. J.; Wiesner, U., Nanoparticle Synthesis via the Photochemical Polythiol Process. *J. Am. Chem. Soc.* **2007,** *129* (33), 10072-10073.

18. (a) Marwitz, A. C.; Nicholas, A. D.; Breuer, L. M.; Bertke, J. A.; Knope, K. E., Harnessing Bismuth Coordination Chemistry to Achieve Bright, Long-Lived Organic Phosphorescence. *Inorg. Chem.* **2021,** *60* (21), 16840-16851; (b) Ayscue, R. L., III; Vallet, V.; Bertke, J. A.; Réal, F.; Knope, K. E., Structure–Property Relationships in Photoluminescent Bismuth Halide Organic Hybrid Materials. *Inorg. Chem.* **2021,** *60* (13), 9727-9744.

19. (a) Lichtenberg, C.; Pan, F.; Spaniol, T. P.; Englert, U.; Okuda, J., The Bis(allyl)bismuth Cation: A Reagent for Direct Allyl Transfer by Lewis Acid Activation and Controlled Radical Polymerization. *Angew. Chem. Int. Ed.* **2012,** *51* (52), 13011-13015; (b) Yamago, S.; Kayahara, E.; Kotani, M.; Ray, B.; Kwak, Y.; Goto, A.; Fukuda, T.,

Highly Controlled Living Radical Polymerization through Dual Activation of Organobismuthines. *Angew. Chem. Int. Ed.* **2007,** *46* (8), 1304-1306; (c) Kayahara, E.; Yamago, S., Development of an Arylthiobismuthine Cocatalyst in Organobismuthine-Mediated Living Radical Polymerization: Applications for Synthesis of Ultrahigh Molecular Weight Polystyrenes and Polyacrylates. *J. Am. Chem. Soc.* **2009,** *131* (7), 2508-2513.

20. (a) Schwamm, R. J.; Lein, M.; Coles, M. P.; Fitchett, C. M., Catalytic oxidative coupling promoted by bismuth TEMPOxide complexes. *Chem. Commun.* **2018,** *54* (8), 916-919; (b) Ramler, J.; Krummenacher, I.; Lichtenberg, C., Well-Defined, Molecular Bismuth Compounds: Catalysts in Photochemically Induced Radical Dehydrocoupling Reactions. *Chem. Eur. J.* **2020,** *26* (64), 14551-14555; (c) Ramler, J.; Schwarzmann, J.; Stoy, A.; Lichtenberg, C., Two Faces of the Bi–O Bond: Photochemically and Thermally Induced Dehydrocoupling for Si–O Bond Formation. *Eur. J. Inorg. Chem.* **2022,** *2022* (7), e202100934.

21. Ramler, J.; Krummenacher, I.; Lichtenberg, C., Bismuth Compounds in Radical Catalysis: Transition Metal Bismuthanes Facilitate Thermally Induced Cycloisomerizations. *Angew. Chem. Int. Ed.* **2019,** *58* (37), 12924-12929.

22. Schwamm, R. J.; Harmer, J. R.; Lein, M.; Fitchett, C. M.; Granville, S.; Coles, M. P., Isolation and Characterization of a Bismuth(II) Radical. *Angew. Chem. Int. Ed.* **2015,** *54* (36), 10630-10633.

23. (a) Beckwith, A. L. J.; Bowry, V. W.; Ingold, K. U., Kinetics of nitroxide radical trapping. 1. Solvent effects. *J. Am. Chem. Soc.* **1992,** *114* (13), 4983-4992; (b) Ingold, K. U.; Pratt, D. A., Advances in Radical-Trapping Antioxidant Chemistry in the 21st Century: A Kinetics and Mechanisms Perspective. *Chem. Rev.* **2014,** *114* (18), 9022-9046; (c) Gentry, E. C.; Rono, L. J.; Hale, M. E.; Matsuura, R.; Knowles, R. R., Enantioselective Synthesis of Pyrroloindolines via Noncovalent Stabilization of Indole Radical Cations and Applications to the Synthesis of Alkaloid Natural Products. *J. Am. Chem. Soc.* **2018,** *140* (9), 3394-3402.

24. (a) Capaldo, L.; Ravelli, D., Hydrogen Atom Transfer (HAT): A Versatile Strategy for Substrate Activation in Photocatalyzed Organic Synthesis. *Eur. J. Org. Chem.* **2017,** *2017* (15), 2056-2071; (b) Capaldo, L.; Ravelli, D.; Fagnoni, M., Direct Photocatalyzed Hydrogen Atom Transfer (HAT) for Aliphatic C–H Bonds Elaboration. *Chem. Rev.* **2022,** *122* (2), 1875-1924.

25. Chinchole, A.; Henriquez, M. A.; Cortes-Arriagada, D.; Cabrera, A. R.; Reiser, O., Iron(III)-Light-Induced Homolysis: A Dual Photocatalytic Approach for the Hydroacylation of Alkenes Using Acyl Radicals via Direct HAT from Aldehydes. *ACS Catal.* **2022,** 13549-13554.

26. (a) Deng, H.-P.; Zhou, Q.; Wu, J., Microtubing-Reactor-Assisted Aliphatic C–H Functionalization with HCl as a Hydrogen-Atom-Transfer Catalyst Precursor in Conjunction with an Organic Photoredox Catalyst. *Angew. Chem. Int. Ed.* **2018,** *57* (39), 12661-12665; (b) Rohe, S.; Morris, A. O.; McCallum, T.; Barriault, L., Hydrogen Atom Transfer Reactions via Photoredox Catalyzed Chlorine Atom Generation. *Angew. Chem. Int. Ed.* **2018,** *57* (48), 15664-15669.

27. Jin, X.; Ye, L.; Xie, H.; Chen, G., Bismuth-rich bismuth oxyhalides for environmental and energy photocatalysis. *Coord. Chem. Rev.* **2017,** *349*, 84-101.

28. (a) Dai, Y.; Poidevin, C.; Ochoa-Hernández, C.; Auer, A. A.; Tüysüz, H., A Supported Bismuth Halide Perovskite Photocatalyst for Selective Aliphatic and Aromatic C–H Bond Activation. *Angew. Chem. Int. Ed.* **2020,** *59* (14), 5788-5796; (b) Riente, P.; Fianchini, M.; Pericàs, M. A.; Noël, T., Accelerating the Photocatalytic Atom Transfer Radical Addition Reaction Induced by Bi_2O_3 with Amines: Experiment and Computation. *ChemCatChem* **2022,** *14* (12), e202200319; (c) Riente, P.; Matas Adams, A.; Albero, J.; Palomares, E.; Pericàs, M. A., Light-Driven Organocatalysis Using Inexpensive, Nontoxic Bi2O3 as the Photocatalyst. *Angew. Chem. Int. Ed.* **2014,** *53* (36), 9613-9616.

29. Park, G.; Karimi, M.; Liu, W.-C.; Gabbaï, F. P., Green-Light-Driven Reductive Elimination of Chlorine from a Carbene-Xanthylium Gold(III) Complex. *Angew. Chem. Int. Ed.* **2022,** *61* (31), e202206265.

30. Gonzalez, M. I.; Gygi, D.; Qin, Y.; Zhu, Q.; Johnson, E. J.; Chen, Y.-S.; Nocera, D. G., Taming the Chlorine Radical: Enforcing Steric Control over Chlorine-Radical-Mediated C–H Activation. *J. Am. Chem. Soc.* **2022,** *144* (3), 1464-1472.

31. (a) Yang, X.; Reijerse, E. J.; Bhattacharyya, K.; Leutzsch, M.; Kochius, M.; Nöthling, N.; Busch, J.; Schnegg, A.; Auer, A. A.; Cornella, J., Radical Activation of N–H and O–H Bonds at Bismuth(II). *J. Am. Chem. Soc.* **2022**; (b) Hanna, T. A.; Rieger, A. L.; Rieger, P. H.; Wang, X., Evidence for an Unstable Bi(II) Radical from Bi–O Bond Homolysis. Implications in the Rate-Determining Step of the SOHIO Process. *Inorg. Chem.* **2002,** *41* (14), 3590-3592; (c) Hering-Junghans, C.; Schulz, A.; Thomas, M.; Villinger, A., Synthesis of mono-, di-, and triaminobismuthanes and observation of C–C coupling of aromatic systems with bismuth(iii) chloride. *Dalton Trans.* **2016,** *45* (14), 6053-6059.

32. For clarity we omitted the formation of $BiCl_4^-$ because it gets immediately reduced and disproportionated to $Bi^{(0)}$ and $BiCl_5^{2-}$ at the indicated reduction potential. See the description of the Figure S4.12 for more information.

33. The reduction of $Bi^{(III)}Cl_5^{2-}$ and oxidation of $Bi^{(0)}$ are complex processes. In both cases 3 electrons are transferred, but we could only observe a single peak in CV. This likely indicates that after the initial single electron transfer (SET), a fast series of disporportionations is triggered which results in $Bi^{(III)}$ and $Bi^{(0)}$. If the processes were stepwise, we should be able to observe more peaks in the CV. Similarly, dissociative LMCT is also a SET reduction which triggers the abovementioned disproportionations leading to the black precipitate - $Bi^{(0)}$.

34. M. Mato, D. S., M. Leutzsch, H. W. Moon, E. Reijerse, J. Cornella, *ChemRxiv* **2022**, DOI 10.26434/chemrxiv-2022-dqj5r. This content is a preprint and has not been peer-reviewed.

35. Megerle, U.; Lechner, R.; König, B.; Riedle, E., Laboratory apparatus for the accurate, facile and rapid determination of visible light photoreaction quantum yields. *Photoch. Photobio. Sci.* **2010,** *9* (10), 1400-1406.

36. Cucka, P.; Barrett, C. S., The crystal structure of Bi and of solid solutions of Pb, Sn, Sb and Te in Bi. *Acta Crystallogr.* **1962,** *15* (9), 865-872.

37. Ito, H.; Renaldo, A. F.; Johnson, R. D.; Ueda, M., ^{13}C chemical shift non-equivalence in methylene carbons of monosubstituted cyclohexanes. *Magnetic Resonance in Chemistry* **1989,** *27* (3), 273-276.

CHAPTER 5

5 Photocatalytic Oxidative Iodination of Electron-Rich Arenes

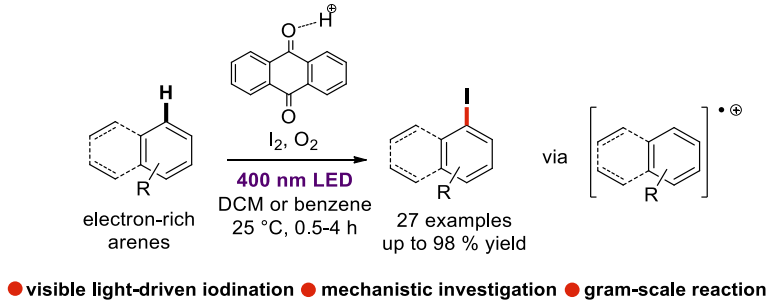

Abstract: A visible-light-mediated oxidative iodination of electron-rich arenes has been developed. 2.5 mol% of unsubstituted anthraquinone as photocatalyst were used in combination with elementary iodine, trifluoroacetic acid and oxygen as the terminal oxidant. The iodination proceeds upon irradiation in non- or weakly-electron donating solvents (DCM, DCE and benzene) wherein a spectral window in strongly coloured iodine solutions can be observed at around 400 nm. The method provides good to excellent yields (up to 98 %) and shows excellent regioselectivity and good functional group tolerance (triple bonds, ketone, ester, amide). Moreover, the photo-iodination was also upscaled to a 5 mmol scale (1.1 g). Mechanistic investigations by intermediate-trapping and competition experiments indicate a photocatalytic arene-oxidation and the subsequent reaction with iodine as a likely mechanistic pathway.

This chapter has been published. For reference see:
Narobe, R.; Düsel, S. J. S.; Iskra, J.; König, B., Photocatalytic Oxidative Iodination of Electron-Rich Arenes. Adv. Synth. Catal. 2019, 361 (17), 3998-4004. Reproduced with permission of John Wiley and Sons publishing house.

Author contribution
RN and SJSD found the reaction. RN performed the optimization, synthesized the scope, and carried out the mechanistic investigations. SJSD helped in the design of the experiments and data evaluation. RN wrote the manuscript with the input of all authors. JI and BK supervised the project and are the corresponding authors.

Most of the experiments describes in this chapter have been performed during Erasmus exchange at UR in the framework of master thesis. Some experimental data has already been presented in a different form in the master thesis. During the PhD additional experiments have been performed (UV-vis, upscale) and the results were summarized in their current form and published in a scientific journal.

5.1 Introduction

Aryl iodides are valuable building blocks in organic chemistry, as they are widely used as synthetic intermediates in various C–C couplings,[1] and for the preparation of hypervalent iodine reagents. Furthermore, they are also used as radiopharmaceuticals.[3] Consequently, the preparation of iodoarenes attracts attention within the synthetic community and the development of new methods for their synthesis is highly desired. Usually, direct C–H bond iodofunctionalization is achieved by employing either iodonium "I^+" donating reagents (*e.g.* Py_2IBF_4[4]) or "I^+" donating systems, wherein the reactive "I^+" species is formed *in situ* (*e.g.* $I_2/HCl/O_2$[5]). The most promising systems in terms of atom and waste economy use elementary iodine or iodide salts as an iodine atom source in combination with Lewis acid activation and environmentally benign oxidants, such as hydrogen peroxide or, even better, oxygen [6]. Much work has already been done in this research area,[6-7] but development of new methods, based on different approaches is an ongoing challenge as these may offer different selectivity and functional group tolerance. In contrast to the traditional polar reactivity manifolds, radical manifolds can be accessed by the use of visible-light photocatalysis.[8] Different light-driven halogenation reactions of arenes were reported before,[9] but to our knowledge no efficient direct visible-light promoted iodination has been reported so far.[10] Although catalytic use of molecular iodine[11] in visible-light photoredox chemistry is lately being exploited,[12] its use in combination with irradiation of photocatalysts is challenging and reports in this area are scarce.[13] The light absorption of iodine and its complexes often overlaps with the absorption bands of photocatalysts and photocatalytic reactions can therefore not be promoted effectively. Consequently, relatively high photocatalyst to iodine ratios are required and systems are limited to low concentrations.[13] In this work, we show how to circumvent iodine coloration issues and present an efficient photocatalytic system that utilizes a stoichiometric amount of iodine to iodinate electron-rich arenes.

5.2 Results and discussion

An iodination reaction is often accompanied by very coloured reaction solutions. Iodide salts (*e.g.* NEt_4I), a colourless iodine atom source, are redox active and get readily oxidized to iodine ($E_{ox} \approx 0.5$ V vs. SHE)[14], which forms coloured polyiodide ions (I_3^-) in the presence of residual iodide ions.[15] The build-up of polyiodide ions prevents any further photochemically promoted reactions, as these species strongly absorb light in an applicable range of the visible spectral region (Figure 5.1a). Another iodine atom source, molecular iodine (I_2), interacts with many commonly used solvents, causing blueshifting (400-510 nm) of the molecular iodine absorption band at 520 nm, or formation of a new charge-transfer (CT) complex band (240-350 nm).[16] The interaction of iodine with a solvent molecule reflects the solvent electron donating ability. In non-interacting solvents (DCM and DCE) or weakly interacting solvents (benzene), a spectral window at around 400 nm is observed (Figure 5.1b). The spectral window at the edge of the visible-light region can in principle be used to perform visible-light promoted reactions.

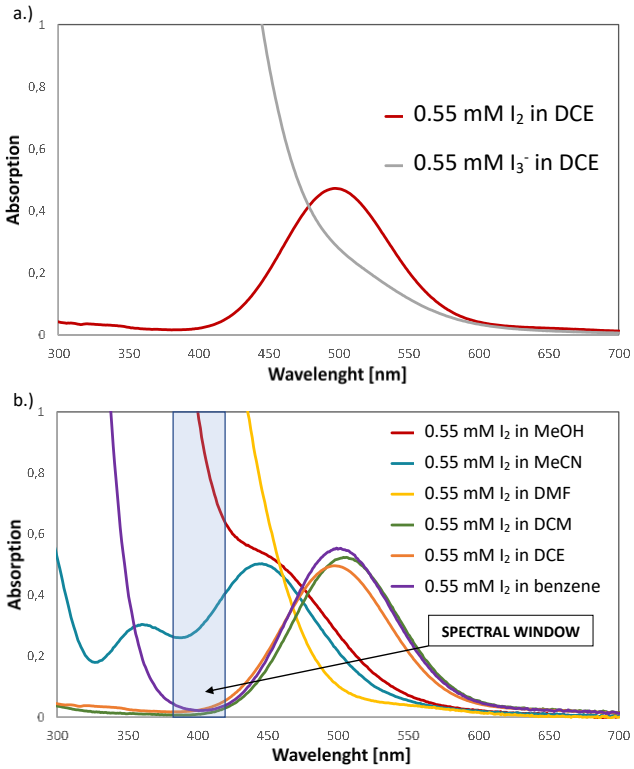

Figure 5.1: a.) UV-VIS spectra of iodine and NEt_4I_3 in DCE and b.) UV-VIS absorption of iodine solutions.

Based on these considerations, we attempted to develop a photoredox-catalyzed iodination system, via irradiation within the spectral window at around 400 nm (Table 5.1). We tested different photocatalysts with relatively high excited state oxidation potentials[17] that are capable of oxidizing anisole,[18] as well as an iodine atom source ($I^-/I_3^-/I_2$ to I_2/I^+).[14] Unsubstituted anthraquinone as photocatalyst provided the highest desired product yield among the tested metal-free dyes (entries 1-4). The oxidation potential of anthraquinone was further enhanced by the addition of TFA,[19] resulting in a drastic increase of the reaction rate and yield of **2** (entry 5). Solvent optimization (Table S5.1) at this stage revealed the highest reaction rate in benzene compared to other tested solvents (*vide infra* for mechanistic rationalization). Iodination in benzene proceeded with 96 % yield of **2** (Entry 6) in only 0.5 h irradiation time. Addition of TFA, can on the other hand, also enhance electrophilicity of iodine molecules by its polarization and thereby trigger electrophilic iodination.

However, negative control experiments with another highly oxidative photocatalyst TPP and without any photocatalyst (entries 7 and 8) hint that this ground state activation of iodine by acid is not an important contribution to the reactivity of the system. Further control experiments (entries 9 and 10) confirmed the essential role of the presence of light and photocatalyst for the reaction's progress. Reactions wherein iodide (in form of a soluble tetraalkyl ammonium salt) was used as iodine atom source did not yield any iodinated product (entries 11 and 12). Other photocatalysts only provided trace amounts of product.

Table 5.1. Screening of the reaction conditions.

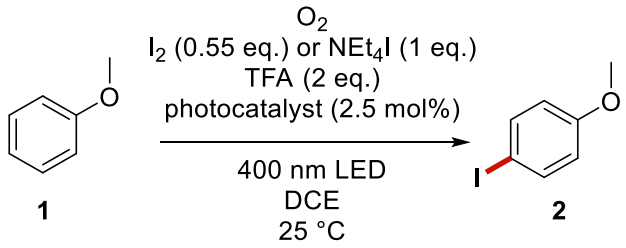

Entry	Iodine ource	PC (5 mol%)	TFA (eq.)	Reaction time	Yield of **2** (%)
1	I_2	RFTA	-	14 h	1
2	I_2	Acr^+-Mes	-	14 h	2
3	I_2	TPP	-	14 h	2
4	I_2	AQ	-	14 h	8
5	I_2	AQ	2.0	0.5 h	64
6[a]	I_2	AQ	2.0	0.5 h	96
7	I_2	TPP	2.0	2 h	3
8	I_2	-	2.0	2 h	2
9[b]	I_2	-	2.0	2 h	0
10[b]	I_2	AQ	2.0	2 h	0
11	NEt_4I	AQ	-	14 h	0
12	NEt_4I	AQ	2.0	14 h	0

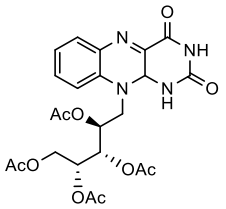
Riboflavin tetraacetate (**RFTA**)

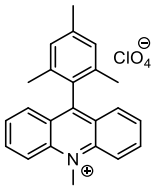
9-Mesityl-10-methylacridinium perchlorate (**Acr^+-Mes**)

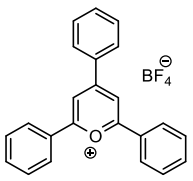
2,4,6-Triphenylpyrylium tetrafluoroborate (**TPP**)

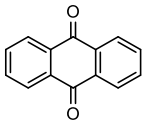
Anthraquinone (**AQ**)

General conditions: anisole (0.1 mmol), applied photocatalyst (2.5 mol%), trifluoroacetic acid (2 eq.) or without, indicated amount of iodine source in 1 mL of DCE. Irradiation with 400 nm LEDs under oxygen atmosphere. Given yields were determined by GC-FID analysis, using naphthalene as internal standard. [a)] Benzene was used as a solvent. [b)] No irradiation.

Next, the synthetic scope of the reaction was explored. First, simple electron-rich iodoarenes (**2-14**) were prepared in good to excellent yields. The method showed high para-regioselectivity for the iodination of anisole yielding less than 4% of the ortho isomer of **2**, presumably due to a non-thermal activation step. For all other compounds a single regioisomer was observed. No side reactions on the benzylic position were observed with methyl substituted arenes and despite the possible steric bulk, the method worked well for both the trimethylbenzene (**12**) and the tert-butyl substituted arene **13**. Notably, no addition of iodine to triple bonds or α-carbonyl position was observed for arenes **17** and **18**, respectively. Despite the acidic conditions, the acid sensitive ester functionality in substrate **19** remained untouched, as there are no strong nucleophiles present in the system. Iodination of the amide derivative required one additional equivalent of acid to break complexes between amide and iodine (see Figures S5.8 and 5.9) and only then proceeded well, affording compound **20** in 98% yield. This approach was applied further for the iodination of other nitrogen containing compounds: protected anilines (**21-23**), phenyl pyrazole (**24**) and biologically active pyrazole derivative phenazone (**25**). The method was also applicable to the iodination of benzothiophene yielding **26**.

Late-stage iodination of biologically active gemfibrozil showed that the sterically hindered carboxylic group (**27**) can be tolerated in the reaction conditions. Notably, we also iodofunctionalized a bioactive naproxen ester derivative that

possesses a chiral benzylic carbon atom. To our delight, we did not observe racemization and obtained this pharmacophore derivative **28** in 92% yield. The method gave lower yields for halogenated anisole derivatives **15** and **16**, as their oxidation potentials are probably on the limit of the anthraquinone excited state potential. Unfortunately, the method is not suitable for more electron-deficient arenes.

Scheme 5.1: Synthetic scope of the photocatalytic iodination.

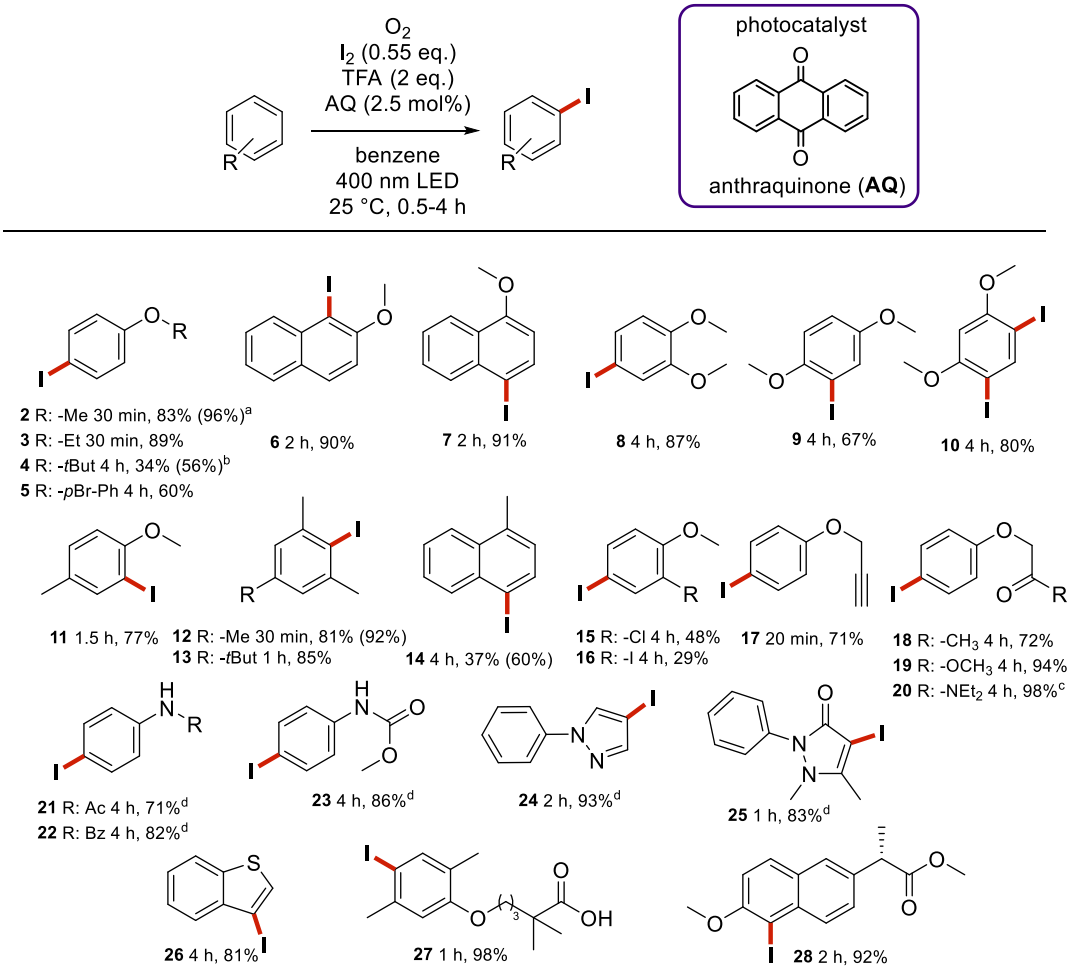

General conditions: 0.1 mmol of substrate, 2.5 mol% of AQ, 2 equiv. of TFA and 0.55 equiv. of I_2 were dissolved in 1 mL of benzene and irradiated at 400 nm for 0.5-4 h. Given yields are isolated. Yields in parenthesis are GC yields determined with naphthalene as an internal standard. [a] <4% of ortho isomer was observed by ^{1}H NMR [b] In parenthesis is NMR yield determined with hexamethylbenzene as an internal standard. [c] 3 equiv. of TFA were used. [d] 4 eq. of TFA were used and the reaction was run in DCE.

In the next step, we performed the reaction on a larger scale. DCM was used as solvent avoiding benzene on a larger scale (Scheme 5.2).

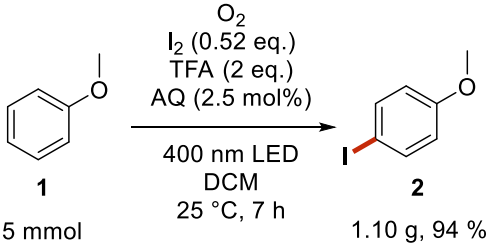

Scheme 5.2: Photocatalytic iodination in a gram scale reaction.

We started our mechanistic investigation of the developed system, by first comparing its performance to the performance of other similar system using classical oxidants. Different conditions using excess of nitromethane, hydrogen peroxide[20] or peracetic acid[21] instead of oxygen and photocatalysts were tested (Table 5). Classic oxidants gave only low yields (entries 2-4) under the selected conditions, while the photocatalytic conditions (entry 1) enabled complete conversion of the starting material. The experiments show an advantage of photocatalytic oxidation over the classic oxidants and suggest that the light-driven iodination may operate via a different mechanism. Additionally, thioxanthene-9-one, a non-redox sensitizer with a similar triplet energy as anthraquinone (265 kJ/mol and 261 kJ/mol, respectively)[22] was tested (entry 5). The latter experiment was performed to disprove singlet oxygen chemistry or other sensitization-driven reactions, as an important contribution to the reactivity of the system.

Table 5.2: Comparison of different oxidants.

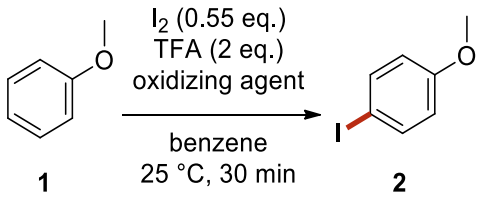

Entry	Oxidizing agent	Yield of **2** (%)
1	O_2, AQ (2.5 mol%), 400 nm LED	96
2	30 % H_2O_2 (5 eq.)	5
3	30-40 % AcOOH in AcOH (5 eq.)	7
4	CH_3NO_2 (5 eq.)	0
5	O_2, thioxanthene-9-one (2.5 mol %), 400 nm LED	0

General conditions: 0.1 mmol anisole, 2 eq. TFA, 0.55 eq. I_2 and 2.5 mol% of applied photocatalyst or 5 eq. of applied oxidizing agent in 1 ml benzene. When photocatalyst was used, the solution was irradiated at 400 nm under oxygen atmosphere. Otherwise, the solutions were stirred in darkness for 30 min. Given yields were determined by GC-FID using naphthalene as an internal standard.

To probe whether the photocatalyst oxidizes the arene in the system, a literature reported trapping reaction with pyrazole as nucleophile[23] was performed in the absence of iodine (Scheme 5.3).[24] The isolated coupled product **29** strongly indicates *in situ* formation of an electrophilic arene radical-cation.

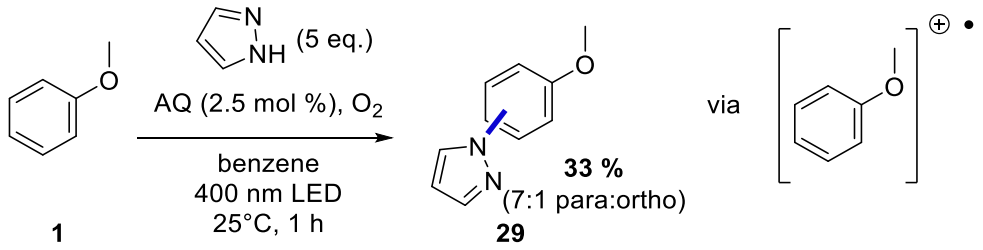

Scheme 5.3: Trapping of the arene radical-cation with pyrazole.

We conducted further mechanistic investigations to prove that the radical cation is an essential intermediate, through which the iodinated product is formed. Galli et al. addressed a similar question before[25] and developed a mechanistic probe that differentiates between a polar and a radical iodination mechanism (Scheme 5.4), based on intermolecular competition between 1,3-dimethoxybenzene (more nucleophilic, forms polar product) and 1,4-dimethoxybenzene (lower oxidation potential, forms radical product). The two compounds compete for the substoichiometric amount of iodinating reagent and the product distribution depends on the prevailing mechanism of the iodination. The obtained calculated ratio of the rate constants $k_{m\text{-OMe}}/k_{p\text{-OMe}}$ in our system is 65±6 (Table S5.3), while the literature

value for classic "I+" iodination is 1420±150[26] and for the only reported system wherein radical iodination was proposed is 210±20[25c]. The result indicates that the photocatalytic iodination might indeed proceed via iodination of the arene radical cation.

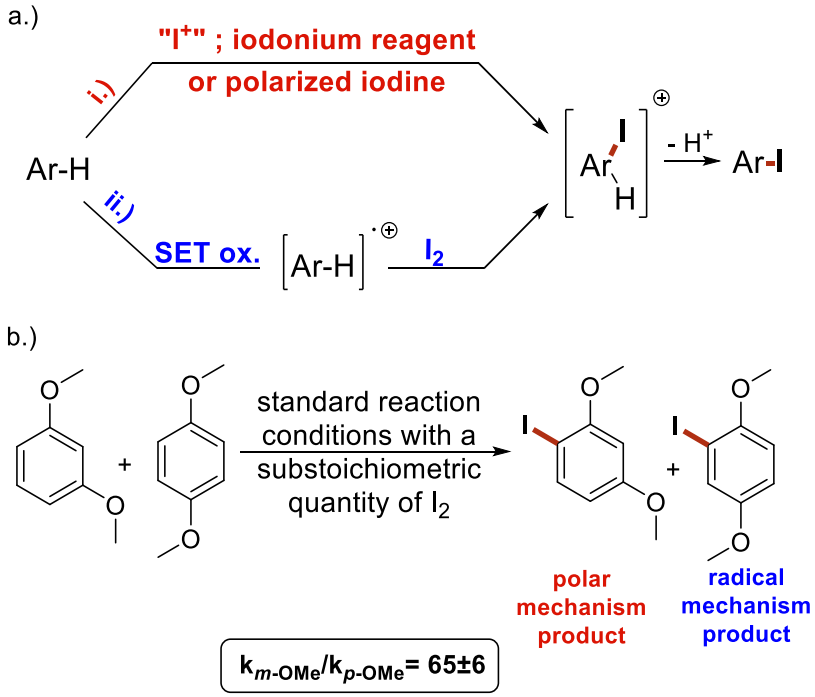

Scheme 5.4: a.) Possible polar and radical mechanism of iodination. b.) Competition experiment to distinguish between the two possible pathways.

The observation of faster reaction rates in benzene compared to other tested solvents, is also in line with the obtained mechanistic evidence, supporting a radical mechanism. Benzene's interaction with iodine is unique in a way, as it forms CT complexes, but does not cause strong blueshifting of the iodine band at 520 nm. This leaves a spectral window at 400 nm, despite the interaction with the solvent. In the iodine-benzene CT, benzene donates π-electrons to the iodine and thus makes the terminal iodine atom of the CT complex more nucleophilic (Scheme 5.5). Enhanced nucleophilicity of iodine is then reflected in a faster reaction with the electrophilic arene radical cations, leading to the iodinated product. Increased reactivity of iodine dissolved in interacting solvents (brown solutions) is a known phenomenon.[27]

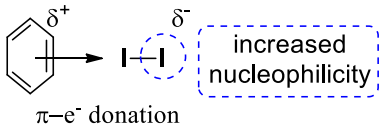

Scheme 5.5: Iodine-benzene CT complex.

Evidently, the main role of acid is not polarization of iodine but rather altering the anthraquinone photoredox properties. A protonation of anthraquinone leads to enhanced absorption at 400 nm and facilitates reduction of anthraquinone (see figures S5.2-5.6).

Based on the previously reported mechanism[19] and our mechanistic investigation, we propose a mechanism (Scheme 5.6) or our photocatalytic oxidative iodination system, wherein protonated AQ acts as a photocatalyst whose excited form oxidizes the arene. The formed arene radical cation subsequently abstracts iodine atom from iodine molecule and forms the iodinated product. The coupled by-product of the reaction is the iodine radical (I·), which can recombine with another I· to form I_2, leading to 100 % iodine economy of the reaction. The photocatalytic cycle is

concluded with the regeneration of anthraquinone by oxygen. It should be noted that a polar mechanism wherein "I⁺" species attacks an arene (Scheme 5.4a i) cannot be fully excluded especially with very electron-rich arenes. In that case AQ's role is oxidation of iodide to molecular iodine (I_2).

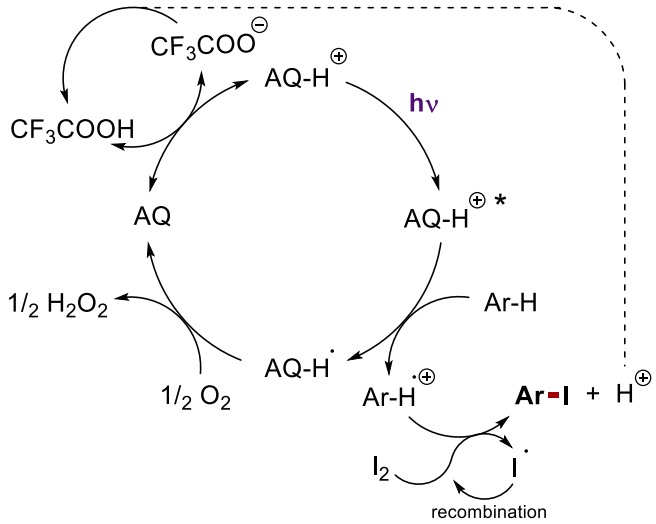

Scheme 5.6: Proposed mechanism of the photocatalytic oxidative iodination reaction.

5.3 Conclusion

In summary, we reported an efficient light-driven method for the iodination of electron-rich aromatic compounds, using iodine, trifluoroacetic acid, inexpensive, unsubstituted anthraquinone photocatalyst, and oxygen as a terminal oxidant. The reactions proceed best in benzene, but also in DCM. The method is fast and shows high regioselectivity and tolerance towards many functional groups. The developed procedure was used on a gram scale reaction, as well as for the late-stage functionalization of bioactive molecules. Mechanistic investigations suggest that the system operates via the oxidation of an arene and subsequent reaction with molecular iodine. The demonstrated approach of irradiation within the solvent dependent iodine spectral window might be important in the development of new light promoted iodination and iodine catalysed methods.

5.4 Experimental information

General information

Starting materials and reagents were purchased from commercial suppliers (Sigma Aldrich, Alfa Aesar, Acros or Fluka) and were used without further purification. Solvents were used as p.a. grade. Reactions were monitored by analytic thin layer chromatography (TLC) using Fluka silica gel F-254 plates. Visualization of the developed TLC chromatogram was performed using 254 NM UV light source. Organic solutions were concentrated using Buchi rotary evaporator. Flash column chromatography was performed either by hand column or on a Biotage® IsoleraTM Spektra. An industrial grade of solvents was used for automated flash column chromatography.

NMR spectroscopy

All NMR spectra were measured at room temperature using a Bruker Avance 300 (300 MHz for ^{1}H, 75 MHz for ^{13}C). All chemical shifts are reported in δ-scale as parts per million [ppm] (multiplicity, coupling constant J, number of protons), relative to the solvent residual peaks as the internal standard. The spectra were analyzed by first order and coupling constants J are given in Hertz [Hz].

Gas chromatography

GC measurements were performed on an Agilent Intuvo 9000 GC system coupled to a FID. The system was equipped with a capillary column (HP-5ms UI, length 30 m, diam. 0.25 mm, film 0.25 µm) and worked with H_2 as carrier gas. GC program: The initial temperature of the GC was set to 40 °C and kept for 1.5 minutes. Subsequently, the oven temperature was increased at a rate of 25 °C/min. until reaching 280 °C, which was maintained for 3 min. Then, temperature was further increased (42 °C/min) until reaching 300 °C and final temperature was hold for 5 minutes. Injector temperature was set to 280 °C and temperature of the detecting unit to 310 °C. A split ratio of 30:1 (split flow 42 mL/min) was applied and the column flow was set to 1.4 mL/min.

Mass spectrometry

All mass spectra were recorded on a Finnigan MAT 95, ThermoQuest Finnigan TSQ 7000, Finnigan MAT SSQ 710 A, Agilent Q-TOF 6540 UHD or Agilent 6224 Accurate Mass TOF instrument.

UV-Vis

Absorption spectra were measured on an Agilent Cary 100 UV/Vis spectrometer in a 0.10 mm thick 10 mm × 10 mm quartz cuvette at 25.0 °C.

Raman spectroscopy

Raman spectra were measured on a Raman Horiba Labram HR instrument in a 0.10 mm thick 10 mm × 10 mm quartz cuvette with He-Ne laser irradiation at 632.8 nm.

Cyclic voltammetry

CV measurements were performed with the three-electrode potentiostat galvanostat PGSTAT302N from Metrohm Autolab by using a glassy carbon working electrode, a platinum wire counter electrode, and a silver wire as a quasi-reference electrode, with ferrocene as internal standard.

Photochemical setup

Photochemical reactions were performed in sealed reaction vials, placed approximately 2 cm above a 400 nm LED array (each LED has 3W electrical power) and stirred under irradiation (Figure S5.1). The reaction temperature was controlled by a thermostated (25°C) metal cooling block. The reactor setup is a custom-made device (University of Regensburg workshop) and is not a commercially available product.

Figure S5.12: Photochemical reaction setup

5.4.1 Solvent screening

Table S5.18: Testing of different reaction solvents.

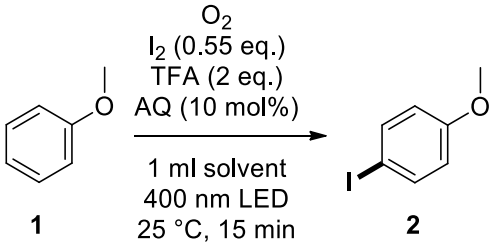

Entry	Solvent	Yield of **2** (%)
1	benzene	76
2	chlorobenzene	53
3	DCE	53
4	chloroform	52
5	DCM	49
6	α,α,α-trifluorotoluene	32
7	toluene	30
8	pentane	18

Standard conditions: anisole (0.1 mmol), anthraquinone (2.5 mol%), TFA (2 eq.), and I_2 (0.55 eq.) in 1 mL of indicated solvent irradiated with 400 nm LEDs under oxygen atmosphere for 15 minutes. Given yield were determined by GC-FID analysis, using naphthalene as internal standard

5.4.1 Mechanistic experiments

5.4.1.1 Arene cation radical trapping experiment

1-(4-methoxyphenyl)-1H-pyrazole and 1-(2-methoxyphenyl)-1H-pyrazole

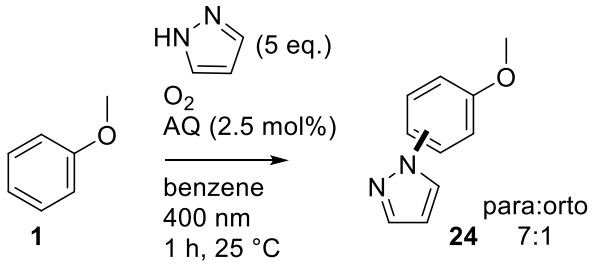

Protocol	Pyrazole (34 mg, 0.05 mmol, 5 eq.) was weighed into a 5 mL crimp vial. A stirring bar, methoxybenzene (10.9 µl, 0.1 mmol) and 1 ml of AQ stock solution (0.5 mg AQ, 0.0025 mmol AQ in 1 ml benzene) were added and the vial was sealed with a crimp cap with a septum. Then, an oxygen balloon was attached to the vial and the atmosphere inside the vial was purged three times with a 20 ml syringe. The reaction mixture was shaken briefly, and the vial was placed approximately 2 cm above a 400 nm LED and stirred under irradiation. The reaction was monitored by TLC After 1 h the reaction mixture turned slightly yellow/brown. It was poured into a 50 mL round bottom flask and diluted with DCM. Silica was added, the solvent was evaporated from the suspension and the residue was used as a dry load for column chromatography on a Biotage® IsoleraTM Spektra. Petroleum ether and ethyl acetate were used as a mobile phase.
Yield	6 mg (7:1 mixture of *para* and *ortho*), 0.034 mmol, 34 %, white crystals
^{1}H NMR	***Para*:** ^{1}H NMR (300 MHz, Chloroform-*d*) δ 7.83 (d, *J* = 2.3 Hz, 1H), 7.70 (d, *J* = 2.3 Hz, 1H), 7.59 (d, *J* = 9.0 Hz, 2H), 6.97 (d, *J* = 9.0 Hz, 2H), 6.48 – 6.40 (m, 1H), 3.85 (s, 3H). ***Ortho*:** ^{1}H NMR (300 MHz, Chloroform-*d*) δ 8.03 (d, *J* = 2.4 Hz, 1H), 7.72 (m, 2H), 7.30 (m, 1H), 7.06 (m, 2H), 6.44 (m, 1H), 3.89 (s, 3H).
^{13}C NMR	***Para*:** ^{13}C NMR (75 MHz, $CDCl_3$) δ 158.2, 140.6, 126.8, 120.9, 114.5, 107.2, 55.6. ***Ortho*:** too low concentration, not observed
HR-MS (EI)*	***Ortho*:** $(M)^{+\cdot}$: calc: 174.0788, found: 174.0787 ***Para*:** $(M)^{+\cdot}$: calc: 174.0788, found: 174.0789
MF	$C_{10}H_{10}N_2O$
MW	166.17 g/mol

* The sample was analysed in a GC-MS system and the determination is based on a separation of both isomers and their ratio (7/1).

Data is in agreement with a literature report.[23]

5.4.1.2 **Competition experiments**

The overall amount of both substrates was 0.1 mmol and the amount of iodine was 0.0082 mmol (substrates to iodine ratio was taken from literature[25c]). Concentrations of anthraquinone (0.5 mg, 0.0025 mmol) and TFA (15.4 µL, 0.2 mmol) were identical to the synthetic scope experiment.

Table S19: Preparation of stock solutions.

stock solution 1	stock solution 2
5.2 mg AQ in 10 ml of benzene	139.7 mg I_2 and 5.2 mg AQ in 10 ml of benzene

Stock solution 1 (2553 µL) and stock solution 2 (447 µL) were transferred into a 5 ml crimp vial. A stirring bar, 1,4-dimethoxybenzene (0.24 mmol, 33.1 mg) and 1,3-dimethoxybenzene (7.9 µL, 0.06 mmol) were added and the solution was stirred. Then, the solution was distributed into two more crimp vials (1 ml each). All three reaction crimp vials were sealed, an oxygen balloon was attached to each vial, and the atmosphere inside the vials was purged three times with a 20 ml syringe. The balloon was removed, the vials were shaken briefly, placed approximately 2 cm above 400 nm LED array (same as for preparative reactions) and stirred. Then, TFA (0.2 mmol, 15.4 µL) was added to each reaction vial and LEDs were switched on. After 3 minutes, the reactions were quenched by adding 0.5 ml sat. $NaHCO_3$ and 0.1 ml sat. $Na_2S_2O_3$. Then, a solution of internal standard (biphenyl ether in benzene) was added and the organic layer of each sample was analysed by GC-FID.

Table S5.20: Competition experiment between *m*- and *p*-dimethoxybenzene.

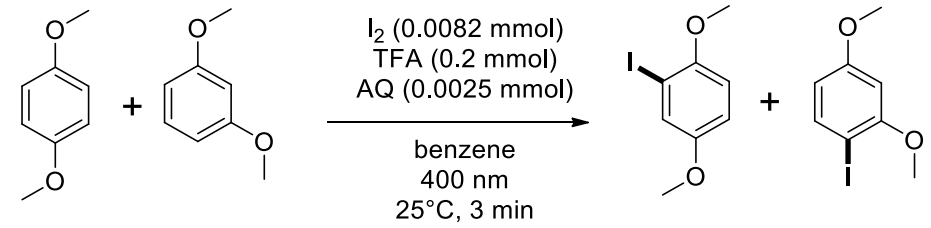

	Concentration after 3 minutes [a]			
Experiment run	I-*m*-OMe [mM]	I-*p*-OMe [mM]	Conversion[b]	$k_{m\text{-}OMe}/k_{p\text{-}OMe}$
1	12.4	1.2	83 %	63
2	13.8	1.3	92 %	71
3	12.7	1.3	85 %	62
				65±6%

[a] Concentrations were determined by using biphenyl ether as an internal standard.

[b] Conversion of starting materials is reported against a limiting reactant - iodine.

Calculation of the ratio of the iodination rate constants

Concentration of product were determined by using biphenyl ether as an internal standard. Concentrations of starting materials were calculated by subtracting the amount of iodinated product from initial starting material concentration.

$$\frac{k_{m\text{-}OMe}}{k_{p\text{-}OMe}} = \frac{\log\left(\frac{C_{m\text{-}OMe\ (0)}}{C_{m\text{-}OMe\ (3\ min)}}\right)}{\log\left(\frac{C_{p\text{-}OMe\ (0)}}{C_{p\text{-}OMe\ (3\ min)}}\right)} = \frac{\log\left(\frac{C_{m\text{-}OMe\ (0)}}{C_{m\text{-}OMe\ (0)} - C_{I\text{-}m\text{-}OMe\ (3\ min)}}\right)}{\log\left(\frac{C_{p\text{-}OMe\ (0)}}{C_{p\text{-}OMe\ (0)} - C_{I\text{-}p\text{-}OMe\ (3\ min)}}\right)}$$

$c_{m\text{-}OMe\ (0)}$ = initial concentration of *meta*-dimethoxybenzene
$c_{m\text{-}OMe\ (3min)}$ = concentration of *meta*-dimethoxybenzene after 3 min
$c_{I\text{-}m\text{-}OMe\ (3min)}$ = concentration of iodinated *meta*-dimethoxybenzene after 3 min

$c_{p\text{-}OMe\ (0)}$ = initial concentration of *para*-dimethoxybenzene
$c_{p\text{-}OMe\ (3min)}$ = concentration of *para*-dimethoxybenzene after 3 min
$c_{I\text{-}p\text{-}OMe\ (3min)}$ = concentration of iodinated *para*-dimethoxybenzene after 3 min

The competition experiments were tried also with a 1,3,5-trimethylbenzene and naphthalene mechanistic probe. This pair was not suitable for our iodination system as it led to formation of dimers of 1,3,5-trimethylbenzene.

5.4.1.3 **Protonation of anthraquinone; NMR, UV-vis and CV**

5.4.1.3.1 NMR

Saturated solution of anthraquinone in *d*6-benzene was prepared. Each time indicated amount of deuterated trifluoroacetic acid was added and NMR was measured.

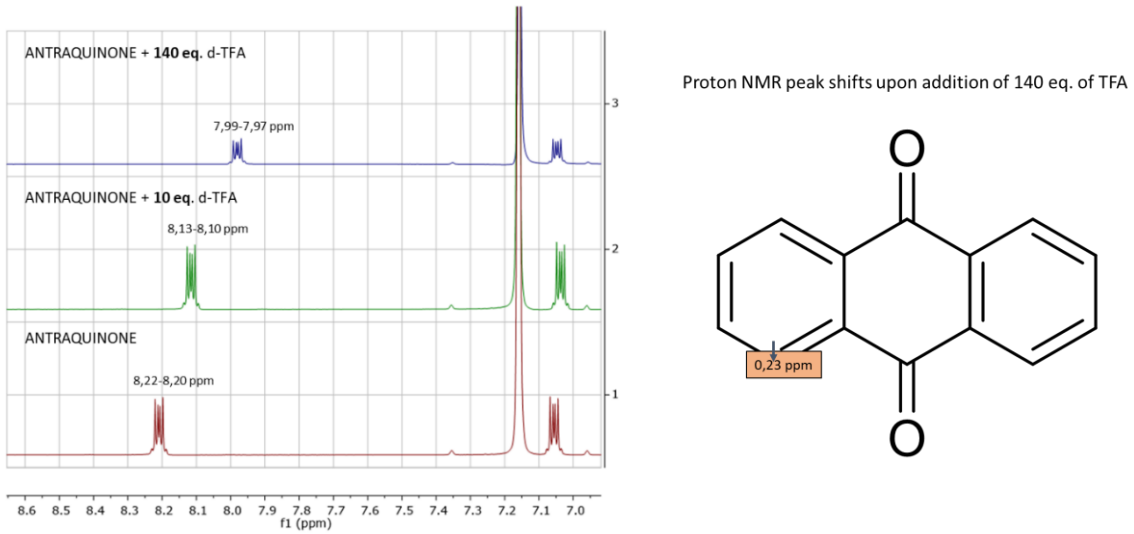

Figure S13: [1]H NMR spectrum upon addition of TFA.

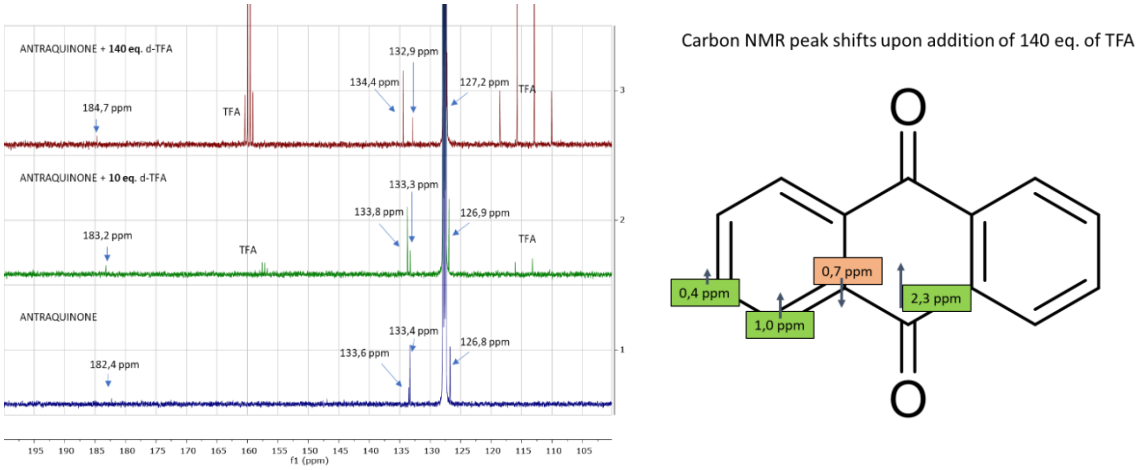

Figure S5.14: [13]C NMR spectrum upon addition of TFA.

The pattern of NMR shifts corresponds to the protonation of carbonyl group.

5.4.1.3.2 UV-vis

Lower concentration AQ: Trifluoroacetic acid was added to 2 ml of 200 µM AQ in benzene. Spectra were measured using a regular quartz cuvette with a 10 mm optical path.

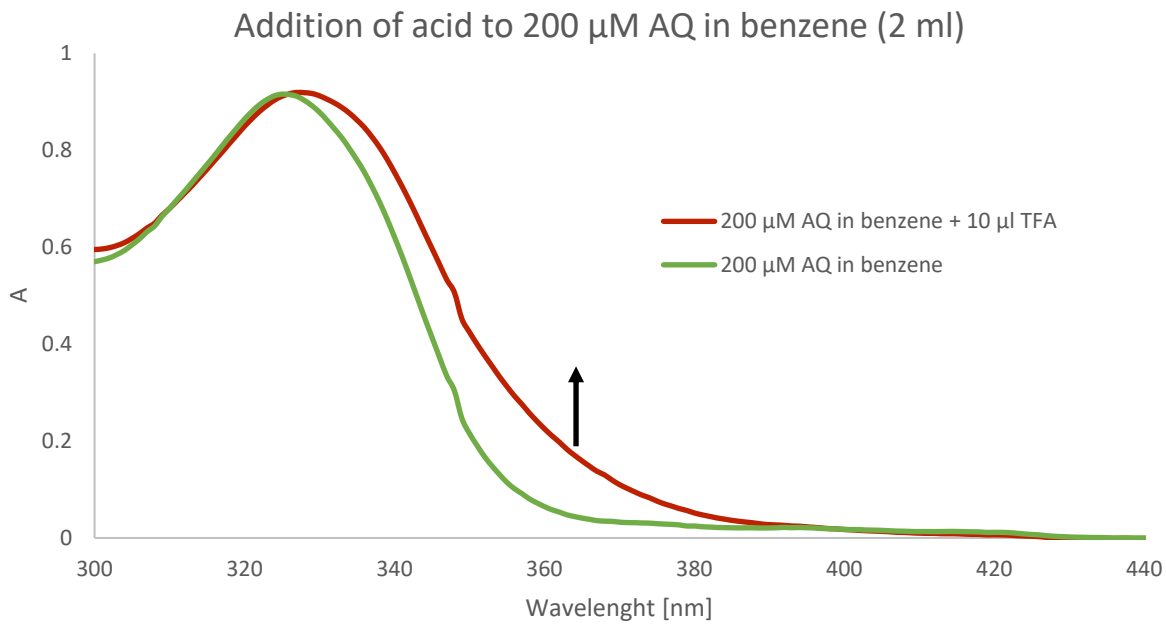

Figure S5.15: UV-vis spectrum of AQ upon addition of TFA.

Higher concentration AQ: Trifluoroacetic acid was added to 2 ml of 1250 µM AQ in benzene. Spectra were measured using a quartz cuvette with a 5 mm optical path.

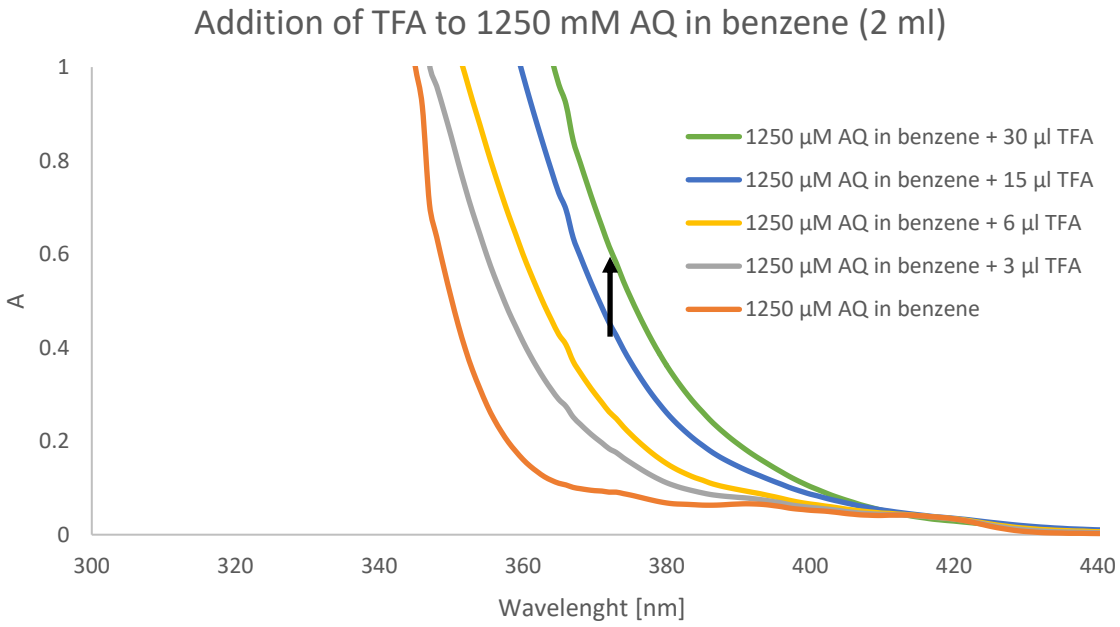

Figure S5.16: UV-vis spectrum of AQ upon addition of TFA.

5.4.1.3.3 Cyclovoltammetry data

Voltammograms were measured in DCE since we could not obtain any relevant data in benzene due to insolubility of commonly used supporting electrolyte (n-Bu_4NBF_4). The substitution of a solvent is justified as we also observed similar reaction rates in DCE and benzene. Values were determined against a ferrocene as an internal standard and then calculated against SCE. [3] [reference value for DCM]

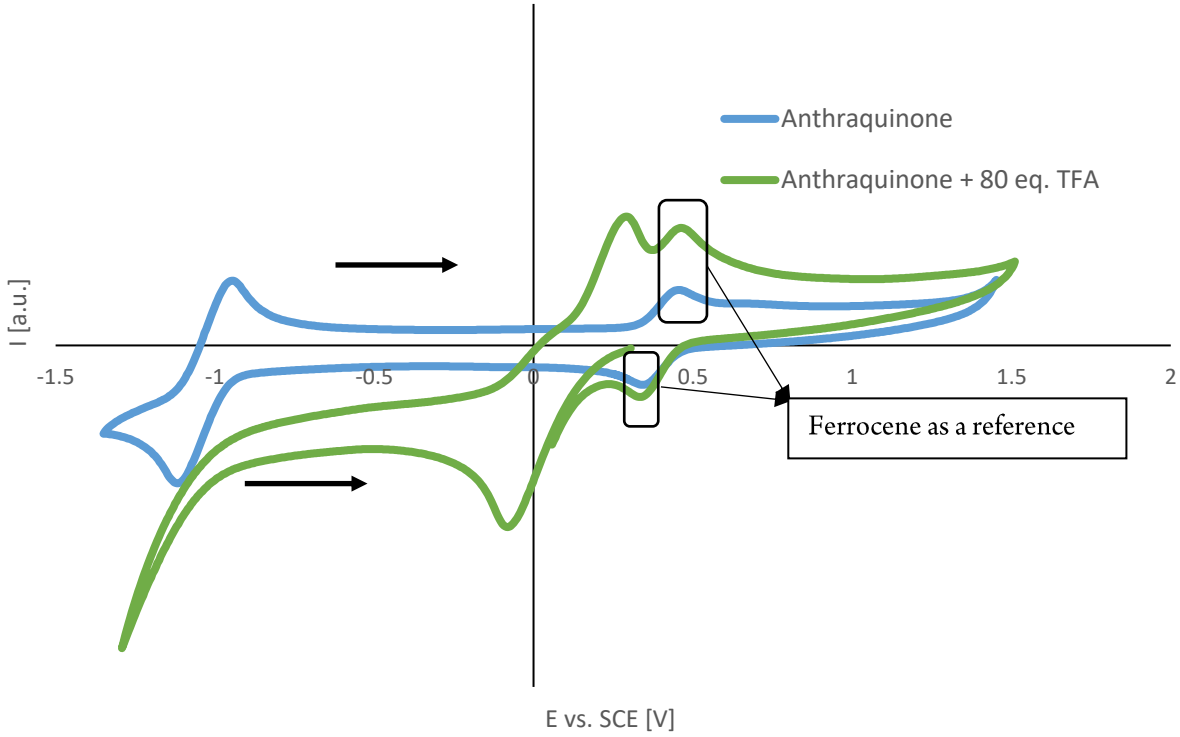

Figure S5.17: Cyclic voltammograms of anthraquinone with and without acid.

Upon the addition of acid, the peak for reduction of anthraquinone shifts by 1.0 V. The result indicates that reduction of anthraquinone is facilitated in the presence of acid.

5.4.1.4 Raman spectroscopic investigation of iodine solutions

To get more insight into the iodine species present in the reaction solution, we performed Raman spectroscopic investigation. First, we measured reference Raman spectra of benzene and solution of iodine in benzene and then compared the spectra to the spectra of iodine solutions with different additives. We did not observe any new signals in Raman spectra upon addition of AQ or TFA to the solution of iodine in benzene. The result indicates that combination of reactants does not promote formation of new iodine species thus implying that molecular iodine is the only iodine species in the solution.

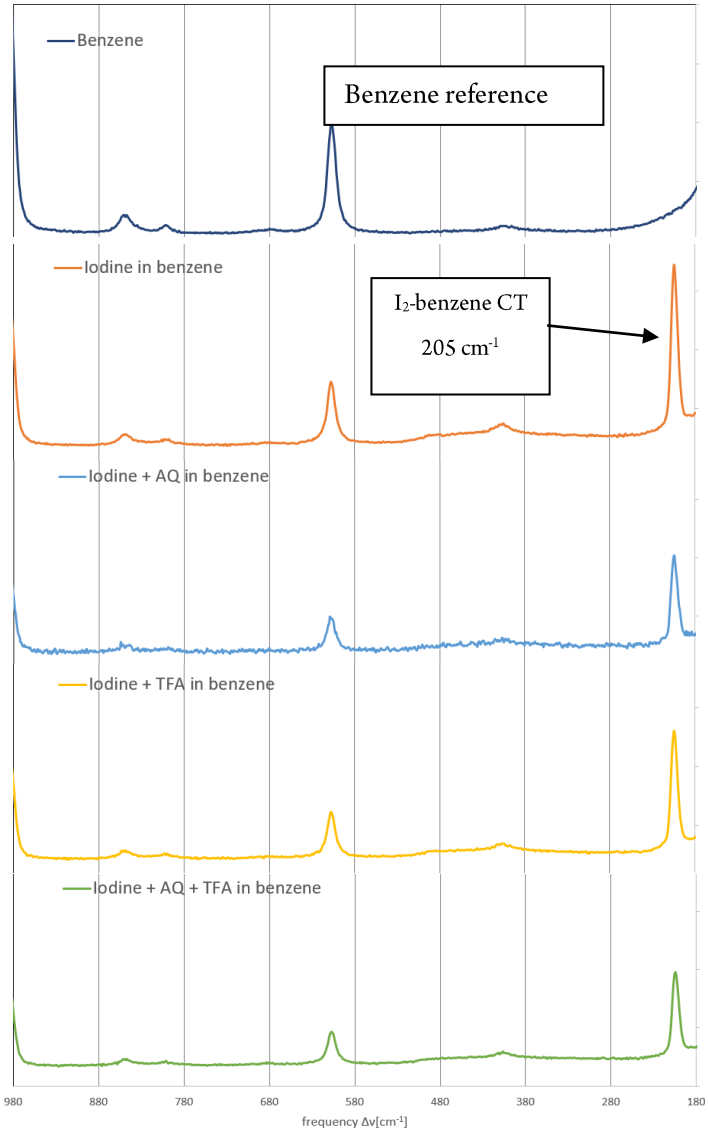

Figure S5.18: Raman spectra of iodine solutions in the presence of TFA and AQ.

Solutions were prepared by dissolving iodine (50.8 mg, 0.2 mmol), TFA (15.4µl, 0.2 mmol) or AQ (5.2 mg, 0.025 mmol) in 4 ml of benzene. The solutions were kept for 3 hours before the measurement.

5.4.1.5 Breaking of amide-iodine complexes with TFA

By adding amide (**20-SM**) to iodine solution, an absorption at 400 nm increases and at 500 nm decreases. This indicates the formation of a complex. The new band prevents efficient irradiation of AQ photocatalyst in the reaction mixture.

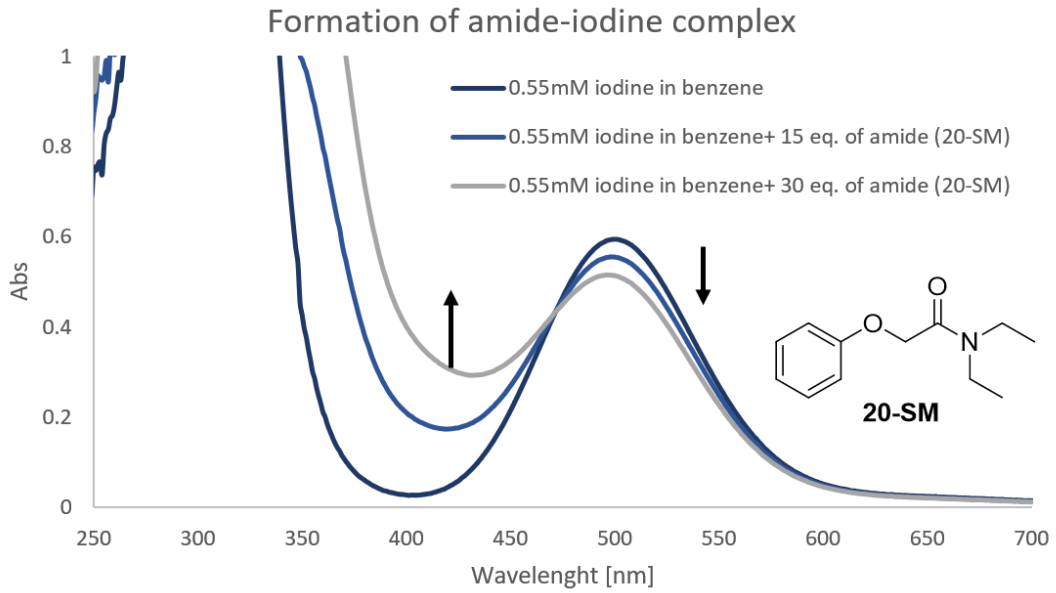

Figure S5.19: Formation of amide-iodine complex.

By adding TFA to the amide-iodine complex solution, the complex breaks and the spectral window for irradiation at 400 nm is regained. Equivalents of TFA are in respect to amide **20-SM**.

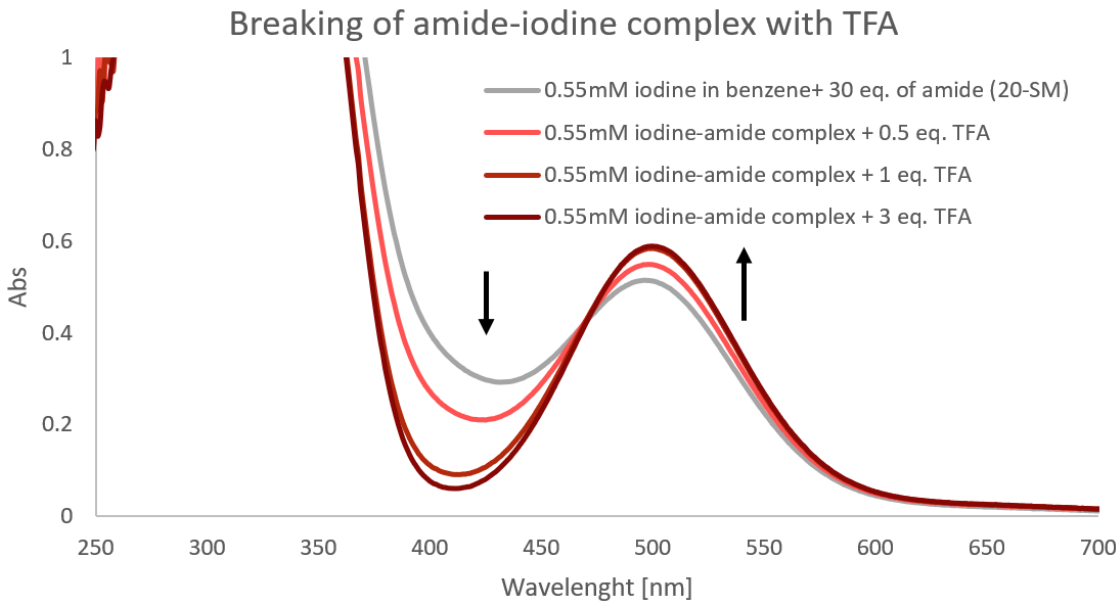

Figure S5.20: Breaking of amide-iodine complex with TFA.

5.4.1.6 **Mechanistic proposal**

Based on the conducted mechanistic study we propose the following mechanism (Scheme S5.7) as described in the manuscript.

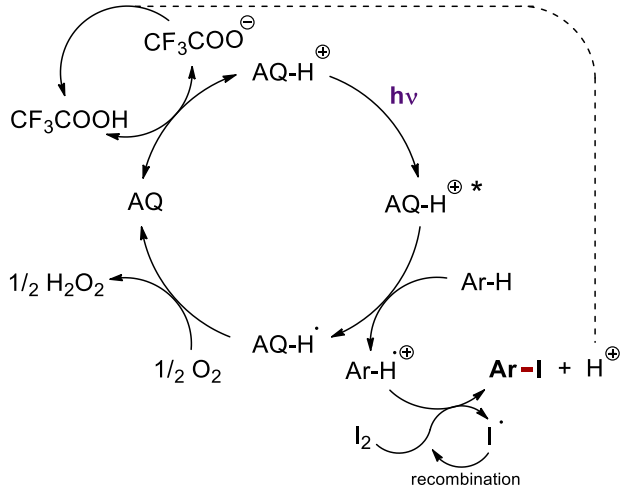

Scheme S5.7: Mechanistic proposal for the photocatalytic iodination.

In addition, we describe an alternative mechanism (Scheme S5.8). Trifluoroacetic acid in the system can also polarize molecular iodine (I_2) and thereby make it more electrophilic and prone to react with electron-rich arenes via classic electrophilic aromatic substitution. This ground state reaction does not seem to be an important contribution for iodination of anisole (Table 5.1 in the manuscript, entries 7-10), but still cannot be excluded from the mechanistic scenario especially for pyrazole derivatives owing to their high nucleophilicity and high oxidation potential. Products of the electrophilic aromatic substitution with iodine (I_2) are the corresponding iodoarene, proton and iodide (I^-) which reacts with residual iodine (I_2) to form triiodide ions (I_3^-). The triiodide ions (I_3^-) can be reoxidized back to iodine (I_2) directly by photocatalyst or by hydrogen peroxide which is formed in the photocatalytic cycle.

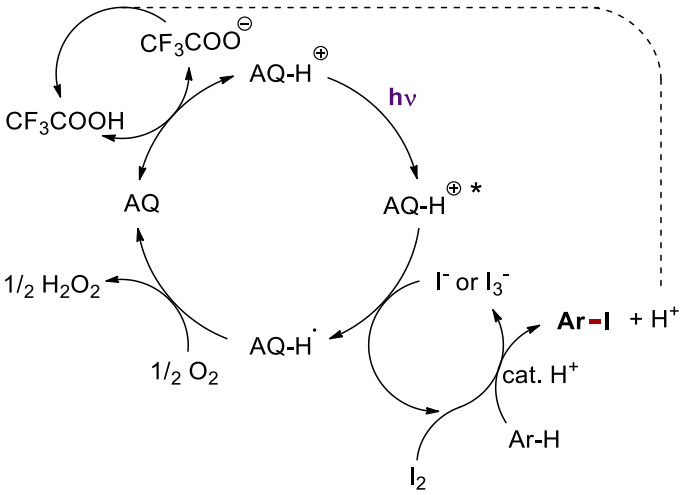

Scheme S5.8: Alternative mechanistic scenario.

5.4.2 Synthetic application of the photoredox iodination

5.4.2.1 Procedures for synthesis of substrates and products

5.4.2.1.1 Synthesis of starting materials

Naproxenmethylester[4] and *tert*-butoxybenzene[5] were synthesized according to the literature known methods and the measured NMR data was in agreement with the previously reported data.

5.4.2.1.2 Typical synthetic scope experiment

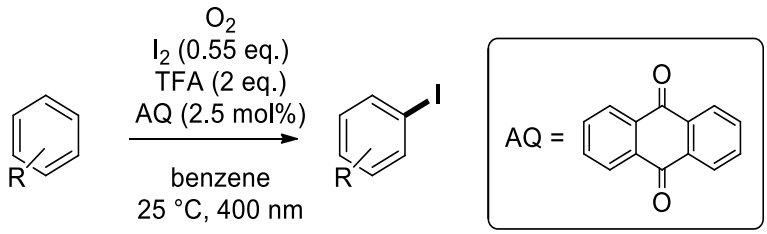

A substrate (0.1 mmol) was weighed into a 5 mL crimp vial. A stirring bar, 1 ml of stock solution (0.5 mg AQ (0.0025 mmol) and 14.0 mg iodine (0.055 mmol) in 1 ml benzene) and 15.4 µL of TFA (0.2 mmol) were added and the vial was sealed with a crimp cap with a septum. Then an oxygen balloon was attached to the vial and the atmosphere inside the vial was purged three times with a 20 ml syringe. The reaction mixture was shaken briefly, and the vial was placed approximately 2 cm above a 400 nm LED and stirred under irradiation at 25 °C. Reaction progress was followed with visual inspection (dark brown to pinky due to iodine consumption), TLC and GC-FID. After completion of the reaction, the reaction mixture was poured into a 50 mL round bottom flask and diluted with DCM. Silica was added, the solvent was evaporated from the suspension and the residue was used as dry load for column chromatography on a Biotage® IsoleraTM Spektra. Petroleum ether and ethyl acetate were used as mobile phase in all cases. A 10 g column was employed with silica gel of type 60 M (40-63 µm, 230-440 mesh) by Merck as a stationary phase. In some cases, a high vacuum pump was used for an additional purification step after column to remove the remaining starting material.

Nitrogen containing compounds (**21**-**25**) are not well tolerated with our standard conditions as they form coloured complexes with iodine or precipitate out from benzene due to protonation. We changed our standard conditions by adding more acid (4 eq.) to break the nitrogen-iodine complexes and by using more polar solvent (DCE) to prevent the precipitation of the formed salts.

Preparative reactions were done on 0.2 mmol scale for most substrates. Reactions were run in two parallel reaction vessels. The reaction mixtures were combined after the reaction step. Exceptionally, iodinated 1,3-dimethoxybenzene (**10**) and the two druglike molecules (gemfibrozil (**27**) and naproxen methyl ester (**28**)) were prepared on 0.1 mmol scale due to relatively high molecular mass of the desired product.

5.4.2.1.3 Large scale reaction

Gram-scale reactions were done in a classic glass tube photochemical reactor setup irradiated from the outside with 18 × 400 nm LEDs (each LED has 3 W electrical power) (Figure S5.21). The glass tube with reaction mixture and LED cooling block were thermostated at 25 °C. The reactor setup is a custom-made device (University of Regensburg workshop) and is not a commercially available product.

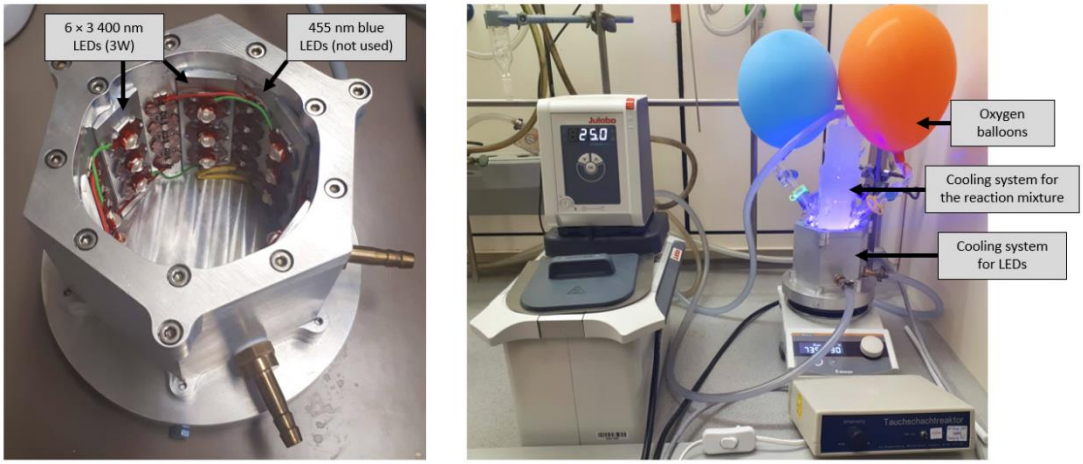

Figure S5.21: Large scale photochemical setup.

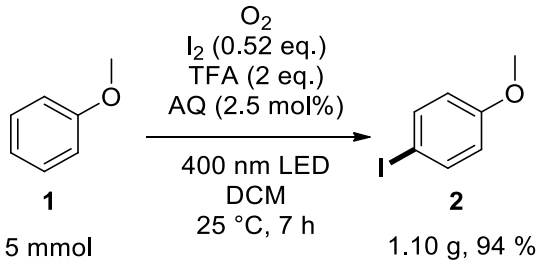

A stirring bar, anthraquinone (26 mg, 0.13 mmol), iodine (667 mg, 2.63 mmol) and anisole (543 µL, 5.00 mmol) were put into the reaction vessel, and dissolved in 50 mL DCM. An oxygen balloon was attached to the reaction vessel and the reaction mixture was purged with oxygen (≈1 L). Then trifluoroacetic acid (765 µL, 10.0 mmol) was added and the two fresh oxygen balloons were attached to the reaction vessel as shown in the Figure S5.21. The reaction mixture was stirred under irradiation for 7 hours at 25°C. The progress of the reaction was monitored by visual inspection (purple colour faints) and GC-FID. After completion of the reaction, the reaction mixture was transferred into the separatory funnel and washed with sat. $NaHCO_3$ (20 mL), sat. $Na_2S_2O_3$ (5 mL) and sat. NaCl (20 mL). The organic fraction was dried over Na_2SO_4 and then mixed with silica gel. The solvent was evaporated *in vacuo* and the obtained crude product (dry load) was purified by automated flash column chromatography using PE/EtOAc as a mobile phase. The pure product was obtained as a white crystalline solid ($m_{product}$= 1.101 g, yield=94 %).

5.4.2.2 Compounds characterization data

***1-Iodo-4-methoxybenzene* (2)**

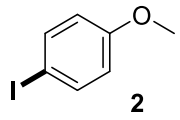

2

Reaction time	30 min
Yield	NMR yield: 96% Isolated yield: 39 mg, 0.167 mmol, 83%, white solid
^{1}H NMR	^{1}H NMR (300 MHz, Chloroform-*d*) δ 7.56 (d, *J* = 9.0 Hz, 2H), 6.68 (d, *J* = 9.0 Hz, 2H), 3.78 (s, 3H).
^{13}C NMR	^{13}C NMR (75 MHz, $CDCl_3$) δ 159.4, 138.2, 116.4, 82.7, 55.3.
HR-MS (EI)	$(M)^{+\cdot}$: calc.: 233.9536, found.: 233.9540

***1-Ethoxy-4-iodobenzene* (3)**

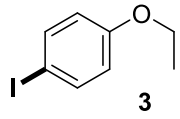

3

Reaction time	30 min
Yield	44 mg, 0.177 mmol, 89 %, white solid
^{1}H NMR	^{1}H NMR (300 MHz, Chloroform-*d*) δ 7.54 (d, *J* = 9.0 Hz, 2H), 6.67 (d, *J* = 9.0 Hz, 2H), 3.99 (q, *J* = 7.0 Hz, 2H), 1.40 (t, *J* = 7.0 Hz, 3H).
^{13}C NMR	^{13}C NMR (75 MHz, $CDCl_3$) δ 158.8, 138.2, 116.9, 82.5, 63.6, 14.7.
HR-MS (EI)	$(M)^{+\cdot}$: calc.: 247.9693, found 247.9698

***1-(tert-Butoxy)-4-iodobenzene* (4)**

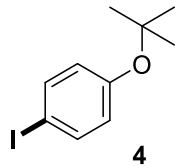

4

Reaction time	4 h
Yield	19 mg, 0.068 mmol, 34 %, colourless oil, NMR yield 56 %
^{1}H NMR	^{1}H NMR (300 MHz, Chloroform-*d*) δ 7.56 (d, *J* = 8.8 Hz, 2H), 6.76 (d, *J* = 8.8 Hz, 2H), 1.34 (s, 9H).
^{13}C NMR	^{13}C NMR (75 MHz, $CDCl_3$) δ 155.3, 137.9, 126.4, 86.8, 79.0, 28.8.
HR-MS (ESI)	$(M+H)^+$: calc.: 276.0011, found: 276.0000

The reaction mixture was first dried in a flow of nitrogen and then the iodinated product was separated from the dry residue by distillation under low vacuum. The method was chosen due to decomposition of the starting material and the product on silica gel, preventing silica gel chromatography for purification. Distillation on a such small scale did not allow the quantitative recovery of the material and therefore the isolated yield is lower.

***1-Bromo-4-(4-iodophenoxy)benzene* (5)**

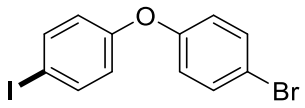

5

Reaction time	4 h
Yield	72 mg (inseparable mixture with 25 % of unconverted starting material), 0.144 mmol, 72 %, white crystalline product.
^{1}H NMR	^{1}H NMR (300 MHz, Chloroform-*d*) δ 7.63 (d, *J* = 8.9 Hz, 2H), 7.45 (d, *J* = 9.0 Hz, 2H), 6.88 (d, *J* = 9.0 Hz, 2H), 6.77 (d, *J* = 8.9 Hz, 2H).
^{13}C NMR	^{13}C NMR (75 MHz, $CDCl_3$) δ 156.9, 155.8, 138.8, 132.9, 121.0, 120.7, 116.3, 86.6.
HR-MS (ESI)	Calc: 373.8803, found:373.8783

***1-Iodo-2-methoxynaphthalene* (6)**

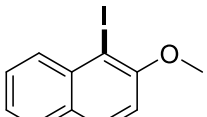

6

Reaction time	2 h
Yield	51 mg, 0.180 mmol, 90 %, white solid
^{1}H NMR	^{1}H NMR (300 MHz, Chloroform-*d*) δ 8.15 (dd, *J* = 8.5, 0.7 Hz, 1H), 7.84 (d, *J* = 8.9 Hz, 1H), 7.75 (dd, *J* = 8.1, 0.6 Hz, 1H), 7.55 (ddd, *J* = 8.5, 6.9, 0.6 Hz, 1H), 7.39 (ddd, *J* = 8.1, 6.9, 0.7 Hz, 1H), 7.22 (d, *J* = 8.9 Hz, 1H), 4.03 (s, 3H).
^{13}C NMR	^{13}C NMR (75 MHz, $CDCl_3$) δ 156.6, 135.6, 131.2, 130.4, 129.9, 128.2, 128.1, 124.4, 112.9, 87.7, 57.2.
HR-MS (EI)	$(M)^{+\cdot}$: calc.: 293.9693, found: 283.9691

***1-Iodo-4-methoxynaphthalene* (7)**

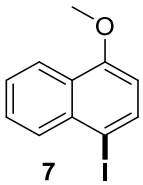

7

Reaction time	2 h
Yield	52 mg, 0.183 mmol, 91 %, pale yellow solid.
^{1}H NMR	^{1}H NMR (300 MHz, Chloroform-*d*) δ 8.24 (d, *J* = 7.3 Hz, 1H), 8.03 (d, *J* = 7.7 Hz, 1H), 7.95 (d, *J* = 8.2 Hz, 1H), 7.64 – 7.55 (m, 1H), 7.55 – 7.48 (m, 1H), 6.60 (d, *J* = 8.2 Hz, 1H), 3.99 (s, 3H).
^{13}C NMR	^{13}C NMR (75 MHz, $CDCl_3$) δ 156.3, 136.9, 134.7, 131.8, 128.2, 126.6, 126.0, 122.5, 105.6, 88.2, 55.7.
HR-MS (EI)	$(M)^{+\cdot}$: calc.: 283.9693, found: 283.9700

4-Iodo-1,2-dimethoxybenzene **(8)**

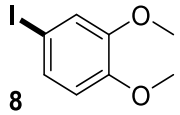

8

Reaction time	4 h
Yield	46 mg, 0.174 mmol, 87 %, colourless oil. (inseparable mixture with anthraquinone)
^{1}H NMR	^{1}H NMR (300 MHz, Chloroform-*d*) δ 7.22 (dd, *J* = 8.4, 2.0 Hz, 1H), 7.11 (d, *J* = 2.0 Hz, 1H), 6.61 (d, *J* = 8.4 Hz, 1H), 3.85 (s, 3H), 3.84 (s, 3H).
^{13}C NMR	^{13}C NMR (75 MHz, $CDCl_3$) δ 149.8, 149.1, 129.7, 120.3, 113.1, 82.3, 56.1, 55.9.
HR-MS (EI)	$(M)^{+\cdot}$: calc.: 263.9642, found: 263.9639

2-Iodo-1,4-dimethoxybenzene **(9)**

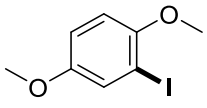

9

Reaction time	4 h
Yield	32 mg, 0.121 mmol, 61 %, colourless oil.
^{1}H NMR	^{1}H NMR (300 MHz, Chloroform-*d*) δ 7.34 (d, *J* = 2.9 Hz, 1H), 6.87 (dd, *J* = 9.0, 2.9 Hz, 1H), 6.76 (d, *J* = 9.0 Hz, 1H), 3.83 (s, 3H), 3.75 (s, 3H).
^{13}C NMR	^{13}C NMR (75 MHz, $CDCl_3$) δ 154.2, 152.7, 124.8, 114.8, 111.6, 86.0, 57.0, 56.0.
HR-MS (EI)	$(M)^{+\cdot}$: calc.: 263.9642, found: 263.9634

1,5-Diiodo-2,4-dimethoxybenzene **(10)**

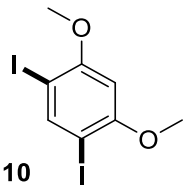

10

Reaction time	4 h
Yield	31 mg, 0.080 mmol, 80 %, white solid.
^{1}H NMR	^{1}H NMR (300 MHz, Chloroform-*d*) δ 8.04 (s, 1H), 6.37 (s, 1H), 3.89 (s, 6H).
^{13}C NMR	^{13}C NMR (75 MHz, $CDCl_3$) δ 159.6, 146.9, 95.8, 75.5, 56.5.
HR-MS (EI)	$(M)^{+\cdot}$: calc.: 389.8608, found: 389.8601

2-Iodo-1-methoxy-4-methylbenzene **(11)**

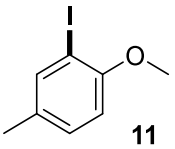

11

Reaction time	1.5 h
Yield	38 mg, 0.154 mmol, 77%, white solid
^{1}H NMR	^{1}H NMR (300 MHz, Chloroform-*d*) δ 7.60 (d, *J* = 2.1 Hz, 1H), 7.10 (dd, *J* = 8.3, 2.1, 1H), 6.72 (d, *J* = 8.3 Hz, 1H), 3.85 (s, 3H), 2.26 (s, 3H).
^{13}C NMR	^{13}C NMR (75 MHz, $CDCl_3$) δ 156.0, 139.8, 132.0, 129.9, 110.7, 85.7, 56.4, 20.0.

HR-MS (EI) $(M)^{+\cdot}$: calc.: 247.9693, found: 247.9687

***2-Iodo-1,3,5-trimethylbenzene* (12)**

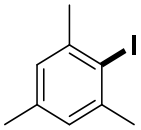

12

Reaction time 30 min

Yield NMR yield 92 %

Isolated yield 40 mg, 0.162 mmol, 81%, white solid.

^{1}H NMR ^{1}H NMR (300 MHz, Chloroform-*d*) δ 6.90 (s, 2H), 2.44 (s, 6H), 2.25 (s, 3H).

^{13}C NMR ^{13}C NMR (75 MHz, $CDCl_3$) δ 141.8, 137.3, 128.0, 104.3, 29.5, 20.7.

HR-MS (EI) $(M)^{+\cdot}$: calc.: 245.9900, found: 245.9901

***5-(tert-Butyl)-2-iodo-1,3-dimethylbenzene* (13)**

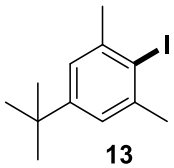

13

Reaction time 1 h

Yield 49 mg, 0.170 mmol, 85%, white solid.

^{1}H NMR ^{1}H NMR (300 MHz, Chloroform-*d*) δ 7.10 (s, 2H), 2.49 (s, 6H), 1.31 (s, 9H).

^{13}C NMR ^{13}C NMR (75 MHz, $CDCl_3$) δ 150.6, 141.5, 124.3, 104.7, 34.3, 31.3, 29.9.

HR-MS (EI) $(M)^{+\cdot}$: calc.: 288.0369, found: 288.0362

***1-Iodo-4-methylnaphthalene* (14)**

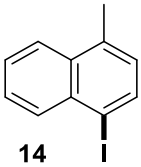

14

Reaction time 4 h

Yield 20 mg (0.074 mmol), 37 % colourless oil

GC yield: 60 %

^{1}H NMR ^{1}H NMR (300 MHz, Chloroform-*d*) δ 8.15 – 8.09 (m, 1H), 7.98 (d, *J* = 7.4 Hz, 1H), 7.96 – 7.91 (m, 1H), 7.61 – 7.53 (m, 2H), 7.04 (d, *J* = 7.5 Hz, 1H), 2.67 (s, 3H).

^{13}C NMR ^{13}C NMR (75 MHz, $CDCl_3$) δ 137.2, 135.5, 134.1, 133.5, 132.8, 127.8, 127.4, 126.6, 124.7, 97.1, 19.3.

HR-MS (ESI) calc: 267.9749, found: 267.9734

The iodinated product and the starting material could not be separated by column chromatography. Therefore, the product was further purified by evaporation in high vacuum (0.05 mbar). As the product is also slightly volatile, the separation resulted in a bit lower yield of the isolated product.

***2-Chloro-4-iodo-1-methoxybenzene* (15)**

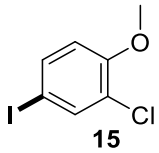

15

Reaction time	4 h
Yield	26 mg, 0.097 mmol, 48 %, white solid.
^{1}H NMR	^{1}H NMR (300 MHz, Chloroform-*d*) δ 7.66 (d, *J* = 2.1 Hz, 1H), 7.51 (dd, *J* = 8.7, 2.1 Hz, 1H), 6.68 (d, *J* = 8.7 Hz, 1H), 3.88 (s, 3H).
^{13}C NMR	^{13}C NMR (75 MHz, $CDCl_3$) δ 155.1, 138.2, 136.6, 123.8, 113.9, 81.9, 56.2.
HR-MS (EI)	$(M)^{+\cdot}$: calc.: 267.9146, found: 267.9150

***2,4-Diiodo-1-methoxybenzene* (16)**

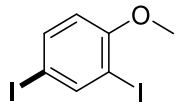

16

Reaction time	4 h
Yield	21 mg, 0.058 mmol, 29 %, white crystalline solid.
^{1}H NMR	^{1}H NMR (300 MHz, Chloroform-*d*) δ 8.04 (d, *J* = 2.1 Hz, 1H), 7.57 (dd, *J* = 8.6, 2.1 Hz, 1H), 6.58 (d, *J* = 8.6 Hz, 1H), 3.85 (s, 3H).
^{13}C NMR	^{13}C NMR (75 MHz, $CDCl_3$) δ 158.2, 146.6, 138.2, 112.8, 87.4, 83.3, 56.5.
HR-MS (EI)	$(M)^{+\cdot}$: calc.: 359.8503, found: 359.8510

***1-Iodo-4-(prop-2-yn-1-yloxy)benzene* (17)**

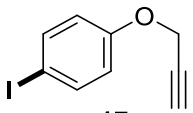

17

Reaction time	20 min
Yield	37 mg (0.142 mmol), white solid
^{1}H NMR	^{1}H NMR (300 MHz, Chloroform-d) δ 7.58 (d, J = 9.0 Hz, 2H), 6.76 (d, J = 9.0 Hz, 2H), 4.66 (d, J = 2.4 Hz, 2H), 2.53 (t, J = 2.4 Hz, 1H).
^{13}C NMR	^{13}C NMR (75 MHz, $CDCl_3$) δ 157.4, 138.3, 117.3, 84.0, 78.1, 75.9, 55.9.
HR-MS (ESI)	calc: 257.9542, found: 257.9537

***1-(4-Iodophenoxy)propan-2-one* (18)**

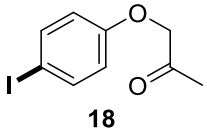

18

Reaction time	4 h
Yield	39 mg, 0.141 mmol, 70 %, slightly yellowish crystals
^{1}H NMR	^{1}H NMR (300 MHz, Chloroform-*d*) δ 7.58 (d, *J* = 9.0 Hz, 2H), 6.66 (d, *J* = 9.0 Hz, 2H), 4.51 (s, 2H), 2.27 (s, 3H).
^{13}C NMR	^{13}C NMR (75 MHz, $CDCl_3$) δ 205.0, 157.6, 138.5, 116.9, 84.1, 73.0, 26.6.
HR-MS (EI)	$(M)^{+\cdot}$: calc.: 275.9642, found: 275.9650

***Methyl 2-(4-iodophenoxy)acetate* (19)**

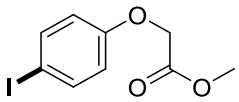

19

Reaction time	4 h
Yield	55 mg, 0.188 mmol, 94 %, white solid.
^{1}H NMR	^{1}H NMR (300 MHz, Chloroform-*d*) δ 7.57 (d, *J* = 9.0 Hz, 2H), 6.68 (d, *J* = 9.0 Hz, 2H), 4.60 (s, 2H), 3.80 (s, 3H).
^{13}C NMR	^{13}C NMR (75 MHz, $CDCl_3$) δ 169.0, 157.7, 138.4, 117.0, 84.2, 65.3, 52.4.
HR-MS (APCI)	$(M)^+$: calc.: 291.9596, found: 291.9597

***N,N-Diethyl-2-(4-iodophenoxy)acetamide* (20)**

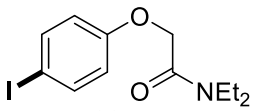

20

Reaction time	4 h
Yield	65 mg, 0.195 mmol, 98 %, slightly yellow oil
^{1}H NMR	^{1}H NMR (300 MHz, Chloroform-*d*) δ 7.56 (d, *J* = 9.0 Hz, 2H), 6.71 (d, *J* = 9.0 Hz, 2H), 4.67 (s, 2H), 3.47 – 3.33 (m, 4H), 1.23 (t, *J* = 7.1 Hz, 3H), 1.15 (t, *J* = 7.1 Hz, 3H).
^{13}C NMR	^{13}C NMR (75 MHz, $CDCl_3$) δ 167.5, 157.8, 138.4, 117.0, 84.0, 66.9, 41.9, 40.9, 14.2, 12.7.
HR-MS (APCI)	$(M+H)^+$: calc.: 334.0298, found: 334.0333

3 eq. of TFA were used to iodinate this substrate.

***N-(4-iodophenyl)acetamide* (21)**[6]

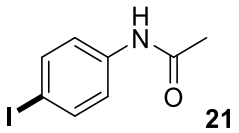

21

Reaction time	4 h
Yield	37 mg, 0.142 mmol, 71 %, white solid
^{1}H NMR	^{1}H NMR (300 MHz, Methanol-d_4) δ 7.61 (d, *J* = 8.8 Hz, 2H), 7.36 (d, *J* = 8.8 Hz, 2H), 2.10 (s, 3H).
^{13}C NMR	^{13}C NMR (75 MHz, MeOD) δ 170.25, 138.45, 137.42, 121.50, 86.21, 22.46.

4 eq. of TFA were used to iodinate this substrate and the reaction was done in DCE.

***N-(4-iodophenyl)benzamide* (22)**

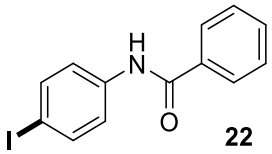

22

Reaction time	4 h
Yield	56 mg, 0. 163 mmol, 82 %, white solid (mixture with 10 mol % of starting material)
^{1}H NMR	^{1}H NMR (300 MHz, DMSO-d_6) δ 10.35 (s, 1H), 7.98 – 7.90 (m, 2H), 7.73 – 7.49 (m, 7H).

^{13}C NMR	^{13}C NMR (75 MHz, DMSO) δ 166.09, 139.50, 137.72, 135.17, 132.17, 128.87, 128.13, 122.89, 87.80, 40.79, 40.51, 40.24, 39.96, 39.68, 39.40, 39.12.
HR-MS (EI)	$(M)^{+\cdot}$: calc.: 322.9802, found: 322.9795

4 eq. of TFA were used to iodinate this substrate and the reaction was done in DCE.

***Methyl (4-iodophenyl)carbamate* (23)**

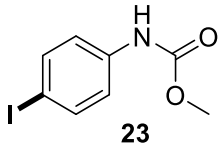

23

Reaction time	4 h
Yield	47 mg, 0.172 mmol, 86 %, crystalline white solid
^{1}H NMR	^{1}H NMR (300 MHz, DMSO-d_6) δ 9.77 (s, 1H), 7.60 (d, J = 8.7 Hz, 3H), 7.29 (d, J = 8.7 Hz, 3H), 3.65 (s, 3H).
^{13}C NMR	^{13}C NMR (75 MHz, DMSO) δ 154.31, 139.50, 137.80, 120.81, 86.02, 52.22.
HR-MS (EI)	$(M)^{+\cdot}$: calc.: 276.9594, found: 276.9599

4 eq. of TFA were used to iodinate this substrate and the reaction was done in DCE.

***4-Iodo-1-phenyl-1H-pyrazole* (24)**

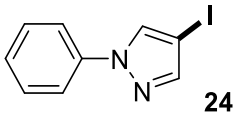

24

Reaction time	2 h
Yield	50 mg, 0.186 mmol, 93 %, white solid
^{1}H NMR	^{1}H NMR (300 MHz, Chloroform-d) δ 7.96 (s, 1H), 7.72 (s, 1H), 7.69 – 7.59 (m, 2H), 7.56 – 7.40 (m, 2H), 7.39 – 7.26 (m, 1H).
^{13}C NMR	^{13}C NMR (75 MHz, $CDCl_3$) δ 145.94, 139.51, 131.32, 129.56, 127.10, 119.12, 58.89.
HR-MS (EI)	$(M)^{+\cdot}$: calc.: 269.9648, found: 269.9643

4 eq. of TFA were used to iodinate this substrate and the reaction was done in DCE.

***4-Iodo-1,5-dimethyl-2-phenyl-1H-pyrazol-3(2H)-one* (25)**

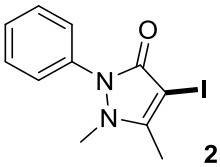

25

Reaction time	1 h
Yield	52 mg, 0.166 mmol, 83 %, white solid
^{1}H NMR	^{1}H NMR (300 MHz, Chloroform-d) δ 7.50 – 7.40 (m, 2H), 7.40 – 7.33 (m, 2H), 7.33 – 7.26 (m, 1H), 3.13 (s, 3H), 2.33 (s, 3H).
^{13}C NMR	^{13}C NMR (75 MHz, $CDCl_3$) δ 163.97, 157.58, 135.07, 129.22, 126.97, 124.10, 61.37, 36.67, 14.75.
HR-MS (EI)	$(M)^{+\cdot}$: calc.: 313.9911, found: 313.9903

4 eq. of TFA were used to iodinate this substrate and the reaction was done in DCE.

***3-Iodobenzo[b]thiophene* (26)**

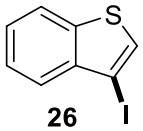

26

Reaction time	4 h
Yield	42 mg, 0.161 mmol, 81 %, yellowish oil.
^{1}H NMR	^{1}H NMR (300 MHz, Chloroform-*d*) δ 7.86 (d, *J* = 7.7 Hz, 1H), 7.77 (d, *J* = 7.7 Hz, 1H), 7.62 (s, 1H), 7.51 – 7.45 (m, 1H), 7.43 – 7.37 (m, 1H).
^{13}C NMR	^{13}C NMR (75 MHz, $CDCl_3$) δ 140.3, 138.4, 129.2, 125.3, 125.2, 122.5, 78.3.
HR-MS (ESI)	$(M)^{+\cdot}$:calc.: 259.9157, found: 259.9158

***5-(4-Iodo-2,5-dimethylphenoxy)-2,2-dimethylpentanoic acid* (27)**

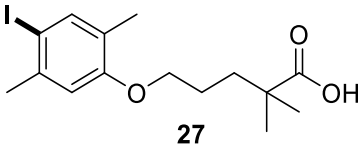

27

Reaction time	1 h
Yield	37 mg, 0.098 mmol, 98 %, white solid
^{1}H NMR	^{1}H NMR (300 MHz, DMSO-d6) δ 12.14 (brs, 1H), 7.52 (s, 1H), 6.91 (s, 1H), 3.91 (t, J = 5.7 Hz, 1H), 2.30 (s, 3H), 2.06 (s, 3H), 1.69 – 1.56 (m, 4H), 1.11 (s, 6H).
^{13}C NMR	^{13}C NMR (75 MHz, DMSO-d_6) δ 178.6, 156.8, 139.1, 138.9, 125.8, 113.2, 89.0, 67.7, 40.9, 36.3, 27.3, 24.8, 24.5, 14.7.
HR-MS (ESI)	$(M+H)^+$: calc.: 377.0608, found: 377.0606

***(S)-Methyl 2-(5-iodo-6-methoxynaphthalen-2-yl)propanoate* (28)**

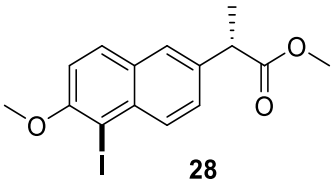

28

Reaction time	2 h
Yield	34 mg, 0.092 mmol, 92 %, white solid
^{1}H NMR	^{1}H NMR (300 MHz, Chloroform-*d*) δ 8.11 (d, *J* = 8.8 Hz, 1H), 7.80 (d, *J* = 9.0 Hz, 1H), 7.65 (d, *J* = 1.6 Hz, 1H), 7.49 (dd, *J* = 8.8, 1.6 Hz, 1H), 7.20 (d, *J* = 9.0 Hz, 1H), 4.02 (s, 3H), 3.89 (q, *J* = 7.2 Hz, 1H), 3.67 (s, 3H), 1.59 (d, *J* = 7.2 Hz, 3H).
^{13}C NMR	^{13}C NMR (75 MHz, $CDCl_3$) δ 174.9, 156.6, 136.5, 134.9, 131.7, 130.2, 129.8, 128.0, 126.3, 113.2, 87.4, 57.2, 52.2, 45.1, 18.5.
HR-MS (APCI)	$(M+H)^+$ calc.: 371.0139, found: 371.0141
Optical rotation	$[\alpha]^{20}$: +45.9 (c 0.3, $CHCl_3$)

5.5 Copies of NMR spectra

Dear reader, for the copies of the NMR spectra click on the URL below to open the full supporting information on the publisher's website (open access).

https://onlinelibrary.wiley.com/action/downloadSupplement?doi=10.1002%2Fadsc.201900298&file=adsc201900298-sup-0001-misc_information.pdf

5.6 References

1. Dohi, T.; Kita, Y., Reaction of Iodo Compounds. In *Iodine Chemistry and Applications*, Kaiho, T., Ed. Wiley: 2014; pp 303-327.
2. Zhdankin, V. V., Synthesis of Hypervalent Iodine Compounds for Oxidation Reactions. In *PATAI'S Chemistry of Functional Groups*, Olofsson, B., Marek, I., Rappoport Z. , Ed. 2018.
3. Adam, M. J.; Wilbur, D. S., Radiohalogens for imaging and therapy. *Chem. Soc. Rev.* **2005,** *34* (2), 153-163.
4. Barluenga, J., Transferring iodine: more than a simple functional group exchange in organic synthesis. *Pure Appl. Chem.* **1999,** *71* (3), 431–436.
5. Bedrač, L.; Iskra, J., Iodine(I) reagents in hydrochloric acid-catalyzed oxidative iodination of aromatic compounds by hydrogen peroxide and iodine. *Adv. Synth. Catal.* **2013,** *355* (7), 1243-1248.
6. Podgoršek, A.; Zupan, M.; Iskra, J., Oxidative halogenation with "green" oxidants: oxygen and hydrogen peroxide. *Angew. Chem. Int. Ed.* **2009,** *48* (45), 8424-8450.
7. Stavber, S.; Jereb, M.; Zupan, M., Electrophilic iodination of organic compounds using elemental iodine or iodides. *Synthesis* **2008,** *2008* (10), 1487-1513.
8. Marzo, L.; Pagire, S. K.; Reiser, O.; König, B., Visible-Light Photocatalysis: Does It Make a Difference in Organic Synthesis? *Angew. Chem. Int. Ed.* **2018,** *57* (32), 10034-10072.
9. Zhang, H.; Lei, A., Visible-light-induced C–H functionalization and C–C/C–X bond-forming oxidative cross-coupling reactions. *Asian J. Org. Chem.* **2018,** *7* (7), 1164-1177.
10. (a) Qiao, H.; Sun, S.; Yang, F.; Zhu, Y.; Kang, J.; Wu, Y.; Wu, Y., Merging photoredox catalysis with iron(III) catalysis: C5-H bromination and iodination of 8-aminoquinoline amides in water. *Adv. Synth. Catal.* **2017,** *359* (11), 1976-1980; (b) Li, L.; Liu, W.; Mu, X.; Mi, Z.; Li, C.-J., Photo-induced iodination of aryl halides under very mild conditions. *Nat. Protoc.* **2016,** *11*, 1948; (c) Li, L.; Liu, W.; Zeng, H.; Mu, X.; Cosa, G.; Mi, Z.; Li, C.-J., Photo-induced Metal-Catalyst-Free Aromatic Finkelstein Reaction. *J. Am. Chem. Soc.* **2015,** *137* (26), 8328-8331; (d) Liu, W.; Yang, X.; Gao, Y.; Li, C.-J., Simple and Efficient Generation of Aryl Radicals from Aryl Triflates: Synthesis of Aryl Boronates and Aryl Iodides at Room Temperature. *J. Am. Chem. Soc.* **2017,** *139* (25), 8621-8627.
11. (a) Breugst, M.; von der Heiden, D., Mechanisms in Iodine Catalysis. *Chem. Eur. J.* **2018,** *24* (37), 9187-9199; (b) Yusubov, M. S.; Zhdankin, V. V., Iodine catalysis: A green alternative to transition metals in organic chemistry and technology. *Resource-Efficient Technologies* **2015,** *1* (1), 49-67; (c) Liu, K.; Song, C.; Lei, A., Recent advances in iodine mediated electrochemical oxidative cross-coupling. *Org. Biomol. Chem.* **2018,** *16* (14), 2375-2387; (d) Jereb, M.; Vražič, D.; Zupan, M., Iodine-catalyzed transformation of molecules containing oxygen functional groups. *Tetrahedron* **2011,** *67* (7), 1355-1387.
12. (a) Liu, Y.; Wang, B.; Qiao, X.; Tung, C.-H.; Wang, Y., Iodine/Visible Light Photocatalysis for Activation of Alkynes for Electrophilic Cyclization Reactions. *ACS Catal.* **2017,** *7* (6), 4093-4099; (b) Yerien, D. E.; Conde, R.; Barata-Vallejo, S.; Camps, B.; Lantaño, B.; Postigo, A., Transition metal- and organophotocatalyst-free perfluoroalkylation reaction of amino(hetero)aromatics initiated by the complex [(TMEDA)I·I3] and visible light. *RSC Adv.* **2017,** *7* (1), 266-274; (c) Sudo, Y.; Yamaguchi, E.; Itoh, A., Photo-oxidative cross-dehydrogenative coupling-type reaction of thiophenes with α-position of carbonyls using a catalytic amount of molecular iodine. *Org.*

Lett. **2017,** *19* (7), 1610-1613; (d) Usami, K.; Nagasawa, Y.; Yamaguchi, E.; Tada, N.; Itoh, A., Intermolecular cyclopropanation of styrenes using iodine and visible light via carbon–iodine bond cleavage. *Org. Lett.* **2016,** *18* (1), 8-11; (e) Yang, J.; Xie, D.; Zhou, H.; Chen, S.; Huo, C.; Li, Z., Visible-light-mediated iodine-catalyzed α-hydroxylation of α-methylene ketones under aerobic conditions. *Org. Chem. Front.* **2018,** *5* (8), 1325-1329; (f) Zhang, H.; Muñiz, K., Selective Piperidine Synthesis Exploiting Iodine-Catalyzed Csp3–H Amination under Visible Light. *ACS Catal.* **2017,** *7* (6), 4122-4125.

13. (a) Becker, P.; Duhamel, T.; Stein, C. J.; Reiher, M.; Muñiz, K., Cooperative light-activated iodine and photoredox catalysis for the amination of C–H bonds. *Angew. Chem. Int. Ed.* **2017,** *56* (27), 8004-8008; (b) Duhamel, T.; Muñiz, K., Cooperative Iodine and Photoredox Catalysis for Direct Oxidative Lactonization of Carboxylic Acids. *Chem. Commun.* **2018**.

14. J. Bard, A.; A. A. Ketelaar, J., *"Encyclopedia of Electrochemistry of the Elements," Vol. II.* 1975; Vol. 122, p 139C-139C.

15. Calabrese, V. T.; Khan, A., Polyiodine and Polyiodide Species in an Aqueous Solution of Iodine + KI: Theoretical and Experimental Studies. *J. Phys. Chem. A* **2000,** *104* (6), 1287-1292.

16. Erdélyi, M., Halogen bonding in solution. *Chem. Soc. Rev.* **2012,** *41* (9), 3547-3557.

17. Romero, N. A.; Nicewicz, D. A., Organic photoredox catalysis. *Chem. Rev.* **2016,** *116* (17), 10075-10166.

18. Roth, H. G.; Romero, N. A.; Nicewicz, D. A., Experimental and Calculated Electrochemical Potentials of Common Organic Molecules for Applications to Single-Electron Redox Chemistry. *Synlett* **2016,** *27* (05), 714-723.

19. Petzold, D.; König, B., Photocatalytic oxidative bromination of electron-rich arenes and heteroarenes by anthraquinone. *Adv. Synth. Catal.* **2017,** *360* (4), 626-630.

20. Iskra, J.; Stavber, S.; Zupan, M., Nonmetal-catalyzed iodination of arenes with iodide and hydrogen peroxide. *Synthesis* **2004,** *2004* (11), 1869-1873.

21. Ogata, Y.; Aoki, K., Iodination of aromatic compounds with a mixture of iodine and peracetic acid. III. Autocatalysis and relative rates. *J. Am. Chem. Soc.* **1968,** *90* (22), 6187-6191.

22. M. Montalti; A. Credi; L. Prodi; Gandolfi, M. T., Handbook of Photochemistry. In *Handbook of Photochemistry,* 3rd ed.; CRC Press: Boca Raton, 2006.

23. Romero, N. A.; Margrey, K. A.; Tay, N. E.; Nicewicz, D. A., Site-selective arene C-H amination via photoredox catalysis. *Science* **2015,** *349* (6254), 1326.

24. No TFA was added, as it also protonates pyrazole to form insoluble precipitate, salt.

25. (a) Galli, C., Aromatic iodination: evidence of reaction intermediate and of the δ-complex character of the transition state. *J. Org. Chem.* **1991,** *56* (10), 3238-3245; (b) Galli, C.; Di Giammarino, S., Studies of substrate selectivity in aromatic iodination and other substitution reactions reinforce previous conclusions about the nature of the mechanism of electrophilic aromatic substitutions. *J. Chem. Soc., Perkin Trans. 2* **1994,** (6), 1261-1269; (c) Fabbrini, M.; Galli, C.; Gentili, P.; Macchitella, D.; Petride, H., Aromatic iodination: a new investigation on the nature of the mechanism. *J. Chem. Soc., Perkin Trans. 2* **2001,** *0* (9), 1516-1521.

26. The value 1420 is reported in a reference 21c. In 21b, the authors report value 1100.

27. Kleinberg, J.; Davidson, A. W., The Nature of Iodine Solutions. *Chem. Rev.* **1948,** *42* (3), 601-609.

6 Summary

Visible light-induced homolysis of different complexes offers a mild approach for the generation of reactive radical intermediates which can be utilized in organic synthesis. The use of photolabile complexes represents a complementing alternative to reaction systems relying on excitation of a photocatalyst. In the thesis, we investigated the applications of light-driven homolysis of hypervalent iodine(III) and bismuth complexes in different reactions.

Chapter 1 summarizes various synthetic transformations based on direct excitation of hypervalent iodine(III) reagents. The diverse reactivity of five different structural classes of hypervalent iodine compounds is presented.

Chapter 2 describes the development of a metal-free system for decarboxylative Ritter-type amination based on iodine(I/III) catalytic manifold. The developed system gives access to carbenium ion intermediates also on electronically disfavoured benzylic positions. The unusually high reactivity of the system stems from a complexation of iodine(III) intermediates with Lewis acid BF_3. These complexes have enhanced oxidation abilities, improved light absorption and higher solubility in the reaction solvent acetonitrile. In the mechanistic study which involved control experiments from potential reaction intermediates and reaction kinetics, two competing operating mechanistic pathways were identified. The faster productive pathway proceeds via direct excitation of iodine(III) - BF_3 complexes, and the slower one via excitation of hypoiodite (RCOOI) species. The synthetic utility of the decarboxylative Ritter-type amination protocol has been demonstrated by the functionalization of benzylic as well as aliphatic carboxylic acids, including late-stage modification of different pharmaceutical molecules.

In **chapter 3,** the application of previously found photolabile iodine(III) - BF_3 complexes was extended to functionalization of abundant C(sp^3)–H bonds. This was enabled by the use of carboxylate ligands which do not undergo fast decarboxylation, but instead serve as hydrogen abstracting catalysts. A screening of different ligands and iodoarenes was done to optimize the performance of the *in situ* formed iodine(III) - BF_3 complex in a Ritter-type amination of benzylic positions. The developed practically simple method complements existing methods for carbenium ions generation by allowing functionalization of certain more challenging substrates (e.g., substrates with primary benzylic positions), which is however negligible under reaction conditions.

Chapter 4 explores the possibility of expanding the concept of ligand-to-metal charge transfer (LMCT) photocatalysis to complexes of less frequently used metals. A screening assay identifying LMCT activity was developed and used to systematically evaluate reactivity of different metal salts under multiple reaction conditions. The assay helped us to discover LMCT activity of simple bismuth salts. These were used for generation of two different electrophilic radicals (chlorine and carboxyl) in net-oxidative as well as redox-neutral photochemical reactions. Mechanistic studies based on cyclovoltammetry and UV-vis spectroscopy revealed that the highly reactive bismuth(II) radical fragment is prone to undergo disproportionation. This represents a competing reaction pathway leading to the catalyst inactivation.

In **Chapter 5**, a development of visible-light-mediated oxidative iodination of electron-rich arenes is described. The topic of the last chapter is not closely related to the general topic of the thesis since the project was designed before the PhD. The method was developed based on the observation of a spectral window in otherwise strongly colored iodine solutions. The window appears when iodine is dissolved in non- or weakly electron-donating solvents at around 400 nm. The excitation of a highly oxidative anthraquinone catalyst in this region allowed photochemical iodination of different electron-rich arenes. Mechanistic investigations by intermediate-trapping and competition experiments indicate a photocatalytic arene-oxidation and the subsequent reaction with iodine as a likely mechanistic pathway.

7 Zusammenfassung

Die Licht-induzierte Homolyse verschiedener Komplexe stellt einen attraktiven und milden Ansatz zur Erzeugung reaktiver radikalischer Zwischenprodukte dar, die in der organischen Synthese genutzt werden können. Die Verwendung photolabiler Komplexe ist eine ergänzende Alternative zu Reaktionssystemen, die auf der Anregung eines Photokatalysators beruhen. In dieser Arbeit wurde die Anwendungen der lichtgetriebenen Homolyse von hypervalenten Iod(III)- und Bismutkomplexen in verschiedenen Reaktionen untersucht.

Kapitel 1 gibt eine Übersicht über verschiedene synthetische Umwandlungen, die auf der direkten Anregung von hypervalenten Iod(III)-Reagenzien basieren. Die vielfältige Reaktivität von fünf verschiedenen Strukturklassen hypervalenter Iodverbindungen wird vorgestellt.

Kapitel 2 beschreibt die Entwicklung einer metallfreien Ritter-Typ Reaktion für die decarboxylative Aminierung mithilfe eines Iod(I/III)-Katalysators. Das entwickelte System ermöglicht den Zugang zu Carbokationen an anspruchsvollen, elektronisch ungünstigen Benzylpositionen. Die außergewöhnlich hohe Reaktivität des Systems beruht auf einer Komplexierung von Iod(III)-Zwischenprodukten mit der Lewis-Säure BF_3. Diese Komplexe sind stärker oxidierend, zeigen verbesserte photophysikalische Eigenschaften und weisen eine höhere Löslichkeit im Reaktionslösungsmittel Acetonitril auf. Bei mechanistischen Untersuchungen, die Kontrollversuche zu potenziellen Reaktionsintermediaten und zur Reaktionskinetik umfassen, wurden zwei mögliche Reaktionswege identifiziert. Der schnellere, produktive Weg verläuft über die direkte Anregung von Iod(III)-BF_3-Komplexen, der Langsamere über die Anregung einer Hypoiodit-Spezies (RCOOI). Der synthetische Nutzen dieser decarboxylierenden Ritter-Typ Aminierung wurde durch die Funktionalisierung von benzylischen und aliphatischen Carbonsäuren gezeigt, insbesondere durch late-stage Modifizierungen verschiedener pharmazeutisch relevanter Moleküle.

In **Kapitel 3** wurde das Konzept der Photolyse von Iod(III)-BF_3-Komplexe auf die Funktionalisierung zahlreicher C(sp^3)-H-Bindungen erweitert. In diesem weiterentwickeltem Reaktionssystem werden Benzoat-Liganden verwendet, die nicht decarboxylieren, und daher als Wasserstoffatom-Transfer Katalysatoren eingesetzt werden können. Durch Screening verschiedener Liganden und Iodoarenen wurde eine optimaler Iod(III)-BF3-Komplex zur C-H Aktivierung und Aminierung benzylischer Positionen ermittelt. Die entwickelte Methode zeichnet sich durch hohe Praktikabilität und einfache Anwendbarkeit aus und stellt damit eine attraktive Alternative zur Erzeugung von Carbenium-Ionen dar, insbesondere zur Funktionalisierung schwieriger Substrate (z. B. Substrate mit primären Benzylpositionen).

In **Kapitel 4** wird die Möglichkeit untersucht, Ligand-Metall-Chargetransfer(LMCT) - Photokatalyse auf weniger häufig verwendete Metalle auszuweiten. Es wurde ein Screening-Assay zur einfachen Identifizierung von LMCT-Aktivität entwickelt und zur systematischen Bewertung der Reaktivität verschiedener Metallsalze eingesetzt. Dieser Test half, die LMCT-Aktivität von einfachen Bismutsalzen zu entdecken. Diese wurden für die Erzeugung von zwei verschiedenen elektrophilen Radikalen (Chlor- und Carboxylradikale) in sowohl oxidativen als auch redox-neutralen photochemischen Reaktionen verwendet. Mechanistische Untersuchungen basierend auf Cyclovoltammetrie und UV-Vis-Spektroskopie ergaben, dass das hochreaktives Bismut(II)-Radikalkatalysatorfragment zur Disproportionierung neigt. Dies stellt einen konkurrierenden Reaktionspfad dar, der zur Inaktivierung des Katalysators führt, der aber unter Reaktionsbedingungen vernachlässigt werden kann.

Kapitel 5 beschreibt die Entwicklung einer Licht getriebenen oxidativen Iodierung von elektronenreichen Aromaten. Dieses Kapitel steht nur in einem losen Zusammenhang mit dem allgemeinen Thema der Dissertation, da das Projekt vor der Promotion konzipiert wurde. Die Methode wurde basierend auf der Beobachtung eines spektralen Fensters in sonst stark gefärbten Iodlösungen entwickelt. Dieses Fenster tritt auf, wenn Iod in nicht oder nur in schwachen

Elektronendonor-Lösungsmitteln bei etwa 400 nm gelöst wird. Die Anregung eines hochoxidativen Anthrachinon-Katalysators im Bereich des Fensters ermöglicht die photochemische Iodierung verschiedener elektronenreicher Aromaten. Mechanistische Untersuchungen, Intermediat-Trapping- und Competition-Experimente deuten auf eine photokatalytische Aren-Oxidation und anschließende Reaktion mit Iod als möglichen Mechanismus hin.

8 Appendix

8.1 Abbreviations

λ	wavelength
APCI	atmospheric-pressure chemical ionization
Ar	arene
AQ	anthraquinone
calc.	calculated
CPS	counts per second
CV	cyclic voltammetry
DCE	1,2-dichloroethane
DCM	dichloromethane
DMA	dimethylacetamide
DMF	dimethylformamide
DMSO	dimethyl sulfoxide
e.g.	for example (lat. exempli gratia)
eq. (or equiv.)	equivalent
EI	electron ionization
ESI	electrospray ionization
et al.	and others (lat. et alii)
EA	ethyl acetate
Fc	ferrocene
FID	flame ionization detector
GC	gas chromatography
HAT	hydrogen atom transer
HRMS	high resolution mass spectrometry
hν	incident photon energy
i.e.	that is (lat. id est)
IR	infrared
J	coupling constant
LED	light emitting diode
LMCT	Ligant-to-metal charge transfer
LRMS	low resolution mass spectrometry
mCPBA	meta-Chloroperoxybenzoic acid
MS	mass spectrometry
n.d.	not detected
NIS	N-iodosuccinimide
NMR	nuclear magnetic resonance
Nu	nucleophile
p.a.	per analysis
ppm	parts per million
PC	photocatalyst
PE	petroleum ether
PG	protecting group

pKa	acid dissociation constant at logarithmic scale
R	alkyl-, aryl- or functional groups
RFTA	riboflavin tetraacetate
rt (or r.t.)	room temperature
SCE	saturated calomel electrode
SET	single electron transfer
TFA	trifluoroacetic acid
THF	tetrahydrofuran
TLC	thin layer chromatography
Tos (or Ts)	toluenesulfonyl
UV	ultra violet light
vis	visible light
vs.	against (lat. versus)

8.2 Curriculum Vitae

Personal Data

Name:	Rok Narobe
Date and place of birth:	10.10.1993; Ljubjana (Slovenia)
Marital Status:	not married
Nationality:	Slovenian

Education

10/2018 – 3/2023	**Ph.D. in Organic Chemistry** University of Regensburg (Germany) *"Synthetic Transformations Based on Homolysis of Iodine and Bismuth Complexes"* Supervisor: Prof. Dr. Burkhard König
10/2015 – 09/2018	**Master of Science, Chemistry** University of Ljubljana (Slovenia) Master thesis: *"Classical and Photocatalytic Oxidative Iodination of Arenes"* Supervisor: Prof. Dr. Jernej Iskra
10/2012 – 09/2015	**Bachelor of Science, Chemistry** University of Ljubljana (Slovenia) Bachelor thesis: *"Study of oxidative iodination of 4-tert-butylphenol with iodine, sulfuric acid and hydrogen peroxide"* Supervisor: Prof. Dr. Marjan Jereb

Conferences

- Seminar day of the graduate research training group "ChemPharm" (4/2021; Regensburg)
- Iberoamerican symposium on organic chemistry (12/2019; Cuba)
- Münster symposium on cooperative effects in organic chemistry (May 5/2019; Münster)
- Seminar day of the graduate research training group „Chemical Photocatalysis"(3/2019; Regensburg)
- Lecture conference on photochemistry (9/2018; München)
- Slovenian Chemical Days (9/2018; Portorož)
- Cutting edge (9/2017; Ljubljana), *best poster award*
- Slovenian Chemical Days (9/2015; Ljubljana)

Awards and recognitions

- Award for the best contribution at the Syngenta Workshop for Talented PhD Chemistry Students (9/2021; Stein, Switzerland)
- DAAD One-Year Research Grant (10/2019-2020; Bonn, Germany)
- Krka Grand Prize for Research Achievements (10/2019; Novo Mesto, Slovenia)
- Participation in 44th International Chemistry Olympiad (7/2012; Washington, DC, USA)

Publication list

- **Narobe, R.;** König, B., Transformations based on direct excitation of hypervalent iodine(III) reagents. *Org. Chem. Front.* **2023,** *10* (6), 1577-1586.
- Birnthaler, D.;† **Narobe, R.;**† Lopez-Berguno, E.; Haag, C.; König, B., Synthetic Application of Bismuth LMCT Photocatalysis in Radical Coupling Reactions. *ACS Catal.* **2023**, *13* (2), 1125-1132. († = equal contribution), *"ACS editors' choice article" recognition*
- **Narobe, R.;** Murugesan, K.; Haag, C.; Schirmer, T. E.; König, B., C(sp^3)–H Ritter amination by excitation of in situ generated iodine(III)–BF_3 complexes. *Chem. Commun.* **2022,** *58* (63), 8778-8781. *Selected as "HOT article"*
- Babawale, F.; Murugesan, K.; **Narobe, R.;** König, B., Synthesis of Unnatural α-Amino Acid Derivatives via Photoredox Activation of Inert C(sp^3)–H Bonds. *Org. Lett.* **2022,** *24* (26), 4793-4797.
- Murugesan, K.; Donabauer, K.; **Narobe, R.;** Derdau, V.; Bauer, A.; König, B., Photoredox-Catalyzed Site-Selective Generation of Carbanions from C(sp^3)–H Bonds in Amines. *ACS Catal.* **2022,** *12* (7), 3974-3984.
- **Narobe, R.;** Murugesan, K.; Schmid, S.; König, B., Decarboxylative Ritter-Type Amination by Cooperative Iodine (I/III)—Boron Lewis Acid Catalysis. *ACS Catal.* **2022,** *12* (1), 809-817.
- Zheng, Y.-W.; **Narobe, R.;** Donabauer, K.; Yakubov, S.; König, B., Copper(II)-Photocatalyzed N–H Alkylation with Alkanes. *ACS Catal.* **2020,** *10* (15), 8582-8589.
- Giedyk, M.; **Narobe, R.;** Weiß, S.; Touraud, D.; Kunz, W.; König, B., Photocatalytic activation of alkyl chlorides by assembly-promoted single electron transfer in microheterogeneous solutions. *Nat. Catal.* **2020,** *3* (1), 40-47.
- **Narobe, R.;** Düsel, S. J. S.; Iskra, J.; König, B., Photocatalytic Oxidative Iodination of Electron-Rich Arenes. *Adv. Synth. Catal.* **2019,** *361* (17), 3998-4004. *Selected as "Very Important Publication" and as journal's front cover picture.*

9 Acknowledgement

First and foremost, I would like to thank my advisor, Professor Dr. Burkhard König for giving me the opportunity to work in his research group first as an exchange and then as a PhD student. I am sincearly grateful for his advice, encouragement and trust to pursue my own ideas. I am thankful also for the opportunities to present my research at different international meetings and conferences.

I am grateful to Prof. Dr. Oliver Reiser and Prof. Dr. Frank-Michael Matysik for the examination of the thesis. Prof. Dr. Arno Pfitzner is acknowledged for serving as a chairperson in my Ph.D. thesis defense.

I would like to especially thank my project collaborators Dr. Simon J.S. Düsel, Dr. Maciej Giedyk, and Dr. Kathiravan Murugesan for many practical solutions, helpful discussions, and their guidance. I thank also other cooperating partners Dominik Birnthaler, Karsten Donabauer, Florence Babawale, Yi-Wen Zheng, and Tobias Schirmer who strongly contributed to the success of our projects. I am grateful as well to a few annonymus colaborators - surprisingly helpful reviewers whose comments significantly improved scientific value of our work. Next, I want to thank my motivated internship students Annette, Becky, Denis, Simon, and Christoph for helping me test and develop different ideas. My sincere thanks go to Indrajit Ghosh, Daniel Petzold, Bartosz Bieszczad, and Shun Wang for their openness to discuss my projects and chemistry in general.

The presented projects were finished in a relatively short time due to excellent administrative and technical support of Regina, Ernst, Barbara, Julija, Britta, Rudi, Simone, and Petra. Thank you!

I warmly thank my former labmates Maciek, Anamitra, Jessi, Kathir, and Alejandro for creating a supportive environment in which many educational and motivating discussions took place.

My time at the University would be quite sad if the research was not properly balanced with some fun activities. For these, I would like to thank all the past and present AK König members, especially Indra, Matthias, Simon D., Petzi, Jonas, Dominik, Elina, Maxim, Michela, Jessi, Alejandro, Alberto, Nikita, Tobi K., Alessa, Uli, Karsten, Tobi S., Vincent, Becky, José, Ritu, Daniel, Saikat, Nicolas, Lea, Sascha, Martin, Ahmad, Alex, Andi, and Marilia. I would like to thank also AK Reiser members Saerom, Peter, Benjamin, Lukas, Urszula, Michi, Carina, Lisa, Kathi, Natalija, Viktor, Sebastian F., Sebastian E., Tomi, Anurag, Quan-Qing, Anna, Aditya, Ruben, Hendrik, Alex, Marco, and Youssef for many pleasant social interactions.

DAAD and Chemical Photocatalysis - GRK 1626 are acknowledged for the financial support and organization of many inspiring meetings.

I thank different communities developing and maintaining web tools and databases which facilitate information exchange between researchers. Specifically, I would like to thank Wikipedia, Inoreader, Grammarly, Thesaurus, Organic Chemistry Portal (OCP), Spectral Database for Organic Compounds (SDBS), cheminfo.org portal, and multiple unit conversion tools. Your services saved me a lot of time.

Velika in zelo pomembna zahvala gre moji družini, ki me podpira pri vseh odločitvah, kljub temu, da morda kdaj ni čisto jasno, kaj želim doseči. Doma sem se priučil vztrajnosti in potrpežljivosti, ki sta mi zelo koristili pri pisanju teh listov. Zahvala gre tudi Evini družini, ki nama vseskozi stoji ob strani in nama tudi zelo pomaga pri organizaciji najinih obiskov Slovenije.

Na koncu se želim zahvaliti punci Evi za njeno neverjetno podporo skozi vsa ta leta. Na tebe se lahko obrnem za karkoli, od kemijskih nasvetov do smiselnega preživljanje prostega časa. Hvala, ker si del mojega življenja!

Eidesstattliche Erklärung

(1) Ich erkläre hiermit an Eides statt, dass ich die vorliegende Arbeit ohne unzulässige Hilfe Dritter und ohne Benutzung anderer als der angegebenen Hilfsmittel angefertigt habe; die aus anderen Quellen direkt oder indirekt übernommenen Daten und Konzepte sind unter Angabe des Literaturzitats gekennzeichnet.

(2) Bei der Auswahl und Auswertung folgenden Materials haben mir die nachstehend aufgeführten Personen in der jeweils beschriebenen Weise unentgeltlich geholfen:
1. _____
2. _____
3. _____

(3) Weitere Personen waren an der inhaltlich-materiellen Herstellung der vorliegenden Arbeit nicht beteiligt. Insbesondere habe ich hierfür nicht die entgeltliche Hilfe eines Promotionsberaters oder anderer Personen in Anspruch genommen. Niemand hat von mir weder unmittelbar noch mittelbar geldwerte Leistungen für Arbeiten erhalten, die im Zusammenhang mit dem Inhalt der vorgelegten Dissertation stehen.

(4) Die Arbeit wurde bisher weder im In- noch im Ausland in gleicher oder ähnlicher Form einer anderen Prüfungsbehörde vorgelegt.

Regensburg, 13.02.2021